Spectral Matching for Elemental Abundances of Evolved Stars of Globular Clusters

Jeffrey D. Simpson

Submitted in partial fulfilment of the
requirements for the degree of
Doctor of Philosophy

University of Canterbury
July 25, 2013

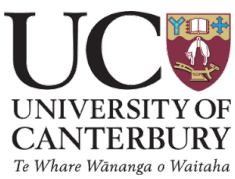

The noble globular cluster ω Centauri, beyond all comparison the richest and largest object of the kind in the heavens. The stars are literally innumerable…

John Herschel (1847)

This thesis has survived:
Getting engaged
Getting married
Moving house once
Three snow days
A 7.1 magnitude earthquake on September 4, 2010 that shut down the university for 2 weeks
A 6.3 magnitude earthquake on February 21, 2011 that shut down the university for 6 weeks
Another 6.3 magnitude earthquake on June 13, 2011 that shut down the university for 1 week
Over 11,000 other earthquakes over the last 2½ years

ISBN 978-0-473-23664-9

Abstract

In order to understand the origin of globular clusters, large samples of their stars need to be observed and analyzed for their chemical composition. This is especially true for the complex, multimetallic cluster ω Centauri, with its large range of iron, carbon, nitrogen, oxygen, sodium and barium abundances. In order to accomplish this, an automated spectral matching pipeline was developed to determine these abundances. This thesis made use of photometry and low resolution spectroscopy to analyze the chemical composition of evolved stars in three clusters: ω Cen, 47 Tuc and NGC 6752. The latter two clusters are monometallic and selected due to their similar metallicities to the metal-rich and metal-poor stars in ω Cen. This allowed them to be used as test-cases for the spectral matching pipeline.

For ω Cen, two analyses were performed. In the first, 221 giant branch stars were selected that had known [O/Fe]. These stars showed the expected anticorrelation in [C/Fe]to [N/Fe]. In the second, spectral indices were used to estimate the oxygen abundance of the stars, leading to a determination of whether a particular star was oxygen-rich or oxygen-poor. From this a catalogue of abundances of iron, carbon and barium of 848 giant branch stars were determined, of which 557 also had well-defined nitrogen abundances.

k-means clustering analysis was used to group the stars in ω Cen into four homogeneous groups based upon these abundances. These groups suggest that there were at least four main periods of star formation in the cluster. The exact order of these star formation events is not yet understood, with some models predicting the groups formed from iron-poorest to iron-richest, while others suggest the potential for iron-poorer groups to form after iron-rich groups.

These results compare well with those found from higher resolution studies and show the value of more extensive lower resolution spectral surveys. They also highlight the need for large samples of stars when working with a complex object like ω Cen.

Contents

List of Figures

List of Tables

Acronyms

2MASS Two Micron All Sky Survey

AAT Anglo-Australian Telescope

AGB asymptotic giant branch

bMS blue main sequence

CMD colour-magnitude diagram

EW equivalent width

FDU first dredge-up

FRMS fast rotating massive stars

GB giant branch

GC globular cluster

HB horizontal branch

hfs hyperfine splitting

HST Hubble Space Telescope

ICM intra-cluster medium

ISM interstellar medium

MInt intermediate metallicity group

MOOG MOOG

MOS multi-object spectroscopy

MP main population

MS main sequence

MSTO main sequence turn-off

RGB red giant branch

rMS red main sequence

RSS Robert Stobie Spectrograph

SALT Southern African Large Telescope

SGB sub-giant branch

SN supernova

TDU third dredge-up

VMP very metal-poor

Disclaimer

I hereby declare that the work in this thesis is that of the candidate alone, except where indicated below or in the text of the thesis.

Chapters 2 and 4 to 6 in part use text and figures that will be published in J. D. Simpson et al. (2012). "Spectral matching for abundances and clustering analysis of stars on the giant branches of ω Centauri". In: MNRAS 427, pp. 1153–1167.

Chapter 5 in part use text and figures that were previously published in J. D. Simpson & P. L. Cottrell (2013). "Spectral matching for abundances of 848 stars of the giant branches of the globular cluster ω Centauri". In: MNRAS 433, pp. 1892–1902.

Spectral data of 47 Tuc in Section 3.1 was acquired in October 2008 by C. Clare Worley at the Anglo-Australian Telescope (AAT). The continuum normalization and [Na/Fe] abundance determination were performed by C. Clare Worley and wavelength calibration were from Andrew Ridden-Harper. Subsequent analysis was performed by the candidate.

Spectral data of 47 Tuc in Section 3.2 was acquired in August 2012 for the candidate at the Southern African Large Telescope (SALT). It was reduced by Peter Cottrell using PySALT (Crawford et al. 2010). Cosmic-ray removal and sky subtraction and subsequent analysis was performed by the candidate.

Spectral data of NGC 6752 in Section 3.5 was acquired C. Clare Worley at the AAT. Initial reduction was performed by C. Clare Worley. Subsequent analysis was performed by the candidate.

Spectral data of ω Cen was acquired in 2000 by Terry Bridges for van Loon et al. (2007) and reduced by them. Their reduced spectra were used by the candidate, but were renormalised by the candidate.

This publication makes use of data products from the Two Micron All Sky Survey, which is a joint project of the University of Massachusetts and the Infrared Processing and Analysis Center/California Institute of Technology, funded by the National Aeronautics and Space Administration and the National Science Foundation.

Figure 1.9 is reproduced from figure 2 of Sneden et al. (2008) with permission of Annual Reviews in this thesis via Copyright Clearance Center.

Jeffrey D. Simpson

July 2013

Chapter 1

Introduction

Globular clusters (GCs) are vast, dense, spherical conglomerations of 10^4–10^6 stars, orbiting a galactic core. At least 157 (Harris 1996, 2010 update) orbit our Milky Way galaxy, a small number compared to some giant ellipticals, which can have tens of thousands. GCs typically inhabit a volume of space usually < 20 pc across. This leads to densities of up to 1000 stars per cubic parsec at their core. Due to their large concentration of stars, they are intrinsically bright, allowing them to be observed at very large distances.

The previous paradigm of GCs was that each cluster existed as a coeval monometallic population; the prototypical simple stellar population. It could be assumed that all the stars had the same distance, reddening and age. The initial mass was the only difference between the individual stars, a fact supported by their simple colour-magnitude diagrams (CMDs). This allowed for them to be used as testing grounds for theories of stellar evolution.

This picture has changed in the last 40 years. It is now understood that, although almost all are monometallic, each GC that has been studied in detail exhibits an anticorrelation in the sodium and oxygen abundances of its stars (e.g., Carretta et al. 2009). This anticorrelation and other abundance ranges exist at all stages of the stellar evolution where it has been measured (reviewed in Gratton et al. 2004, 2012). This has led to a new paradigm in which GCs had a primordial population that polluted the intra-cluster medium (ICM)[1], from which one or more subsequent generations formed with different sodium and oxygen abundances to the first generation (first proposed by Cottrell & Da Costa 1981). This is known as self-enrichment, although the exact form of the polluters is not yet understood, with some favouring asymptotic giant branch (AGB) stars (e.g., D'Antona & Ventura 2007), some fast rotating massive stars (FRMS) (e.g., Decressin et al. 2007) and some including supernovæ (SNe) (e.g., J.-W. Lee et al. 2009).

There are some clusters that are outliers to this picture. The main topic of this thesis, ω Cen, is one such anomaly. Visible to the naked eye in the southern constellation Centaurus, it was first reported as non star-like by Halley (1714). It is about 5.2 kpc from the Sun. Its luminosity and mass set it apart from almost all other Galactic GCs, where physical extent is usually anticorrelated with luminosity (Fig. 1.1). Instead, ω Cen is one of two clusters to break this trend, with the other being NGC 2419. The situation with NGC 2419 is not fully understood, due to its large distance (apparent brightness 100 times fainter ω Cen) and its small apparent size (5 times smaller than ω Cen; Harris 1996). Cohen et al. (2010) found a spread of ~ 0.2 dex in the calcium abundance from the Ca II infrared triplet, which they interpreted as being a metallicity range of the cluster. However Mucciarelli et al. (2012) dispute this, suggesting that the spread is not real, instead being the result of Cohen et al. (2010) not taking into account a spread in magnesium. Higher resolution work by Cohen & Kirby (2012) found a calcium spread but no spread in iron. Whatever is the case, it is an extremely large cluster for its luminosity, which could be the result of it having an extragalactic origin. It warrants further scrutiny. For completeness, there are four other clusters with known metallicity spreads: NGC 3201 (Δ[Fe/H] < 0.4; Simmerer et al. 2013)[2], Terzan 5 (Δ[Fe/H] ~ 0.5; Ferraro

[1] In this thesis, the phrase intra-cluster medium (ICM) is used to refer to the gas and dust inside the potential of a cluster from which subsequent generations of stars can form. This is to distinguish it from the interstellar medium (ISM) which surrounds the cluster and in some models enters into the cluster's potential and mixes with the ICM to change its composition.

[2] This cluster has a retrograde orbit with a high radial velocity, is differentially reddened, and has an inhomogeneous distribution of stars (Kravtsov et al. 2010). It also has a low mass, unlike the other multimetallic clusters.

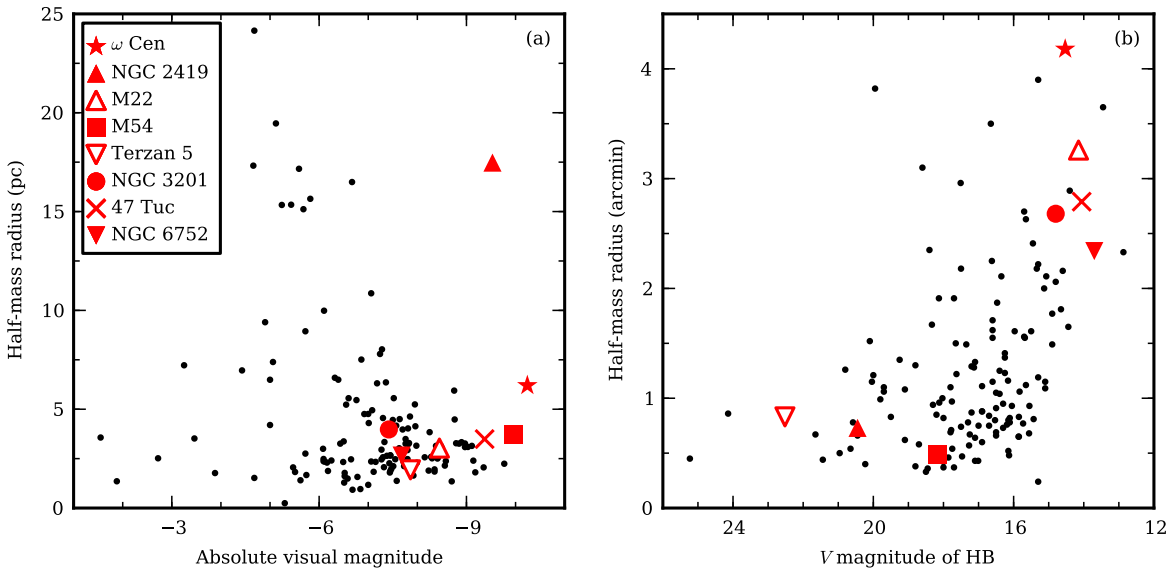

Figure 1.1 — The (a) physical sizes and luminosities and (b) apparent angular extents and apparent magnitudes of GCs of the Milky Way (Harris 1996). Highlighted are the GCs mentioned in this chapter to show their normal or in some cases anomalous luminosities. The first two on the legend are anomalous properties, the next three have metallicity spreads and the last two were analyzed in Chapter 3.

et al. 2009)[3], M22 (Δ[Fe/H] ~ 0.14; Marino et al. 2009), and M54 (Δ[Fe/H] ~ 0.19, found within the core of the Sagittarius dwarf spheroidal; Carretta et al. 2010a).

Due to ω Cen's brightness, it was possible to produce CMDs of its giant branch (GB) stars as early as Belserene (1959). The first to suggest that there was an intrinsic width to the GB that was not related measurement uncertainties was Geyer (1967), with confirmation by Cannon & Stobie (1973). However they did not provide any suggestions as to the cause for the GB colour spread beyond the potential for differential reddening in the cluster. That there was an abundance range in the cluster was first determined by Freeman & Rodgers (1975), who measured the Ca II K line in 25 RR Lyræ stars and found a 1.2 dex range in the [Ca/H] showing, for the first time, that ω Cen was not homogeneous in its elemental abundances.

It has now become clear in the four decades since Cannon & Stobie (1973) that ω Cen is unlike most GCs. In both spectroscopy and photometry it presents a complex picture of an object that underwent multiple star formation events, each with different elemental abundances. It has a huge metallicity range for even the non-monometallic GCs (Δ[Fe/H]> 1.5 dex compared to ~ 0.5 dex for Terzan 5.). This thesis is an exploration of using spectroscopy and photometry to determine basic stellar parameters ($T_{\rm eff}$, $\log g$) and elemental abundances ([Fe/H], [C/Fe], [N/Fe], [Ba/Fe] and [O/Fe]) of evolved stars, and to place these stars into groups of similar abundances.

This introductory chapter presents previous observational results of 47 Tuc and NGC 6752 (Section 1.1); the observations of multiple populations in the photometry and spectroscopy of ω Cen (Section 1.2); an overview of stellar nucleosynthesis in the context of GC stars (Section 1.3); and an overview of this thesis (Section 1.4).

1.1 Observational History of 47 Tuc and NGC 6752

In addition to ω Cen, this thesis used two monometallic GCs, 47 Tuc and NGC 6752, as test-cases for calibrating the spectral matching pipeline that was used for the automated abundance analysis. The basic parameters of these clusters are found in Table 1.1. These clusters cover the range of metallicities observed in ω Cen, with both exhibiting

[3]Origlia et al. (2011) found there was no aluminium-oxygen anticorrelation within the two populations of stars in the clusters found by Ferraro et al. (2009), [Fe/H] = −0.25, +0.27, so Massari et al. (2013) suggest that Terzan 5 is not a true GC, but instead is a remnant fragment of the Galactic bulge. It also has a very high metallicity for a GC.

Table 1.1 — Basic parameters of the GCs investigated in this thesis (Harris 1996).

Cluster	[Fe/H]	m_V	$V_{\rm HB}$	half-light radius	E($V-K$)	$m-M$
47 Tuc	−0.72	3.95	14.06	3′.17	0.12	13.37
NGC 6752	−1.54	5.40	13.70	1′.91	0.11	13.24
ω Cen		3.68	14.51	5′.00	0.30	13.70

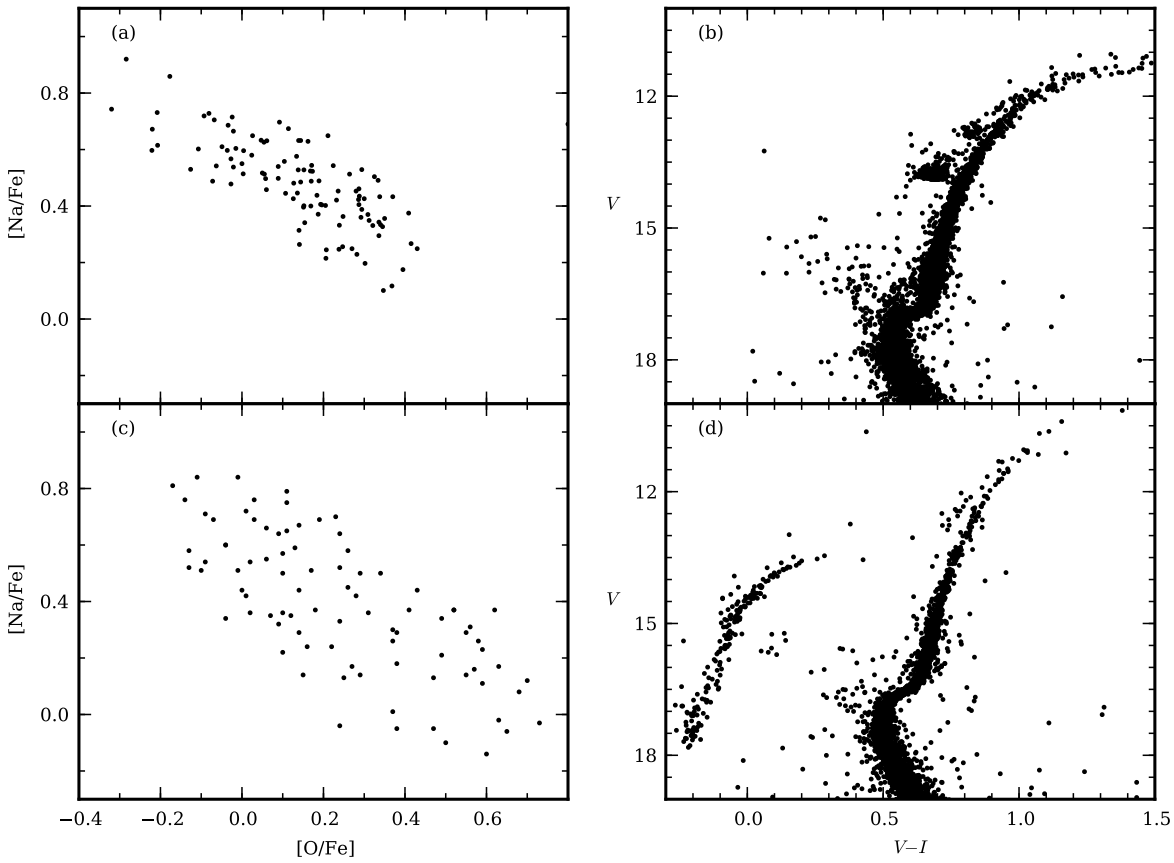

Figure 1.2 — The sodium-oxygen anticorrelations and the CMDs of the two monometallic GCs: (a) & (b) 47 Tuc; (c) & (d) NGC 6752. The photometry is from the Globular Cluster Treasury (Sarajedini et al. 2007). The [Na/Fe] and [O/Fe] abundances are from Carretta et al. (2007, 47 Tuc) and Carretta et al. (2009, NGC 6752)

typical monometallic GC features: light element abundance correlations and some very slight evidence for multiple populations in their photometry (Fig. 1.2).

In this section is a brief overview of the observational properties of these clusters with a particular focus on their carbon, nitrogen, sodium, oxygen and s-process abundances.

1.1.1 47 Tucanæ

Due to its brightness, 47 Tuc has been well studied. At [Fe/H] = −0.7, it is metal-richer than 75 % of all Galactic GCs. Although different papers in the literature have reported a range of different metallicities for the cluster, there is no evidence for any intrinsic spread of the iron content of the stars. Photometrically it has been found to have a split sub-giant branch (SGB) with a range of about 1 mag (Anderson et al. 2009; Piotto et al. 2012). Anderson et al. (2009) also found that the main sequence (MS) had a larger width than would be expected from just photometric errors. These spreads in luminosity could be interpreted as a 0.02–0.03 dex spread in helium abundance (Di Criscienzo et al. 2010; Nataf et al. 2011). In the latter of those works, it was also suggested that the helium-rich population was more centrally concentrated than the stars with the primordial helium abundance.

Like all well-studied Galactic GCs there is a range in the abundances of light elements. On the MS, Briley et al. (2004) observed 115 stars and showed that there was a 1.5 dex range in nitrogen and a 0.7 dex range in carbon. This confirmed previous work which had shown a significant range in the strength of the CN and CH spectral indices (e.g., Harbeck et al. 2003). It was through these indices that these abundance ranges were first discovered. One of the key results was the bimodality of the CN strength of the stars (Cannon et al. 1998). The CN-strong stars are more centrally located, implying from the result of Nataf et al. (2011) that these stars are also helium enhanced.

In the case of the sodium-oxygen anticorrelation, this does not appear to be bimodal, instead having a continuous distribution (Carretta et al. 2009). Sodium is correlated with CN strength on the red giant branch (RGB) (Worley & Cottrell 2012), a result also observed on the MS (Briley et al. 1996). So the stars form two groups: either N- & Na-poor and C- & O-rich; or the converse. The Na-O result of Carretta et al. (2009) is used in Chapter 3 to determine [O/Fe] from [Na/Fe] determined by Worley (2013).

In the cluster NGC 6752 (also studied in this thesis), Norris et al. (1981) found that, while the RGB had many stars with strong CN bands, the AGB was devoid of CN-strong stars. This result was confirmed by Campbell et al. (2010). However little such work has been done on 47 Tuc, though there have been some CN-strong AGB stars observed by Worley & Cottrell (2012).

For this thesis, over 100 GB in 47 Tuc stars were analyzed from spectra taken with AAOmega on the Anglo-Australian Telescope (AAT), and the Robert Stobie Spectrograph (RSS) on the Southern African Large Telescope (SALT).

1.1.2 NGC 6752

NGC 6752 is the most metal-poor of the two monometallic clusters studied for this thesis. It has less than the median metallicity of Galactic GCs, with a metallicity of [Fe/H] = −1.5 (Harris 1996). This metallicity makes its stars similar in iron content to the bulk of the stars in ω Cen ([Fe/H] peak at −1.7 dex, see Fig. 1.6). Chemically the Na-O anticorrelation has been observed for both its unevolved (Carretta et al. 2005) and evolved stars (Yong et al. 2008). This was the first cluster for which the Na-O anticorrelation was observed in unevolved stars, showing that the anticorrelation must be intrinsic to GC stars, rather than either the result of an interior mixing process that would dramatically alter the surface composition on the GB, or from material accreted onto the surface of the stars from other stars (proposed by D'Antona et al. 1983). This process would have been peculiar to the GC environment as the Na-O anticorrelation is not observed in field stars (e.g., Ramírez et al. 2012). The observed ranges of sodium and oxygen in NGC 6752 are typical of GCs. It has been found to have a broadened (but not split) MS (Milone et al. 2010) and RGB (Grundahl et al. 2002; Yong et al. 2008) and shares an extended blue horizontal branch with clusters which have been found to have multiple populations NGC 2808 (Piotto et al. 2007), ω Cen and M54 (Carretta et al. 2010a).

For this thesis, spectra from AAOmega on the AAT of 11 RGB stars in NGC 6752 were analyzed.

1.2 Observational History of ω Cen stars

Together with the monometallic clusters 47 Tuc & NGC 6752, ω Cen was investigated extensively for this thesis. In this section there is a focus on the main evolutionary stages of ω Cen stars: the main sequence (MS), sub-giant branch (SGB), red giant branch (RGB), horizontal branch (HB) and asymptotic giant branch (AGB). They are presented in the order of stellar evolution, which is not the same as the historical order of the observations, which concentrated on the bright GB and HB stars first.

1.2.1 Main sequence

As discussed in Section 1.1.2, the MS of GCs are of great interest as they exhibit the composition of the gas cloud from which they formed. As such any abundance results are not affected by first dredge-up (FDU) or third dredge-up (TDU). Results from the MS of ω Cen have shown that the cluster has multiple populations with very different chemical properties and that these abundances are intrinsic to the stars.

Using the Wide-Field Planetary Camera 2 images from the the Hubble Space Telescope (HST), Bedin et al. (2004) were able to definitively show that the MS of ω Cen is bifurcated, a feature that had been hinted at by Anderson (1997, 2002, 2003). This was followed by a third MS found by Villanova et al. (2007). Between these two papers was the counter-intuitive result that the blue main sequence (bMS) was in fact metal-richer than the red main sequence (rMS) (Piotto et al. 2005). All else being equal, metal-poorer stars are hotter (and therefore bluer) than metal-richer stars. The explanation for them being swapped on the MS is that the stars of the bMS are helium enhanced relative to the stars of the rMS (Norris 2004; King et al. 2012). There are two effects that explain these features. An increased helium abundance makes a star hotter and brighter, changing the location of the zero-age main sequence on the CMD, which is why the bMS is metal-richer than the rMS. Because the stars are hotter, they will evolve off the MS sooner than a star with a lower helium abundance, and in the process cross-over the rMS. A similar feature is observed in the monometallic cluster NGC 2808 (Piotto et al. 2007), meaning that multiple MSs are not unique to multimetallic clusters.

Abundances of carbon and nitrogen for MS stars were determined by Stanford et al. (2010). They found a significant spread in the CH band strength for all metallicity ranges ([Fe/H] < -1.5, $-1.5 >$ [Fe/H] > -1.1, and [Fe/H] ≥ -1.1). This was not observed in the other GCs they compared to: NGC 6397, NGC 6752 and 47 Tuc. They could not be as definitive with nitrogen due to low sensitivity of the index in faint stars to changes in [N/Fe]. Using spectrum synthesis they measured abundances of a small number of stars directlyOne feature they observed was a sub-solar [C/Fe] for their [Fe/H] ≥ -1.1 stars, while the metal-poorer groups were all super-solar in [C/Fe]. They were unfortunately not sensitive to low carbon in their metal-poor stars. It would be highly desirable to extend the samples of MS stars, with their primordial surface compositions. It is important to understand how the different main sequences (MSs) link through to the RGBs through the sub-giant branches (SGBs).

1.2.2 Sub-giant branch

The SGB region has provided evidence for intrinsic abundance ranges in all GCs, as like MS stars, they have not undergone mixing processes that would change their surface composition. The existence of the anomalous RGB-a (Section 1.2.3 and Table 1.2) was first noted by Pancino et al. (2000) and this was connected to the SGB by Ferraro et al. (2004). They were able to trace it to at least $V = 18.4$. Further work by Villanova et al. (2007) identified that there were four distinct SGBs and made age estimations of these branches (which are controversial, as will be discussed in Section 6.2). Pancino et al. (2011b) investigated six SGB stars with UVES at the Very Large Telescope, three of which were found on what they called the "lower" (fainter in V) SGB and three on the "upper" (brighter in V). Of interest to this thesis are the abundances that they determined for [C/Fe], [N/Fe], [Ba/Fe] and [Fe/H]. Figures 1.3 and 1.4 shows the abundances that they found in comparison to abundances found on the RGB by other researchers (Norris & Da Costa 1995; Stanford et al. 2010; Villanova et al. 2010; Marino et al. 2011a, 2012). Whether they were upper or lower SGB stars does not appear to have been correlated with their [N/Fe] abundance, though the upper SGB stars are all found at [C/Fe] ~ 0.1. The very low metallicities they found for their upper SGB stars is metal poorer than that of the bulk of the main population (MP) ([Fe/H] ~ -1.7). They suggest these stars are members of a very metal-poor (VMP) population of stars. These are either remnants of the first generation of stars, or the remnant of stars that formed a hypothesized dwarf galaxy parent of ω Cen (see Section 6.3). The [Ba/Fe]

Table 1.2 — Metallicity groups of ω Cen per Sollima et al. (2005) and Johnson & Pilachowski (2010). These groupings are sometimes used to describe the different populations of stars in ω Cen.

Group name	[Fe/H] range
MP	[Fe/H] ≤ −1.6
MInt1	−1.6 < [Fe/H] ≤ −1.3
MInt2+3	−1.3 < [Fe/H] ≤ −0.9
RGB-a	[Fe/H] > −0.9

abundances for the metal-richer stars in their sample show that any s-process enhancements are definitely intrinsic to the material that formed this generation of stars, and not a consequence of any mixing processes on the RGB, since they are as enhanced in barium as the RGB stars of the same metallicity.

Sollima et al. (2005) observed 256 SGB stars with $R \sim 6500$ to determine their metallicity via the infrared calcium triplet, selecting stars that had been photometrically identified as belonging to one of the four SGB branches (they selected equal numbers of stars on each branch which means that this is a biased sample). They determined four [Fe/H] bands: −1.7, −1.4, −1.1 and −0.6, confirming that the branches observed on the RGB map onto the SGB. Norris et al. (1997) found that metal-rich RGB-a to be "dynamically cooler" than the metal-poor stars. However Sollima et al. (2005) found that their metal-rich stars had the same σ_v as the metal-poor stars, with the intermediate metallicity populations being 2–3 km s^{-1} less dispersed.

The SGB-a contains the metal-rich SGB stars and is about a magnitude fainter than the other SGBs and merges with the MS at a fainter magnitude than the main sequence turn-offs (MSTOs) of the other populations. Pancino et al. (2011a) determined the α-element abundance for this region. It had been found that the RGB-a stars had a lower [α/Fe] than the metal-poorer stars (Pancino et al. 2002; Origlia et al. 2003), implying a contribution of SNe 1A. But these studies were in contradiction to Johnson & Pilachowski (2010) who looked at some of the same stars and found higher [α/Fe]. There is still a trend where [Ca/Fe] raises with iron until −1.2 and then drops off gently, which could mean than SNe 1A could still be invoked for the metal-rich population but does not explain why the most metal-poor stars are also low in calcium. For barium, Pancino et al. (2011a) found that [Ba/Fe] > 0.5 for their sample of [Fe/H] > −1.0 stars, which is consistent with results for the RGB.

The "combed" structure of the SGB and RGB seems to be scrambled in some way. In order to understand them, we require many stars observed at high resolution. Currently there are few stars at high resolution and many at low resolution. The problem is that the structure of the RGB is related to the metallicity of the star, while the structure of the SGB is related to the age, C, N, O and He of the stars. No SGB stars were analyzed in this thesis.

1.2.3 Red giant branch

It is on the RGB of the cluster that the most research has taken place. As mentioned, this has the added complication that abundances can change due to mixing[4] (I. Iben J. 1964). However AGB and RGB stars are the brightest stars in the cluster, especially important for high resolution spectroscopy and efficient use of telescope time.

Unlike the subtle photometric evidence for multiple populations in some monometallic clusters, the CMD of ω Cen is remarkable (Fig. 1.5). With high precision photometry it is possible to observe multiple RGBs. These multiple branches were first (independently) discovered by Y.-W. Lee et al. (1999) and Pancino et al. (2000). Somehow the three MSs described in Section 1.2.1, split into at least five SGBs and RGBs. As mentioned in Section 1.2.2, there is an anomalously red RGB known as the RGB-a (Pancino et al. 2000). This branch has been found to contain the most metal-rich (Pancino et al. 2002; Sollima et al. 2005) and sodium-rich (Johnson & Pilachowski 2010) stars in the cluster.

Most of the GB stars are found to be around [Fe/H] ~ −1.75 (Norris & Da Costa 1995; Stanford et al. 2006; Johnson & Pilachowski 2010; Marino et al. 2011a). There is a second peak in the metallicity distribution [Fe/H] ~ −1.50, with evidence for further peaks at −1.15, −1.05 and −0.75 (Fig. 1.6) (Johnson & Pilachowski 2010). These peaks correspond to different GBs that have been observed photometrically (Rey et al. 2004).

[4] e.g., Merrill (1952) who identified technetium, an element with no stable isotopes, in field RGB stars, showing it must be produced in the star and mixed to the surface in a cosmologically short time.

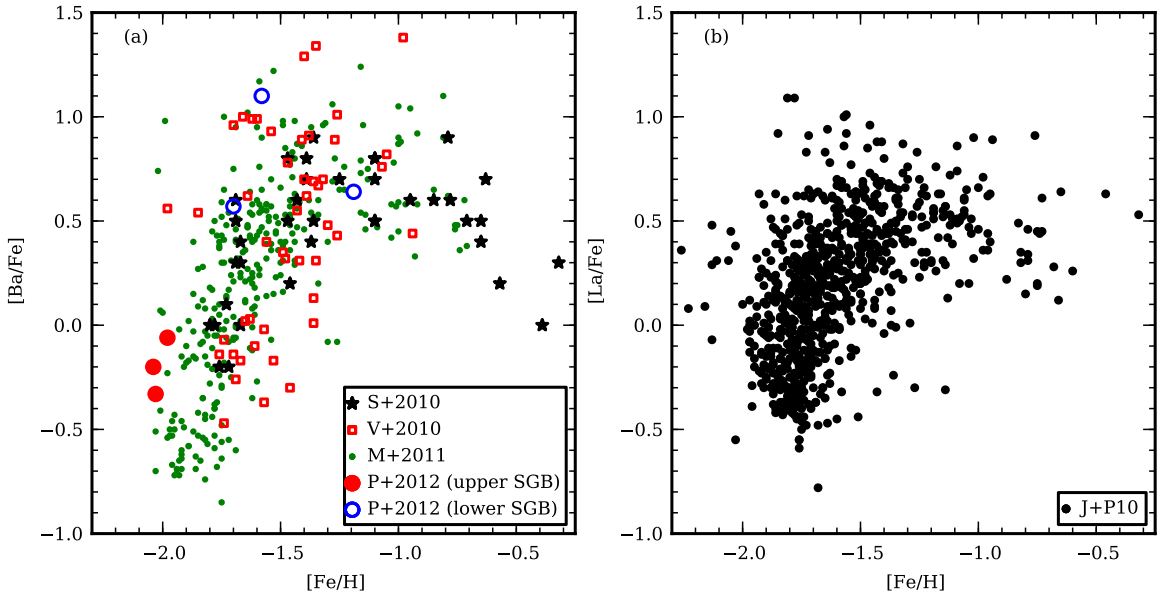

Figure 1.3 — Abundances for s-process elements of SGB and RGB stars in ω Cen. (a) [Ba/Fe] determined for the RGB stars by Stanford et al. (2010, S+2010), Villanova et al. (2010, V+2010), and Marino et al. (2011a, M+2011) for ω Cen stars. Also plotted are six SGB stars from Pancino et al. (2011b, P+2011). The large red circles are the "upper" SGB stars, which were all very metal-poor (VMP), and the large blue filled circles are the "lower" SGB stars. (b) [La/Fe] (another s-process element) from Johnson & Pilachowski (2010). All studies have found a rapid increase of s-process elemental abundance with metallicity and then a flattening off at [Fe/H] ~ −1.5. The results of Stanford et al. (2010) and Johnson & Pilachowski (2010), which had the most metal-rich stars, suggest that the [s-process/Fe] could decrease at the highest metallicities.

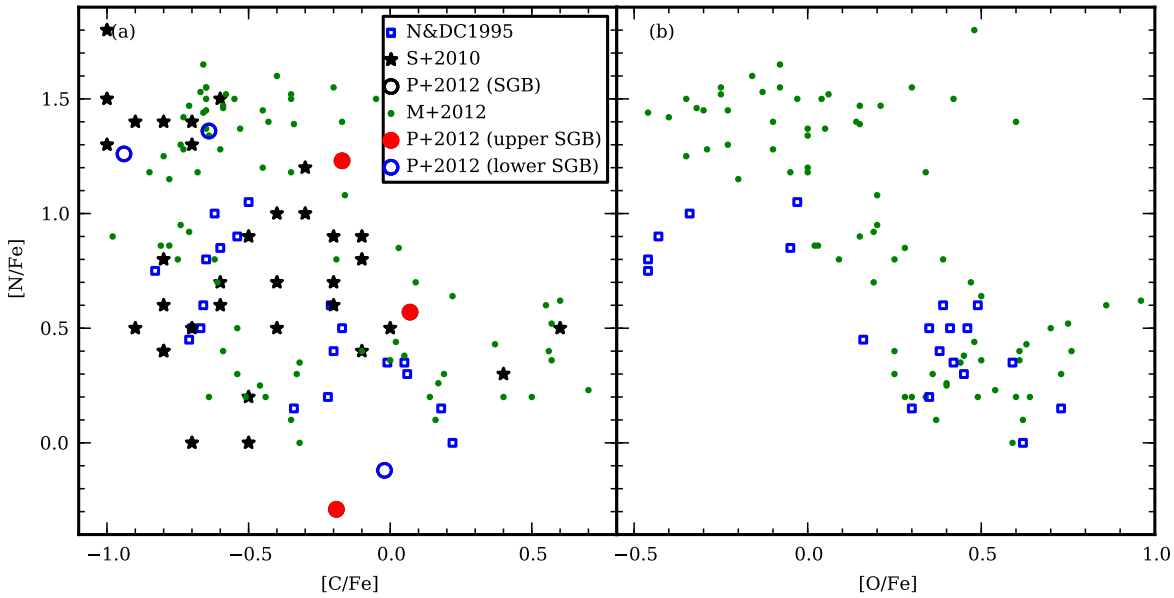

Figure 1.4 — (a) The [N/Fe] & [C/Fe] and (b) [N/Fe] & [O/Fe] abundances for the RGB as determined by Norris & Da Costa (1995, N&DC1995), Stanford et al. (2010, S+2010; no [O/Fe]) and Marino et al. (2012, M+2012). Also plotted are six SGB stars of Pancino et al. (2011b, P+2011) for comparison of evolved and unevolved stars.

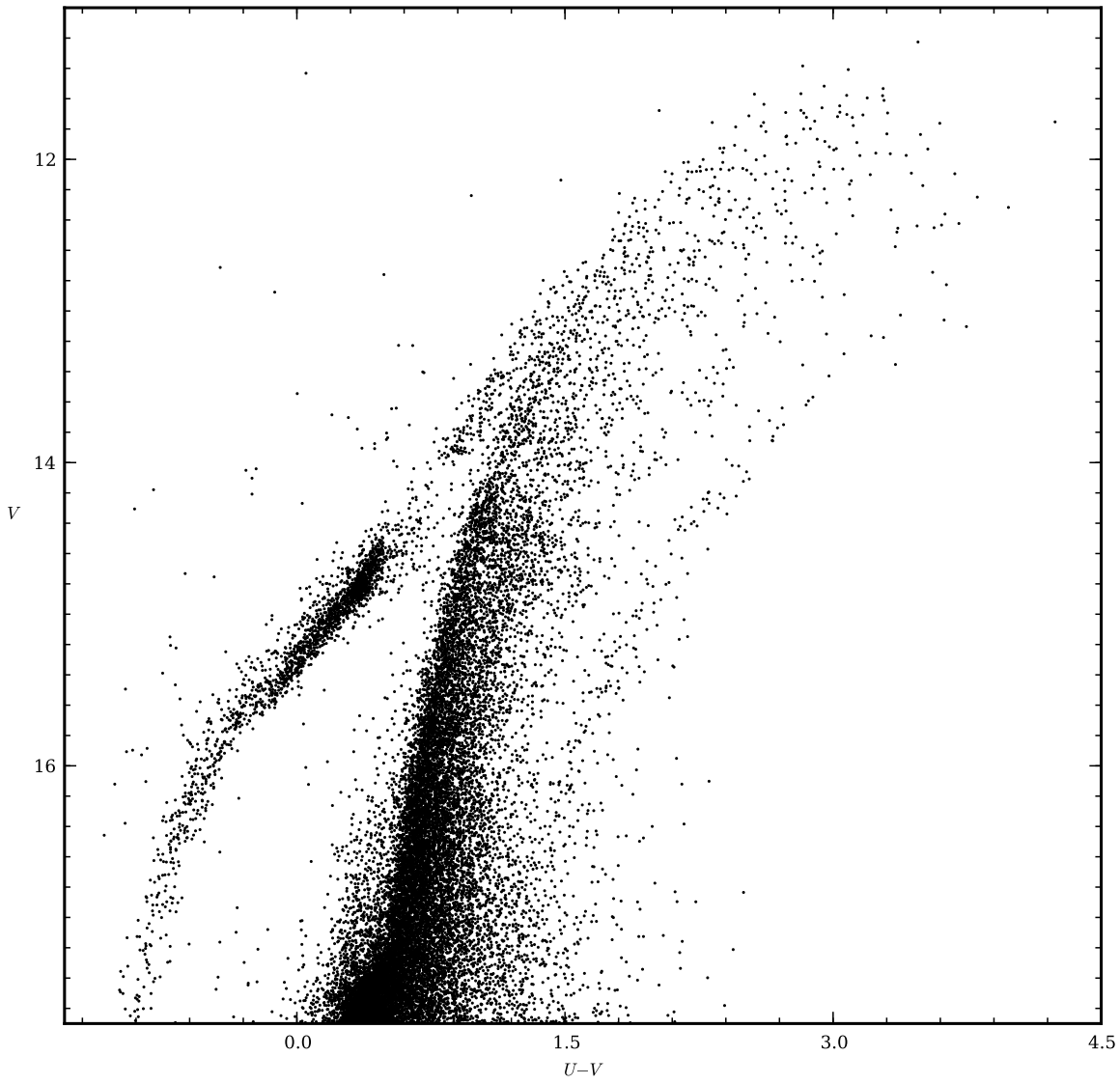

Figure 1.5 — U-($U-V$) CMD of ω Cen from about the MSTO to the top of the GB, showing the multiple GBs and the extended HB. (Bellini et al. 2009a).

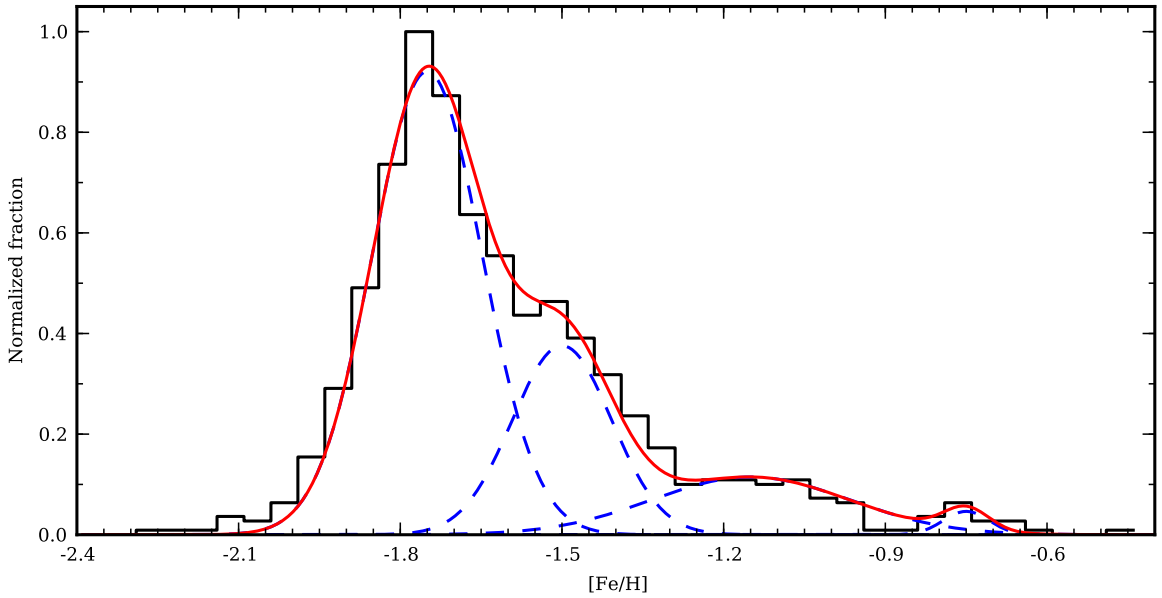

Figure 1.6 — Metallicity histogram from Johnson & Pilachowski (2010) of ω Cen, with a solid red line showing the best fitting result of adding together four Gaussians with $\mu_{[Fe/H]}$ of −1.75, −1.50, −1.15 and −0.75 (dashed blue curves). It does not include the [Fe/H] = −1.05 peak found by Johnson & Pilachowski (2010) for sake of clarity.

ω Cen differs from most monometallic clusters not only in its metallicity range but in its neutron-capture element abundances. Most monometallic clusters show no variation in their s- or r-process abundances[5] (e.g., 47 Tuc as observed by Worley & Cottrell 2012), while within ω Cen there is a positive correlation of s-process abundances with metallicity (Fig. 1.3). In fact there is over a 1 dex increase in the abundance of [La/Fe] and [Ba/Fe] between [Fe/H] = −1.9 and −1.5. Barium abundances from Villanova et al. (2010) have a 1.5 dex scatter at all [Fe/H]. This was also found for the light s-process elements, yttrium and zirconium. Villanova et al. (2010) reported evidence for bimodality in the [Ba/Fe] to [Fe/H] distribution. For stars with [Fe/H] < −1.5 there were two populations: [Ba/Fe] ~ +1.0 or ~ −0.2. This result does not agree with the larger samples of Johnson & Pilachowski (2010) and Marino et al. (2011a) who found no such bimodality in the s-process elements. Instead there was a continuous trend of increasing [Ba/Fe] or [La/Fe] with increasing [Fe/H], at least up to [Fe/H] = −1.5. Above this metallicity there is a flattening or even turning over of [Ba/Fe] with respect to [Fe/H] (Stanford et al. 2010).

The sodium-oxygen anticorrelation of ω Cen is much more complex that any observed for other GCs (Fig. 1.7). Per the results of Johnson & Pilachowski (2010), there are three regions: an oxygen-rich region with Δ[Na/Fe] ~ 1 dex; a sodium-rich region with Δ[O/Fe] ~ 0.5 dex; and a sodium-oxygen correlated region. The first two regions appear like the sodium-oxygen anticorrelation that is observed in other GCs (e.g., Fig. 1.2), but the correlated region has not been observed in other globular clusters. These stars with the correlated sodium and oxygen have been found to be metal rich (Johnson & Pilachowski 2010), which would mean that its stars correspond to those identified photometrically as the RGB-a. Another aspect of the oxygen abundance of ω Cen is that Johnson & Pilachowski (2010) found that there were no oxygen-poor stars at large radial distances in the cluster. This would suggest that these stars were formed preferentially close to the core, consistent with some formation theories of the cluster, where oxygen-rich ICM settled to the core.

D'Orazi et al. (2011) measured Pb and other neutron capture elements of 12 RGB stars. Their interest in Pb was that it can only be produced through the "main" component of the s-process which occurs in 1–3 $M_\odot$ AGB stars (Section 1.3). Detection of significant enhancements of lead would suggest that the weak component of the s-process cannot be invoked to explain the production of the majority of s-process elements in ω Cen. Their

[5] One monometallic cluster with a neutron-capture spread is M15 ($\Delta \log \varepsilon(\mathrm{Ba}) = 0.48$; Sobeck et al. 2011). See also Chapter 6 for further discussion of s-process element abundance ranges in GCs.

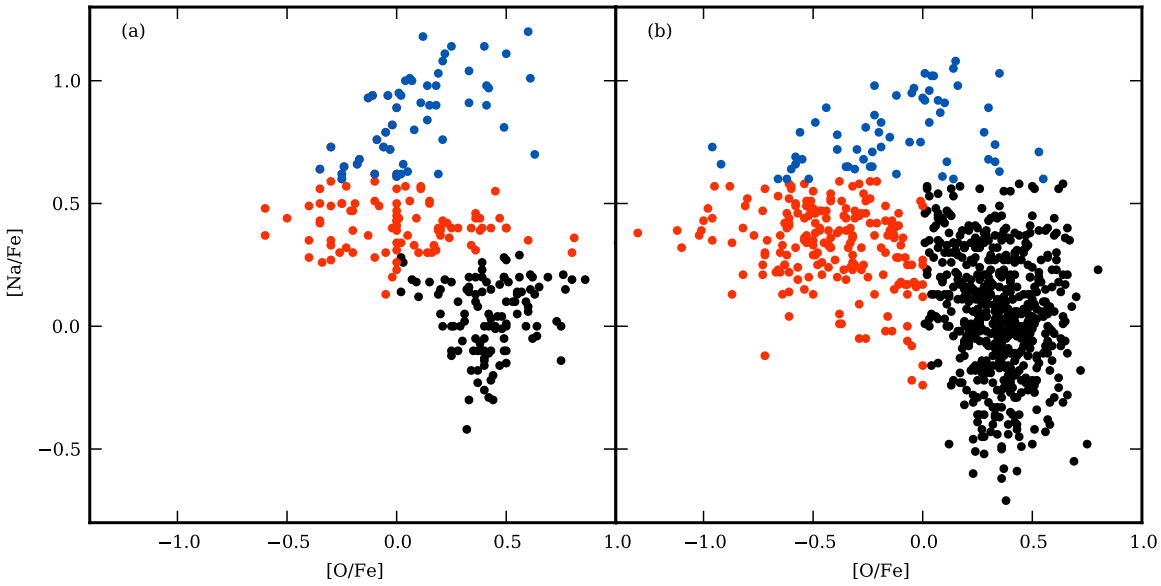

Figure 1.7 — The sodium-oxygen (anti)correlation from (a) Marino et al. (2011a), and (b) Johnson & Pilachowski (2010) for stars in ω Cen. The colours are used to define the three general regions discussed in the text, namely the oxygen-rich group (black), the sodium rich group (red) and the Na-O correlated groups (blue).

[Pb/Fe] abundances were in agreement with the main component being the primary source, instead of the "weak" component that occurs in higher mass AGB stars and therefore could resolve the conflicting time frames that come from the Na-O anticorrelation and the s-process enhancement (see Section 6.2).

There are a number of small studies of the carbon and nitrogen abundances in ω Cen (Fig. 1.4). Brown & Wallerstein (1993) analyzed six stars finding $-0.45 <$ [C/Fe] $< +0.1$ and $0.75 <$ [N/Fe] < 1.25. These stars had a large range of metallicities but did not include any stars with [Fe/H] > -1.25. Norris & Da Costa (1995) had a larger sample of 40 (biased) stars for which they determined a larger range for both carbon and nitrogen than seen by Brown & Wallerstein (1993). They found that there was a floor to their [C/Fe] values at ~ -0.8, a feature that they pointed out was not due to their abundance analysis method. Their most carbon-rich objects were roughly solar in their carbon abundance.

The most recent study and at the highest resolution ($R\sim$ 20,000) is Marino et al. (2012). They observed 77 GB stars and found a correlation between the overall C+N+O abundance and the metallicity. Using the sodium-oxygen anticorrelation, they were able to distinguish what they referred to as first- and second-generation stars. Their results show a clear bifurcation between CN-weak and CN-strong stars (Fig. 1.4). The nitrogen-rich stars are grouped together with little spread in carbon. The CN-weak stars show a range of [C/Fe] from −0.5 to 0.5. They found many more stars that were more carbon rich than compared to what had been previously observed on the RGB.

D'Orazi et al. (2011) (who also measured Pb) determined [C/Fe] and [N/Fe]. They had only one C-rich star in their sample. Looking at the ratio of ''heavy''-s (hs) process elements (i.e., Ba, La, Nd) to ''light''-s (ls) process elements (i.e., Y, Zr), this star is peculiar. It sits outside their trend of [hs/ls] to [Fe/H] and [Pb/ls] to [hs/ls]. With only one star it is not possible to draw any real conclusions but it did have a much lower [hs/ls] for its [Pb/ls] than they found for their C-poor stars.

One of the most important pieces in the puzzle of ω Cen is the helium content of the stars. Norris (2004) was the first to propose that the split MS could be the result of differing helium abundances in the stars. This has been confirmed, but only a small sample of GB stars have had their helium spectral line equivalent widths measured, which limits the conclusions that can be drawn from this. Dupree et al. (2011) found that of their twelve GB stars, five had helium lines present in their spectra. The average [Na/Fe] abundance for those stars with no helium present was [Na/Fe] $= 0.0 \pm 0.3$, while for stars with helium present it was 0.4 ± 0.1. Further work is needed to increase the

number of stars with helium inferred, so that the He abundances can be correlated with other elemental abundances to aid the identification of different populations of stars. However, the Dupree et al. (2011) result would suggest that the it is the sodium-rich stars which are the brethren of the stars on the bMS.

This thesis considers the stars as single entities but due to the sheer number of stars in ω Cen there will be a large number of binaries in the cluster. Its low central density means that many that formed primordially will have survived to the present day (Davies 1997; Ivanova et al. 2006). With the complex CMD, it is not possible to search for binaries by assuming they will be 0.7 mag brighter (twice the flux) that the main RGB. One method of searching for them is to use X-ray imaging. Chromospherically active stars may be the result of enhanced coronal activity due to tidal locking. Cool et al. (2013) used the Advanced Camera for Surveys on HST to look for optical counterparts to X-ray sources identified by the Chandra X-ray Observatory. In all there were 109 X-ray sources; 59 had identifiable optical counterparts and about 40 of these were likely cluster members. Of interest to this thesis is that eight of their candidate counterparts were found on the RGB-a and SGB-a, while 14 were on the "main" RGB. Since there are about 10 times more stars on the main RGB than the RGB-a, this would suggest that X-ray sources are 5–15 times more likely to be found on the RGB-a. Unfortunately none of their stars were observed by van Loon et al. (2007) so it is not possible to confirm their metallicity. That there are potentially more binaries in the metal-rich population does not correspond to the observations of field stars, where there is no correlation between metallicity and binary fraction. It is also opposite to the work of Vesperini et al. (2011) who suggested that the first generation would have more binaries than the second generation in GCs. If these stars are in fact not high metallicity, then they could be examples of "red stragglers" (Albrow et al. 2001).

1.2.4 Horizontal branch

The stars visible on the HB of ω Cen are old, low-mass stars that are undergoing core helium burning. In GCs, there is the so-called "second parameter problem", where the morphology of the HBs of GCs depends not only on the [Fe/H] of the cluster but also on some other second (or third parameter) parameter (Gratton et al. 2010). GCs of the same metallicity can have very different HB morphologies (e.g., NGC 288 and NGC 362; Shetrone & Keane 2000). With the range of metallicities observed in ω Cen it is currently not possible to disentangle the various populations of stars present on the HB and how this would affect the morphology of the HB. First, the HB stars are very hot compared to the GB, meaning their metal lines become very weak, requiring very high-resolution spectroscopy. Second, diffusion processes completely alter the surface composition of HB stars hotter than ~ 11,500 K (Michaud et al. 1983, 2008). One element that may still be used to understand the potential population membership is helium. As observed for MS stars, at least one of the populations of stars in ω Cen is greatly enhanced in helium. It should be the bluest HB stars that would be the most He-rich stars (Y.-W. Lee et al. 2005).

Moni Bidin et al. (2011) acquired spectra of 116 HB stars with $R \sim 1600$ and used the Balmer and He lines to determine $T_{\rm eff}$, $\log g$ and the metallicity. They found that the stars were consistent with a $Y = 0.33$ model (compared to the canonical $Y = 0.23$). However they noted that their calculated masses were very low, on average smaller than the mass required to ignite helium in the core ($\sim 0.45\,M_\odot$). So it is not completely possible to draw any absolute conclusions, though these HB stars of ω Cen are definitely different from those observed in other clusters.

Like other massive GCs, ω Cen has a blue hook on its HB. This is a population of stars that are even hotter and bluer than the usual end of the HB in less massive clusters. Moni Bidin et al. (2012) measured the helium abundance of 100 HB stars including the blue hook stars. They found about 15 % of their extreme horizontal branch ($T_{\rm eff} \geq 20{,}000$ K) stars had a surface helium abundance ~ 1 dex lower than the rest of the sample, with the same feature also observed in NGC 2419 (Di Criscienzo et al. 2011). Moni Bidin et al. (2012) note that due to the measurement errors they cannot tell if this is a bimodal or continuous distribution. For the blue hook stars, they found a similar fraction of helium deficient stars, with the suggested cause of them being post-HB stars, which are evolving directly to the white dwarf phase, without first ascending the AGB.

1.2.5 Asymptotic Giant Branch

In a monometallic GC, to the first-order, there is one isochrone through the CMD[6]. This makes the identification of AGB stars simple, apart from at the brightest magnitudes where the AGB and the RGB merge. However, in

[6] With the Na-O anticorrelation showing there have been multiple star formation events in monometallic GCs, there will be an age spread between the stars, which would result in difference paths on the CMD. However these abundance and age differences do not give rise to large differences in the shape of the GB on the CMD for these clusters.

the case of ω Cen it is not possible to identify all of the AGB stars, as the AGBs of the most metal-rich RGBs will overlap with the most metal-poor RGBs (for the LMC, estimates are that 30 % of ''RGB'' stars are actually AGB stars; Cole et al. 2004). This means that studies looking at the RGB of ω Cen are almost certainly also investigating AGB stars as well.

As mentioned in Section 1.1.2, the AGB of NGC 6752 seems to lack CN-strong stars. Similar results have been found for other clusters, i.e., M13 lacks sodium-rich stars on its AGB, which are abundant on the RGB (Pilachowski et al. 1996). There are few papers that have looked at samples of AGB stars in ω Cen. Recently there was Simpson et al. (2012, candidate is the lead author), where 55 AGB stars were identified in the van Loon et al. (2007) spectral library and they found them to have low-CN index strengths compared to the rest of the stars in the cluster. Consistent with the idea that the visible AGB of ω Cen is from the metal-poor population, Hilker & Richtler (2000) found over 100 stars that they classified as AGB stars, which had a peak metallicity of [Fe/H] = −1.7.

The AGB results of Simpson et al. (2012) are discussed in this thesis and expanded with [C/Fe] and [N/Fe] abundances for half the AGB stars identified photometrically as belonging to the AGB (Section 6.4).

1.3 Stellar Nucleosynthesis

Along with the observational results of 47 Tuc, NGC 6752 and ω Cen, it is important to understand the processes through which these different chemical elements (Fig. 1.8) are produced in stars. This section outlines the life stages of stars and how the elements of importance to this thesis are synthesized.

Only the four lightest elements (H, He, Li, Be) were produced in any extant quantity in the Big Bang. The rest of the elements were, and continue to be, synthesized in the interiors of stars, through the fusion of charged nuclei, the addition of neutrons to nuclei, or the disintegration of larger nuclei. The previous research in this area was reviewed and collated in the landmark paper of Burbidge et al. (1957) who outlined eight different processes through which most of the elements could be produced. In terms of this thesis, the most important processes are hydrogen burning, α-process, and the s- and r-processes. Their model is accepted today with some modifications and improvements, with further reviews by Trimble (1975), Wallerstein et al. (1997), and Iliadis (2007).

The beginning, and majority, of a star's life fusing charged nuclei is spent on the MS. For the stars visible on the MS of GCs today, all are less than a solar mass, meaning they will have lifetimes of the order of 10^{10} years. The most massive stars in a cluster ($> 25\,M_{\odot}$) would have had MS lives of $< 10^{6}$ years (the MS lifetime is roughly proportional to the ¾th power of the stellar mass). The MS is the stage of a star's life where it is burning hydrogen into helium, either predominantly through the pp-chain or the CNO cycle. For the pp-chain, which takes place in stars with masses less than about $1.5\,M_{\odot}$, the main process, known as ppl, is $p(p,e^{+})^{2}H(p,\gamma)^{3}He(^{3}He,2p)^{4}He$. The ppl chain accounts for about 90 % of the Sun's energy production. For more massive stars, the predominant process is the CNO cycle, which uses isotopes of carbon, nitrogen, oxygen and fluorine as catalysts to convert four protons in ^{4}He. The classical version of this CNO cycle is $^{12}C(p,\gamma)^{13}N(e^{+},\nu)^{13}C(p,\gamma)^{14}N(p,\gamma)^{15}O(e^{+},\nu)^{15}N(p,^{12}C)^{4}He$. Certain steps of the cycle, and reactions with ^{13}N before it can decay, create characteristic signatures in isotopic ratios. For instance, during first dredge-up (FDU) on the RGB, material that is rich in ^{13}C (from $^{12}C(p,\gamma)^{13}N(e^{+},\nu)^{13}C$) is brought to the surface. Measurement of the relative abundances of different elements and isotopes can help us to understand the material from which the stars formed: ICM formed from just the stellar ejecta of previous stars in the cluster; the ICM material mixing with the ISM; or just pure ISM material.

As the helium abundance of the core increases, the hydrogen burning continues in a shell surrounding the core. The core contracts to retain hydrostatic equilibrium, increasing its temperature, and therefore increasing the hydrogen burning rate. This moves the star off the MS and onto the SGB. At the point when the star's envelope becomes fully convective, it becomes an RGB star. Once the core of the star reaches $T \sim 0.1$ GK, it begins converting helium to carbon via the triple-α process, $^{4}He(^{4}He)^{8}Be(^{4}He,\gamma)^{12}C$. At the time of Burbidge et al. (1957), it was thought that this addition of α-particles would continue onwards, forming elements such as ^{20}Ne and ^{24}Mg, but this is now known not to be the case (Wallerstein et al. 1997). The rate of α-particle captures occurs too slowly at the temperatures and densities present, and the process will terminate at ^{16}O.

Elements heavier than this are formed through carbon, neon, oxygen, and silicon burning in the core. For solar mass stars, such as those observed today in ω Cen, the temperatures and densities in the core are never high enough for these burning processes to take place. Instead their degenerate helium core undergoes what is known as a helium core flash, when it suddenly overcomes the degeneracy that did not allow it to expand as its temperature increased. This extinguishes the hydrogen shell that has been providing the luminosity at the stellar surface and the

Figure 1.8 — Periodic table of the elements (updated version of http://www.texample.net/tikz/examples/periodic-table-of-chemical-elements/)

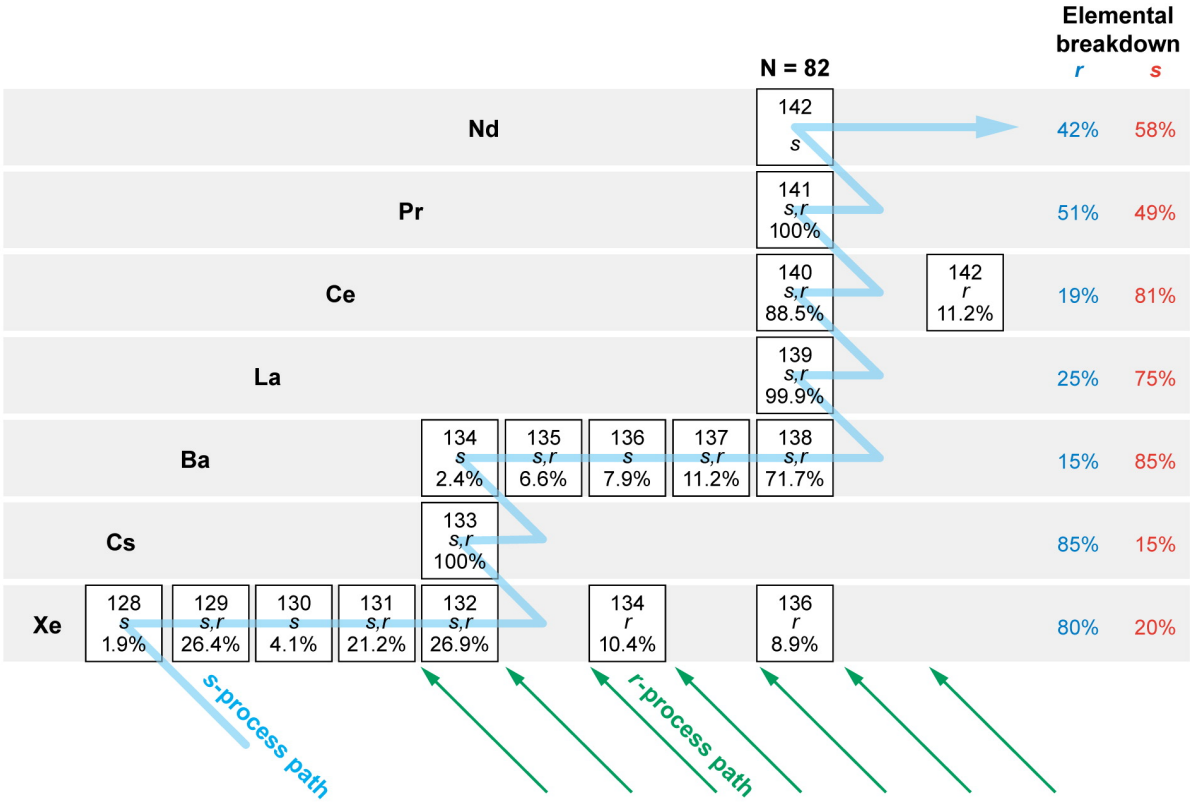

Sneden C, et al. 2008.
Annu. Rev. Astron. Astrophys. 46:241–88

Figure 1.9 — Reproduction with permission of Figure 2 of Sneden et al. (2008). Their caption reads "A portion of the nuclear chart showing elements Xe to Pr and the production of each isotope by the p-, s-, and r-processes. The s-process (light blue line) operates close to stability—the black boxes show stable nuclei—whereas the r-process is formed out of very neutron-rich (unstable) nuclei that β decay back (green lines) to stability. We also add one isotope of Nd to this chart to indicate the next steps in the s-process chain, but do not indicate the other Nd isotopes. Listed to the outside right are the total percentage breakdowns by process for each element."

star moves onto the HB, where it burns the now non-degenerate helium in its core. The hydrogen shell surrounding it continues to burn through the CNO cycle. Once the helium core is exhausted, it is left as a CO core with a helium shell and a hydrogen envelope, which places it on the AGB. The importance of these stars is discussed later.

In stars more massive than the Sun, further core burning can take place. Carbon burning takes three principle forms: ^{12}C(^{12}C,^{4}He)^{20}Ne, ^{12}C(^{12}C, p)^{23}Na, and ^{12}C(^{12}C, n)^{23}Mg. Once carbon is exhausted in the core, neon is photodisintegrated and the resultant α particles combine with ^{20}Ne to form ^{24}Mg. Oxygen is the next element to undergo core burning, producing primarily ^{28}Si, ^{31}P and ^{31}S but also all elements up to mass number 40 (Ar, K, Ca). Together, neon and oxygen burning are the modern equivalent of the α-process of Burbidge et al. (1957). The final exothermic reaction is silicon burning, where photodisintegration frees α-particles, protons and neutrons from nuclei in the core. These free particles combine with elements to form the nuclei with mass numbers A ~ 40–56. These stars were extremely important in the chemical evolution history of ω Cen, as they produced the core-collapse SNe that polluted the ICM with Fe-rich material. With ω Cen's large metallicity range, not seen in most GCs, something different to monometallic clusters must have happened in the cluster to keep this material inside the gravitational potential of the cluster, so that the iron-richer generations could form.

Very few isotopes heavier than ^{56}Ni can be produced by charged-particle reactions. This leaves neutron-capture as the primary method to produce elements heavier than the iron peak of the nuclear binding-energy diagram

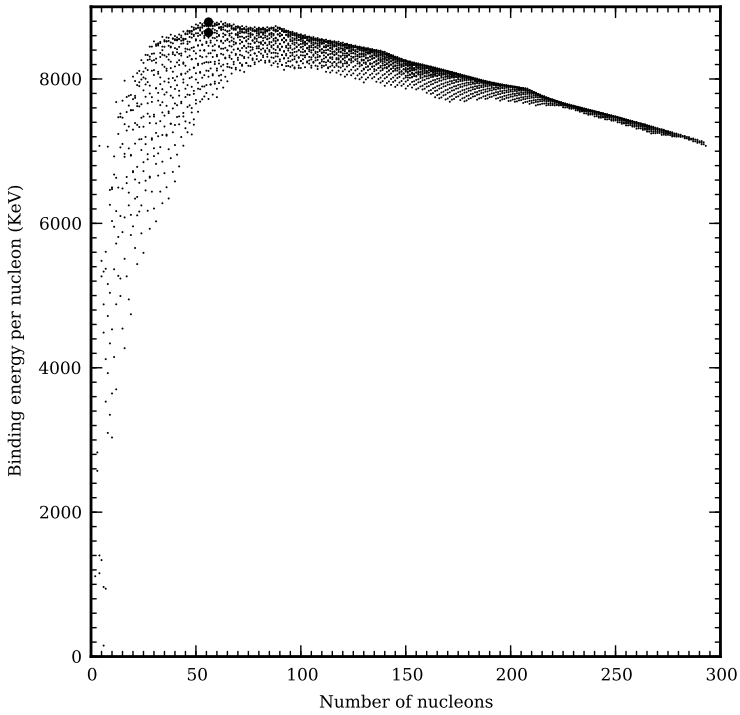

Figure 1.10 — Curve of binding energy per nucleon (Audi et al. 2003). The two large dots mark ^{56}Ni and ^{56}Fe (largest and smallest binding energy respectively of the two indicated isotopes). ^{56}Ni is the isotope with the highest binding energy per nucleon and ^{56}Fe is the isotope that is commonly regarded end of the charged nuclei fusion.

(Fig. 1.10). Burbidge et al. (1957) identified and named the two neutron-capture processes: the s(low)-process and the r(apid)-process. During the s-process, an isotope (i.e., ^{134}Ba) is exposed to a flux of neutrons, resulting in the following nuclear reactions (illustrated in Fig. 1.9): ^{134}Ba(n,γ)^{135}Ba(n,γ)^{136}Ba(n,γ)^{137}Ba(n,γ)^{138}Ba(n,γ)^{139}Ba. This addition of neutrons cannot continue as ^{139}Ba is radioactive with a half-life of $t_{½}$ = 83 min (National Nuclear Data Center 2013). The s-process is slow in the sense that the time between neutron captures by a given nucleus are long enough that the nucleus has time to β-decay if it is unstable. It is estimated that the mean neutron-capture rate is once every 10 years for a given nucleus during the s-process. So ^{139}Ba decays: ^{139}Ba(e$^+$,ν)^{139}La. The resulting nucleus of ^{139}La is stable and the addition of neutrons can continue: ^{139}La(n,γ)^{140}La. But ^{140}La is radioactive ($t_{½}$ = 1.7 days; National Nuclear Data Center 2013), so decays via β-decay to ^{140}Ce. This addition of neutrons and β-decay continues along the so-called valley of β-stability: ^{140}Ce(n,γ)^{141}Ce(e$^+$,ν)^{141}Pr(n,γ)^{142}Pr(e$^+$,ν)^{142}Nd.... The termination of the s-process occurs at ^{209}Bi[7]. This is the heaviest isotope with an extant amount that is produced via the s-process. Heavier isotopes are not possible as ^{210}Bi has a half-life of $t_{½}$ = 5.012 d, so it proceeds, ^{209}Bi(n,γ)^{210}Bi(e$^+$,ν)^{210}Po(α)^{206}Pb.

There is not a single path for the creation of elements through the s-process. This is because some isotopes have half-lives close to the average capture rate. For example ^{147}Pm has a half-life of 2.6 years (National Nuclear Data Center 2013). These longer-lived isotopes cause 15–20 significant branches in the path through the nuclides (Wallerstein et al. 1997).

Conversely, the r-process occurs in an environment where the neutron flux is so large that most nuclei do not have any time to decay before another neutron is captured (~ 10,000 times per second). The addition of neutrons continues until photodisintegration and/or β-decay stop the nucleus from growing any larger. The nucleus decays when the neutron flux decreases, arriving at a stable (or long-lived) isotope. These isotopes are important as they

[7] It was once thought that this was a stable isotope but is now known to have a half-life of ~ 10^{19} years (de Marcillac et al. 2003), leaving ^{208}Pb as the heaviest stable isotope.

Table 1.3 — Stable and long-lived isotopes of barium are produced by three different processes, though the s-process is dominant in terms of the overall fraction. Isotopic percentages from Asplund et al. (2009) and s-process percentage from McWilliam (1998).

Mass number	Isotopic fraction (%)	Production process
130	0.106	p
132	0.101	p
134	2.417	s
135	6.592	s (60 %), r
136	7.854	s
137	11.232	s (68 %), r
138	71.698	s (80 %), r

shield other isotopes from the r-process, leaving them as purely s-process (or p-process elements[8]). For instance ^{136}Xe is formed purely via the r-process and with a half-life of $t_{½} \sim 10^{21}$ years (National Nuclear Data Center 2013), shields ^{136}Ba from any r-process production (Fig. 1.9).

With two main processes that can produce heavy elements, it could be difficult to disentangle the different sites where elements are produced. Fortunately, the shielding by stable isotopes, and blocking by unstable isotopes means that some isotopes are produced solely by the s-process while some are produced solely by the r-process (the p-process accounts for only a small proportion of nucleosynthesis). There are also some isotopes that are produced mainly by one of the processes. For example, the neutron-capture element of interest in this thesis, barium, has five stable isotopes and two very long-lived isotopes[9]: ^{130}Ba and ^{132}Ba are produced via the p-process; ^{134}Ba and ^{136}Ba via the s-process; and ^{135}Ba, ^{137}Ba and ^{138}Ba via the s- and r-processes. From the isotopic ratios and the relative production rates from the s- and r-process (Table 1.3), about 80 % of barium is produced by the s-process. With its strong spectral lines, it is good element to use as a s-process tracer in the stellar atmosphere.

The main component of s-process production is thought to take place in the helium shell of low-mass AGB stars. These stars consist of a core of CO or ONe, above which sits a He shell, then an He-rich intershell (by mass 75 % He, 25 % ^{12}C), then an H-rich envelope. Some protons from the envelope are mixed into the intershell, allowing ^{12}C(p,γ)^{13}N(e^{+},ν)^{13}C(p,γ)^{14}N to occur. Some regions become ^{13}C rich and other parts are ^{14}N rich. Hydrogen burning in the H-envelope increases the abundance of He in the intershell, which means the He shell below becomes denser and helium burning can ignite in it, triggering a thermal pulse. This causes the expansion of the He shell outwards, extinguishing the H-envelope burning. After a short while, the He shell stops burning and contracts, allowing the H envelope to return to temperatures at which H burning can resume. This repetition of helium flashes can repeat 10–100 times in a star's life on the AGB. Current theory predicts that above 90 MK, the ^{13}C pocket can be completely destroyed via ^{13}C(α,n)^{16}O, leading to a flux of neutrons. This flux of neutrons can then be captured by iron-peak elements and form heavy elements via the s-process. In addition, during the thermal pulse, the higher temperatures allow ^{14}N(α, γ)^{18}F(e^{+},ν)^{18}O(α, γ)^{22}Ne(α,n)^{25}Mg, giving a second (but smaller) flux of neutrons. This source is important as it occurs at temperatures which cause more branchings to happen. To explain the distribution of s-process elements observed in the solar system, a weak component is required which is attributed to fast rotating massive stars (FRMS). Due to their temperatures, ^{14}N(α, γ)^{18}F(e^{+},ν)^{18}O(α, γ)^{22}Ne occurs rapidly at the beginning of core helium burning, using up all the ^{14}N. At the end of the He core burning phase of the star, ^{22}Ne(α,n)^{25}Mg creates a flux of neutrons.

Along with the neutron flux, the cross-section of the nucleus to neutron absorption plays an important role in the abundance pattern. Ba, La, Nd sit at the "heavy s" (hs) peak and Sr, Y, Zr at the "light s" (ls) peak. These elements have small cross sections to neutrons, so there is a build up of their nuclei. So the abundance of elements beyond the ls and hs peaks is affected by the abundance of seed nuclei more massive than these peaks that existed in the ICM.

[8] The p-process is the nucleosynthetic process that creates isotopes with less neutrons relative to other stable isotopes of the same element. It is thought to occur via the photodisintegration of more massive nuclei, i.e, ^{136}Ce(γ,α)^{132}Ba.

[9] The isotopes ^{130}Ba and ^{132}Ba are "observationally stable" with half-lives of $\sim 10^{21}$ years (Meshik et al. 2001).

In stellar astronomy, almost all physical measurements are sampling light that comes from the top few hundred kilometres of the star[10] (~ 0.01 % of the radius). The rest of the interior is obscured. As a result, the abundances that are determined are only for the top layer of the star. We are not able to determine the abundances of the stellar interior, where nucleosynthesis is occurring. So it is only during mixing processes that we can see the result of nucleosynthesis, when new nuclei are brought to the surface. These dredge-up events occur when a nuclear burning event ends, resulting in the core contracting and the envelope expanding. There are up to four major dredge-up events in a star's life. In the stars observed in GCs only the first dredge-up (FDU) and third dredge-up (TDU) will occur.

FDU occurs at the end of core hydrogen burning as the helium core contracts and heats up. This causes the H shell to expand and cool, lowering its density, and as a result becoming more opaque. This requires that energy transfer via convection. This convection moves inwards, changing the surface composition. First the lithium abundance drops as the lithium-poor material is mixed upwards. Then the $^{12}C/^{13}C$ ratio lowers due to ^{13}C-rich material from $^{12}C(p,\gamma)^{13}N(e^{+},\nu)^{13}C$, which has been occurring in the core. The amount of ^{14}N also increases as ^{12}C has been converted in ^{14}N.

TDU (Schwarzschild & Härm 1967, first found by) occurs during the thermal pulses of AGBs described above, which are an important part of the s-process. Each thermal pulse provides the necessary conditions for the convective envelope to move inwards at the end of the shell flash. It moves into regions that have undergone partial helium burning. This allows the surface composition of carbon to increase. In some stars several of these TDU events can change the surface C/O ratio to larger than unity and result in a carbon star. It is also during the TDU that the elements produced during the s-process will reach the surface where they can be observed.

1.4 Science Goals

This thesis is an investigation of abundances of light elements (carbon, nitrogen, oxygen and sodium) and heavy elements (iron and barium) in different types of GCs. It is motivated by the need to provide abundance results for hundreds (and even thousands) of stars, the direction that GC and general astronomy is moving towards, i.e., GALactic Archaeology with HERMES (Zucker et al. 2012) and GAIA (Lindegren 2010). It also investigates the strengths and weaknesses of low-resolution spectroscopy. A further impetus is understanding the abundance results that will be possible with multi-object spectroscopy of a telescope such as SALT, of which the University of Canterbury is a consortium member.

Multi-object spectrographs allow for hundreds of stars to be observed in one night, making it possible to efficiently sample an object like a GC with 10^4–10^6 stars. Recent papers, such as Marino et al. (2011a), used the VLT to obtain spectra of 300 stars of ω Cen, and Johnson & Pilachowski (2010) published results for 855 stars of ω Cen. They confirmed the peculiar chemical make-up of the cluster. This thesis makes use of both of these datasets and extends them with an investigation of the van Loon et al. (2007) spectral library.

The first task of this thesis is to describe the spectral matching pipeline (Chapter 2). This used a combination of photometry and spectroscopy of the individual stars to determine common stellar parameters ($T_{\rm eff}$, $\log g$, [Fe/H]) as well as s-process, carbon, and nitrogen abundances. It makes use of spectral indices for stars where no [O/Fe] abundance is available. The importance of [O/Fe] is discussed in Chapter 2 as well as throughout this thesis.

The first clusters investigated in this thesis are the monometallic clusters 47 Tuc and NGC 6752 (Chapter 3). These clusters were selected as they had metallicities which were similar to the main peaks in the metallicity distribution of ω Cen. That chapter shows that the spectral matching pipeline worked well and returned results that are consistent with previous researchers.

After analyzing the monometallic clusters, the pipeline was then used on the multimetallic cluster ω Cen, using the van Loon et al. (2007) spectral library. In this case, there were two different analyses undertaken. The first analysis looked at 221 stars that had [O/Fe] abundances from Johnson & Pilachowski (2010) (Chapter 4) and the second analysis used CN and CH spectral indices to estimate the oxygen abundance of over 800 stars of ω Cen (Chapter 5). These abundance results were used to identify groups of stars with common chemical abundances which represent the different population of stars.

These abundance results are discussed in the context of proposed models of GC creation and nucleosynthetic yields of stars (Chapter 6). There is also discussion of the AGB, and the radial velocity and spatial distributions of

[10] The notable exception being observation of neutrinos, which can come from the stellar core.

the stars of ω Cen in this chapter. A concluding chapter (Chapter 7) provides a summary of the work carried out in this thesis and some possible directions for future work.

Chapter 2

Stellar Parameter Determination and Spectral Matching

This chapter is a discussion of the methods used to determine the stellar parameters of interest for the globular cluster (GC) stars: $T_{\rm eff}$, $\log g$, [Fe/H], [C/Fe], [N/Fe], [Ba/Fe] and [O/Fe]. This required the use of a combination of photometric and spectroscopic data, in conjunction with parameters determined by other researchers. These methods were used for 47 Tuc and NGC 6752 (Chapter 3) and ω Cen (Chapters 4 and 5). The methods are generally discussed in this chapter in the context of ω Cen. As such, unless otherwise stated, the synthetic spectra in this Chapter have been computed at the same spectral resolution as the van Loon et al. (2007) spectra: R = 1600.

The first parameters determined were the temperature and gravity (Section 2.1), which used empirical relationships between the stellar colour and $T_{\rm eff}$. The spectrum normalization method is defined in Section 2.2. Also important to the pipeline are the molecular equilibria involving molecules of carbon, nitrogen and oxygen (Section 2.3); the carbon and barium isotopic ratios (Section 2.4); strong spectral lines (Section 2.5). Finally, the full the spectral matching pipeline is described in Section 2.6.

2.1 Temperature and Gravity from Photometry

The most basic parameters of a star include its effective temperature ($T_{\rm eff}$) and surface gravity ($\log g$). In this work, these were determined for each star using photometry.

At the spectral resolution and with the wavelength coverage of the spectra used in this thesis, it was not possible to use a spectral-temperature indicator such as the Hβ spectral line. Therefore the temperature-colour relationships of Alonso et al. (1999, 2001) were used. These could then be combined with the luminosity relationship to estimate the surface gravity of each star.

2.1.1 Temperature

For stars of unknown metallicities, an appropriate colour for temperature determination is $V-K$, due to the lack of line blanketing would affect the $B-V$ colour, which was formerly used for photometry-based temperature determination (also discussed in Section 2.3 of Alonso et al. 1999). In the case of ω Cen, there is a 1.5 dex range in [Fe/H], with the [Fe/H] unknown for the majority of stars investigated in this thesis. That made the selection of a metallicity-independent determinator of $T_{\rm eff}$ from the the colour important. For the range of $V-K$ and $B-V$ in ω Cen, Table 2.1 shows how the range of [Fe/H] affects the derived temperature and gravity using the Alonso et al. (1999) empirical equations. If $B-V$ were selected there is a strong dependence on the input [Fe/H], with $B-V$ = 0.8 having a 260 K range in $T_{\rm eff}$, while in $V-K$ there is a 5 K range.

For each spectral library used in this work, V photometry was available from its creators, which was combined with J and K_S photometry from the Two Micron All Sky Survey (2MASS) (Skrutskie et al. 2006) to find the $V-K$ colour. 2MASS observed the sky in the near-infrared covering three photometric bands: J (1.25 μm), H (1.65 μm), and K_S (2.17 μm). Alonso et al. (1999) requires the $V-K$ photometry to be in the Carlos Sánchez Telescope (TCS)

Table 2.1 — The colour-temperature equations of Alonso et al. (1999) have [Fe/H] and $T_{\rm eff}$ dependences, which has an effect on the temperature determined from them. This table gives the $T_{\rm eff}$ (in K) found across the full range of $B-V$ and $V-K$ for the possible [Fe/H] found in ω Cen. The blank entries are where the constraints of Alonso et al. (1999) in colour and/or [Fe/H] were not met.

	$T_{\rm eff}$ (K) for a given [Fe/H]					$T_{\rm eff}$ (K) for a given [Fe/H]			
$B-V$	−0.5	−1.0	−1.5	−2.0	$V-K$	−0.5	−1.0	−1.5	−2.0
0.4	6343	6244	6178	6142	1.0	6580	6612		
0.6	5630	5522	5441	5386	1.5	5752	5760	5777	5803
0.8	5063	4938	4851	4799	2.0	5108	5099	5097	5103
1.0	4684	4599	4545	4520	2.5	4586	4572	4564	4562
1.2	4360	4305	4276	4273	3.0	4218	4205	4197	4194
1.4	4078	4047			3.5	3951	3937		
1.6	3832	3819			4.0	3760	3745		
1.8	3614	3617			4.5	3627	3611		

photometric system. The photometry was converted to this system using a method developed by Johnson et al. (2005), which uses the J and K_S from 2MASS and the V in the Johnson photometric system,

$$(J-K)_{\rm ESO} = \frac{(J-K_S)_{\rm 2MASS} + (0.008)}{0.956}, \tag{2.1}$$

$$K_{\rm ESO} = K_{\rm 2MASS} - (0.005)(J-K)_{\rm ESO} + 0.045, \tag{2.2}$$

$$K_{\rm TCS} = K_{\rm ESO} - 0.042 + 0.006(J-K)_{\rm ESO}, \tag{2.3}$$

$$(J-K)_{\rm TCS} = -0.012 + 0.910(J-K)_{\rm ESO}, \tag{2.4}$$

$$K_{\rm J} = K_{\rm TCS} + 0.048 + 0.014(J-K)_{\rm TCS}, \tag{2.5}$$

$$(V-K)_{\rm TCS} = 0.050 + 0.993(V-K)_{\rm J}. \tag{2.6}$$

With the photometry in the correct photometric system, Equations 8 & 9 of Alonso et al. (1999, 2001) were used,

$$\frac{5040}{T_{\rm eff}} = a_0 + a_1(V-K) + a_2(V-K)^2 + a_3(V-K)[{\rm Fe/H}] + a_4[{\rm Fe/H}] + a_5[{\rm Fe/H}]^2. \tag{2.7}$$

For their Equation 8: $a_0 = 0.5558; a_1 = 0.2105; a_2 = 1.981\times10^{-3}; a_3 = -9.965\times10^{-3}; a_4 = 1.325\times10^{-2}; a_5 = -2.726\times10^{-3}$. For Equation 9: $a_0 = 0.3770; a_1 = 0.3660; a_2 = -3.170\times10^{-2}; a_3 = -3.074\times10^{-3}; a_4 = -2.765\times10^{-3}; a_5 = 2.973\times10^{-3}$. These equations have constraints on $V-K$ and [Fe/H] (Table 2.2) which determined if Equation 8 or 9 were used. If the star satisfied the constraints for both equations then a linear interpolation between $2.00 < V-K < 2.50$ was used to avoid any discontinuities in the temperatures. If neither set of constraints were satisfied then the star was excluded from future analysis.

2.1.2 Gravity

The surface gravity was determined using the elementary equation,

$$\log g_\star = 0.40(M_{\rm bol,\star} - M_{\rm bol,\odot} + \log g_\odot + 4\log(T_\star/T_\odot) + \log(M_\star/M_\odot), \tag{2.8}$$

with $M_{\rm bol,\odot} = +4.75$, $T_\odot = 5777$ K and $\log g_\odot = 4.44$ (Allen & Cox 2000). The stellar mass was set to 0.8 $M_\odot$, which is thought to be typical of the giant branch (GB) stars in the GCs being studied. With ω Cen's multiple populations (Section 1.2), an age range is highly likely and this would cause a mass range of the stars present on the GB today. This mass range would extend down to 0.6 $M_\odot$. However, since the logarithm of the stellar mass is used in Eq. (2.8), this would reduce the effect on the final gravity value to 0.1 dex at the most extreme. As such, the probable mass range was ignored.

Table 2.2 — Constraints from Alonso et al. (1999) for their Equations 8, 9, 17 and 18, which are given here as Eqs. (2.7) and (2.9). E.g., for a star with [Fe/H] = −1.7, then its $V-K$ must be in this range $1.20 \leq V-K \leq 2.50$.

Metallicity range	Equation	Colour range	Equation	Temperature range
$+0.2 \geq$ [Fe/H] > -0.5	8	$0.20 \leq V-K \leq 2.50$	17	$3.50 \leq \log(T_{\rm eff}) \leq 3.67$
$-0.5 \geq$ [Fe/H] > -1.5		$1.00 \leq V-K \leq 2.50$		$3.56 \leq \log(T_{\rm eff}) \leq 3.67$
$-1.5 \geq$ [Fe/H] > -2.5		$1.20 \leq V-K \leq 2.50$		$3.58 \leq \log(T_{\rm eff}) \leq 3.67$
$-2.5 \geq$ [Fe/H] > -3.0		$1.70 \leq V-K \leq 2.50$		$3.61 \leq \log(T_{\rm eff}) \leq 3.67$
$+0.2 \geq$ [Fe/H] > -0.5	9	$2.00 \leq V-K \leq 4.90$	18	$3.65 \leq \log(T_{\rm eff}) \leq 3.96$
$-0.5 \geq$ [Fe/H] > -1.5		$2.00 \leq V-K \leq 4.60$		$3.65 \leq \log(T_{\rm eff}) \leq 3.83$
$-1.5 \geq$ [Fe/H] > -2.5		$2.00 \leq V-K \leq 3.40$		$3.65 \leq \log(T_{\rm eff}) \leq 3.80$
$-2.5 \geq$ [Fe/H] > -3.0		$2.00 \leq V-K \leq 2.80$		$3.65 \leq \log(T_{\rm eff}) \leq 3.74$

The bolometric correction was taken from Alonso et al. (1999, their Equations 17 & 18),

$$BC = \frac{b_0}{X} + b_1 + b_2 X + b_3 X^2 + b_3 X[\text{Fe/H}] + b_4[\text{Fe/H}] + b_5[\text{Fe/H}]^2, \tag{2.9}$$

where $X = \log(T_{\rm eff}) - 3.52$. The constraints are given in Table 2.2. For Equation 17, $b_0 = -5.531 \times 10^{-2}$, $b_1 = -0.6177$, $b_2 = 4.420$, $b_3 = -2.669$, $b_4 = 0.6943$, $b_5 = -0.1071$, $b_6 = -8.612 \times 10^{-3}$ and for Equation 18, $b_0 = -9.930 \times 10^{-2}$, $b_1 = 2.887 \times 10^{-2}$, $b_2 = 2.275$, $b_3 = -4.425$, $b_4 = 0.3505$, $b_5 = -5.558 \times 10^{-2}$, $b_6 = -5.375 \times 10^{-3}$. There is a small [Fe/H] in Eq. (2.7) dependence which across the metallicity range of ω Cen would affect the surface gravity by 0.01 dex.

Using the uncertainty of the photometry and the empirical equations of Alonso et al. (1999), propagation of uncertainties resulted in errors of 1 % in $T_{\rm eff}$ and $\log g$. There was a strong correlation between the V magnitude of the star and its uncertainty. For the brightest stars in ω Cen, the uncertainty in temperature was 40 K, while for the faintest stars it was about 150 K. The photometric gravities were good estimates but are based on empirical equations. In Figure 17 of Alonso et al. (1999), they show that there was up to ±0.2 magnitude difference between their bolometric correction and those of other researchers.

Differences in gravity can be mimicked by differences in metallicity, especially with the ionized barium line at 4554 Å, used in this study for determining [Ba/Fe]. Increasing the gravity of a star will decrease the strength of spectral lines of ionized species (for all other parameters remaining constant). It was found that a 0.3 dex change in gravity (for a $T_{\rm eff} = 4000$ K, $\log g = 0.8$, [Fe/H] = −1.7 star) could be compensated for by a 0.05 dex change in the metallicity (Fig. 2.1). For a gross change of metallicity it was not possible to use the gravity to compensate. This provides confidence that even having the surface gravity wrong by 0.3 dex will not affect the results of this thesis.

For ω Cen, where there is a large number of stars that have been studied by multiple researchers, these temperature and gravity determinations compared well. Johnson & Pilachowski (2010), Marino et al. (2011a) and Marino et al. (2012) all found essentially the same temperatures and gravities (Fig. 2.2) as for the sample of stars used in Chapters 4 and 5, since they used the same method (Johnson et al. 2005) and in some cases the same photometry (from van Leeuwen et al. 2000; Bellini et al. 2009a). Any small differences were due to distance moduli, reddening, stellar mass selections, and corrections for systematic difference between photometry (the last is discussed in Section 5.2).

2.2 Spectrum Normalization

The previous section described the application of the photometry. Now we move to the analysis of the spectral data.

The spectra used in this research ranged in spectral resolution from $R \sim 1600$ for the van Loon et al. (2007) spectra of ω Cen, to ~ 6000 for the AAOmega spectra of 47 Tuc and NGC 6752. With the focus on the analysis of a blue-end of the optical spectrum which is rich in spectral lines, it was not possible, at these resolutions, to find true continuum points. This required the development of a method that used pseudo-continuum points instead.

The raw spectrum was continuum normalized by mapping the observed spectrum onto the synthetic spectrum. Three anchor points were selected: 4088 Å, 4220 Å and 4318 Å (as also used in Worley & Cottrell 2012). These three

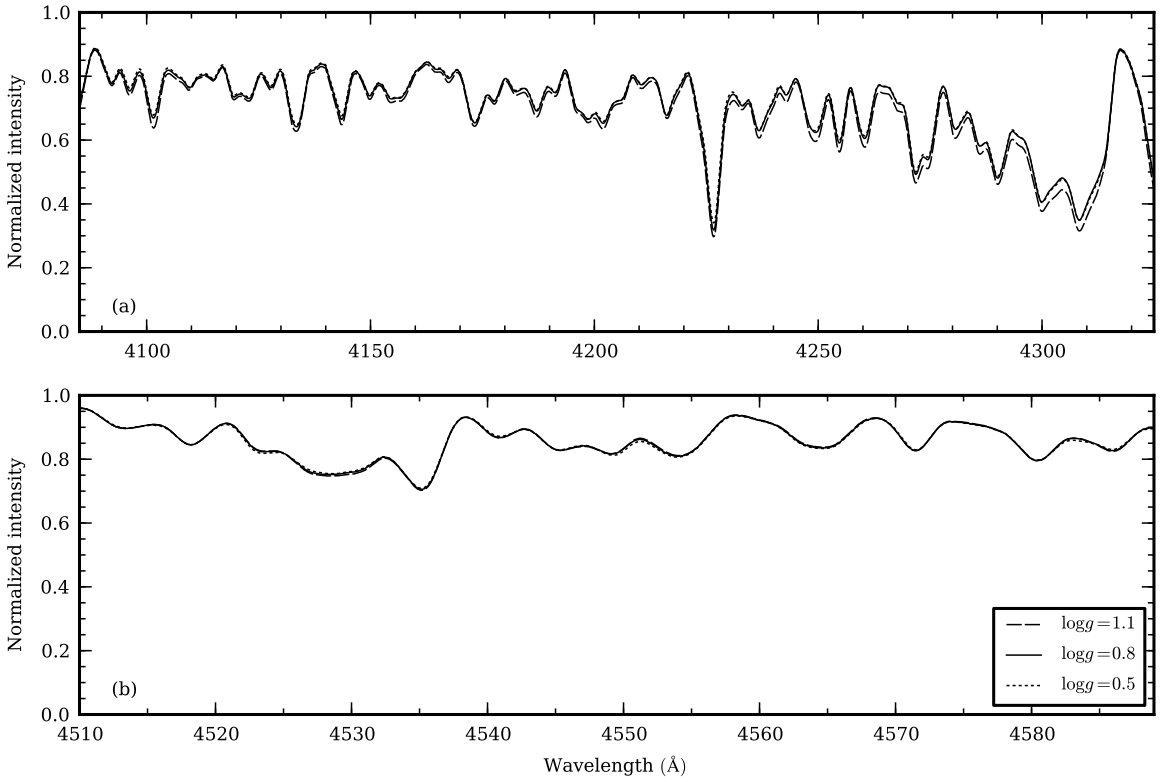

Figure 2.1 — Synthetic spectra ($T_{\rm eff}$ = 4000 K, [Fe/H] = −1.7, [C/Fe] = −0.2, [N/Fe] = 0.4, [O/Fe] = −0.1) illustrate the small effect that gravity has on the strength of spectral features: (a) CN and CH region of the spectrum; (b) the Ba II 4554 Å line. Changing $\log g$ by ±0.3 dex (doubling or halving the surface gravity of the star), while keeping the other stellar parameters the same is shown to have a negligible effect on the spectra.

points were joined by two straight lines and these lines were mapped from the raw spectrum onto the equivalent lines in the synthetic spectrum (Fig. 2.3). This method has a dependence on the synthetic spectrum being used, as the continuum placement was recomputed at each iterative step. These three points were selected due to their stability across the $T_{\rm eff}$, $\log g$, [Fe/H], [C/Fe] and [N/Fe] abundance ranges that are found in the most extreme object studied, ω Cen (Fig. 2.4). Although the point at 4088 Å does change with different metallicities, the regions of the spectra used for the abundance analysis were closer to the other two points, so were not be affected by this.

In the van Loon et al. (2007) spectral library of ω Cen (used in Chapters 4 and 5), there are continuum-normalized spectra available, but these have some relative intensity problems in the 4000–4300 Å region: namely that the CH band head was at a lower normalized intensity than the CN band head. This was not found in any of the synthetic spectra that were examined (Fig. 2.4). This is why a new normalization was performed on their unnormalized spectra, instead of simply using their normalized spectra.

2.3 Molecular Equilibria

Knowing the [O/Fe] abundance of each star is of great important when undertaking an abundance analysis involving carbon and nitrogen, because of the equilibria that exist between CO, CH, CN (and other) molecules in the stellar atmosphere. The amount of oxygen affects the amount of carbon that is bound up in the CO molecule. The amount of C left over is then bound preferentially into CH, with the remainder forming CN. In the Bmolec.f routine of moog (used for the spectrum synthesis in this thesis), the equilibrium constant ($K_{\rm p}$) (Petrucci et al. 2001) is calculated in order to determine which molecules are preferred in the stellar atmosphere. For example, in a $T_{\rm eff}$ = 4000 K star,

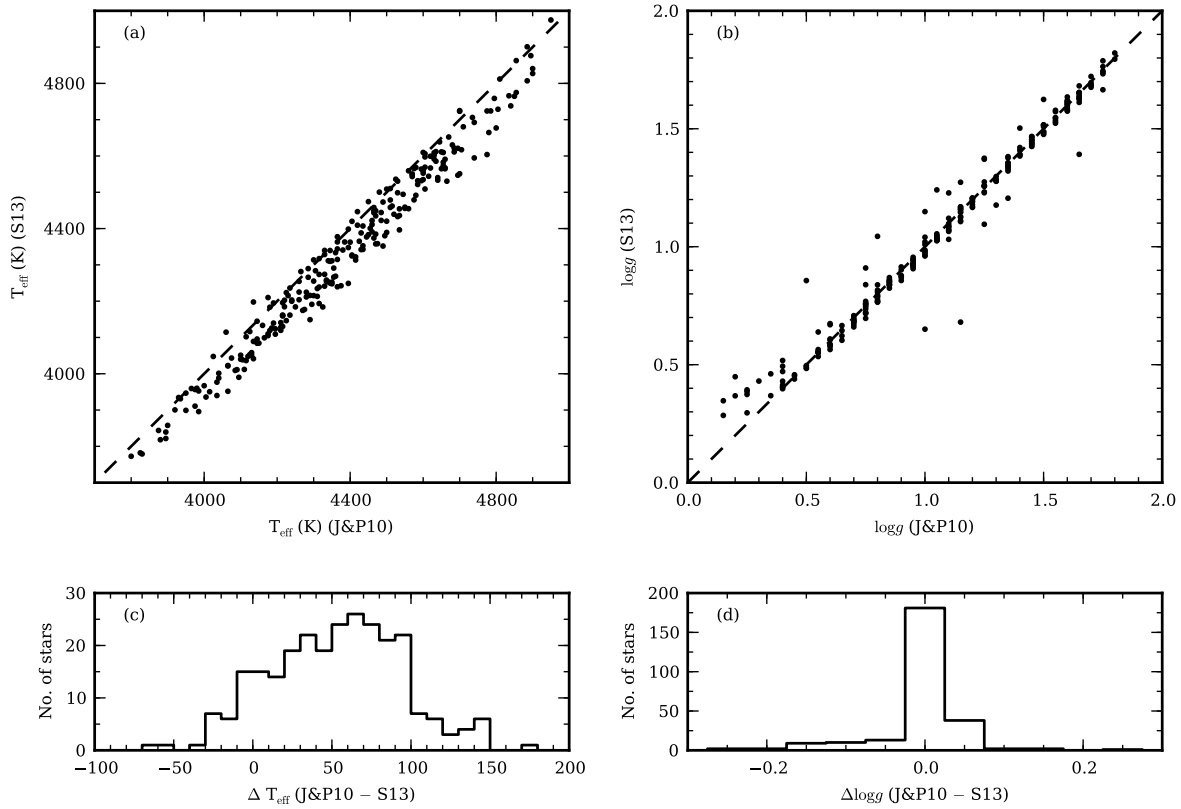

Figure 2.2 — (a) & (c) Comparison of the $T_{\rm eff}$ found by this work (S13) and that of Johnson & Pilachowski (2010, J&P10), and (b) & (d) show the comparison for $\log g$. The dashed lines in (a) & (b) are one-to-one lines as a guide. The temperatures found by Johnson & Pilachowski (2010) were about 50 K hotter than those found by in this thesis. This can be attributed to the systematic magnitude difference between the photometry of van Leeuwen et al. (2000) and Bellini et al. (2009a), which is described in Section 5.2.

$\log K_{\rm p}$ for CO, CH and CN are −50, −31 and 160 respectively. This tells us that the molecule CO is favoured in the equilibrium reaction (CO $\rightleftharpoons$ C + O) and so is CH in its reaction (CH $\rightleftharpoons$ C + H). Conversely, it is the reactants that are favoured in the equilibrium of CN (CN $\rightleftharpoons$ C + N). This fact can also be seen in the dissociation energies of the different molecules: for CO, CH and CN they are respectively 1077 kJ mol^{-1}, 339 kJ mol^{-1} and 732 kJ mol^{-1} (Darwent 1970). Here CO is much harder to break apart than the other two molecules of interest.

The effects on the synthetic spectrum of changing [O/Fe] (while keeping [C/Fe] and [N/Fe] constant) are shown in Fig. 2.5a. Increasing the [O/Fe] abundance decreases the strength in the spectrum of both the CN and CH bands, while the converse is true if [O/Fe] is decreased. This shows that knowing the oxygen abundance of the stars is fundamental to any inference of the carbon and nitrogen abundances in the star from the CN and CH molecular bands. Figures 2.5b and 2.5c show the effect of changing [C/Fe] and [N/Fe]. The effect of changing [N/Fe] is only to change the strength of the CN band, which consistent with the equilibrium constant of CN $\rightleftharpoons$ C + N favouring the reactants, C & N. while changing carbon affects both CN & CH.

2.4 Carbon Isotopic Ratios and Hyperfine Splitting of Barium Spectral Lines

The ^{12}C/^{13}C ratio has a small effect on the spectrum (Fig. 2.6a). It is thought that the primordial ratio is ~ 90, which is also observed in the Sun (Anders & Grevesse 1989) (though it is still unknown for halo dwarfs in the field and in clusters), while it is between 5–30 in field GB stars (Keller et al. 2001). The ratio for fully processed material is 3.5. Observations of ω Cen stars have found a mean value of 4.3 ± 0.4 (V. Smith et al. 2002). Figure 2.6a shows the

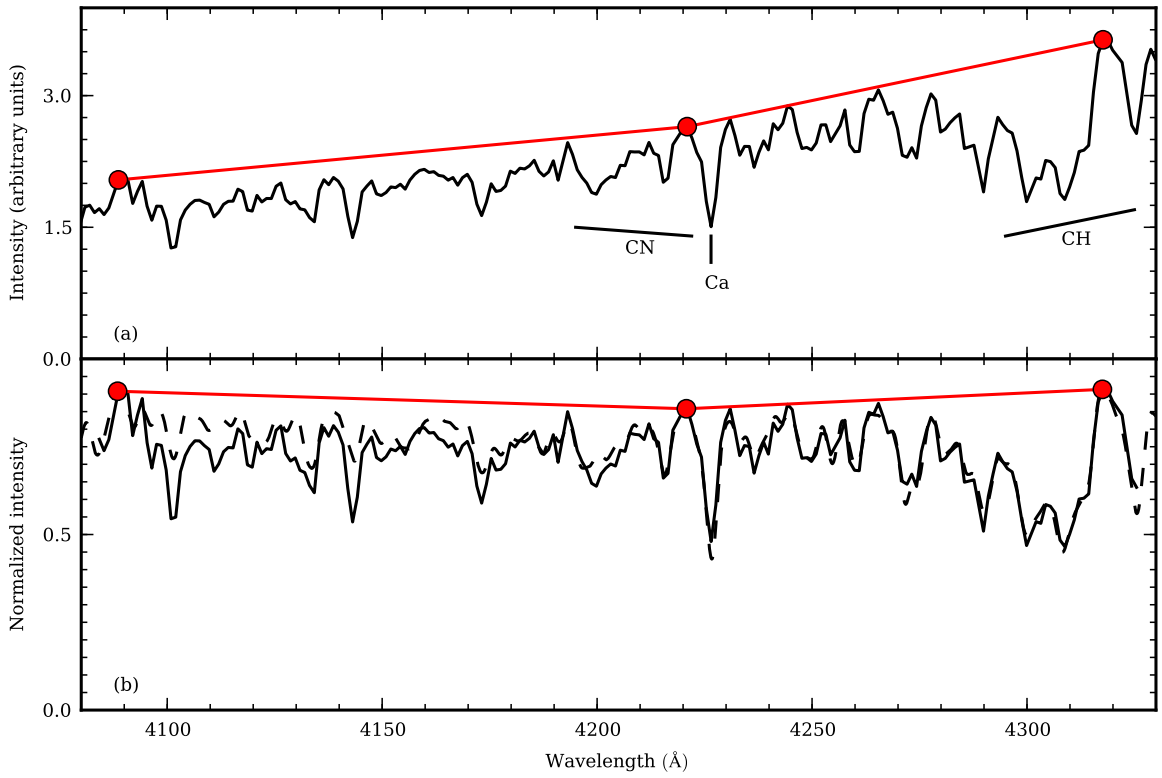

Figure 2.3 — (a) Portion of the reduced spectrum of LEID48049 (from van Loon et al. 2007). (b) Normalized spectrum of LEID48049 (solid line) and best fitting synthetic spectrum (dashed line), as found in Chapter 5 ($T_{\rm eff}$ = 4000 K, log g = 0.5, [Fe/H] = −1.8, [O/Fe] = +0.4, [C/Fe] = 0.2, [N/Fe] = 0.3.) The red dots in each panel show the pseudo-continuum points that were used for the spectrum normalization, and the lines joining them are the lines that were mapped onto each other: such that the left line segment in (a) was mapped onto the left line in (b), and the same for the right line segments. In this way, the relative intensity difference between the band heads in the synthetic spectra was preserved.

effect of different carbon isotopic ratios from the 90 to 3.5. For this work a ^{12}C/^{13}C ratio of 8 was used. This was selected as the stars in this thesis would have undergone a range of processing and mixing, which could not be determined simply from their brightness due to the complex GB structure of ω Cen's colour-magnitude diagram (CMD). The different carbon ratios only affects the CN spectral bands by an observable amount, with the changes in the spectrum at 4207 Å due to the ^{13}C^{14}N band head. Even then, this large change is between the most extreme values. For the likely observed range in these GCs (< 10), there is a negligible difference between different spectra.

Hyperfine structure is caused by the interaction of the nuclear spin with the momentum vector of the rest of the atom, splitting the energy levels of isotopes with odd numbers of nucleons, and especially in odd atomic-numbered elements (Gray 2005). Of importance to stellar spectroscopy, hfs causes a strong line to become desaturated, resulting in features with larger equivalent widths (EWs) than single lines with no hfs component (Prochaska & McWilliam 2000). In other words, hfs will cause the line to have a larger EW for a given abundance compared to when hfs is not included in the spectrum synthesis.

With about 18 % of barium in stars having an odd mass number (primarily ^{135}Ba and ^{137}Ba; see Table 1.3), the strong spectral lines of barium exhibit hfs. For the 4554 Å line of barium, two line lists were created: one that included all the isotopic species of the barium feature and one that did not. It was found that across the temperature and gravity ranges of ω Cen, the effect was negligible (Fig. 2.6b). Such results confirmed what was found by Stanford et al. (2010) for main sequence (MS) stars. They found a Δ[Ba/Fe] < 0.05 dex between abundances found with hfs and those without. As such hfs was not included in the analysis in Chapters 4 and 5 where [Ba/Fe] is determined.

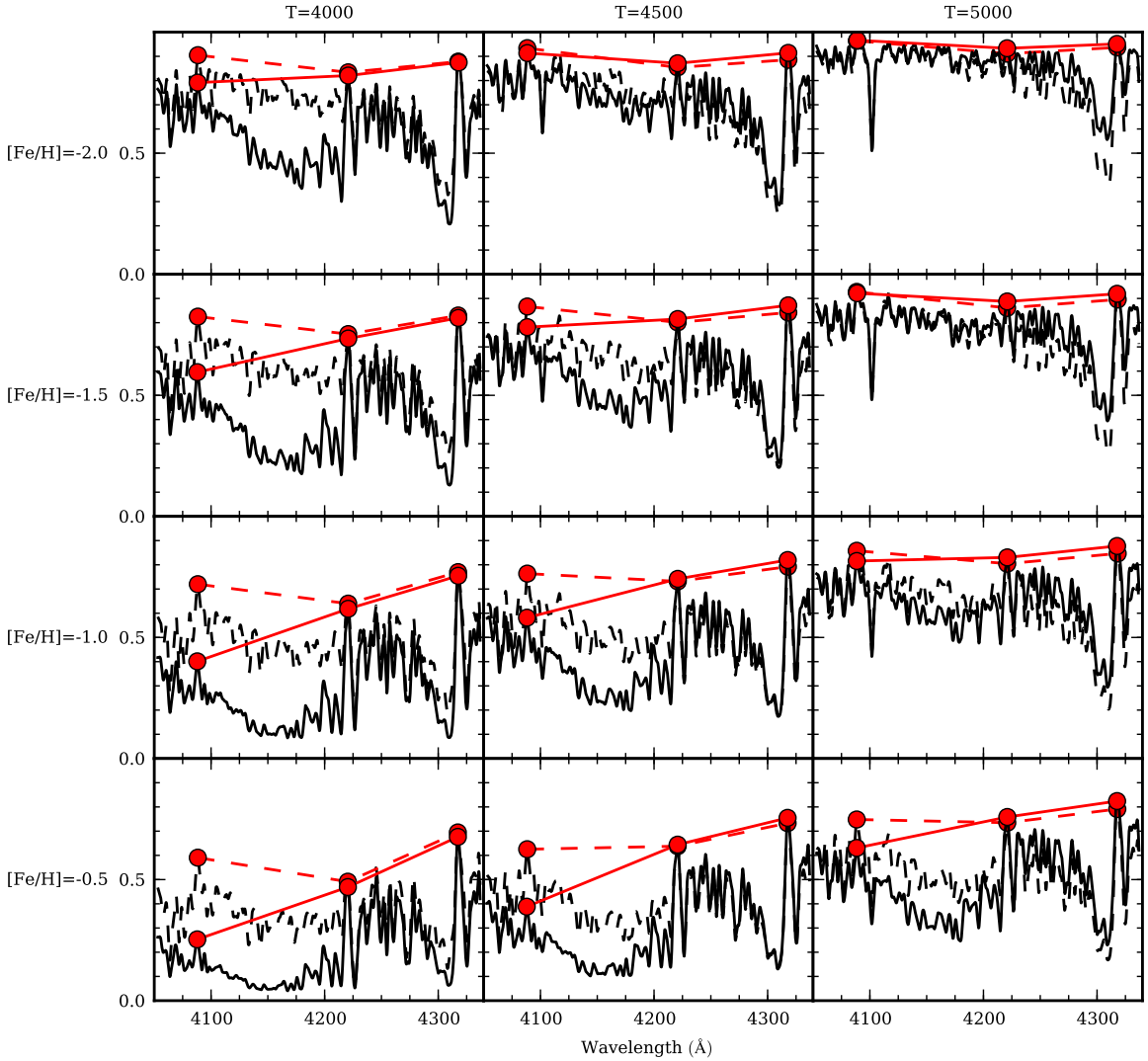

Figure 2.4 — Grid of synthetic spectra across the range of $T_{\rm eff}$, [Fe/H], [C/Fe], [N/Fe] and [O/Fe] of ω Cen. The solid lines used a model atmosphere with [C/Fe] = 0.0, [N/Fe] = 1.0, [O/Fe] = −0.5, and the dashed line used [C/Fe] = 0.5, [N/Fe] = 0.0, [O/Fe] = 0.4. The red dots are the pseudo-continuum points and they are joined by line segments, which were used in the continuum normalization shown in Fig. 2.3.

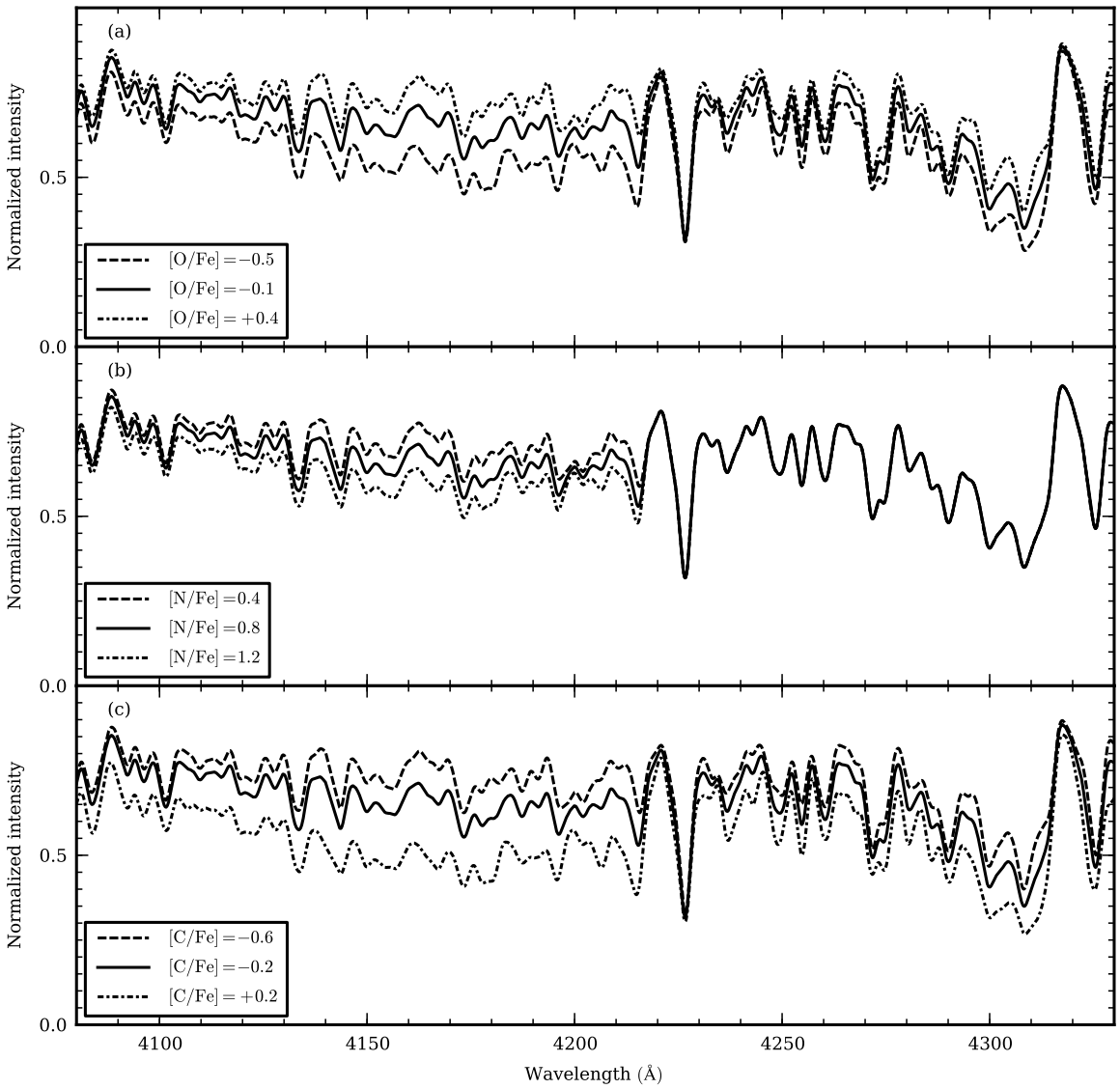

Figure 2.5 — Three sets of spectra showing the effects of changing (a) [O/Fe], (b) [N/Fe], and (c) [C/Fe]. The ranges for each element were chosen from the peaks of the distribution for ω Cen found in Section 5.1, and especially in Fig. 5.13. In each panel, the solid line shows the same model ($T_{\rm eff}$ = 4000 K, [Fe/H] = −1.7, [C/Fe] = −0.2, [N/Fe] = 0.4, [O/Fe] = −0.1). The equilibria involving CH and CO favour creating those molecules, unlike CN, where the equilibrium favours the reactants (C and N). From (a) it is clear that knowing the [O/Fe] abundance is of vital importance for determining the carbon and nitrogen abundances of stars from molecular bands.

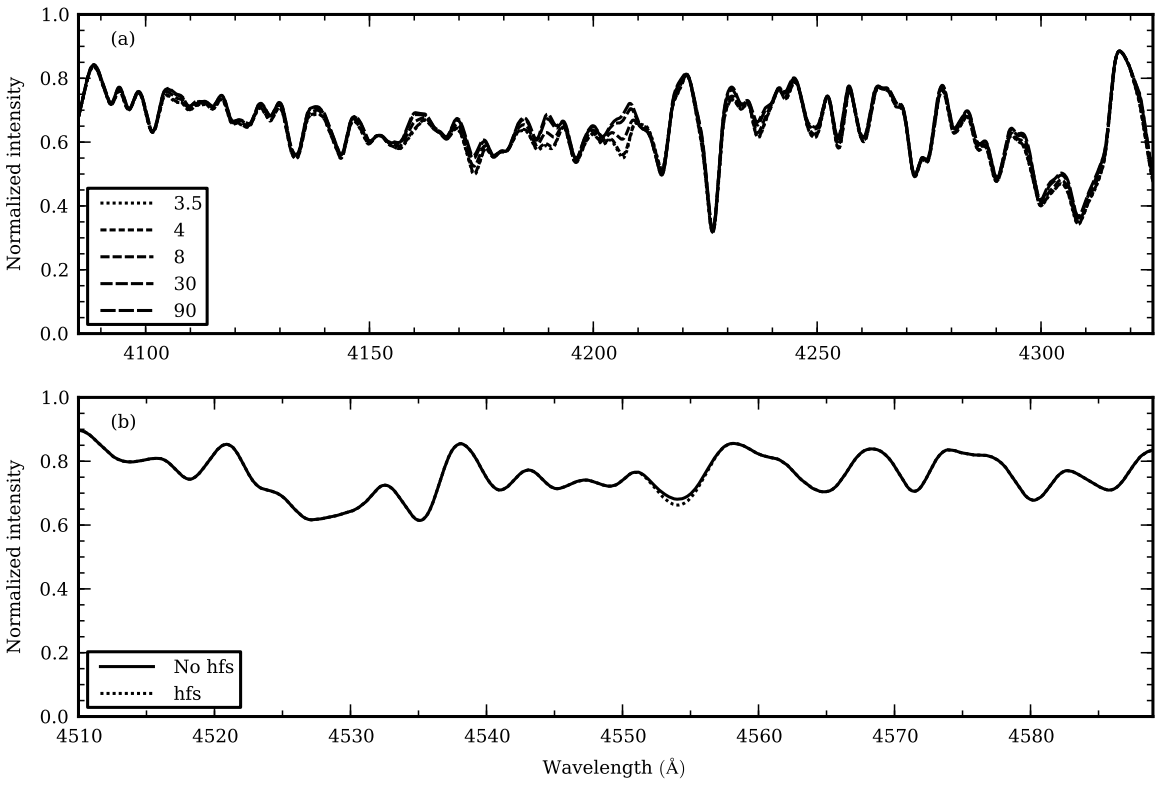

Figure 2.6 — (a) The effect of different carbon isotopic ratio on the spectrum. From the shortest to the longest dash (strongest to weakest spectral lines), the ratios are 3.5, 4, 8, 30 and 90. The regions with the largest changes are where the $^{13}C^{14}N$ band heads form (4205 Å). The models with the lowest $^{12}C/^{13}C$ ratio have the strongest $^{13}C^{14}N$ band heads. (b) The effect of hfs on the spectrum. The Ba II 4554 Å spectral line experiences hfs. At the resolution of the van Loon et al. (2007) spectral library it is a very small effect and was ignored for the abundance analysis of ω Cen.

2.5 Strong Lines

The Ca I and Ba II lines were regarded as strong lines by MOOG, sitting on the upper portion of the curve of growth. Throughout this work MOOG would normally only consider ±1 Å for opacity contributions from neighbouring transitions. By placing a spectral line on the strong line list, MOOG would consider the line's opacity contributions for every wavelength step in the synthesis. Without being considered as a strong line, the Ca I line would appear as if formed in a star with about 0.3 dex less in [Ca/Fe] (Fig. 2.7a). In terms of the pipeline used in this work, where [Ca/Fe] is fixed, it would instead cause [Fe/H] to come out 0.3 dex metal-richer as well as changes in [C/Fe] and [N/Fe] that would flow from this. There was a small effect on the Ba II 4554 Å line as well (Fig. 2.7b).

Sections 2.2 to 2.5 have discussed the aspects of the spectrum synthesis that must be considered in this analysis. The following section brings these threads together to describe the spectral matching pipeline.

2.6 Spectral Matching Pipeline

This section describes the automated spectral matching pipeline by which the abundances were determined for the stars from their observed spectra.

Spectrum synthesis was performed using the 2012 version of MOOG (Sneden 1973). MOOG is FORTRAN code that performs a variety of local thermodynamic equilibrium line analysis and spectrum synthesis tasks. Around this

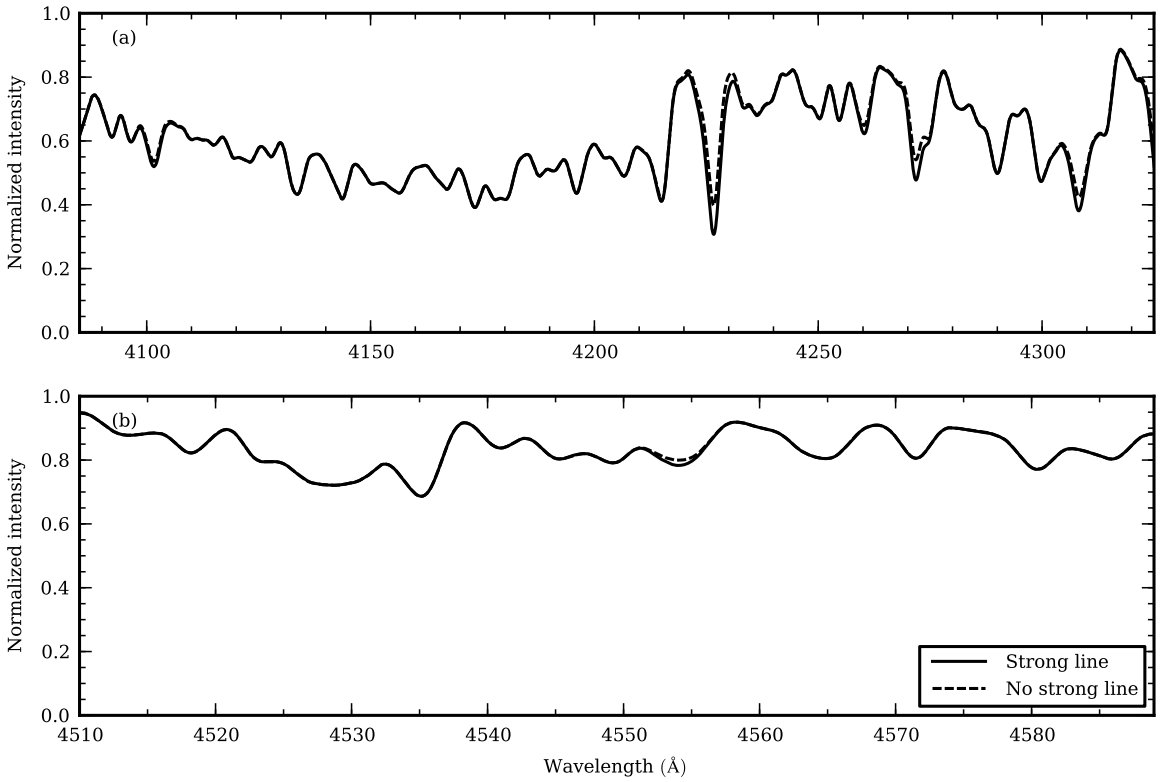

Figure 2.7 — Effect of the strong line list in MOOG for (a) Ca I 4226 Å, (b) Ba II 4554 Å using a $T_{\rm eff}$ = 4050 K, [Fe/H] = −1.5 model. The solid line in both panels is with the a strong line list, while the dashed line is with no strong line list.

was created a PYTHON wrapper to code the spectral matching pipeline which found the best matching synthetic spectrum using known parameters and physically reasonable estimates for the unknown parameters of the stars.

At the start of the pipeline, the $T_{\rm eff}$ and $\log g$ (as calculated in Section 2.1) were rounded to 50 K and 0.1 dex respectively as it was not necessary to be more precise than that given the spectral resolution. Initial random guesses were made for [Fe/H], [C/Fe] and [N/Fe]. The ranges of these guesses depended on the cluster being studied, and the known ranges of the elemental abundances of their stars: e.g., for ω Cen's CN-strong stars: −1.0 < [C/Fe] < 0.2, −0.5 < [N/Fe] < 2.0.

At this point, each star had a $T_{\rm eff}$, $\log g$, and starting inputs for [Fe/H], [C/Fe], and [N/Fe]. The final two parameters required were [O/Fe] and [Ca/Fe]. The values of these depended on the dataset that was being investigated. In the case of some objects, [O/Fe] was estimated from spectral indices (Chapter 5 and Section 3.1.1) and in other cases the abundances used were from other researchers (Chapter 4 and Sections 3.1.2 and 3.5). For [Ca/Fe], fixed values were assumed used for the monometallic clusters and in Chapter 5. In Chapter 4, values from Johnson & Pilachowski (2010) were used for the individual stars.

The microturbulence (v_t) was assumed to be 2.0 km s^{-1} for all of the stars. It was not possible to be refine this value due to the lack of unblended iron lines to remove the trend in iron abundance with line strength, the usual method for refining the microturbulence. For comparison, Johnson & Pilachowski (2010) had a mean of $\langle v_t \rangle = 1.7 \pm 0.2$ km s^{-1} for their study of 855 GB stars of ω Cen.

These input stellar parameters were used to create a stellar atmosphere models using ATMOSPHY[1]. This is PYTHON code that interpolates the desired model atmosphere from the Castelli-Kurucz grid of stellar models

[1] https://github.com/andycasey/atmosphy

Table 2.3 — Example of how the minimum was determined through the iterative process. For the Ca I spectral line at 4226 Å, the EW difference between the observed and synthetic spectra was determined. In this case the first guess was [Fe/H] = −1.5, then the next guess was [Fe/H] = −1.4, which did not make the difference smaller, so it proceeded back to [Fe/H] = −1.5 and continued in this direction until it reached [Fe/H] = −1.9, which had a larger EW difference than the previous metallicity of [Fe/H] = −1.8. The pipeline then went back to −1.8 and then −1.7 and finally to −1.8. At this point the last five metallicity values tried were −1.8, −1.7, −1.8, −1.9 and −1.8. With the first, third and fifth values of this list being equal, this [Fe/H] value was determined to be −1.8.

Iteration step	[Fe/H]	EW difference (mÅ)
1	−1.5	0.102
2	−1.4	0.125
3	−1.5	0.102
4	−1.6	0.048
5	−1.7	0.025
6	−1.8	**0.001**
7	−1.9	0.007
8	−1.8	**0.001**
9	−1.7	0.013
10	−1.8	**0.001**

(Castelli & Kurucz 2003). This model also instructed MOOG to include H_2, CH, NH, OH, C_2, CN, CO, N_2, NO, O_2, OH_2, CO_2, Mg^+H, MgH, SiH, TiO and MgO in the molecular equilibria of the spectrum synthesis. The solar abundances of Anders & Grevesse (1989) were used.

For the CH and CN region of the spectrum, line lists were from Norris (2012, private communication). These line lists were found to match to the high-resolution atlas of α Boo (Hinkle et al. 2000) using abundances determined by Decin et al. (2004). α Boo was selected as it is a GB star like the GC stars analyzed in this thesis (though metal rich at [Fe/H] = −0.5). They also matched the α Boo spectrum convolved to the resolution of the van Loon et al. (2007) spectra. The atomic $\log gf$ values in the empirical line list for the barium region investigated (400–500 nm) were adjusted so that the synthetic spectrum matched the α Boo spectrum, again at both resolutions.

The spectrum for the region from 4050–4340 Å was produced in three overlapping segments (4050–4150 Å, 4140–4250 Å and 4230–4340 Å) due to a limitation in MOOG of the number of spectral lines it can handle at any one time. The [Fe/H] was determined using the metallicity sensitive CaI line at 4226 Å. The other two spectral features used were the carbon-dependent G band region (mainly CH: $A^2\Delta - X^2\Pi$) (4295–4325 Å) and the CN blue-system ($B^2\Sigma - X^2\Sigma$) (4195–4222 Å).

After normalizing the observed spectrum (Section 2.2), the first step of the spectral matching process was to minimize the EW difference between the observed and synthetic spectrum of the Ca I line at 4226 Å. The synthetic spectrum was used to define the position of the calcium line: the left and right "shoulders" were defined as being at the maximum intensity between 4218–4223 Å and 4227–4235 Å respectively. Their positions changed slightly with different input parameters which is why it was not at fixed values. The trapezium method was used to find the EW of the line in the synthetic and observed spectra and the difference calculated. This value was stored and the [Fe/H] increased by 0.1 dex, with a new model and synthetic spectrum created. The continuum was normalized with this new synthetic spectrum and the EW difference determined. If the difference in the EW was smaller than that found at the previous [Fe/H] value, the [Fe/H] was increased by another 0.1 dex and the process repeated. Otherwise [Fe/H] was decreased by 0.1 dex.

The computer would store the last five EW differences. It would compare the most recently calculated [Fe/H] value to the third-most-recent and fifth-most-recent values. If they were the same, a minimum had been found, which the pipeline assumed was the global minimum. An example of this is shown in Table 2.3. With the [Fe/H] determined, the spectral matching pipeline moved first to the CH and then the CN band heads. This iterative process was repeated for each of these. First the CH band head (4295–4325 Å) had the χ^2 between the synthetic and observed spectra minimized by changing [C/Fe] in the model atmosphere. The method was the same as for [Fe/H], where the assumed global minimum was found when [C/Fe] was oscillating between two values. Finally [N/Fe] was found by minimizing the χ^2 for the spectral region 4195–4222 Å, in the same way as for [C/Fe].

Table 2.4 — Example of the refinement of [Fe/H], [C/Fe], [N/Fe] by the spectral matching pipeline. In steps 3 and 4 it converges to the same triplet of values.

Iteration step	[Fe/H]	[C/Fe]	[N/Fe]
1	−0.7	−0.4	0.5
2	−1.0	−0.7	0.4
3	−0.9	−0.8	0.4
4	−0.9	−0.8	0.4

Table 2.5 — Results of the delta analysis performed on four stars to understand the effect of changing the input temperature by 100 K and the gravity by 0.3 dex.

LEID	$T_{\rm eff}$	[Fe/H]		[C/Fe]		[N/Fe]	
		$\Delta T_{\rm eff}$ = 100 K	$\Delta \log g$ = 0.3 dex	100 K	0.3 dex	100 K	0.3 dex
25062	3965	−0.1	+0.1	−0.3	−0.2	+0.1	+0.3
61085	3965	+0.2	0.0	−0.2	0.0	−0.4	+0.1
30013	4485	−0.1	0.0	0.0	0.0	−0.1	+0.1
57114	4470	+0.2	−0.1	0.0	0.0	−0.1	+0.1

As discussed in Section 2.3, there exist molecular equilibria between [C/Fe], [N/Fe] and [O/Fe]. This means that the [C/Fe] determined is dependent on the [N/Fe], which could have been subsequently changed by fitting the CN band head. The overall metallicity of the model could also have been changed to fit the calcium spectral line at 4226 Å. As such it was necessary to take the triplet of [Fe/H], [C/Fe] and [N/Fe], and feed them back into the spectral matching pipeline. The pipeline would continue modifying the triplet of abundances until two successive iterations returned the same triplet (example given in Table 2.4). There were some cases where two sets of triplets would be alternated between. In those cases, the pipeline had a built-in limit and would exit with the last found triplet.

For the barium region of the spectrum (4500–4600 Å), the [Fe/H] value was used from the CH/CN region of the spectrum and [Ba/Fe] was determined by minimizing the χ^2 difference over the whole region, which was centred on the strong Ba II line at 4554 Å. Because of the simpler nature of the spectral line, this would simply increase or decrease [Ba/Fe] from 0.0 dex until the χ^2, reached a minimum. There was no iteration necessary.

This chapter has described the generic method used in the abundance determination of GC stars. This method was used, with some minor modification, for all the stars of the objects investigated in this study.

2.7 Uncertainties

A delta analysis was performed to understand the sensitivity of the spectral matching method to the input parameters of temperature and gravity. Four stars were selected, one from each group identified in Section 4.3, with two stars being low temperature (~ 4000 K) and two being higher (~ 4500 K). The results of this analysis are presented in Table 2.5. It was found that increasing the temperature by 100 K results in 0.1 to 0.2 dex increase in [Fe/H] and [C/Fe]. [N/Fe] changed by ±0.1 dex except for the most N-rich star which decreased by 0.4 dex. Changing the gravity by 0.3 dex had little to no effect on the abundances (see also Fig. 2.1).

2.8 Summary

This Chapter has described the methods used in this thesis for determining the stellar parameters and abundances of the GC stars. The $T_{\rm eff}$ and the $\log g$ were estimated from the photometry using the temperature-colour relationships. The temperature and gravity were used to create synthetic spectra that were used to continuum normalize the observed spectra and find the abundance of evolved stars of GCs.

The next three chapters use the spectral matching pipeline for three different clusters. In Chapter 3 it analyzed spectra of 47 Tuc and NGC 6752, and in Chapters 4 and 5 for ω Cen using different [O/Fe] estimates for the stars.

Chapter 3

Monometallic Globular Clusters as Test-Cases

To test the pipeline described in the previous chapter, it was decided to investigate monometallic clusters as test-cases. Within a monometallic cluster, the stars have the same metallicity. This means that for the spectral matching pipeline, either the metallicity can be fixed for each star at the known value of the cluster, or metallicities can be determined for each star, and compared to the literature value for the cluster. In order to cover the [Fe/H] range observed of ω Cen, two clusters were selected: 47 Tuc ([Fe/H] = −0.7) and NGC 6752 (−1.5) (basic parameters for each are summarized in Table 1.1).

There were three sources of spectral data for this thesis, summarized in Table 3.1. Each cluster was observed at low resolution, sampling the red giant branch (RGB) and the asymptotic giant branch (AGB), with a few horizontal branch (HB) stars in 47 Tuc and NGC 6752. These clusters are of similar brightnesses, meaning that the signal-to-noise is comparable across the different spectra. For ω Cen, van Loon et al. (2007) had a spectral resolution of $R \sim 1600$. For the monometallic clusters, the spectral resolution was higher and the wavelength coverage was different: van Loon et al. (2007) covered 3800–5000 Å, while the AAOmega spectra covered 4000–4300 Å in the blue and 5750–6200 Å in the red; and the Southern African Large Telescope (SALT) multi-object spectroscopy (MOS) was ~ 3700–4500 Å. Therefore it was not possible to determine the [Ba/Fe] for 47 Tuc and NGC 6752. With regards to their wavelength resolution, van Loon et al. (2007) had a somewhat low sampling of the spectrum, with a data point every ~ 1.1 Å, while the AAOmega spectra had a data point every ~ 0.15 Å and the SALT MOS spectra about every ~ 0.25 Å. This changed the possible precision to which the equivalent width (EW) could be calculated for the Ca I 4226 Å spectral line. A further complication with the spectra from SALT is that there are gaps between the three CCD chips that make up the detector. This means for these stars there are small portions of the spectra which had no data. This became a problem when this coincided with a spectral region of interest, meaning that not all the stars observed could be analyzed.

The clusters discussed in this chapter are 47 Tuc in Sections 3.1 and 3.2 and NGC 6752 in Section 3.5. Oxygen abundances were estimated for each star and [C/Fe], [N/Fe], and [Fe/H] determined. Using literature abundances for the clusters (and in some cases abundances for the same stars from other researchers) the spectral matching pipeline is shown to return abundances that are in good agreement with those found by previous researchers.

3.1 AAOmega Spectra of 47 Tucanæ

47 Tuc is a large cluster in the southern sky that exhibits the classical features of a globular cluster (GC), including a single metallicity ([Fe/H] = −0.7) and the sodium-oxygen anticorrelation (Fig. 3.1). As with some other GCs, there

Table 3.1 — Sources of spectral data for this thesis.

Source	Object	Wavelength coverage	Resolution
van Loon et al. (2007)	ω Cen	3800–5000 Å	1600
AAOmega	47 Tuc and NGC 6752	4040–4300 Å and 5750–6200 Å	6500
SALT MOS	47 Tuc	3700–4500 Å	3000

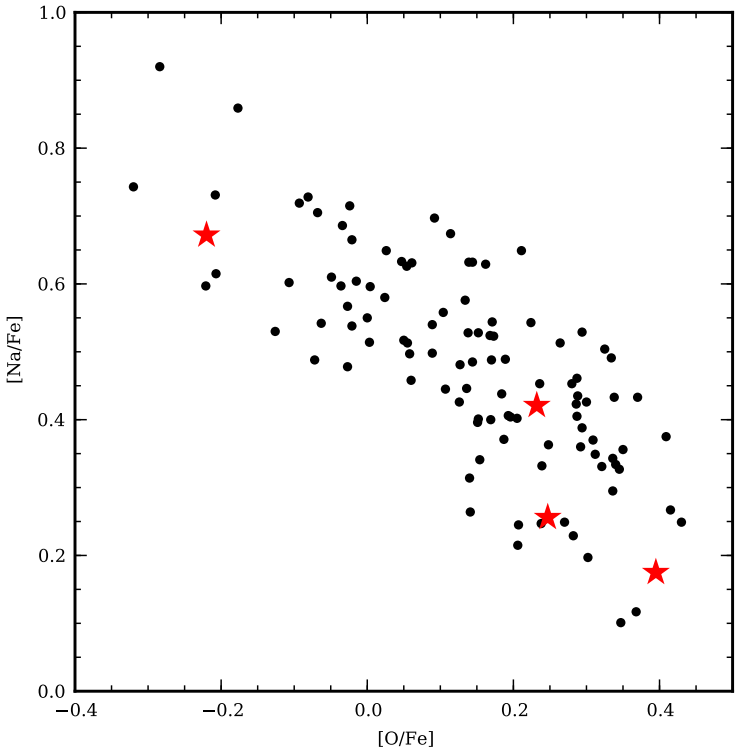

Figure 3.1 — The sodium-oxygen anticorrelation of 47 Tuc (Carretta et al. 2009). The red stars mark those stars that are in common between Carretta et al. (2009) and Worley & Cottrell (2012), which are discussed in Section 3.3.

is now photometric evidence for multiple populations of stars in the cluster (Milone et al. 2012). It has been well studied due to its brightness ($V_{\rm HB}$ = 14.06) and apparent angular size: in the SIMBAD database, there are 2625 references from 1850 to 2012, compared to 2058 for ω Cen. Its southerly position (Dec = −72°) means that it is not possible to observe from the northern hemisphere, but it is well placed for observations from SALT and other observatories in Australia, Chile and New Zealand.

47 Tuc was part of the the focus of two preceding Ph.D. students at the University of Canterbury (Wylie-de Boer 2006; Worley 2009). In part they used the well-studied fiducial star Lee 2525 (Frogel et al. 1981; Norris et al. 1984; Brown et al. 1990; Eggen & J. I. Iben 1991; Brown & Wallerstein 1992; Eggen 1992; Tucholke 1992; Norris et al. 1996; Cayrel de Strobel et al. 1997; Eggen 1998; Ramdani & Jorissen 2001; Worley et al. 2009; Soubiran et al. 2010; Worley et al. 2010). By observing the same star, it is possible to calibrate the abundance results at multiple spectral resolutions and when using different analysis techniques. The usual source of systematic offsets is the placement of the continuum: in high resolution spectra, the true continuum can be more readily identified, while at lower resolution the true continuum is not present. This requires the use of pseudo-continuum points, as described in Section 2.2.

The first set of spectra analyzed in this chapter for 47 Tuc was observed at the Anglo-Australian Telescope (AAT) with the AAOmega instrument in October 2008. A sample of the spectra as shown in Fig. 3.2 and their sky locations in Fig. 3.3. The 94 giant branch (GB) and HB stars were observed by Worley & Cottrell (2012)[1], covering a 2 magnitude range from $12.5 < V < 14.5$ and a colour range of $0.8 < B-V < 1.4$ (Fig. 3.4). The sample of stars covered the RGB, AGB and HB of 47 Tuc and as such provided a good indicator of the temperature sensitivity of

[1]Worley & Cottrell (2012) had 97 stars, but three were not analyzed in this thesis as their $V-K$ colours were not correct. In addition, the photometric temperature determination used in that work was incorrect. However, 13 of the 94 stars had their temperatures determined spectroscopically, and it is these stars that are discussed in Section 3.1.1 with regards to their [Na/Fe].

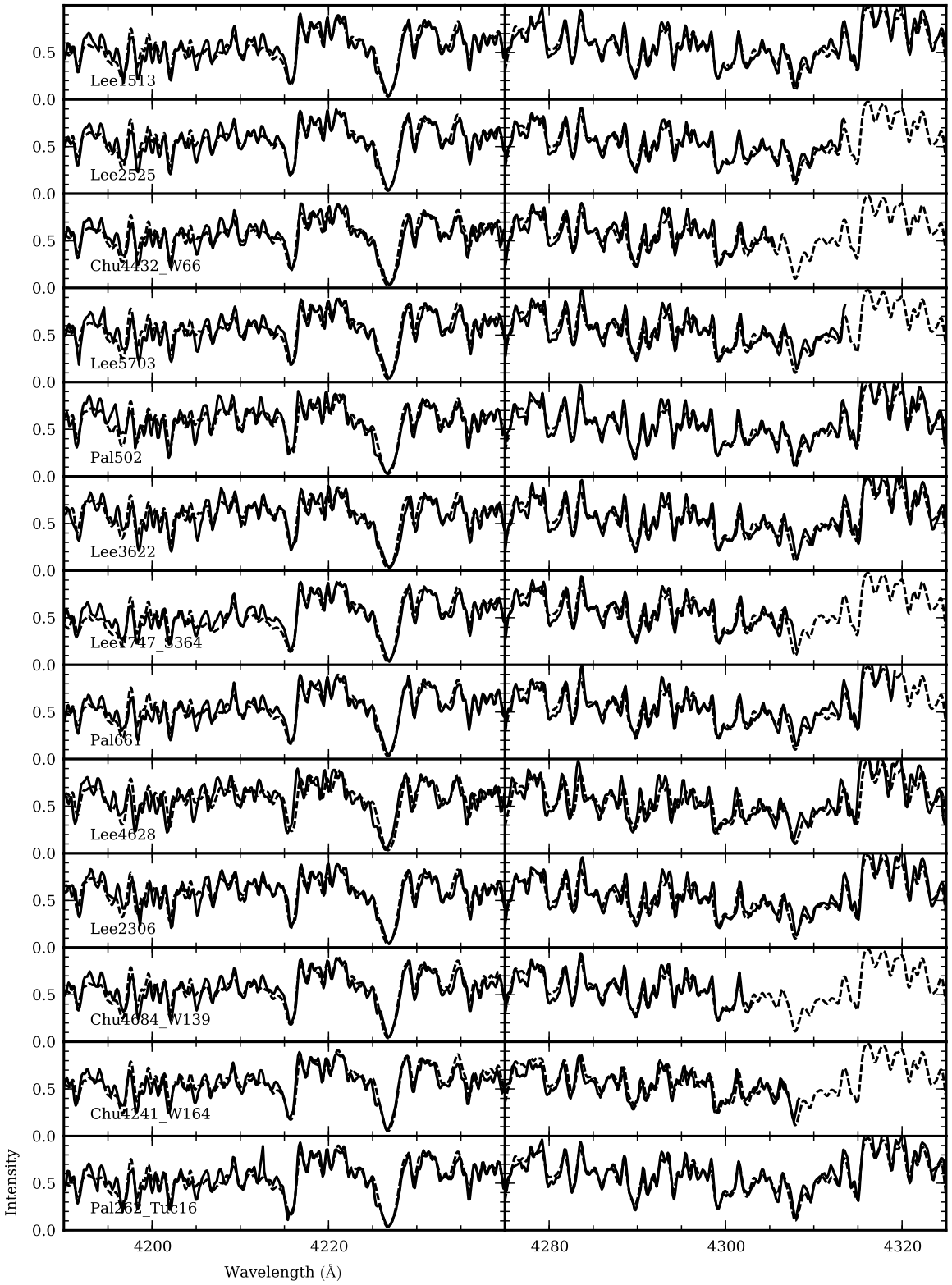

Figure 3.2 — Sample of the AAOmega spectra of 94 stars of 47 Tuc. The solid lines are the observed spectra and the dashed lines are the synthetic spectra fit.

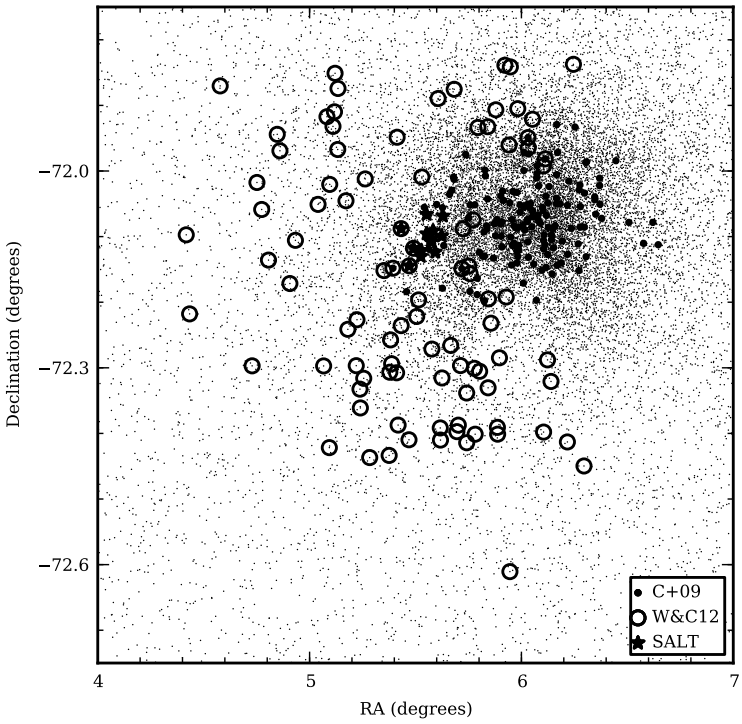

Figure 3.3 — Sky location of different datasets of 47 Tuc over the background of the 2MASS catalogue: Carretta et al. (2009, C+09),Worley & Cottrell (2012, W&C12), and SALT data used in Section 3.2.

the spectral matching pipeline. The spectral resolution was $R \sim 6500$ and the signal-to-noise was 30–50 in the spectral region of interest. The spectra were reduced using the 2dFDR pipeline and continuum normalized by Worley (2013, private communication). An example spectrum is shown in Fig. 3.5 for Lee 2525.

The spectra of 47 Tuc had coverage from 4000–4300 Å (blue arm) and 5750–6200 Å (red arm). This meant that some stars did not have the band head at 4320 Å observed due to the radial velocity dispersion of the cluster, and the changing wavelength coverage with different positions in the field of view of the telescope (i.e., Lee 2525 in Fig. 3.5). As such the [C/Fe] was determined for these stars using a smaller portion of the spectrum than stated in Section 2.6: from 4295 Å to the end of the observed spectrum.

Each star was positionally matched to the Two Micron All Sky Survey (2MASS) to give photometry in the J, H, K band passes. This allowed for the determination of the temperature of the stars from the $V-K$ colour using the method described in Section 2.1. As described in that Section, this colour is much less affected by line blanketing due to metal lines. This reduces the dependency of the temperature determined on the metallicity of the star.

3.1.1 Abundances Determined using Oxygen from Spectral Indices

The spectral library from AAOmega was analyzed in two ways: (1) with the carbon, nitrogen and metallicity determined as per the method described in Section 2.6 (referred to in this thesis as "floating" [Fe/H]); or (2) with the metallicity at a fixed value of [Fe/H] = −0.7. These two methods were used to understand how the [C/Fe] and [N/Fe] determined were affected by using a floating or fixed [Fe/H] for the stars.

As discussed in Section 2.3, knowing the [O/Fe] of the stars is crucial to determining precise and accurate abundances of carbon and nitrogen when using molecular bands. In the case of the 94 stars in 47 Tuc, thirteen had [Na/Fe] determined by Worley & Cottrell (2012). As well as the sodium-oxygen anticorrelation, there also exists a correlation between sodium and nitrogen in GCs (Norris & Pilachowski 1985). Worley & Cottrell (2012) measured

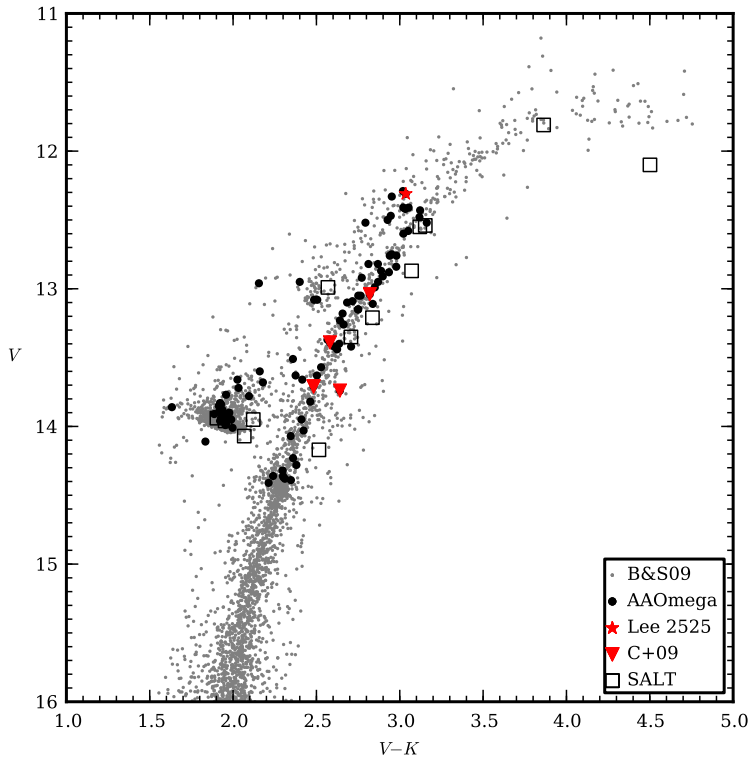

Figure 3.4 — The positions of the 94 stars in 47 Tuc on a V-($V-K$) CMD. The black dots, red star, & triangle symbols are the 94 stars observed by Worley & Cottrell (2012). In order of brightness from brightest to faintest, the red triangles mark the positions of Lee 5717, Lee 2737, Lee 2601, and Lee 5705, the four stars are in common between Carretta et al. (2009) and Worley & Cottrell (2012). For context, the grey dots show a combination of photometry from Bergbusch & Stetson (2009, B&S09) and 2MASS. Also indicated are the 13 SALT stars.

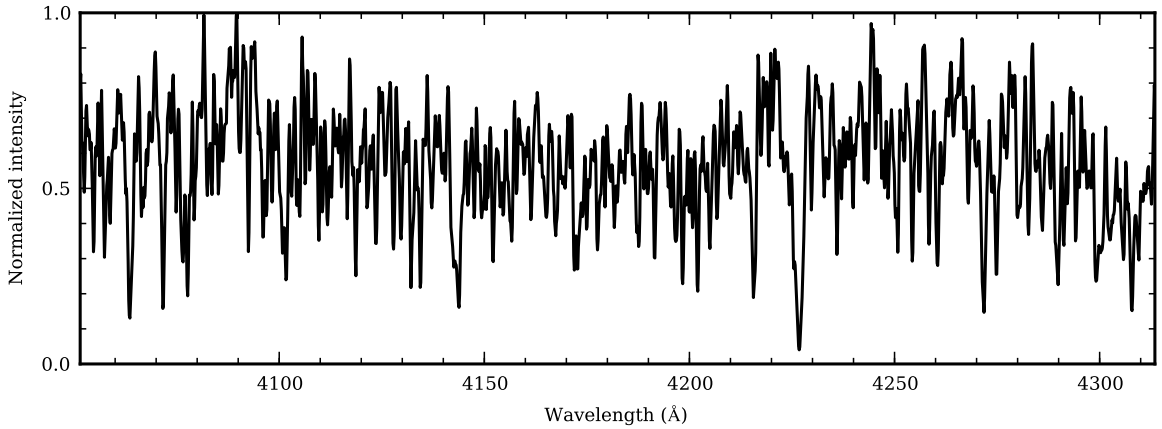

Figure 3.5 — The spectrum of Lee 2525 as observed by AAOmega. It is an example of one of the stars which did not have the full wavelength coverage to include the 4320 Å CH band head.

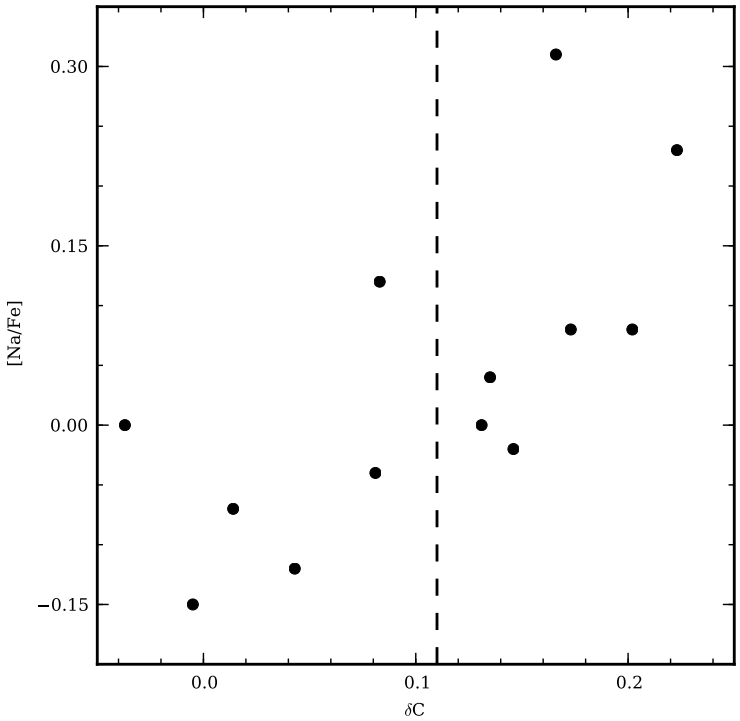

Figure 3.6 — Reproduction of Figure 10 of Worley & Cottrell (2012) showing the correlation between their CN-sensitive δC spectral index and the [Na/Fe] determined for 13 stars. The dashed line is at $\delta C = 0.11$ and divides the CN-weak stars from the CN-strong stars, which was used to define if a star was Na poor or Na rich, and therefore O rich or O poor, respectively.

the CN-sensitive δC spectral index, defined by them,

$$\mathrm{S}(4142) = -2.5 \log \left(\frac{\int_{4120}^{4216} F_\lambda d\lambda}{\int_{4216}^{4290} F_\lambda d\lambda} \right), \tag{3.1}$$

$$\mathrm{C}(4142) = 0.742 \times \mathrm{S}(4142) + 0.236, \tag{3.2}$$

$$\delta\mathrm{C} = \mathrm{C}(4142) - [0.304(B-V) - 0.275]. \tag{3.3}$$

This spectral index correlated with the sodium abundance of the stars and the Na-rich/Na-poor stars could be divided at an index value δC = 0.11 (Fig. 3.6). Therefore having a δC > 0.11 meant the star was Na-rich and therefore O-poor, and vice versa. For stars with δC > 0.11, the oxygen abundance was estimated to be [O/Fe] = −0.2, and for those with δC ≤ 0.11 the estimate was [O/Fe] = +0.4. These estimated [O/Fe] values were based upon the sodium-oxygen anticorrelation (Fig. 3.1). Of the 94 stars, 49 (52 %) were classified as CN-rich per their δC index.

These spectra were continuum normalized, in the same way as described in Section 2.2, by Worley (2013, private communication) using a template of α Boo for all the stars, which has a similar temperature and metallicity (T_{eff} = 4290 K, [Fe/H] = −0.50) as the GB stars of 47 Tuc. Initially the stars were analyzed by the spectral matching pipeline using this continuum placement but it was found that there was a correlation between the temperature of the star and the metallicity determined (Fig. 3.7). The coolest stars had [Fe/H] ∼ −0.9, while the hottest HB stars were [Fe/H] ∼ −0.2 (T_{eff} = 1000 K hotter than α Boo). It was found that the depression of the continuum as determined by MOOG for the hotter stars was less than that determined by Worley (2013) using the α Boo template (Fig. 3.8). This therefore required a much higher metallicity to return the same EW of the Ca I line in both the observed and synthetic spectra. To compensate for this, a simple multiplicative shift was applied to force the position of the left-hand edge of the Ca I line to be at the same intensity in the observed and synthetic spectra.

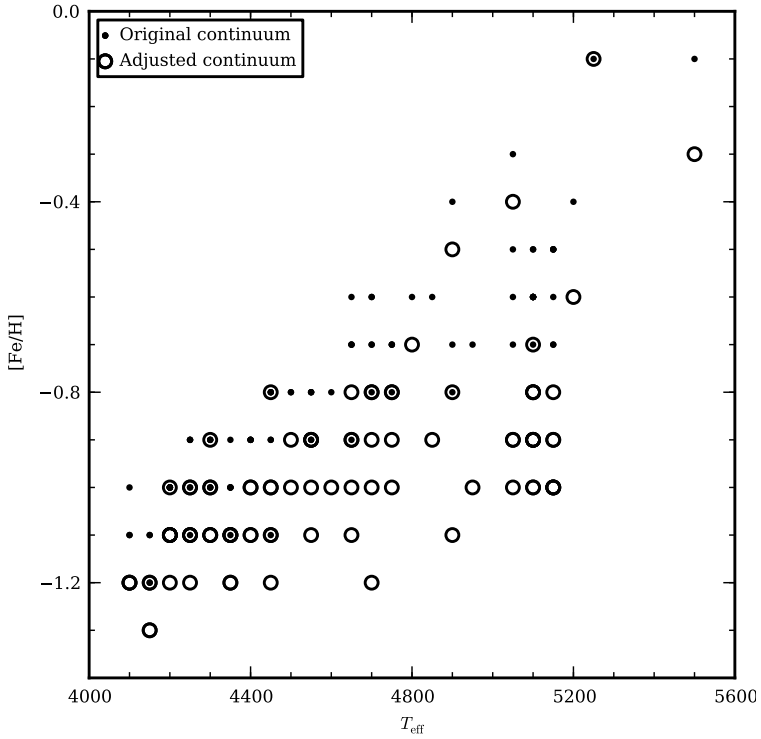

Figure 3.7 — The trend of the determined [Fe/H] with $T_{\rm eff}$ for the 47 Tuc stars with AAOmega spectra. With the original continuum placement of Worley (2013), the hottest stars were found to be much more metal rich than those with the continuum adjustment to correct for the use of the α Boo template for all the stars.

The values discussed in this chapter were found using the spectra for which this continuum adjustment had been applied.

Figure 3.9a presents the [Fe/H] of the 47 Tuc stars determined using the calcium line. It is obvious that the method returned a metal poorer value than the accepted metallicity of [Fe/H] = −0.70. In this case the $\langle$[Fe/H]$\rangle$ = −0.94 ± 0.20, which is about 0.2 dex metal-poorer than the literature value for the cluster. The distribution of metallicities is symmetrical about this mean value, which would imply that the scatter is caused by the fact a single [Ca/Fe] was used for all the stars, whereas there is a small range of calcium abundances in the cluster: an interquartile range of 0.4 dex was found by Koch & McWilliam (2008a,b). The systematic offset means that the EW of the Ca I 4226 Å line was not as great as MOOG determined for the stars, possibly caused by a further continuum placement problem.

[C/Fe] and [N/Fe] individually are bimodal and are anticorrelated with each other (Figs. 3.9b, 3.9d and 3.10a) for the floating [Fe/H] analysis. There is one group of stars with a peak at [C/Fe] = −0.4 and [N/Fe] = 0.8 (49 stars) and one group at −0.8 and 1.7 (45 stars) respectively.For the fixed [Fe/H] analysis, the [C/Fe] distribution is flatter (Fig. 3.9c), while the [N/Fe] abundances are multimodal (Fig. 3.9d).

The differences between the carbon and nitrogen abundances from the two metallicity values for each stars are shown in Fig. 3.11. Neither [C/Fe] nor [N/Fe] have a trend between the [X/Fe] found with the floating and fixed [Fe/H]. The lower metallicity determined from the calcium line compared to the canonical [Fe/H] required that [C/Fe] and [N/Fe] be larger to compensate and match the band strength of the observed spectrum. [C/Fe] was on average 0.1 dex smaller, while for [N/Fe] the N-poor stars decreased 0.2 dex and the N-rich stars decreased by 0.4 dex. Overall, this did not change the distribution of stars in the [C/Fe]-[N/Fe] abundance plane (comparing Figs. 3.10a and 3.10b) as can be seen in Figs. 3.11a and 3.11b where there is a one-to-one trend. As would be expected from their [N/Fe] abundances, the two groups are split in their δC index values, with N-poor group have an average of $\langle\delta C\rangle$ = 0.06 ± 0.05 and the N-rich group have $\langle\delta C\rangle$ = 0.18 ± 0.04 (for the floating [Fe/H]). In Fig. 3.12,

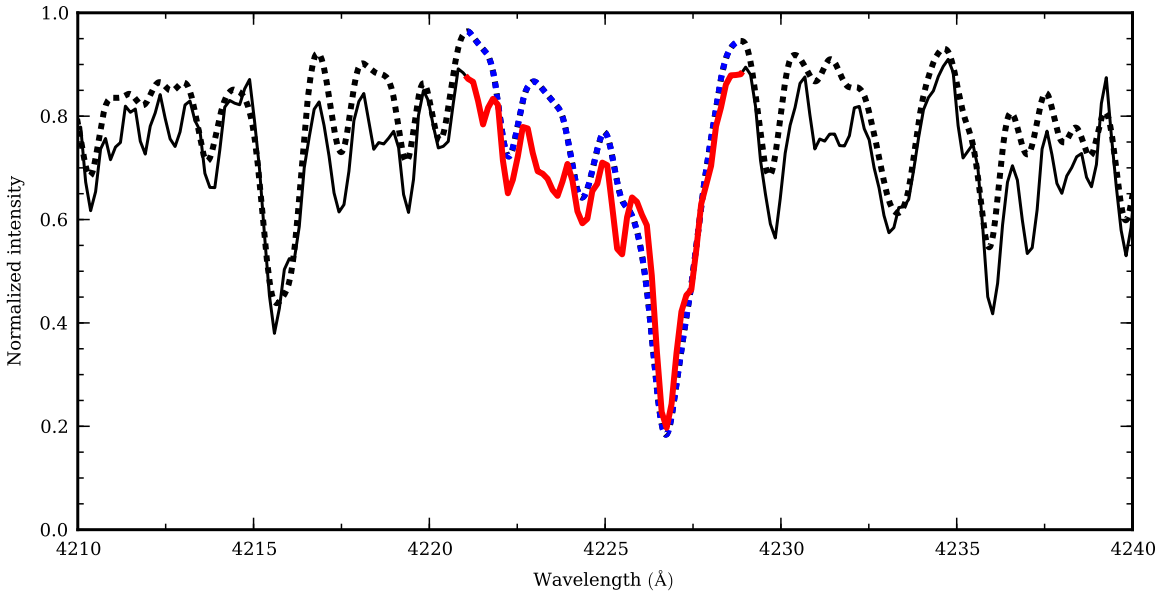

Figure 3.8 — An example of the continuum placement problems for the hot stars (in this case, Lee 1315; $T_{\rm eff}$ = 5100 K). The dotted line shows the synthetic spectrum and the solid line the observed spectrum. The thicker red line and thicker dotted blue line show the regions of the observed and synthetic spectra that was used to calculate the EW of the Ca I line. The synthetic spectrum is not depressed as much as the observed spectrum meaning that in order to achieve the same EW it is necessary to increase the metallicity of the model atmosphere.

the correlation between the δC spectral index (defined to be sensitive to the CN feature at 4142 Å) and [N/Fe] is confirmed. This is of course not unexpected but is a useful validation of the correctness of the spectral matching pipeline when it comes to the nitrogen abundance.

3.1.2 Abundances Determined using [O/Fe] derived from [Na/Fe]

Unlike the more complicated sodium-oxygen anticorrelation of ω Cen (e.g., Fig. 1.7), where sodium-rich and sodium-poor stars can be at the same oxygen abundances, it is possible to use the [Na/Fe] of a star in 47 Tuc to get a good estimate of its [O/Fe]. In this thesis the results of Carretta et al. (2009) were used in conjunction with sodium abundances for all 94 stars (Worley 2013, private communication). A parabola was fitted through the distribution of sodium and oxygen abundances of Carretta et al. (2009) and was used to interpolate [O/Fe] from [Na/Fe]. It was required to additively adjust the [Na/Fe] of Worley (2013) by 0.4 dex to have them on the same abundance scale as Carretta et al. (2009). The abundance determination proceeded as described in Sections 2.6 and 3.1.1, with the two analyse: one using a floating [Fe/H]; and one using a fixed [Fe/H].

Repeating the same analysis as in the previous section, histograms and scatterplots were created. Again it was found that there was an underestimation of the metallicities of the stars (Fig. 3.13a) with the average metallicity of $\langle$[Fe/H]$\rangle$ = −1.08 ± 0.20. Comparing Figs. 3.9b and 3.9c to Figs. 3.13b and 3.13c, there is no longer any bimodal behaviour of the [C/Fe] abundances. Both Figs. 3.13b and 3.13c instead show a single peak. Looked at from a slightly different angle, Figs. 3.14a and 3.14b show that the [N/Fe] to [C/Fe] distribution is steeper than in Figs. 3.10a and 3.10b, which corresponds to the smaller range of [C/Fe] found in the histograms. The difference in [Fe/H] again manifests itself as a systematic difference between the abundances found for the fixed and floating analyses (Fig. 3.15).

In the previous Section, the δC index was used to estimate that [O/Fe]. For those stars that were classified O-rich previously, their mean oxygen abundance in this Section was 0.17 ± 0.23 dex and for the O-poor stars it was 0.03 ± 0.36 dex, where previously it was 0.4 and −0.2 respectively. Using the two extreme oxygen abundances in

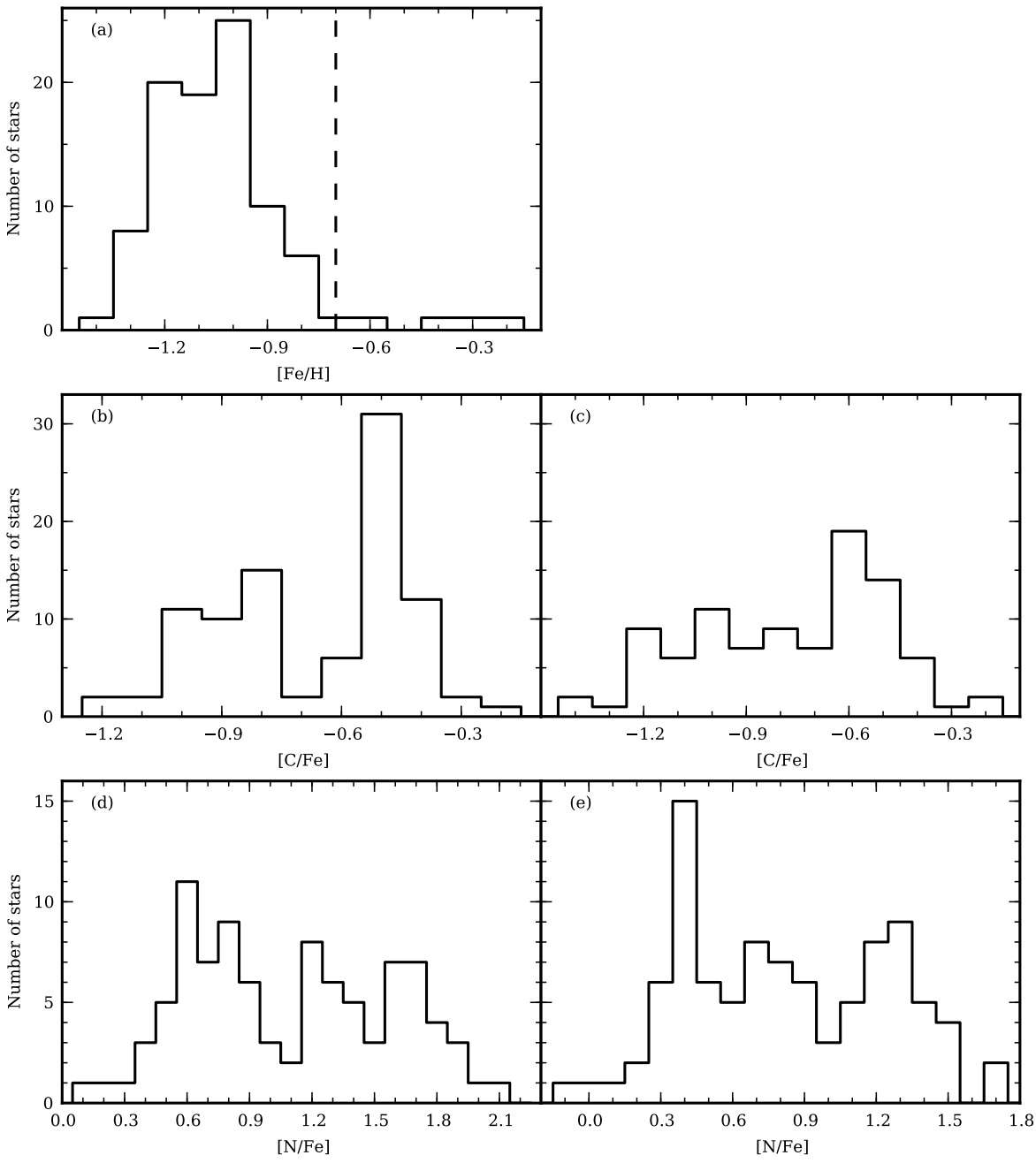

Figure 3.9 — Histograms of [Fe/H], [C/Fe] and [N/Fe] determined for 47 Tuc stars with [O/Fe] determined from the δC, using the AAOmega spectra. (a), (b) & (d) show the abundances that were determined with a floating [Fe/H], and (c) & (e) show the abundances when the metallicity was fixed at [Fe/H] = −0.7. The dashed line in (a) shows [Fe/H] = −0.7 for comparison.

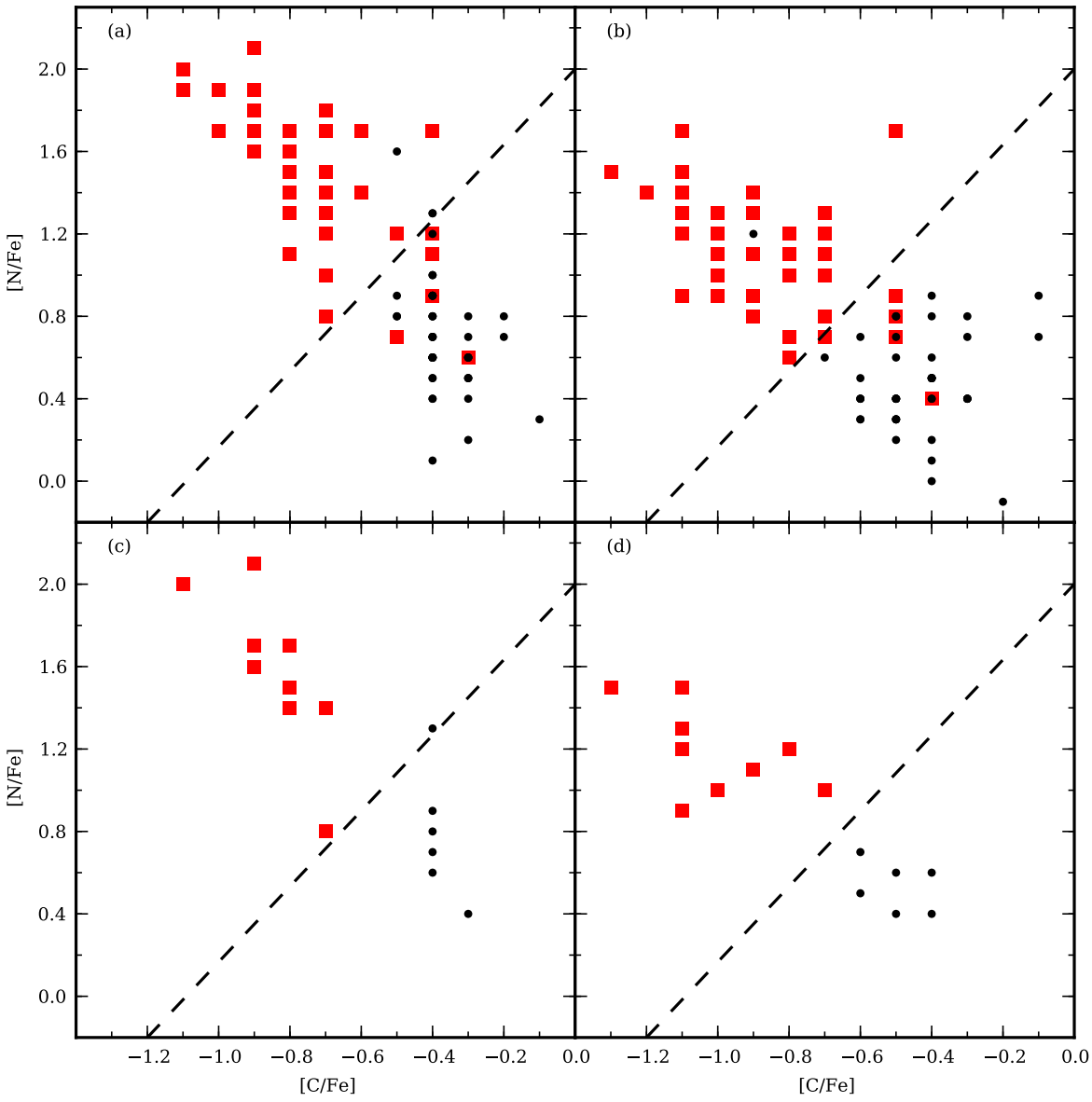

Figure 3.10 — The [N/Fe] and [C/Fe] for 47 Tuc stars using the AAOmega spectra, with [O/Fe] determined from the δC. Abundances determined with: (a) & (c) floating [Fe/H]; (b) & (d) fixed [Fe/H]. In (c) & (d) only those stars on the AGB are shown. In all panels, the red squares are stars where $\delta C > 0.11$ ([O/Fe] = −0.2) and the black dots are for $\delta C \leq 0.11$ ([O/Fe] = +0.4). The dashed line is the same in all panels and can be used to separate the N-rich group from the N-poor group.

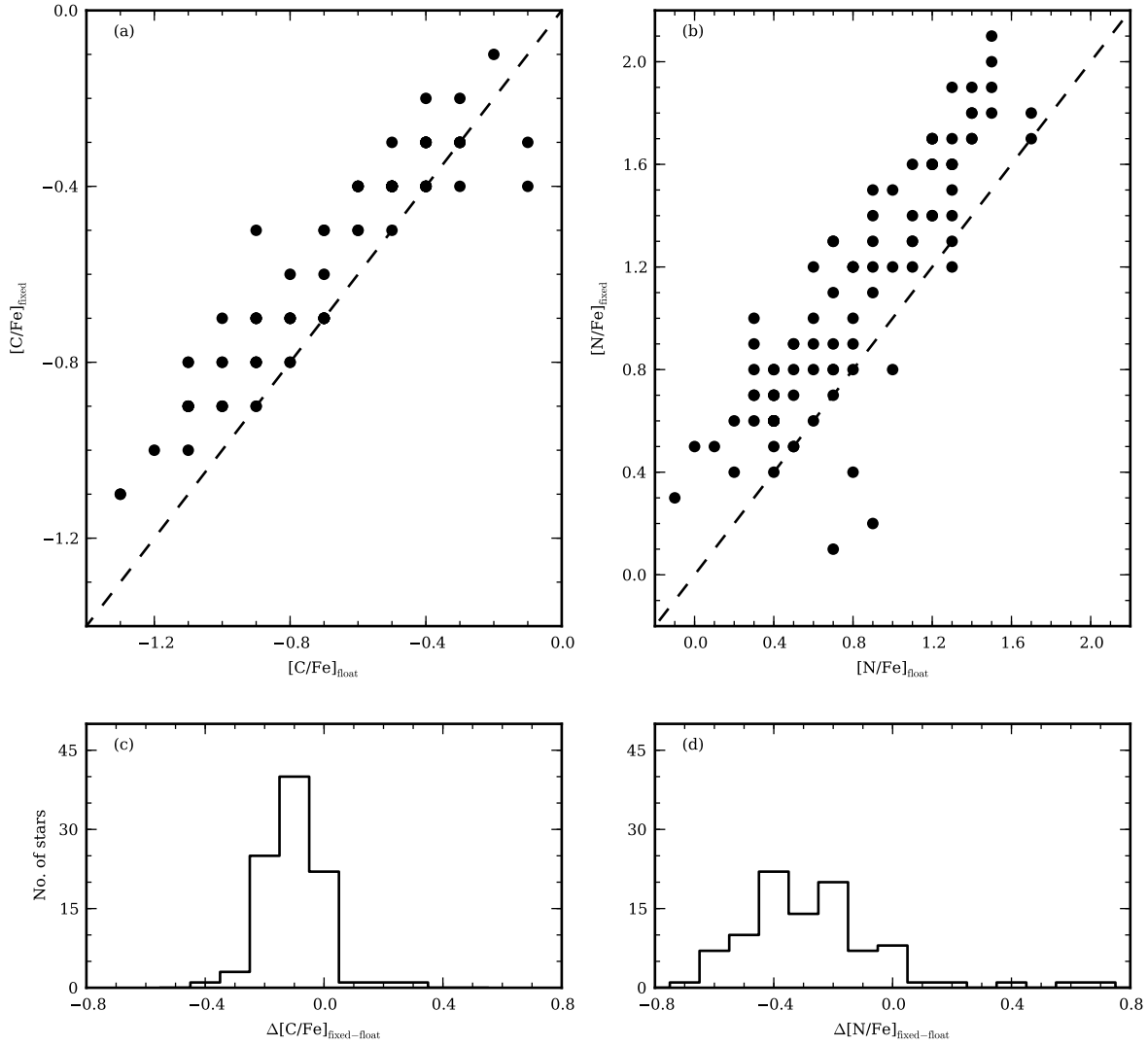

Figure 3.11 — Differences for the abundances found for 47 Tuc stars using AAOmega spectra for the different metallicity values ($[X/Fe]_{Ca} - [X/Fe]_{fixed}$) when using [O/Fe] derived from δC. (a) & (c) [C/Fe] and (b) & (d) [N/Fe].

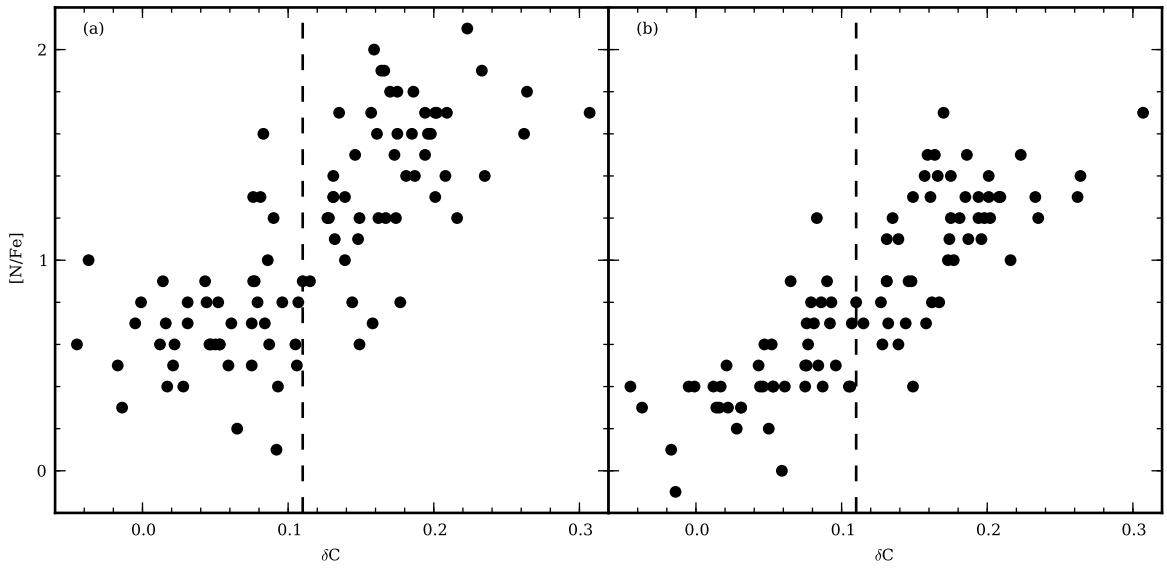

Figure 3.12 — The correlation between [N/Fe] and δC, found for the 47 Tuc stars using the AAOmega spectra: (a) using the floating [Fe/H]; and (b) using the fixed [Fe/H]. The [O/Fe] abundance was derived from the δC index.

the previous Section caused the [C/Fe] to have a larger range than when using an individualized [O/Fe] in this Section. This can be seen in Figs. 3.16a and 3.17a, where the [C/Fe] found for the C-rich stars from $[O/Fe]_{\delta C}$ is bigger than those found from $[O/Fe]_{Na}$, while for the C-poor stars the [C/Fe] is smaller.

The [N/Fe] abundances show a similar range and hints of bimodality (or even trimodality) in Figs. 3.13d and 3.13e as in Figs. 3.9d and 3.9e. This is supported by the scatterplots (comparing Figs. 3.14a and 3.14b to Figs. 3.10a and 3.10b) and the comparison between the abundances found from the two different oxygen abundances (Figs. 3.16b, 3.16d, 3.17b and 3.17d). Again there is a good correlation between the δC index and the [N/Fe] abundance (Fig. 3.18). There is no obvious trend between the [N/Fe] abundance found by one method and that [N/Fe] found by another (unlike for [C/Fe] in Figs. 3.16a and 3.17a). There is however an average systematic offset of 0.07 dex between the [N/Fe] derived from the $[O/Fe]_{Na}$ compared to [N/Fe] derived from $[O/Fe]_{\delta C}$ (Figs. 3.16 and 3.17). This systematic offset is not the result of the [Fe/H] difference derived from the two [O/Fe] abundances, where only 28/94 (30 %) of the stars had any difference between the [Fe/H] abundances (Fig. 3.19). The systematic difference exists even for the analysis where the [Fe/H] was fixed at −0.7 for all the stars (Figs. 3.17b and 3.17d). Since the [C/Fe] abundance was somewhat larger for the analysis using δC derived [O/Fe] (Figs. 3.16b and 3.17b), this would require the [N/Fe] to be smaller to result in the same strength of the CN band head used in the analysis (with more carbon available from the increased [C/Fe], less nitrogen is required to form the same amount of CN in the atmosphere of the star). This does not appear to explain why there is a very systematic offset, as some of the stars having lower [C/Fe] in the δC analysis compared to the [Na/Fe] analysis. However since the effect is small (~ 0.1 dex), it was not a concern and does not invalidate the results presented in this thesis.

The resolution of the AAOmega spectra (R ~ 6000) is three times that of the 2dF spectra of the van Loon et al. (2007) spectral library used in Chapters 4 and 5. It was therefore decided to observe a selection of 47 Tuc stars with a lower resolution to provide a bridge between the higher and lower spectral resolutions.

3.2 SALT MOS Spectra of 47 Tucanæ

In September 2012, the Robert Stobie Spectrograph (RSS) on SALT was used to observe 23 evolved stars of 47 Tuc. This spectra provided a spectral resolution (R ~ 3000), intermediary to the resolution of AAOmega (R ~ 6000) and 2dF (R ~ 1600). Of the 23 stars, 17 were observed with 1.″5 slits and 5 were alignment stars with slit widths of 5″. The

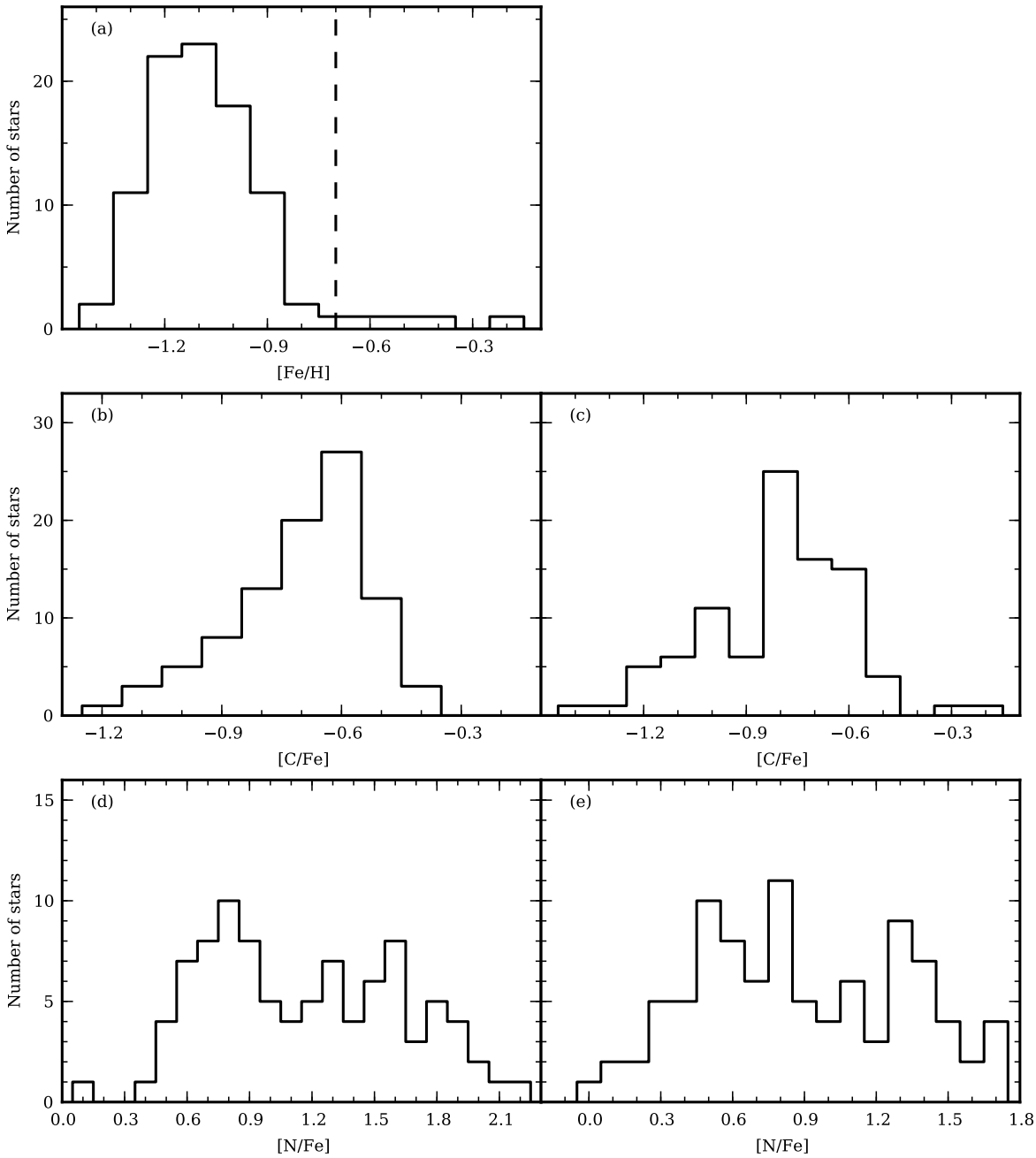

Figure 3.13 — Same as Fig. 3.9, but with abundances determined from [O/Fe] derived from [Na/Fe].

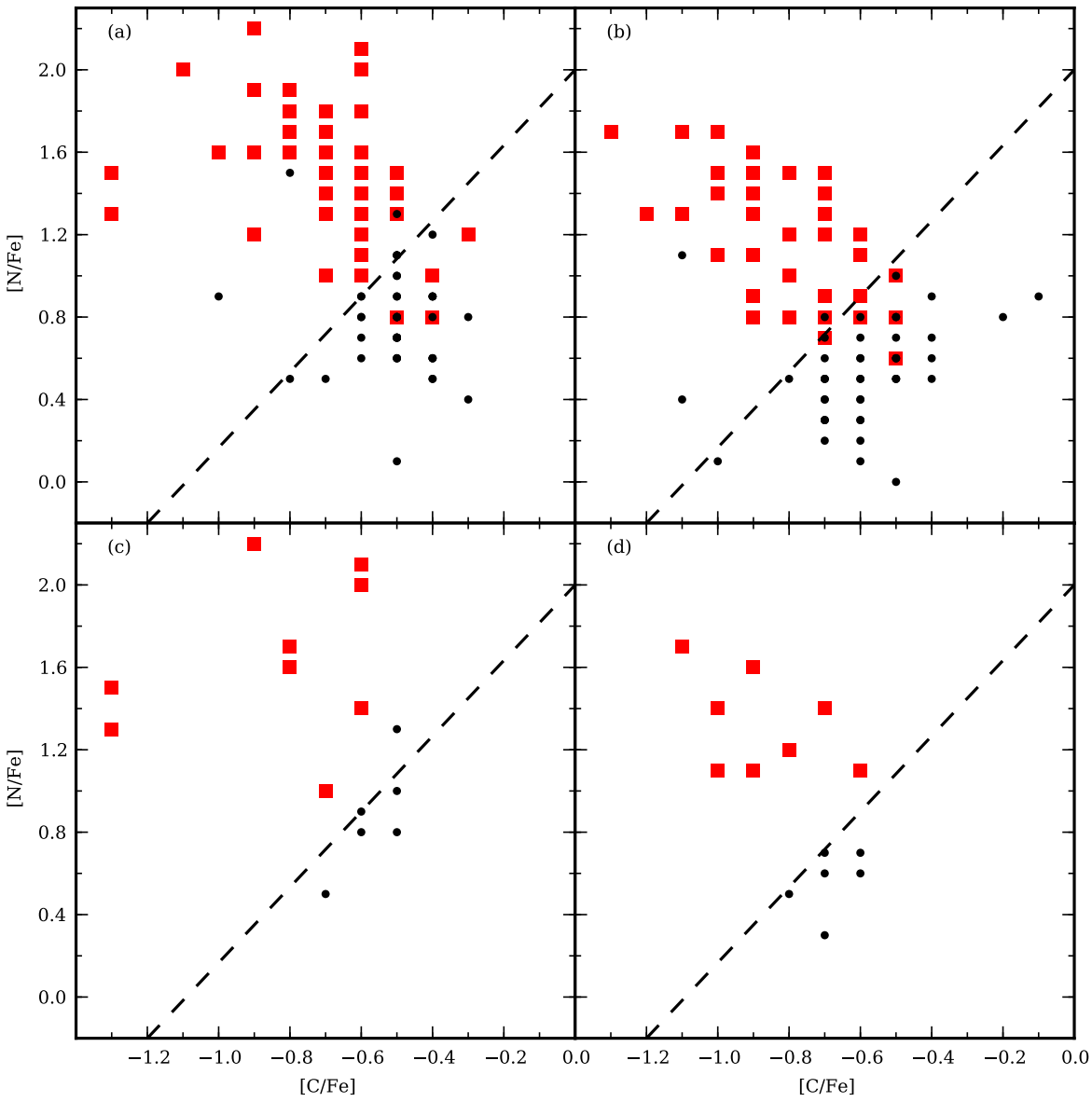

Figure 3.14 — Same as Fig. 3.10, but with abundances determined from [O/Fe] derived from [Na/Fe].

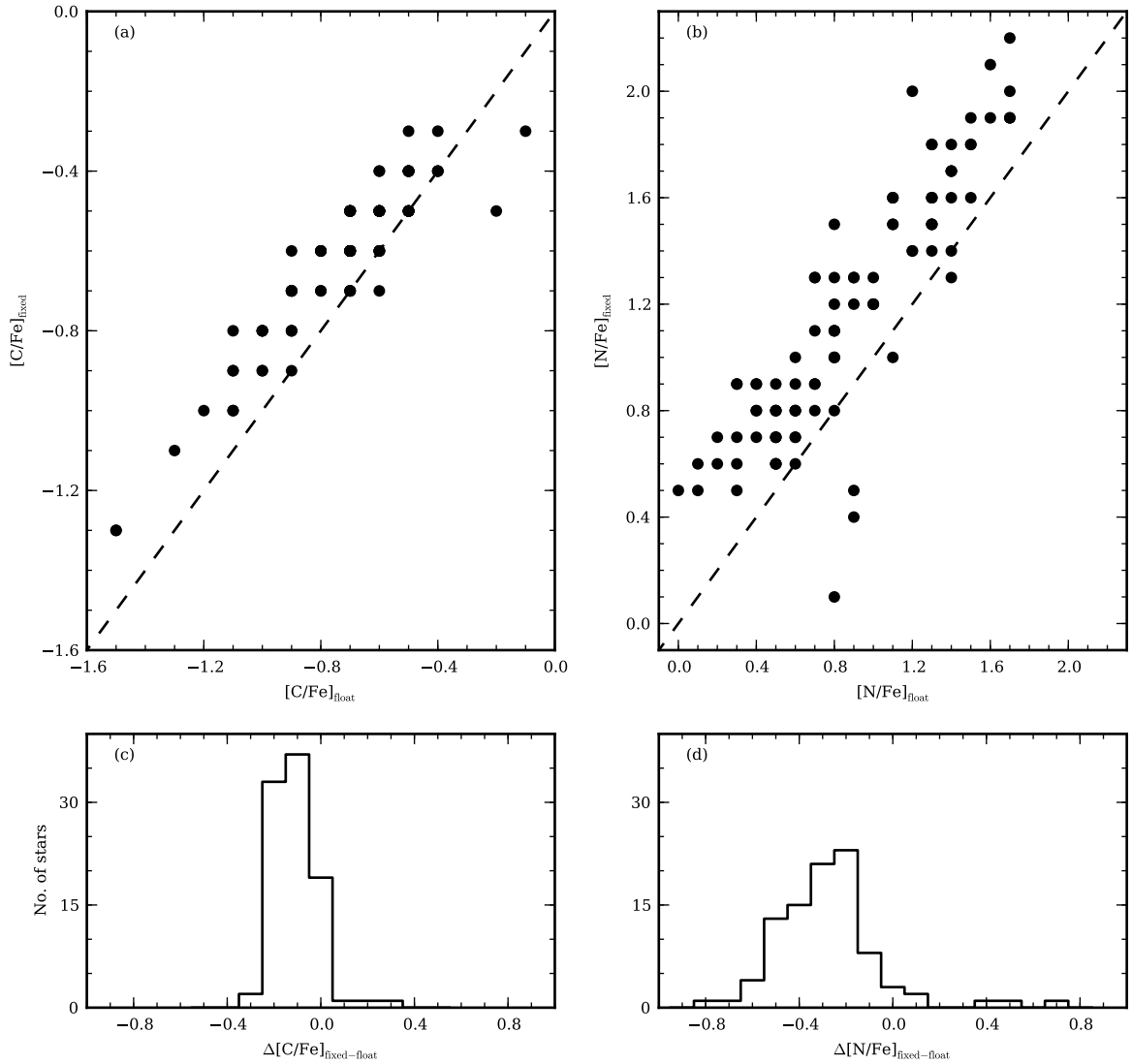

Figure 3.15 — The same as Fig. 3.11 but for a [Na/Fe]-derived [O/Fe].

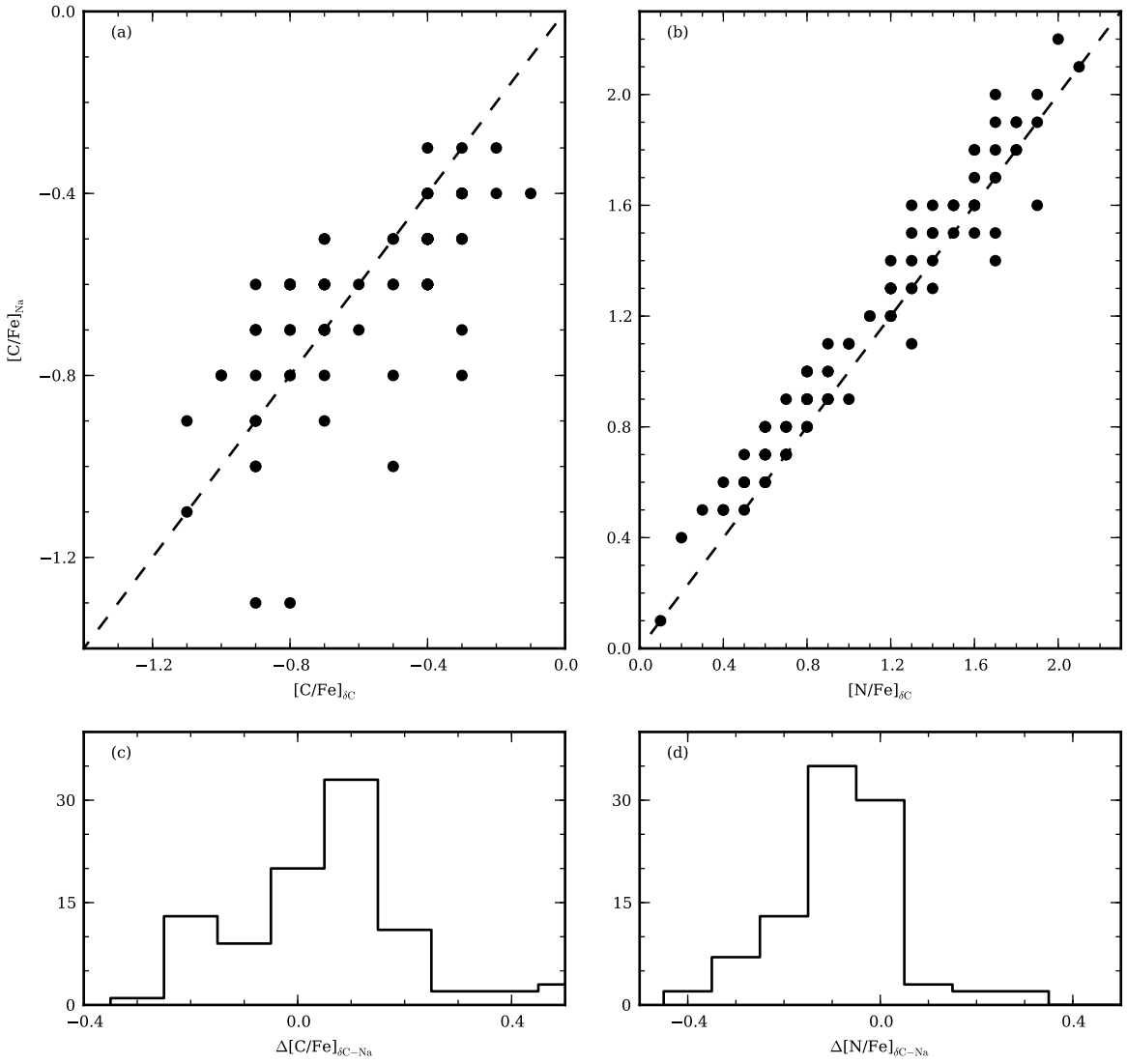

Figure 3.16 — Comparison of the (a) & (c) [C/Fe], and (b) & (d) [N/Fe] abundances (using a floating [Fe/H]) found for the different methods of estimating the [O/Fe] of the 47 Tuc stars (from δC or [Na/Fe]).

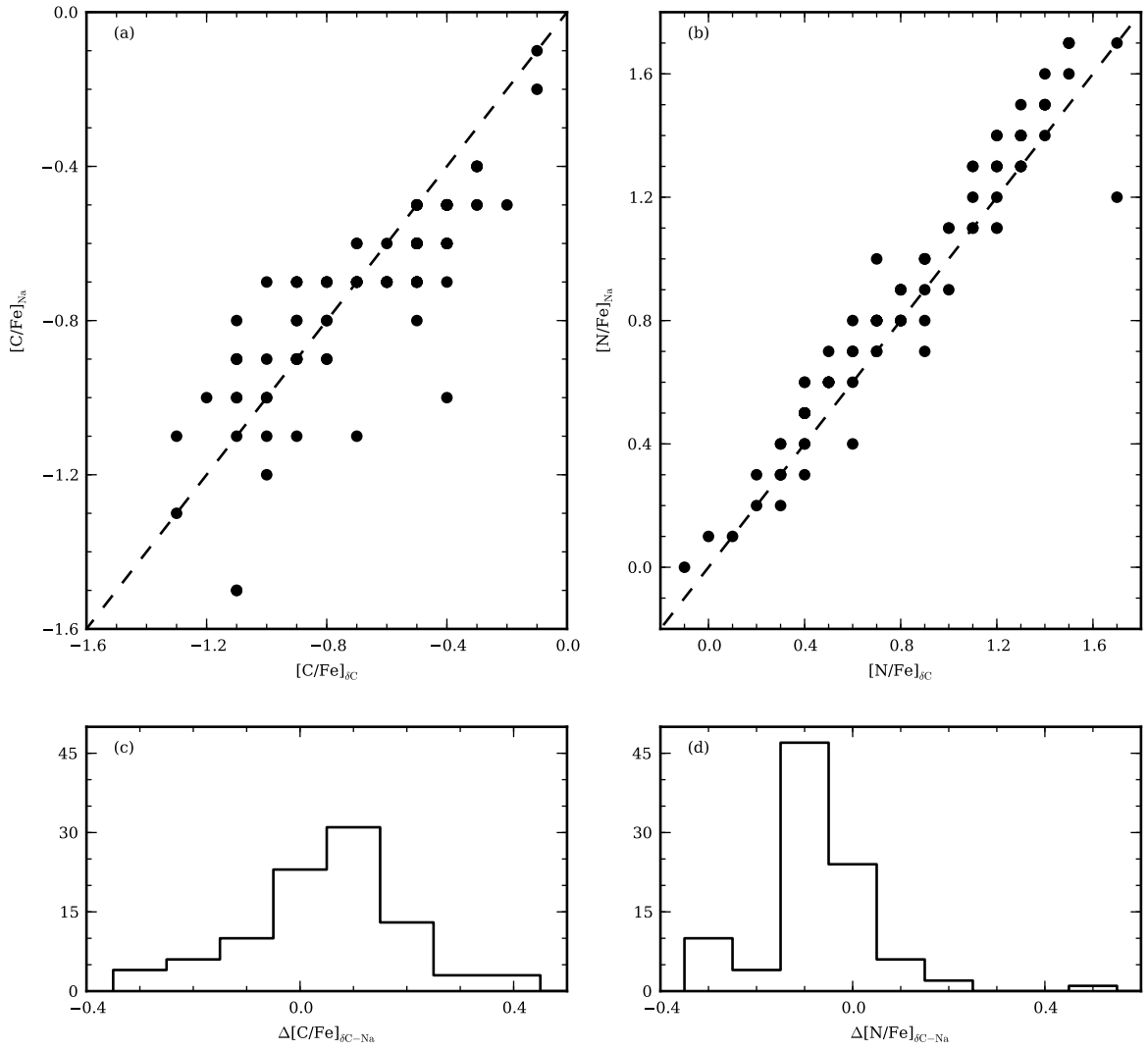

Figure 3.17 — The same as Fig. 3.16 but for a fixed [Fe/H].

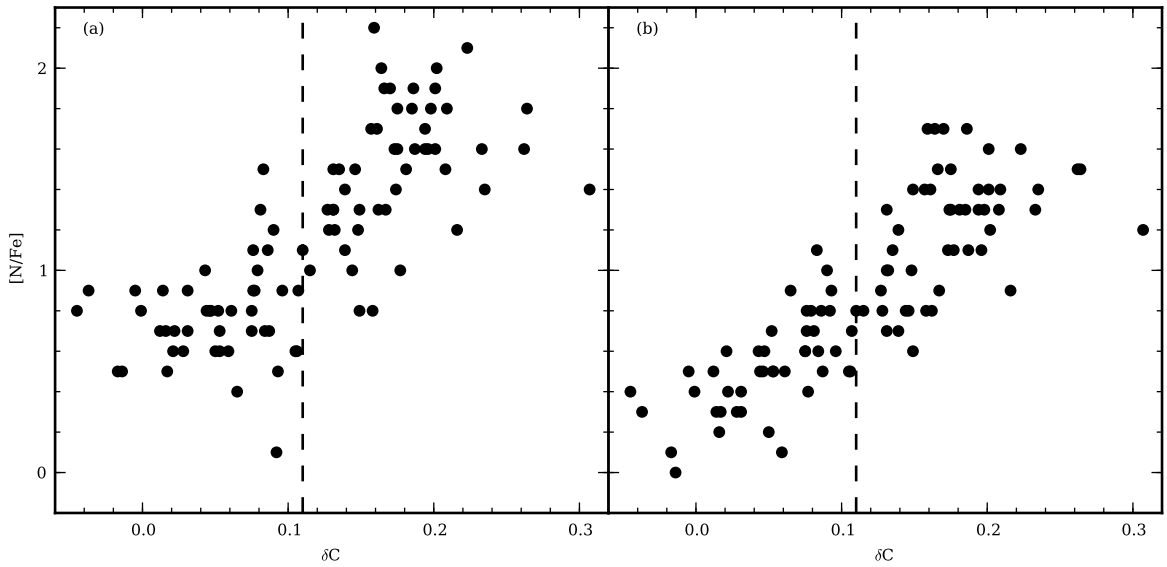

Figure 3.18 — Same as Fig. 3.12 but with [O/Fe] derived from [Na/Fe].

alignment stars have usable spectra, but have not been analyzed in this thesis as their spectral resolution ($R \sim 1000$) is lower than 2dF. Analysis of them will be conducted at a later date. The spectra were reduced by Cottrell (2013, private communication) using PyRAF (Crawford et al. 2010). Cosmic-ray removal and sky subtraction were undertaken by the candidate. One complication of the SALT spectra is that the detector of RSS consists of three CCDs side by side, such that there are two gaps in the spectra. This means that there are portions of the spectra missing for the stars, which in some cases occurs in regions of the spectrum that are used for continuum fitting or abundance determination. Examples of these missing portions can be seen for Lee 2707, Lee 3708, and Pal 661 in Fig. 3.20. Unfortunately four of the 17 stars had this occur, so their spectra was not analyzed for this thesis. For three more, the chip gaps fell on the CH and CN molecular band regions so the number of spectrum points used for the determination of [C/Fe] and [N/Fe] was reduced. The spectra and the model fits of one of the analyses is shown in Fig. 3.20

The spectra were analyzed four times: at [O/Fe] = +0.4 or −0.2, and with each oxygen abundance with a fixed [Fe/H] or floating [Fe/H]. The stars were blindly selected so there was no guarantee that they would show a full range of carbon and nitrogen abundances. In this case, the stars appear to be mostly CN-weak (Fig. 3.21). The outlier in Fig. 3.21 (and especially in Fig. 3.21a) is Lee 2705, though it was found to have a metallicity of [Fe/H] = −1.3 and $T_{\rm eff}$ = 3650 K, suggesting the technique may not work very well for the coolest stars at the top of the GB.

There were three matches between this Section and the AAOmega spectra: Lee 2608, Lee 2616 and Pal 661 (Table 3.2). The results were very similar from two independent analyses. The first two stars were classified as oxygen rich via their δC, while Pal 661 was oxygen poor. In both sets of analyses (AAOmega and SALT), Pal 661 was found to be carbon poorer than the other two stars and also nitrogen richer. Each of the different analyses of the stars returned slightly different abundances. However all the abundances are within the expected uncertainties (Section 2.7). This is a very good result: abundance analysis using the same spectral matching pipeline of spectra at different resolutions ($R \sim 6500$ for AAOmega versus $R \sim 3000$ for SALT) meant that the pipeline was able to return consistent results. This meant that it could be applied to the lower resolution spectra of van Loon et al. (2007) and the abundances determined would be consistent and astrophysically useful.

3.3 Discussion of 47 Tuc Results

There were the four stars that were in common between Carretta et al. (2009) and Worley (2013) (Table 3.3). This allowed for a direct comparison of the [Na/Fe] derived by the two works. For their sample of 47 Tuc stars,

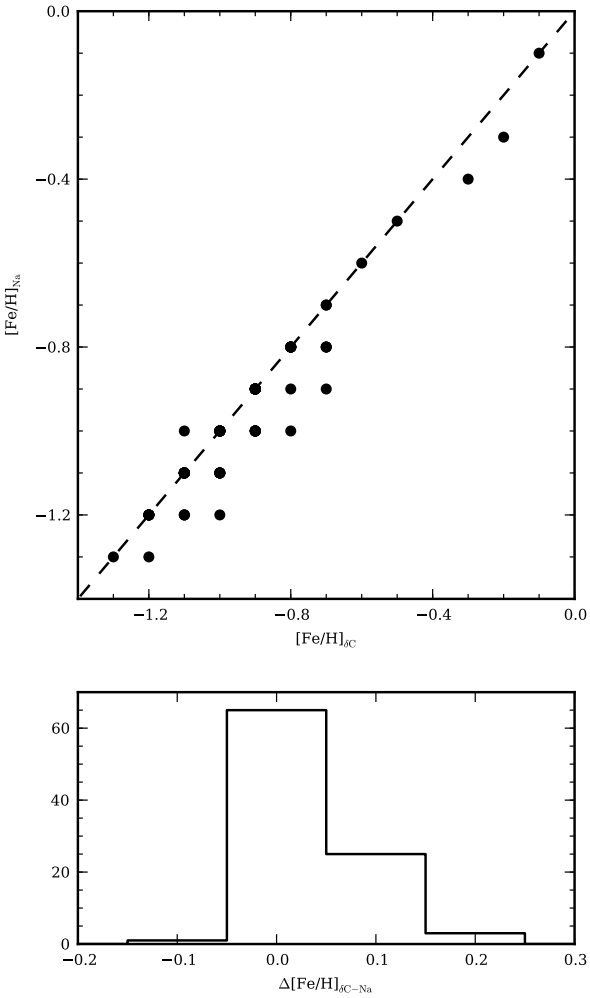

Figure 3.19 — Comparison of the [Fe/H] found when using different methods of estimating the [O/Fe] of the 47 Tuc stars (from δC or [Na/Fe]).

Carretta et al. (2009) found $\langle$[Fe/H]$\rangle$ = −0.74 ± 0.03, while Worley (2013) adopted a [Fe/H] = −0.7 for all their stars. Although there is a scatter between these [Na/Fe] values, we are comparing abundance analysis performed on high resolution ($R > 22,000$; Carretta et al. 2009) to results from lower resolution spectra ($R \sim 6000$). More comparison stars would be required to be definitive as to any systematic offsets between Carretta et al. (2009) and Worley (2013), but it does appear that Worley (2013) found lower sodium abundances than Carretta et al. (2009). This justifies the use of a corrective offset to place the [Na/Fe] abundances of Worley (2013) onto the same scale as Carretta et al. (2009). As mentioned in Section 3.1.2, 0.4 dex was added to the [Na/Fe] abundances of Worley (2013) to match the range of sodium of Carretta et al. (2009).

As discussed in Section 3.1, four analyses were performed on these 94 AAOmega stars. Two used a fixed [Fe/H] (Fig. 3.17) and two allowed the [Fe/H] to be determined (Fig. 3.16). One of each of these two used [O/Fe] estimated from the δC index of Worley & Cottrell (2012), while the other used Na-O anticorrelation and [Na/Fe] as found by Worley (2013). The different analyses found the same results for all the stars in terms of identifying their relative carbon and nitrogen abundances. All returned a carbon-nitrogen anticorrelation. Between the fixed and floating [Fe/H], the changes were systematic. For the different oxygen abundances, [N/Fe] changes were also systematic (though the cause of this is not understood). For [C/Fe], there was not a one-to-one trend. Instead there was a large

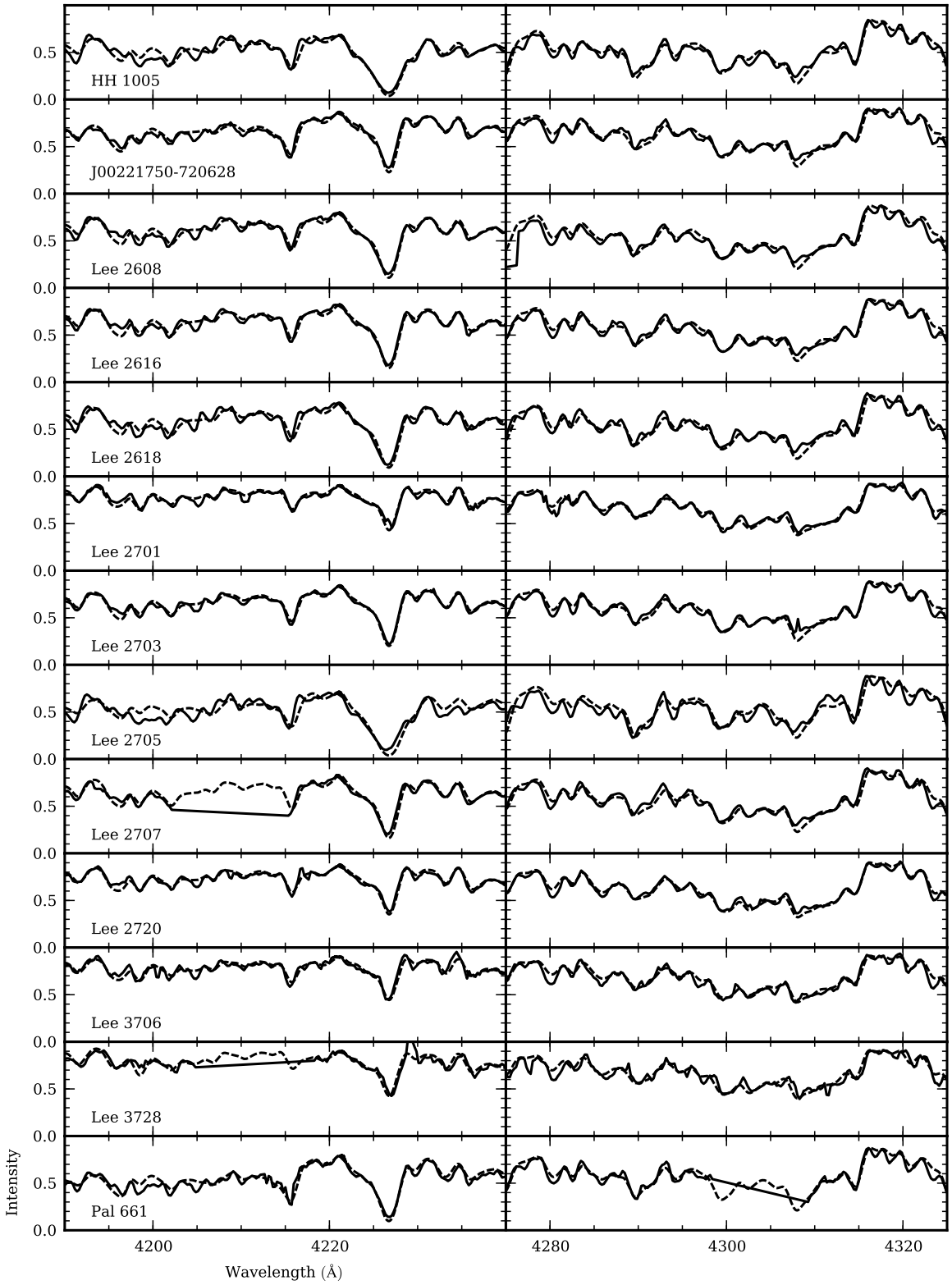

Figure 3.20 — SALT spectra of the 13 stars analyzed for 47 Tuc. The solid line is the observed spectra and the dashed line is the best fitting synthetic spectra. Where there was a chip gap is a long straight line, i.e., for Lee 2707 between 4202–4216 Å.

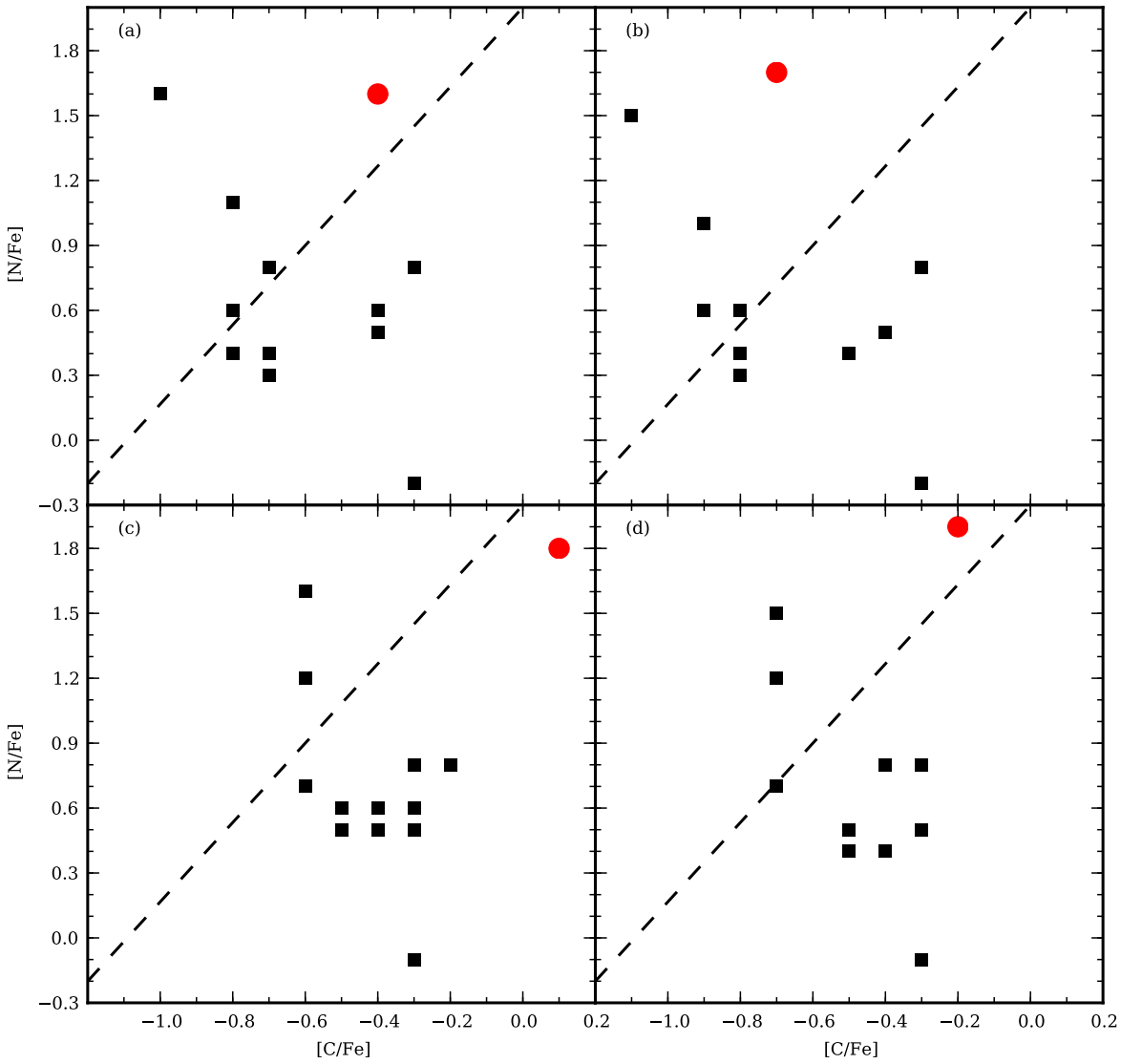

Figure 3.21 — [C/Fe] and [N/Fe] abundances for the 47 Tuc SALT spectra. (a) Floating [Fe/H] and [O/Fe] = −0.2; (b) fixed [Fe/H] and [O/Fe] = −0.2; (c) floating [Fe/H] and [O/Fe] = +0.4; and (d) fixed [Fe/H] and [O/Fe] = +0.4. The red circle marks Lee 2705. The dashed line is the same as in Fig. 3.10.

Table 3.2 — Three 47 Tuc stars in common between AAOmega and SALT spectra.

	PAL 661	LEE 2616	LEE 2608
AAOmega			
$[Fe/H]_{floating,[Na/Fe]}$	−1.3	−1.0	−1.0
$[C/Fe]_{floating,[Na/Fe]}$	−0.6	−0.5	−0.5
$[N/Fe]_{floating,[Na/Fe]}$	+2.0	+0.7	+0.7
$[C/Fe]_{fixed,[Na/Fe]}$	−0.8	−0.7	−0.6
$[N/Fe]_{fixed,[Na/Fe]}$	+1.2	+0.5	+0.3
$[Fe/H]_{floating,\delta C}$	−1.2	−0.9	−1.0
$[C/Fe]_{floating,\delta C}$	−0.8	−0.4	−0.4
$[N/Fe]_{floating,\delta C}$	+1.7	+0.6	+0.7
$[C/Fe]_{fixed,\delta C}$	−1.1	−0.5	−0.5
$[N/Fe]_{fixed,\delta C}$	+1.2	+0.4	+0.3
SALT			
$[Fe/H]_{[O/Fe]=+0.4}$	-1	-0.9	-1
$[Fe/H]_{[O/Fe]=-0.2}$	-1	-0.9	-1
$[C/Fe]_{fixed,[O/Fe]=+0.4}$	-0.7	-0.5	-0.4
$[C/Fe]_{fixed,[O/Fe]=-0.2}$	-1.1	-0.8	-0.8
$[C/Fe]_{floating,[O/Fe]=+0.4}$	-0.6	-0.5	-0.4
$[C/Fe]_{floating,[O/Fe]=-0.2}$	-1	-0.7	-0.7
$[N/Fe]_{fixed,[O/Fe]=+0.4}$	1.5	0.4	0.4
$[N/Fe]_{fixed,[O/Fe]=-0.2}$	1.5	0.3	0.4
$[N/Fe]_{floating,[O/Fe]=+0.4}$	1.6	0.6	0.6
$[N/Fe]_{floating,[O/Fe]=-0.2}$	1.6	0.4	0.4

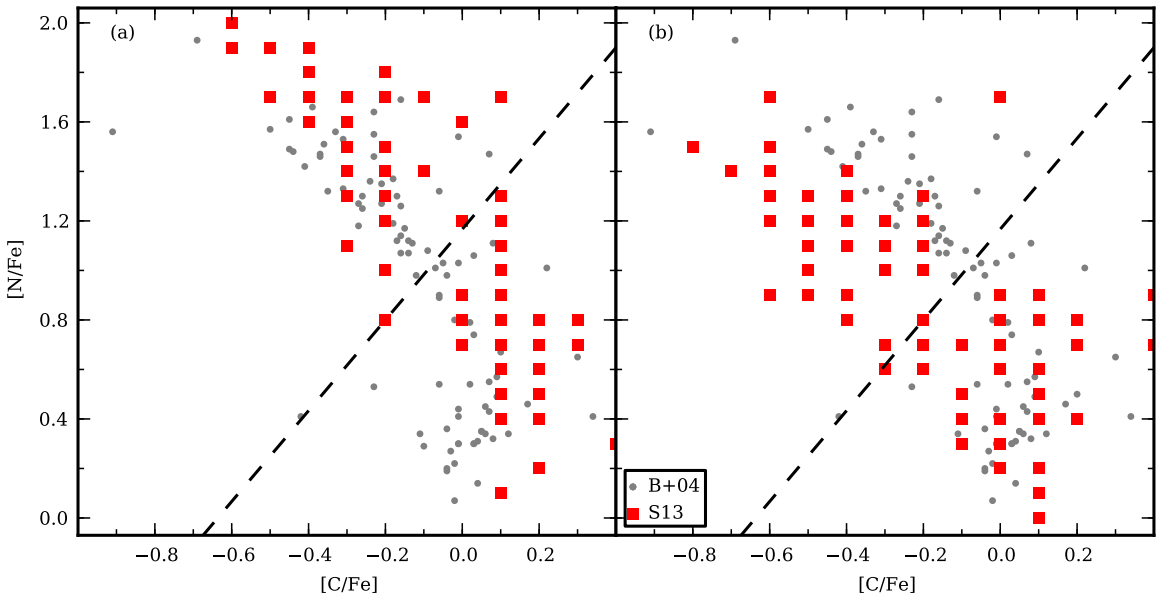

Figure 3.22 — (a) [C/Fe] and [N/Fe] for the stars for the floating [Fe/H] by this work (S13). (b) [C/Fe] and [N/Fe] fixed at [Fe/H] = −0.7 for all the stars.The dashed line is the same as in Fig. 3.10. In both panels, the values determined in this thesis have been shifted: [C/Fe] by 0.5 dex and the [N/Fe] by 0.0 dex. The grey dots show the abundances determined by Briley et al. (2004, B+04) for their MS stars.

Table 3.3 — Four stars in common between Carretta et al. (2009, C+09) and Worley (2013, W&C13).

W&C13 ID	ID C+09	$[Na/Fe]_{W\&C13}$	$[Na/Fe]_{C+09}$	$\Delta[Na/Fe]_{W\&C13-C+09}$
Lee 2601	6808	0.11	0.42	−0.32
Lee 2737	9518	−0.44	0.26	−0.70
Lee 5705	1389	0.38	0.18	−0.20
Lee 5717	42866	−0.10	0.67	−0.77

spread, with the $[C/Fe]_{\delta C}$-poor stars being carbon richer than when using $[O/Fe]_{[Na/Fe]}$. And the $[C/Fe]_{\delta C}$-rich stars had lower carbon for $[O/Fe]_{[Na/Fe]}$. All of this meant that there was a steeper carbon-nitrogen anticorrelation for the $[O/Fe]_{[Na/Fe]}$ results than for the $[O/Fe]_{\delta C}$ results.

There are only a few papers in the literature with determinations of [C/Fe] and [N/Fe] abundances for large numbers of stars in 47 Tuc. Carretta et al. (2005) determined carbon and nitrogen abundances for 9 sub-giant branch (SGB) stars, finding a range of $-0.50 < [C/Fe] < -0.11$ and $-0.35 < [N/Fe] < +1.10$. This covers a similar range to the N-poor group found for the GB and HB stars reported in this thesis. A much larger group of stars was investigated by Briley et al. (2004), although they were looking at unevolved, MS stars, these are compared to this thesis in Fig. 3.22. Their CN-weak group had a range from $-0.1 < [C/Fe] < 0.2$ and $0.0 < [N/Fe] < 0.5$, and their CN-strong group ran from $([C/Fe], [N/Fe]) = (-0.5, +1.5)$ to $(+0.0, +1.0)$. By eye, this would require the [C/Fe] values determined in this thesis to be increased by 0.5 dex and no change to the [N/Fe]. Of course it is not entirely appropriate to compare evolved stars with unevolved stars, due to the former having undergone mixing processes that will change their surface compositions, especially true for carbon and nitrogen. With regards to Lee 2525, only Brown et al. (1990) determined [C/Fe] and [N/Fe] for this star: [Fe/H] = −0.85, [C/Fe] = −0.11, [N/Fe] = 1.10. In this thesis similar values were found using these correction: for the δC analysis, $[Fe/H]_{floating} = -1.2$, $[C/Fe]_{floating} = +0.1$, $[N/Fe]_{floating} = 1.3$, $[C/Fe]_{fixed} = -0.2$, $[N/Fe]_{fixed} = 0.7$; for the [Na/Fe] analysis, $[Fe/H]_{floating} = -1.2$, $[C/Fe]_{floating} = -0.1$, $[N/Fe]_{floating} = 1.3$, $[C/Fe]_{fixed} = -0.2$, $[N/Fe]_{fixed} = 0.7$.

Norris et al. (1981) and Campbell et al. (2010) found that there is a lack of CN-strong stars on the AGB of NGC 6752. For 47 Tuc however, CN-rich AGB stars are found (see Figs. 3.10c, 3.10d, 3.14c and 3.14d). There are 15 of the 94 stars of the AAOmega spectra on the AGB. Using the dividing lines in Figs. 3.10c, 3.10d, 3.14c and 3.14d as the division between the CN-rich and CN-poor stars, there are 66 %, 60 %, 71 % and 57 % of these AGB stars that are CN-rich. In the overall sample, the stars are evenly divided between CN rich and CN poor. From these results, it can be concluded that in the case of 47 Tuc, all the CN-rich HB stars do evolve to become AGB stars, and in fact it would seem that we are maybe missing CN-weak stars.

During an initial analysis for Section 3.1.1 of the AAOmega spectra, all the stars were analyzed with the wrong [O/Fe]: the O-rich stars with [O/Fe] = −0.2 and the O-poor stars with +0.4. This caused a large change in [C/Fe], with the N-rich stars becoming 0.3 dex more abundant in carbon, and vice versa for the N-poor stars. A smaller effect occurred in [N/Fe] with the N-rich stars becoming 0.1 dex richer, and vice versa for the N-poor stars. This actually caused the two populations of stars on the RGB to be completely bimodal, with the AGB stars intermediary. Since the [O/Fe] was wrong for the stars it is not useful in an astrophysical sense, but it is a clear illustration of the importance of knowing the oxygen abundance of stars when considering the CN and CH molecular bands in their spectrum.

3.4 NGC 362

As part of the same observing campaign that provided that spectra in Section 3.2, 25 GB stars of NGC 362 were also observed with the same instrument configuration. Again the spectra were reduced by PLC and then cosmic ray removed & sky subtracted by the candidate. This reduction was preliminary in nature (i.e., there is not barycentric correction applied).

This cluster was selected as it was intermediary in metallicity to 47 Tuc and NGC 6752. Although cited as an example of a "second parameter pair" with NGC 288, there is not a lot of large-scale analyses of its stars. As shown in Fig. 1.2, the largest sample of stars for which sodium and oxygen abundances have been measured in twelve stars

Table 3.4 — Abundance results for NGC 6752 for the two analyses (floating and fixed [Fe/H]).

				Floating			Fixed	
ID C+05	ID	$T_{\rm eff}$	$\log g$	[Fe/H]	[C/Fe]	[N/Fe]	[C/Fe]	[N/Fe]
4625	f155	4700	1.9	−1.6	−0.5	0.7	−0.5	0.5
4787	f261	4800	2.1	−1.9	−0.6	1.4	−0.8	1.0
6860	f380	4900	2.3	−1.9	−0.5	1.3	−0.6	0.6
21647	f463	4950	2.4	−1.7	−0.6	1.0	−0.7	0.3
27083	f390	4950	2.3	−1.8	−0.8	1.7	−0.9	1.2
27778	f115	4650	1.7	−1.8	−0.6	1.3	−0.6	0.8
29265	f20187	4900	2.3	−1.8	−0.5	1.2	−0.6	0.8
32829	f20015	4650	1.7	−1.6	−0.7	0.9	−0.7	0.8
32978	f372	4900	2.3	−1.6	−1.0	1.5	−1.0	1.3
36022	f236	4800	2.1	−1.9	−0.4	0.5		
36058	f20061	4650	1.8	−1.7	−1.0	1.4	−1.0	1.2

(Shetrone & Keane 2000). This means that it is not possible to perform any direct comparisons of the stars to check the correctness of the $T_{\rm eff}$, $\log g$ or abundances determined. However based upon the observation that most (all?) Galactic GCs exhibit a sodium-oxygen anticorrelation and also an bimodality or range of CN spectral indices, it is likely that there will be an anticorrelation between the [N/Fe] and the [C/Fe].

The spectral matching pipeline was identical to that used in Section 3.2 had the same properties (wavelength coverage, chip gaps). A feature common to all the stars was a strong spectral feature at 4222–4223 Å. This feature had been present in the other clusters, but in this case, the spectral matching pipeline had trouble achieving a consistent fit to it and the CH & CN band heads. The feature was caused by CH lines, as evidenced by the fact that increasing the [C/Fe] abundance of the stars allows for the feature to be fit. However the [C/Fe] which works with the known metallicity of the cluster is far too large to fit the CH band head feature by about 1 dex.

It was not possible that this discrepancy is caused by having an incorrect [O/Fe] abundance for the stars. As illustrated in Fig. 3.23, any changes to the [O/Fe] to increase the strength of the 4223.2 Å feature will cause the CH band head at 4320 Å to also increase in strength. This makes perfect sense: the reason that the 4223.2 Å feature increases in strength is that there is more carbon in the atmosphere of the star, which will make all the carbon features increase in strength. Another possibility that can be discounted is that the carbon isotopic ratio is unusual for these stars. As shown in Fig. 3.24, the full range of ^{12}C/^{13}C ratios (90–3.5) affect the strength of the 4223.2 Å feature only by a small amount. The CH band head at 4320 Å has a small change as well but of equal magnitude and not of the order needed.

Having the wrong temperature would affect the line strength, with models showing that decreasing the temperature by 4000 K for a typical NGC 362 star would result in the Ca I line strength increasing, which would also increase the strength of 4223.2 Å feature due to the large wings of the Ca I line. At the same time, the CH band head would be weaker for a 4000 K star than for a 4400 K star.

3.5 NGC 6752

NGC 6752 is a metal-poor globular cluster that was the target of observations by Worley (2009). Like 47 Tuc, these 97 GB stars were observed with the AAOmega on the AAT, and have the same wavelength coverage and spectral resolution. The reduction of the spectra was only preliminary for this thesis and they had not been analyzed before, so there was no δC index available for the stars to provide an estimate of the [O/Fe] abundance. However Carretta et al. (2007) observed NGC 6752 with the European South Observatory's high resolution multifibre spectrograph FLAMES/GIRAFFE mounted on the Very Large Telescope UT2. With a spectral resolution of $R \sim 20{,}000$, they were able to obtain precise oxygen abundances for 110 stars. Of the 97 stars observed by Worley (2009), 11 were in common with Carretta et al. (2007) and had spectra that were compatible with the spectral matching pipeline, in particular covering all the pseudo-continuum points that are used in the continuum normalization. The sky location of the stars is shown in Fig. 3.26. The 11 stars were analyzed using the spectral matching pipeline with

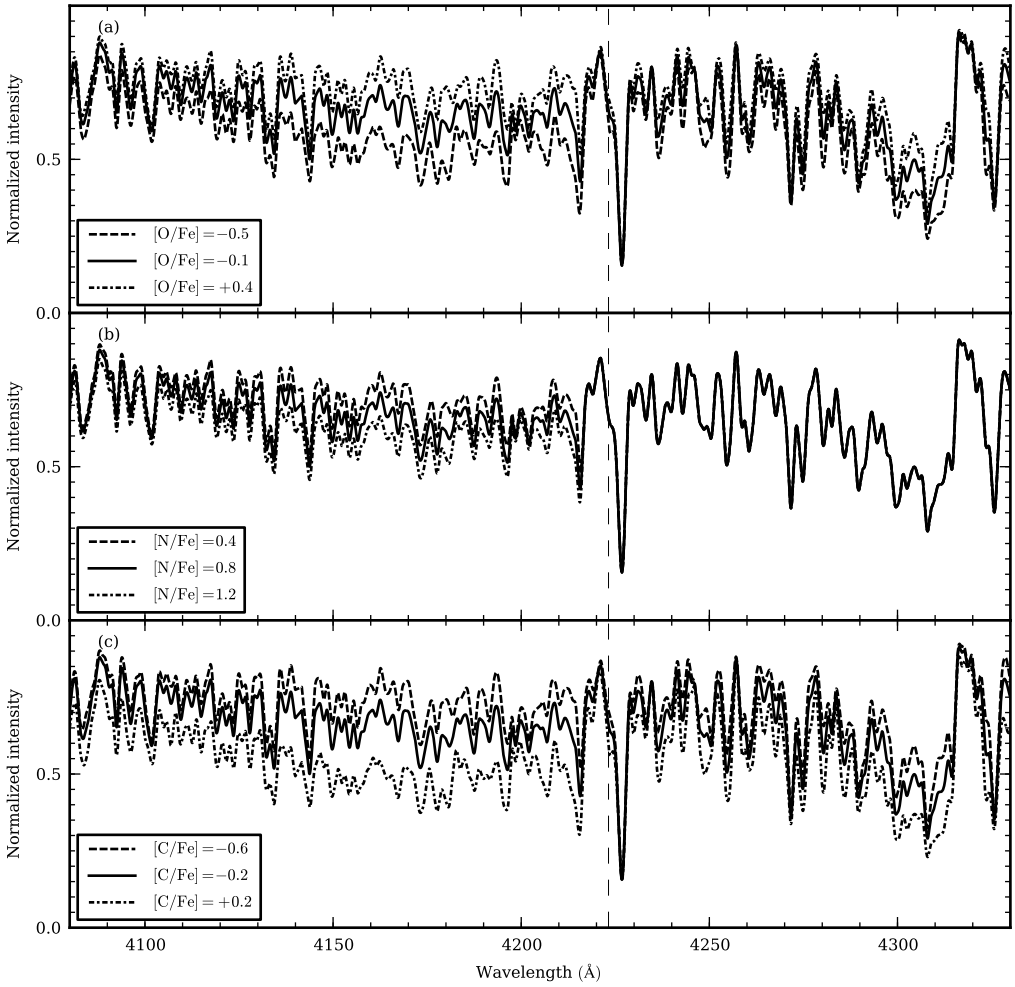

Figure 3.23 — The same as Fig. 2.5 but for the resolution of the SALT MOS spectra of NGC 362 ($R \sim 3000$). The wavelength of the CH lines at 4223.2 Å is marked with the vertical thin dashed line.

$E(V-K) = 0.11$ and $m - M = 13.24$. A small wavelength shift had to be applied for each star as the wavelength calibration was not accurate. This was done by eye to have the position of the Ca I 4226 Å at the same wavelength in both the observed and synthetic spectra. In Section 3.1, the spectra of the 47 Tuc stars had been previously continuum normalized (Worley & Cottrell 2012; Worley 2013), and this normalization (with a small adjustment) was used for all the stars. In the case of NGC 6752, the full spectral matching pipeline was used as these spectra had not previously been continuum normalized, with the spectra normalized as described in Section 2.2.

As in Sections 3.1 and 3.2, the stars were analyzed with two different metallicity values: fixed at a reasonable literature value (in this case [Fe/H] = −1.5); or with the [Fe/H] determined from the Ca I spectral line ("floating"). The spectra with model fits are shown in Fig. 3.27. The results are found in Table 3.4 and Fig. 3.28. The average metallicity determined was $\langle$[Fe/H]$\rangle$ = −1.75±0.12. This can be compared to literature abundances of [Fe/H] = −1.54 (Harris 1996), −1.56 (Carretta et al. 2007), −1.62 (Yong et al. 2008). As with the analyses of 47 Tuc, the metallicity found here is slightly metal-poorer than those other researchers.

Figure 3.28 shows the abundance results that were found for the stars. The stars covered the full range of sodium and oxygen abundances present in the cluster which resulted in them showing a wide range of carbon and nitrogen values (Figs. 3.28a and 3.28b). There are only 18 stars, all only slightly evolved, for which [C/Fe] and [N/Fe] have been determined in NGC 6752 (Carretta et al. 2005). As with the results of 47 Tuc it was found that the [C/Fe]

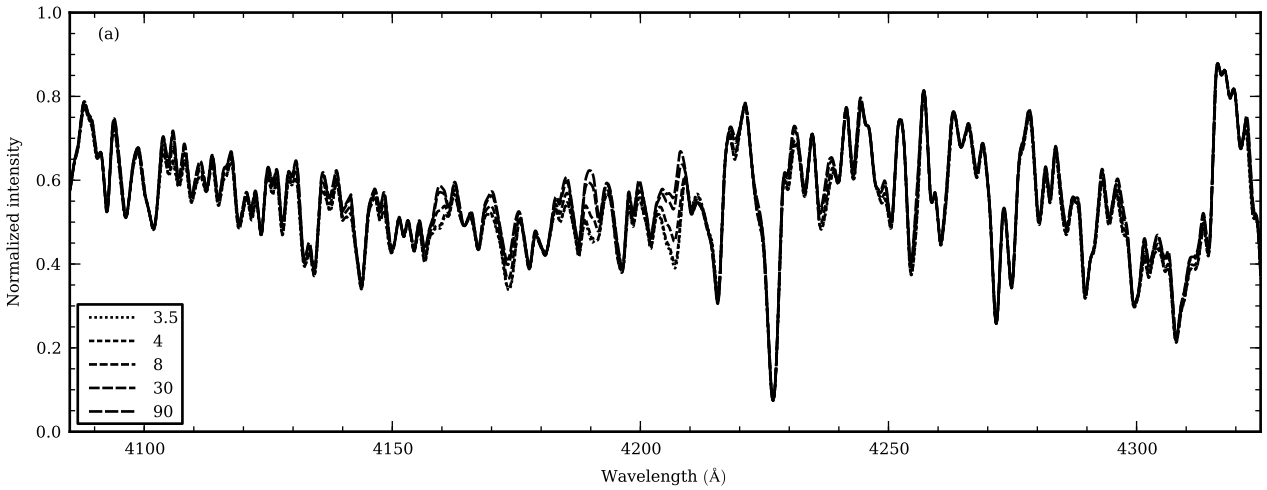

Figure 3.24 — The same as Fig. 2.6a but for the resolution of the SALT MOS spectra of NGC 362 ($R \sim 3000$).

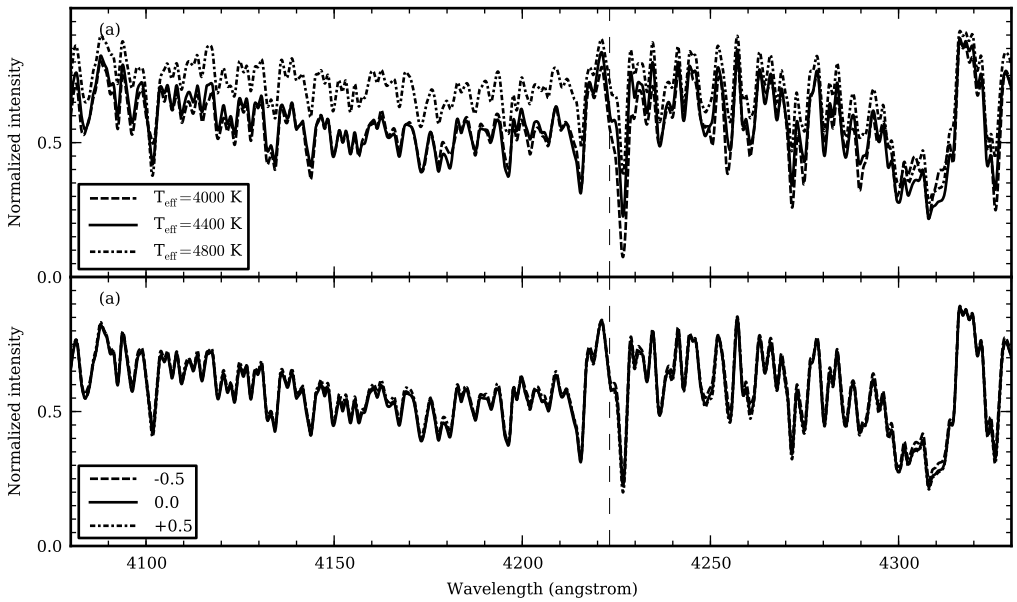

Figure 3.25 — The effect of (a) $T_{\rm eff}$ and (b) $\log g$ on the spectra.

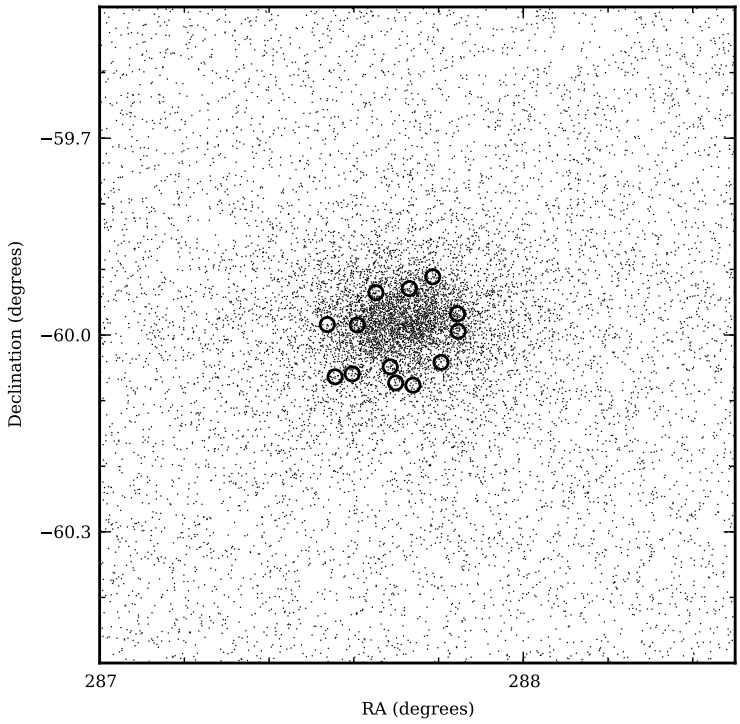

Figure 3.26 — Sky location of 11 stars analyzed for NGC 6752 over the background of the 2MASS catalogue.

abundances determined in this work were lower than those found by other researchers, by about 0.5 dex. Since we are comparing stars that are well up to the GB, to stars that are just evolving off the MS or just moving off the SGB (Fig. 3.28f), it is not possible to directly compare these results. The two most sodium-poor stars of the eleven are found to be much more nitrogen-poor than similar stars in Carretta et al. (2005). Confirming the result of Norris & Pilachowski (1985), there is a positive correlation between the sodium abundance and the nitrogen abundance (Figs. 3.28b and 3.28c).

3.6 Summary

This chapter has investigated two monometallic clusters using the spectral matching pipeline described in Chapter 2. This pipeline was developed to analyze low resolution spectra of ω Cen and these monometallic clusters were selected to provide assurances that the method worked and to calibrate the results it returned. In the case of 47 Tuc, two sets of spectra were analysed. For the AAOmega spectra, two analyses were performed: first using [O/Fe] abundance estimated from the spectral index of CN, and second using [O/Fe] estimated from the [Na/Fe] of each star. These two cases will be used in this thesis's investigation of ω Cen, with Chapter 4 using previously determined [O/Fe] for 221 stars, and Chapter 5 using a spectral index to estimate if a star is oxygen rich or oxygen poor.

A smaller sample of NGC 6752 stars used [O/Fe] previously determined (Carretta et al. 2007). In all cases it was found that the results returned by the spectral matching pipeline were consistent with the results in the literature and the metallicities were compatible with a monometallic cluster. The scatter of the iron abundances are understandable due to the precision possible when using a single spectral line of calcium to determine [Fe/H].

There are some systematic differences between the abundances determined in this chapter and those found by other researchers. As such, it was useful for the analysis of ω Cen stars to identify results with which the results can be compared. This provided a consistent abundance scale that the results of this thesis can be placed onto. In the case of these monometallic clusters, it was found that [Fe/H] was 0.1–0.2 dex lower than the literature values and the [C/Fe] of the 47 Tuc stars was 0.5 dex lower than the abundances found for unevolved stars in the cluster. For

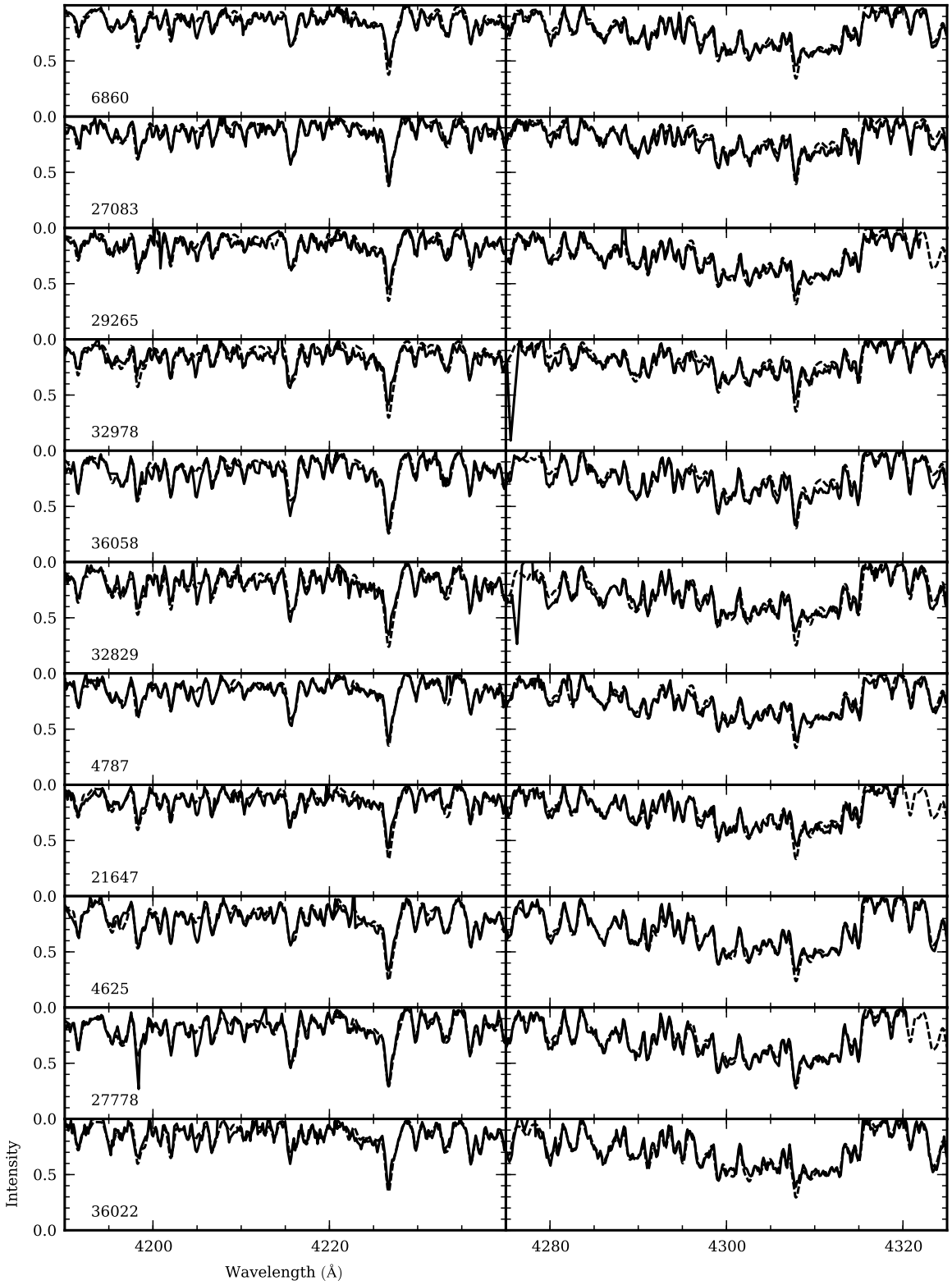

Figure 3.27 — Spectra from AAOmega of the NGC 6752 stars in common with Carretta et al. (2007). The solid line is the observed spectra and the dashed line is the best fitting synthetic spectra.

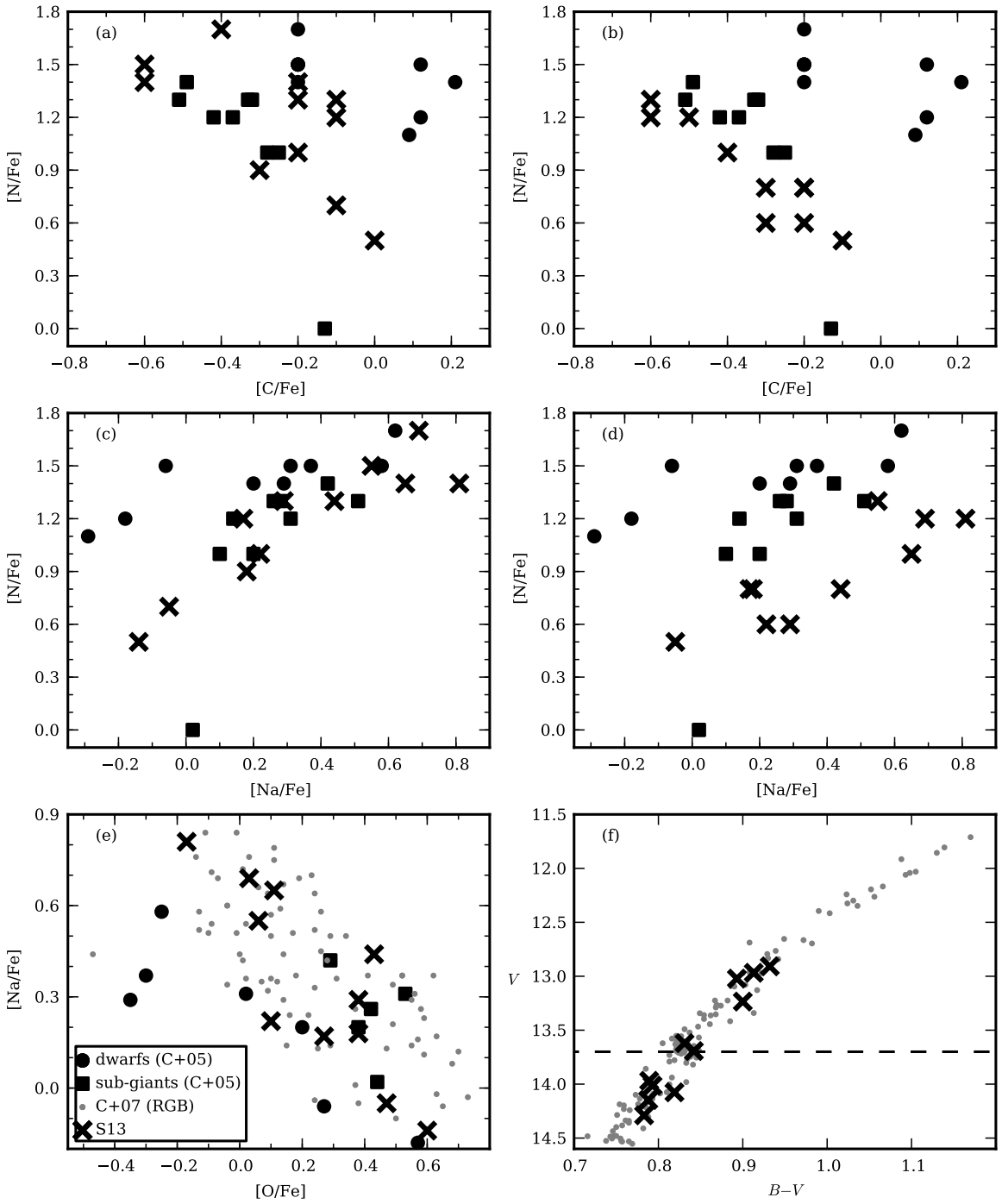

Figure 3.28 — (a) & (b) The [N/Fe] and [C/Fe] abundances for NGC 6752 stars for this work (S13) and Carretta et al. (2005, C+05), with (a) floating [Fe/H] and (b) fixed [Fe/H]. The [C/Fe] from this work have been adjusted by 0.4 dex. (c) & (d) are the same but for [N/Fe] and [Na/Fe]. (e) The eleven stars analyzed in this thesis highlighted on the full Carretta et al. (2007, C+07) dataset and also showing the Carretta et al. (2005, C+05) stars. (f) CMD showing the eleven stars and the full Carretta et al. (2007) dataset (the dashed line indicates the level of the HB: $V_{\rm HB}$ = 13.70). A CMD of the SGB stars is in Fig. 3.29.

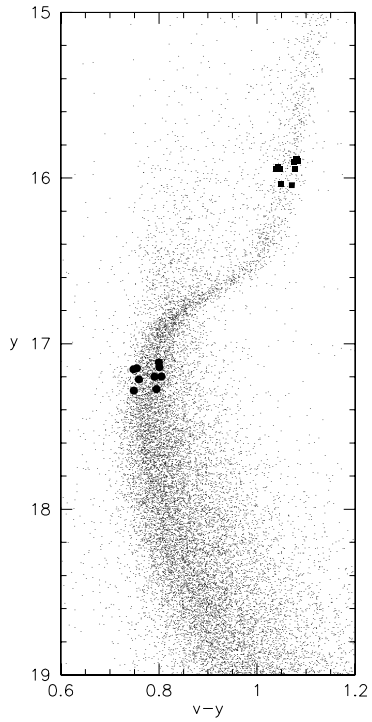

Figure 3.29 — Reproduction with permission of Figure 1 of Gratton et al. (2001) showing the location of the stars on the CMD from Carretta et al. (2005) in Fig. 3.28. Photometry is from Grundahl et al. (2000).

NGC 6752, [C/Fe] was about 0.5 dex lower than other results for stars of the cluster. In the case of both clusters, there was no difference in [N/Fe], apart from for NGC 6752 for one of the analysis (Fig. 3.28d). In Chapters 4 and 5 the focus changes to ω Cen, a multimetallic cluster with complex abundances, first using a subset of the van Loon et al. (2007) spectral library.

Chapter 4

ω Centauri: 221-Star Set with known [O/Fe]

The results of the monometallic clusters showed that the spectral matching pipeline can recover the [Fe/H], [C/Fe] and [N/Fe] of stars from lower resolution spectra. They also showed that knowledge of the [O/Fe] abundance is important for these stars in order to have accurate abundances of carbon and nitrogen. With that in mind, the next stage of this research was to move to the main target of this thesis, ω Cen, working with stars with known [O/Fe] from previous researchers (Johnson & Pilachowski 2010). This would allow for the same number of "unknowns" to be present as in monometallic stars, where the [Fe/H] was known but not the [O/Fe] precisely. Since the aim of Chapter 5 was to investigate stars with unknown [Fe/H], in this Chapter the [Fe/H] would also be determined. So for these stars [O/Fe] was known but not the [Fe/H].

This chapter discusses an investigation of a 221-star subset created from the combination of the van Loon et al. (2007) spectral library and the abundance dataset of Johnson & Pilachowski (2010). Section 4.1 discusses the observational data sources; Section 4.2 presents the results and quality assurance; Section 4.3 presents a statistical clustering analysis of the dataset from this work and of Marino et al. (2011a, 2012) that places the stars into groups with common abundances; and Section 4.4 puts these groups into the context of abundance planes.

This chapter is based primarily on Simpson et al. (2012).

4.1 Observational Data Sources

A dataset of 221 giant branch (GB) stars (including 14 stars that were observed twice spectroscopically) was created by combining information from the Two Micron All Sky Survey (2MASS), van Loon et al. (2007), Bellini et al. (2009a), and Johnson & Pilachowski (2010). Table 4.1 describes the data sources that were combined and used in this Chapter and the next.

4.1.1 van Loon et al. (2007) Spectral Library

The van Loon et al. (2007) dataset is a spectral library of 1518 post-main sequence (MS) stars in ω Cen. Spectra were obtained with the 2dF instrument at the Anglo-Australian Telescope, covering approximately $\lambda\sim$ 3840–4940 Å at a resolving power of $\lambda/\Delta\lambda\sim$ 1600 and a signal-to-noise per pixel ranging from ~ 50 in the blue to > 100 in the redder

Table 4.1 — Overview of different data sources used in this and the following chapter.

Source	Type	Stars
van Loon et al. (2007)	Spectroscopy	1518
Johnson & Pilachowski (2010)	Abundances	855
Marino et al. (2012)	Abundances	77
Bellini et al. (2009a)	Photometry	359,391
2MASS	Photometry	26,985

part of the wavelength range. For each star van Loon et al. (2007) provided an ID assigned by van Leeuwen et al. (2000) (known as the LEID), positional information, B magnitude, $B-V$ colour and radial velocity. van Loon et al. (2007) also did a stellar parameter determination for their catalogue, solely from the spectra and assuming solar-scaled abundances. For this thesis, it was decided to use their raw spectra and analyse the stars ourselves with appropriate globular cluster (GC) abundances and concentrating on small sections of the spectrum. The continuum was normalized by mapping the raw spectrum onto the synthetic spectrum, as described in Section 2.2.

At the resolution of the van Loon et al. (2007) spectra, and with its wavelength coverage, it was not possible to use a spectral-temperature indicator such as Hβ. Therefore the temperature-colour relationships of Alonso et al. (1999) were used. This could then be combined with the luminosity relationship to estimate the surface gravity of the stars. For stars of unknown metallicities, the most appropriate colour to use is $V-K$, as discussed in Section 2.1. Consequently, additional photometry of the stars in the van Loon et al. (2007) catalogue was needed, since they only had B and V for the stars.

4.1.2 Photometry Data Sources

The Two Micron All Sky Survey Photometry

The 2MASS data were sampled for a circular region around RA = $13^{\mathrm{h}}26^{\mathrm{m}}14\overset{\mathrm{s}}{.}16$, Dec. = $-47°31'11\overset{''}{.}95$, the centre of the van Loon et al. (2007) data. This created a catalogue of 26,985 stars with J, H and K_S magnitudes in the 2MASS photometric system. The majority of the stars in the raw dataset were from the GC with obvious contamination by field stars. The photometry extended well below the ω Cen's main sequence turn-off (MSTO), covering all the van Loon et al. (2007) stars.

Bellini et al. (2009a) Photometry

Bellini et al. (2009a) used ESO archive data to create a new, CCD-based, proper-motion catalogue for ω Cen extending to $B \sim 20$, containing 359,391 stars with photometry in the U, B, V, R_C, I_C, and Hα band passes. They used 279 archive images acquired at the ESO/MPI2.2m telescope at La Silla (Chile) equipped with the wide-field imager camera (WFI). It covered 83 % of the stars of the van Loon et al. (2007) spectral library (Fig. 4.1). This catalogue improved upon the previous large proper motion catalogue of ω Cen, produced by van Leeuwen et al. (2000) from photographic plates. Although van Loon et al. (2007) had B and V magnitudes for all of their stars van Leeuwen et al. (2000), it was decided to use the Bellini et al. (2009a) photometry instead as it provided a very precise colour-magnitude diagram (CMD) that could be used to distinguish the metal-poor asymptotic giant branch (AGB) (the bluest stars on the GB) from all of the red giant branch (RGB). Other AGBs will be mixed with the RGBs as a consequence of the different evolutionary paths followed by stars of different ages, metallicities, C+N+O and helium abundances.

4.1.3 Positional Matching

To determine the T_{eff} and $\log g$ of the stars, the $V-K$ colour was needed. This required the positional matching of van Loon et al. (2007) sources and the photometric sources of Bellini et al. (2009a) and 2MASS. The closest positional match within $5''$ was found for all the stars of van Loon et al. (2007). If no match existed, then the star was excluded from the analysis of this Chapter.

2MASS stated that their positional accuracy should be less than 130 microarcseconds (mas) for saturated sources and < 80 mas for the best unsaturated sources. The van Leeuwen et al. (2000) dataset, from which the van Loon et al. (2007) is derived, had positional errors mostly less than 100 mas in right ascension and declination. Bellini et al. (2009a) stated that based upon ~ 5500 reference stars, their error was 45–50 mas in each coordinate. The positional matching of the three photometric catalogues was done using TOPCAT (Taylor 2005). There were 982 stars in common between van Loon et al. (2007) and 2MASS, with 672 of these stars also matching to Bellini et al. (2009a).

4.1.4 Selection Of Stars

Johnson & Pilachowski (2010) determined several elemental abundances including [Fe/H], [O/Fe], [Na/Fe] and [Ca/Fe] for the 855 GB stars. For the analysis presented in this chapter only those stars that were also in the Johnson

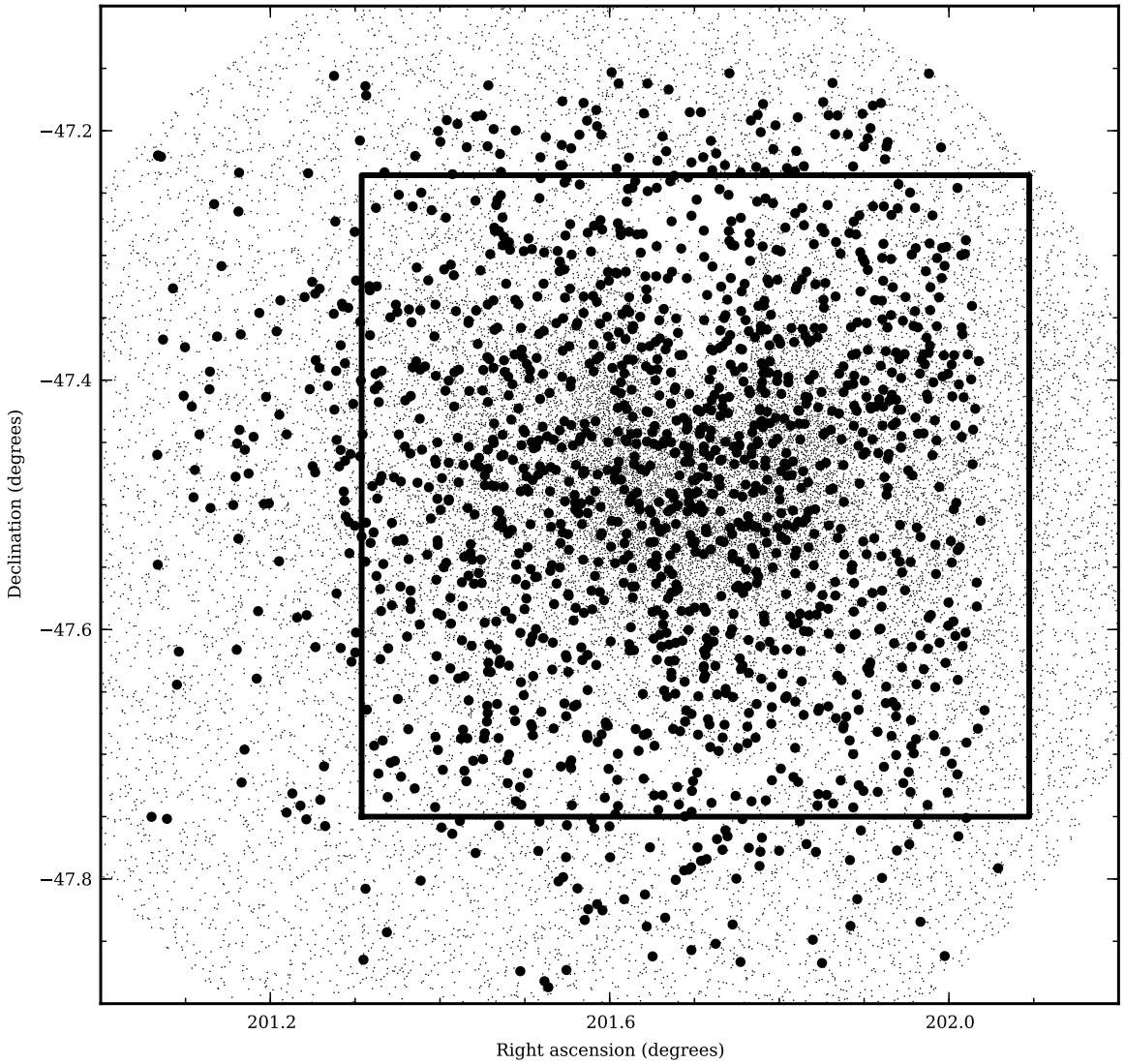

Figure 4.1 — The sky coverage of van Loon et al. (2007) (dots) and Bellini et al. (2009a) (inside the box), showing that 83 % of van Loon et al. (2007) stars are inside the region observed by Bellini et al. (2009a).

Table 4.2 — Photometry of the 221 stars. The LEID is the star label given by van Loon et al. (2007). The *U* and *V* photometry is from Bellini et al. (2009a) and the *J* and *K* photometry is from 2MASS. All the photometry is in their original system. The spectral indices ,CH(4300) and S(3839), and the number of spectra of each star in the van Loon et al. (2007) spectral library, are also given.

LEID	U	V	J	K	S(3839)	CH(4300)	N. of Spectra
15022	14.19	12.10	9.730	8.95	0.108	0.229	1
15023	14.15	12.26	9.964	9.23	0.075	0.264	1
16019	14.78	13.28	11.268	10.62	0.475	0.400	2
16027	14.83	13.55	11.532	10.86	0.089	0.239	1
17029	14.42	13.17	11.201	10.54	0.090	0.135	1
17046	14.41	13.31	11.364	10.74	0.049	0.120	1

This table is available in its entirety in a machine-readable format.

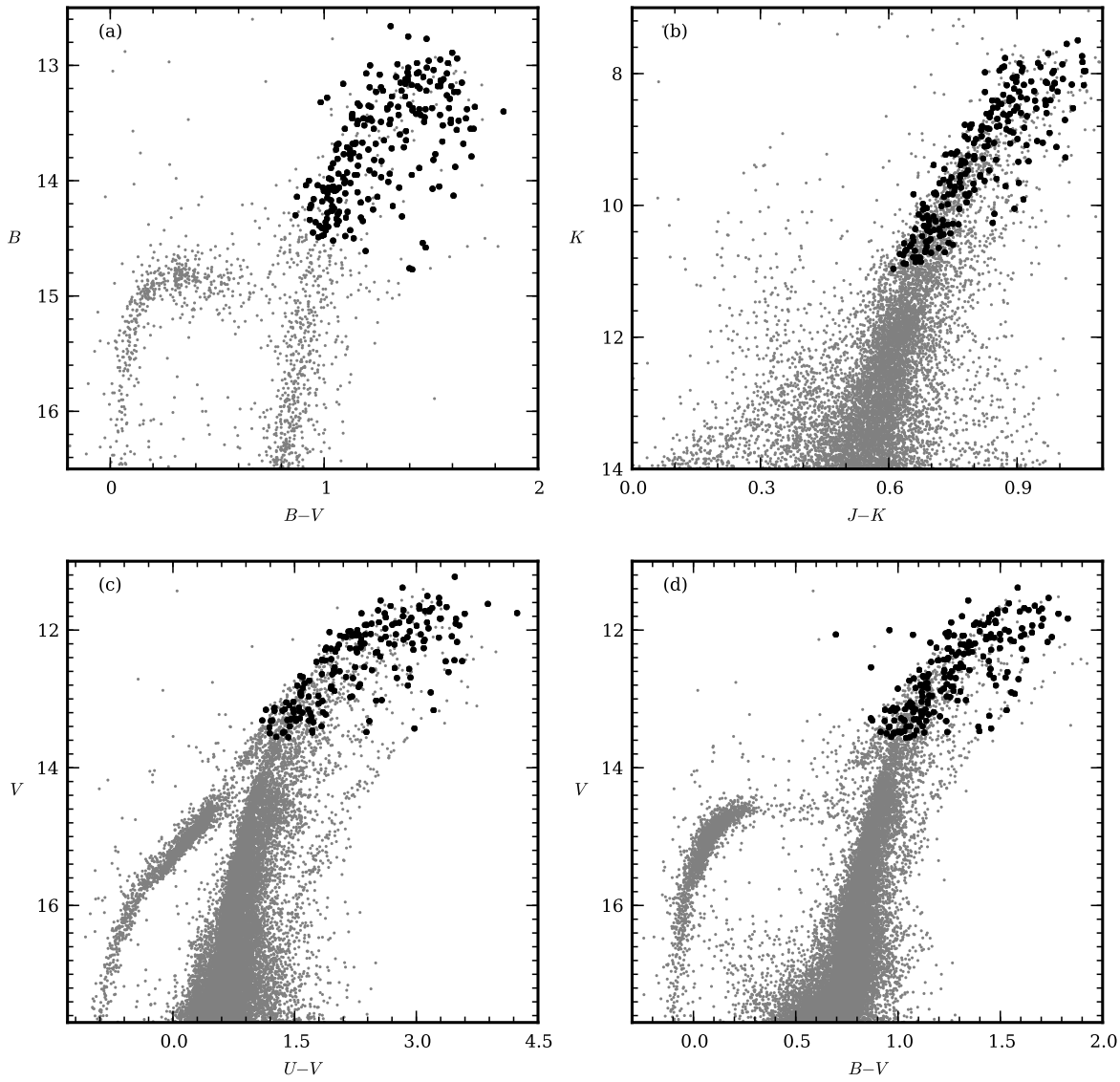

Figure 4.2 — Four CMDs showing the positions of the 221 stars (black dots) in various colour planes against the background of the full set of photometry (grey dots). (a) B–V (van Loon et al. 2007); (b) J–K from 2MASS; (c) U–V (Bellini et al. 2009a); (d) $B-V$ (Bellini et al. 2009a). The limiting magnitude ($V < 13.5$) of Johnson & Pilachowski (2010) meant that these stars were all well above the HB level and the magnitude of the easily discernible AGB is barely reached. The abundances determined are presented for the stars in Table 4.3.

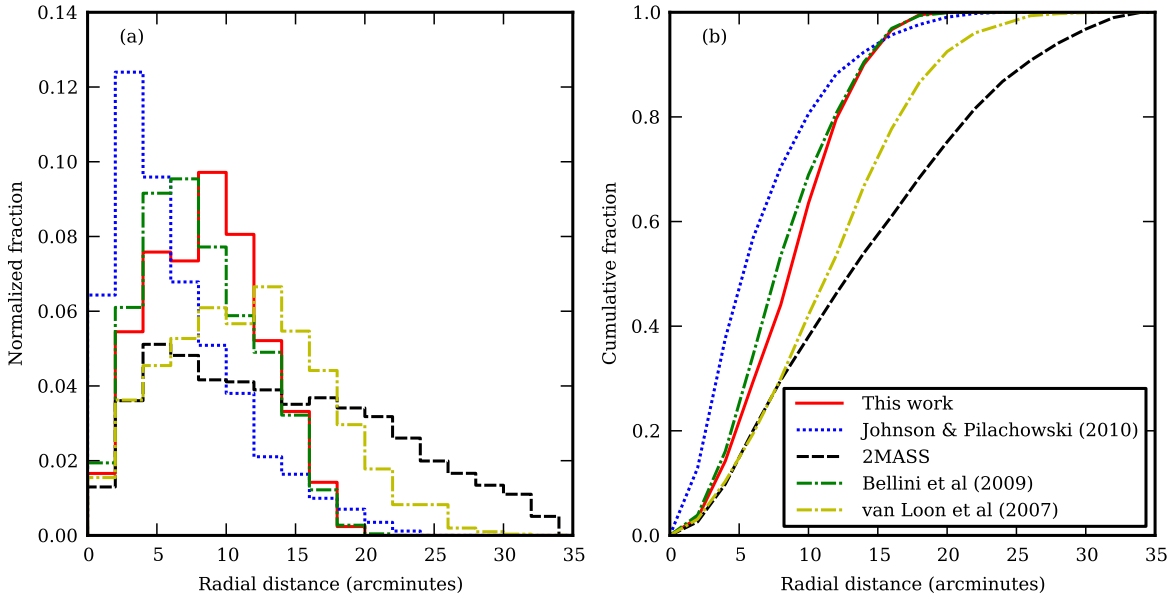

Figure 4.3 — The radial distributions of this work, Johnson & Pilachowski (2010), 2MASS, Bellini et al. (2009a) and van Loon et al. (2007). The work presented in this chapter has a similar radial distribution as Bellini et al. (2009a), which is unsurprising as it was dependent on their photometry.

& Pilachowski (2010) catalogue were used, as it would result in more precise abundances that did not have further uncertainty due to unknown oxygen and calcium abundances. A full analysis of the complete van Loon et al. (2007) spectral library, with reasonable estimates of oxygen and calcium, is in Chapter 5.

Johnson & Pilachowski (2010) selected their stars from van Leeuwen et al. (2000) and there were 291 matches in total between van Loon et al. (2007) and Johnson & Pilachowski (2010) based upon matching the star IDs. Of the 672 stars is common between the 2MASS, van Loon et al. (2007) and Bellini et al. (2009a) libraries, 221 were also in common with Johnson & Pilachowski (2010) (Fig. 4.2 and Table 4.2).

Overall, the 221 stars have a magnitude range of $11.2 < V < 13.6$ and a colour range of $0.8 < (B-V) < 1.8$. This corresponds to stars with $T_{\rm eff}$ from 3800–4900 K and $\log g$ from 0.3–1.8.

This dataset does have a selection bias against the core of the cluster, due to the bias of the Bellini et al. (2009a) catalogue (Fig. 4.3). Comparing the radial distributions of the Johnson & Pilachowski (2010) dataset and the 221 stars, their stars are much more centrally concentrated: 57 % of the stars in the Johnson & Pilachowski (2010) dataset are within $6'$ of the cluster centre while for the 221 star set it is 29 %. In Section 4.4 it is noted that this selection effect does not appear to have greatly biased the sample, as there is a similar proportion of O-rich and O-poor stars as found by Johnson & Pilachowski (2010). The radial distribution of the stars in the abundance groupings is discussed in Section 6.1.

4.2 Results

For each star the following parameters were determined: $T_{\rm eff}$, $\log g$, [Fe/H], [C/Fe], [N/Fe] and [Ba/Fe] (Table 4.3). The CMD position of the stars is shown in Fig. 4.2. There were 221 stars that were analysed with 14 having two spectra. An estimate of the uncertainty in the abundances determined was made using the doubly observed stars. The average standard deviation in the difference in [Fe/H] was ±0.2 dex, [C/Fe] was ±0.2 dex, [N/Fe] was ±0.3 dex and [Ba/Fe] was ±0.6 dex.

Plotting the metallicity found by this work against that of Johnson & Pilachowski (2010) shows a good correlation (Fig. 4.4). Most of the stars had [Fe/H] from −2.0 to −1.5, resulting in a large concentration around these values. As would be expected when results derived from spectra with a resolution of 1600 is compared to spectra with a

Table 4.3 — Stellar parameters determined for the 221 stars. The LEID is the star label given by van Loon et al. (2007). Abundances of [O/Fe] and [Na/Fe] are from Johnson & Pilachowski (2010). The offsets described in Section 4.2 and Fig. 4.6 have been applied to [C/Fe] and [N/Fe]. The group number is described in Section 4.3.

LEID	$T_{\rm eff}$	log g	[Fe/H]	[C/Fe]	[N/Fe]	[O/Fe][a]	[Na/Fe][a]	[Ba/Fe]	Group
15022	4400	0.9	−1.8	−0.5	0.3	0.44	−0.36	0.4	2
15023	4450	1.0	−1.6	−0.6	0.1	0.42	−0.29	−0.2	1
16019	4800	1.6	−1.7	0.7	−0.1	0.64	0.01	0.8	2
16027	4750	1.7	−2.3	−0.1	−1.0	0.46	−0.16	−0.1	1
17029	4800	1.6	−1.9	−0.8	−0.9	0.35	0.49	−0.2	1
17046	4850	1.7	−2.3	−0.6	1.0	0.14	0.16	1.0	3
37318	3950	0.8	−1.0	−0.4	2.0	0.35	1.03	0.5	4
38115	4150	0.8	−1.6	0.4	0.1	0.28	0.14	0.2	2
44449	4100	0.6	−1.5	−0.6	1.5	−0.73	0.47	0.5	3

(This table will be available in its entirety in a machine-readable form. A portion is shown here for guidance regarding its form and content.)

Table 4.4 — Stellar parameters determined (this work ≡ S13) for the nine stars in common with Marino et al. (2012). The LEID is the star label given by van Loon et al. (2007) and the ID is the numbering scheme from Marino et al. (2012, M+12). The [Fe/H], [C/Fe], [N/Fe] from Marino et al. (2012) are shown for comparison. The [O/Fe] is from Johnson & Pilachowski (2010, J&P10).

ID			[Fe/H]		[C/Fe]		[N/Fe]		[O/Fe]	
LEID	M+12	$T_{\rm eff}$	S13	M+12	S13	M+12	S13	M+12	J&P10	M+12
35090	246585	4100	−1.3	−1.64	−0.55	−0.65	1.05	1.55	−0.32	−0.25
36156	245724	4150	−2.0	−1.97	−0.45	−0.44	−0.05	0.20	0.43	0.30
36179	244812	4050	−1.5	−1.40	−0.75	−0.17	2.05	1.40	−0.42	−0.10
37253	242745	4150	−1.9	−1.91	−0.25	−0.35	0.15	0.10	0.43	0.37
38115	241359	4200	−1.6	−1.69	+0.35	0.17	0.05	0.26	0.28	0.40
46150	224500	3950	−1.6	−1.51	+0.25	0.40	0.65	0.20	0.44	0.49
46194	225246	4200	−1.9	−1.87	−0.65	−0.61	0.65	0.70	−0.05	0.19
48235	220325	4050	−1.5	−1.61	−0.65	−0.45	1.15	1.20	−0.32	0.00
51091	215367	4400	−2.0	−1.93	−0.55	−0.98	0.75	0.90	0.28	0.15

resolution of 20,000, there is a spread of values. About 70 % of the stars were within ±0.2 dex of the value found by Johnson & Pilachowski (2010). The average difference for all the stars was 0.1 dex: Johnson & Pilachowski (2010) found a slightly more metal-rich value than that found by this work.

Among the 221 stars there were nine stars in common with Marino et al. (2012) (Figs. 4.5 and 4.6 and Table 4.4). Marino et al. (2012) analyzed of 77 RGB stars of ω Cen using spectra from FLAMES/GIRAFFE (R ~ 20,000). They determined [Fe/H], [C/Fe], [N/Fe] and [O/Fe] for their stars (Fig. 1.4). These stars were used for direct comparison of the [C/Fe] and [N/Fe] abundances found in this thesis, as Johnson & Pilachowski (2010) did not determine abundances for these elements. The nine stars in common between this Chapter's work and Marino et al. (2012) had a range of $T_{\rm eff}$ from 4050–4400 K and in metallicity from −1 > [Fe/H] > −2. According to the abundances determined by Marino et al. (2012), four would be classed as CN-strong ([N/Fe] > 0.6), while four were CN-weak with high carbon abundances. This meant that they provided a good sample across the range of stellar parameters which was not clumped at a particular metallicity, [C/Fe] or [N/Fe].

A comparison of the [C/Fe] and [N/Fe] to that of Marino et al. (2012) showed that there was a systematic offset between the two datasets. In order to place this work onto the same abundance scale as Marino et al. (2012), it was necessary to apply some systematic corrections to our values. Using the eight of the nine stars in common (LEID36179 was excluded as an outlier), it was found that the [C/Fe] needed the addition of 0.45 dex (the same as in Chapter 3 for 47 Tuc and NGC 6752), while the offset in [N/Fe] was −0.55 dex. This offset was likely caused by continuum placement and the positive feedback between [C/Fe] and [N/Fe]. If the [C/Fe] is too low, then the

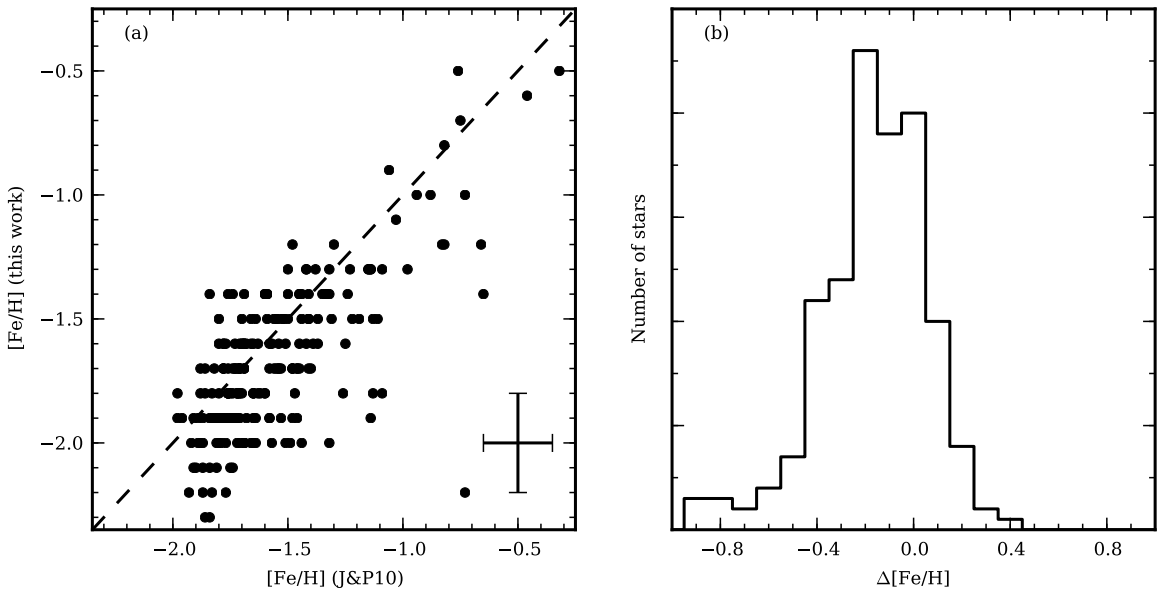

Figure 4.4 — (a) direct comparison of the metallicities found for each star in this study and the abundances found for the same stars by Johnson & Pilachowski (2010) (with the one-to-one line shown). This figure excludes three stars for which [Fe/H] < −2.4 were found for this thesis. (b) Difference in [Fe/H] between the value found by Johnson & Pilachowski (2010) compared to the value from this thesis.

[N/Fe] will have to be increased in order to reach the same strength of the CN region. The comparison of the corrected [C/Fe] and [N/Fe] values are shown in Fig. 4.6.

The significant outlier in Fig. 4.6b is LEID36179. Figure 4.7 shows the synthetic spectra produced using our parameters and the parameters of Marino et al. (2012) for this star. This clearly shows that the Marino et al. (2012) C and N abundances do not provide a good fit to the CN and CH spectral features in the van Loon et al. (2007) spectrum. One note about this star is that Marino et al. (2012) determined an [O/Fe] = −0.1 while Johnson & Pilachowski (2010) have [O/Fe] = −0.42. This is the largest difference for these nine stars in terms of the oxygen abundance determined by the two groups. The overall results in this Chapter & thesis are not compromised by this outlier.

A qualitative comparison of the [C/Fe] to [N/Fe] shows that the automated spectral matching method worked well (Fig. 4.8): it did not find stars that were both carbon and nitrogen rich, the upper-right quadrant on that abundance plane. There was not the clear bifurcation that was seen by Marino et al. (2012), but there was clearly the same anti-correlation between [C/Fe] and [N/Fe]. Some very N-poor stars were found. These were the result of the spectral matching pipeline. It would keep searching for the parameters that minimized the χ^2, which could sometimes lead to extremely small values as the χ^2 difference between the steps in [C/Fe] or [N/Fe] were very small. This was the cause of the extremely low [N/Fe] values that are not shown on Fig. 4.8. These stars have so little detectable nitrogen that that the automated process determined values as low as [N/Fe] = −3. This combination of the parameters and the resolution gives just an upper limit on the [N/Fe], rather than a definitive abundance for these stars.

4.3 Clustering Analysis

k-means clustering is a method to create *k* groups (or clusters) from a dataset of *n* entries using *m* parameters. It minimizes the distance of each member from the group (or cluster) centre. It was first described by Steinhaus (1956) and MacQueen (1967). In the work presented here, the method was implemented using the *R* statistical package (R Development Core Team 2011), a freely available system for statistical computation and graphics. The default *k*-means clustering contained in *R* (Hartigan & Wong 1979) was employed in this thesis.

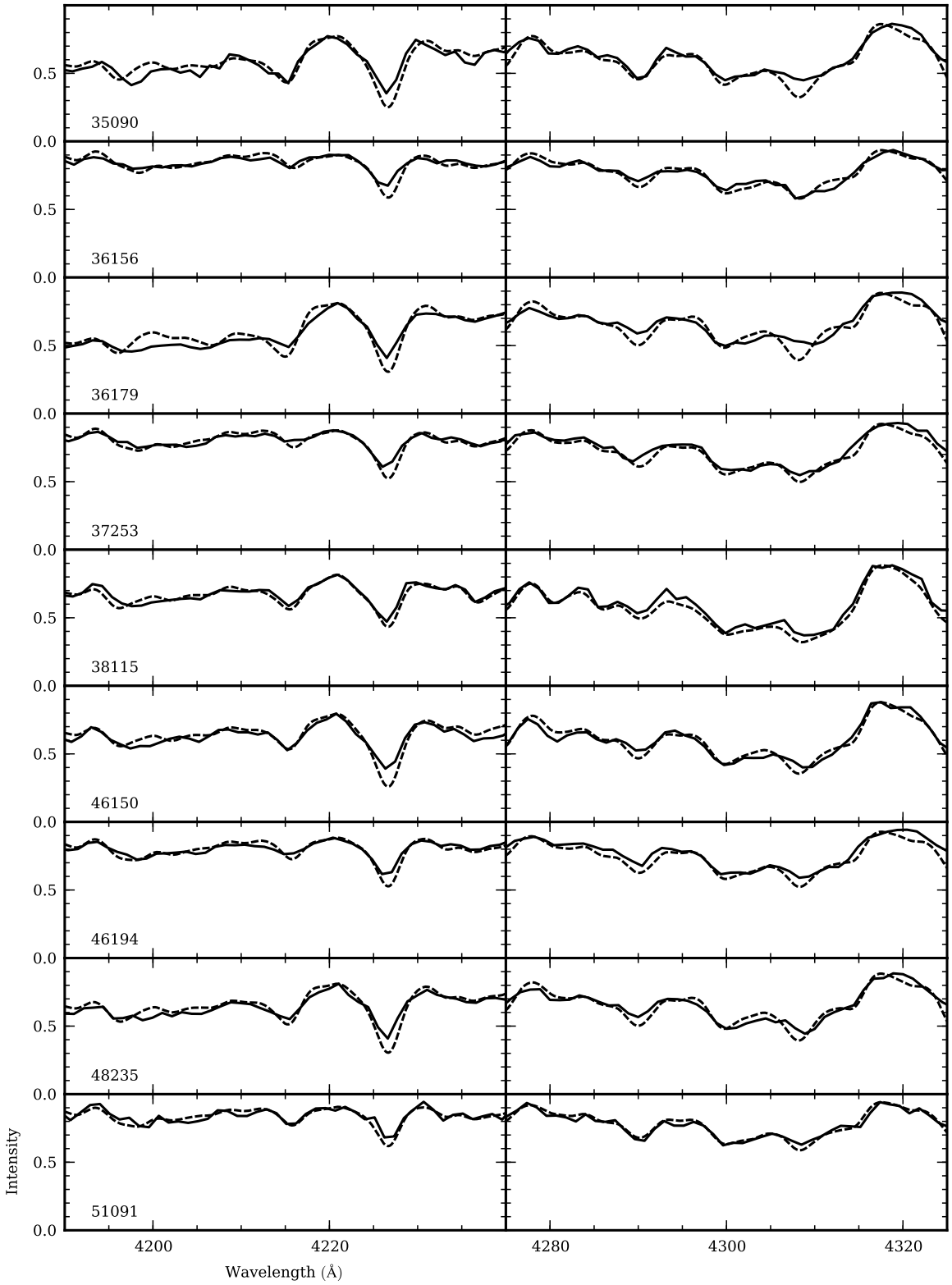

Figure 4.5 — Spectra of the nine stars in common with Marino et al. (2012). The solid line is the observed spectra and the dashed line is the best fitting synthetic spectra.

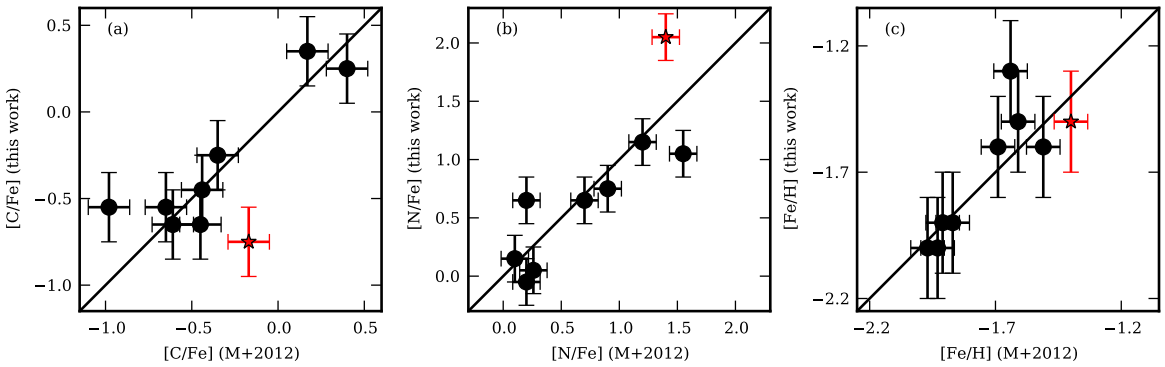

Figure 4.6 — The nine stars in common between this work and Marino et al. (2012) were used to determine systematic offsets. (a) [C/Fe] values were adjusted by 0.45 dex, (b) [N/Fe] by −0.55 and (c) [Fe/H] were unadjusted. The star marked with a red star is LEID36179, the outlier discussed in Section 4.2 and Fig. 4.7.

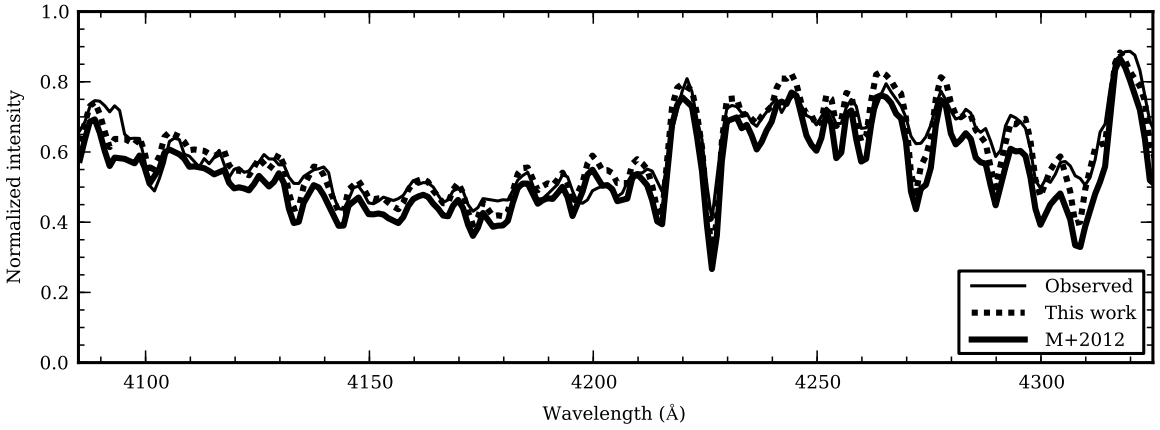

Figure 4.7 — LEID36179 is the significant outlier on Fig. 4.6b. We determined [N/Fe] = 2.35, while Marino et al. (2012) determined 1.4 dex. The thick solid line shows the synthetic spectrum that results using Marino et al. (2012)'s stellar parameters and abundances (adjusted using the offsets described in Section 4.2 and Fig. 4.6). The thin solid line is the observed spectrum from van Loon et al. (2007) and the dotted line is our fit to this spectrum.

Table 4.5 — The cluster centres found using k-means clustering analysis of the 221 stars from the van Loon et al. (2007) spectral library. For each parameter, the average and standard deviation are given, along with the number of stars in each group. The symbol is the identifier used for that group in the figures.

Group	Symbol	N. stars	[Fe/H]	[C/Fe]	[N/Fe]	[O/Fe]	[Na/Fe]	[Ba/Fe]
1	∗	62	−1.8 ± 0.3	−0.4 ± 0.2	0.3 ± 0.3	0.3 ± 0.1	−0.1 ± 0.3	−0.4 ± 0.5
2	○	86	−1.7 ± 0.2	0.0 ± 0.3	0.4 ± 0.3	0.4 ± 0.1	0.0 ± 0.2	0.4 ± 0.3
3	△	49	−1.7 ± 0.3	−0.5 ± 0.2	1.0 ± 0.3	−0.3 ± 0.4	0.3 ± 0.2	0.5 ± 0.4
4	×	24	−1.3 ± 0.4	−0.6 ± 0.2	1.8 ± 0.4	−0.2 ± 0.2	0.7 ± 0.2	0.8 ± 0.4

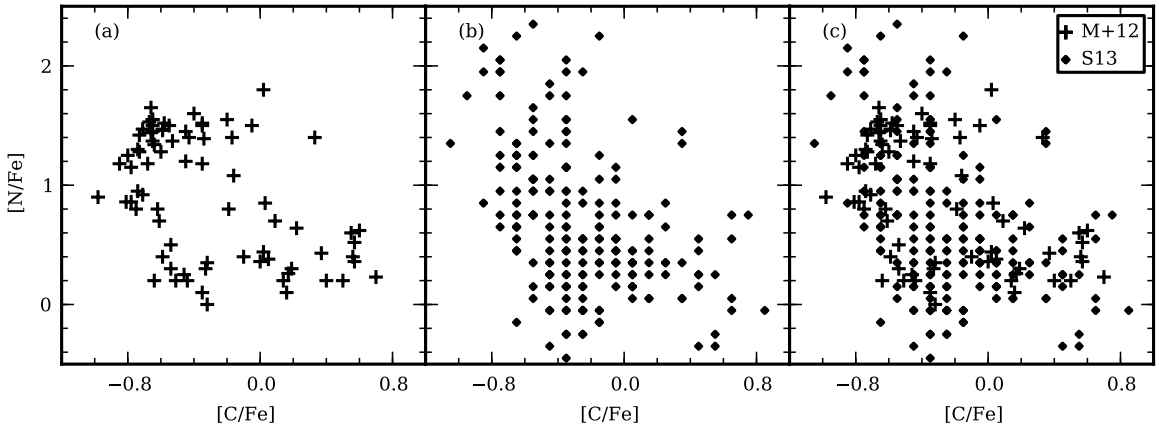

Figure 4.8 — The [C/Fe] and [N/Fe] for (a) Marino et al. (2012, M+12) (b) and this thesis (S13). (c) shows the combination of the two datasets. The abundances in this thesis were only determined to a precision of 0.1 dex due to the spectral resolution of the spectra. It shows the expected anticorrelation, as observed by Marino et al. (2012). This plot excludes eight stars that had extremely low [N/Fe] abundances determined in this thesis.

Table 4.6 — The cluster centres for the 74 stars from the Marino et al. (2011a, 2012) data. The column descriptions are the same as those in Table 4.5.

Group	Symbol	N. stars	[Fe/H]	[C/Fe]	[N/Fe]	[O/Fe]	[Na/Fe]	[Ba/Fe]
1	*	17	−1.9 ± 0.1	−0.5 ± 0.3	0.5 ± 0.3	0.3 ± 0.1	0.1 ± 0.2	−0.4 ± 0.2
2	○	18	−1.6 ± 0.2	0.3 ± 0.2	0.4 ± 0.2	0.6 ± 0.2	0.1 ± 0.1	0.4 ± 0.2
3	△	19	−1.6 ± 0.1	−0.6 ± 0.2	1.3 ± 0.2	0.0 ± 0.2	0.4 ± 0.2	0.3 ± 0.2
3b	▲	13	−1.5 ± 0.1	−0.5 ± 0.2	1.4 ± 0.1	−0.1 ± 0.2	0.6 ± 0.1	0.9 ± 0.2
4	×	7	−1.1 ± 0.1	−0.3 ± 0.3	1.6 ± 0.1	0.2 ± 0.2	1.0 ± 0.1	0.8 ± 0.1

There are two caveats for *k*-means clustering. First, the Euclidean distance is used. This could require the input data be transformed to give an appropriate range of values. This was not done in this thesis as the range of values was of similar magnitudes. Otherwise the clustering will be dominated by the parameter with the largest range. For example, if the radial velocity were included unchanged, the stars would simply be grouped in bands of radial velocity, as its have a 100 km s^{-1} range, much larger than the 1 dex range of the abundances. Second, the number of groupings must be appropriate for the dataset. Too few or too many groupings can lead to less definitive results. In this case, there was experimentation to determine an appropriate numbers of clusters.

Gratton et al. (2011) used *k*-means clustering on the Johnson & Pilachowski (2010) dataset to create seven groupings of stars in ω Cen. They used the [Fe/H], [α/Fe], [Na/O] and [La/Fe] to show there are three metallicity regimes in the cluster with a range of α-, light-, and neutron capture element properties. Their analysis confirmed each metallicity regime has its own correlations and anticorrelations amongst the different elements. Of particular interest was the very metal-rich group that showed a Na-O **correlation** and had the highest average neutron-capture element abundances of the groups in the cluster they identified.

It was recognized that the low resolution spectra of van Loon et al. (2007) meant there were larger uncertainties in each parameter than existed for Gratton et al. (2011) using the Johnson & Pilachowski (2010) data. This would make group identification harder. In order to first understand the groups that could be found when carbon and nitrogen were used in conjunction with some of the abundances that Gratton et al. (2011) used, it was decided to combine the Marino et al. (2011a, 2012) datasets and identify groups in them. There were 74 stars which had an [Fe/H] and [C,N,O,Na,Ba/Fe]. These six parameters were chosen to look for groupings as they could be also used for the dataset of 221 stars. Neither Marino et al. (2011a) nor Marino et al. (2012) determined an α-element abundance. However, Gratton et al. (2011) found that there was simply a positive correlation between metallicity and their α-element average for their groups, so it was not important to the clustering analysis.

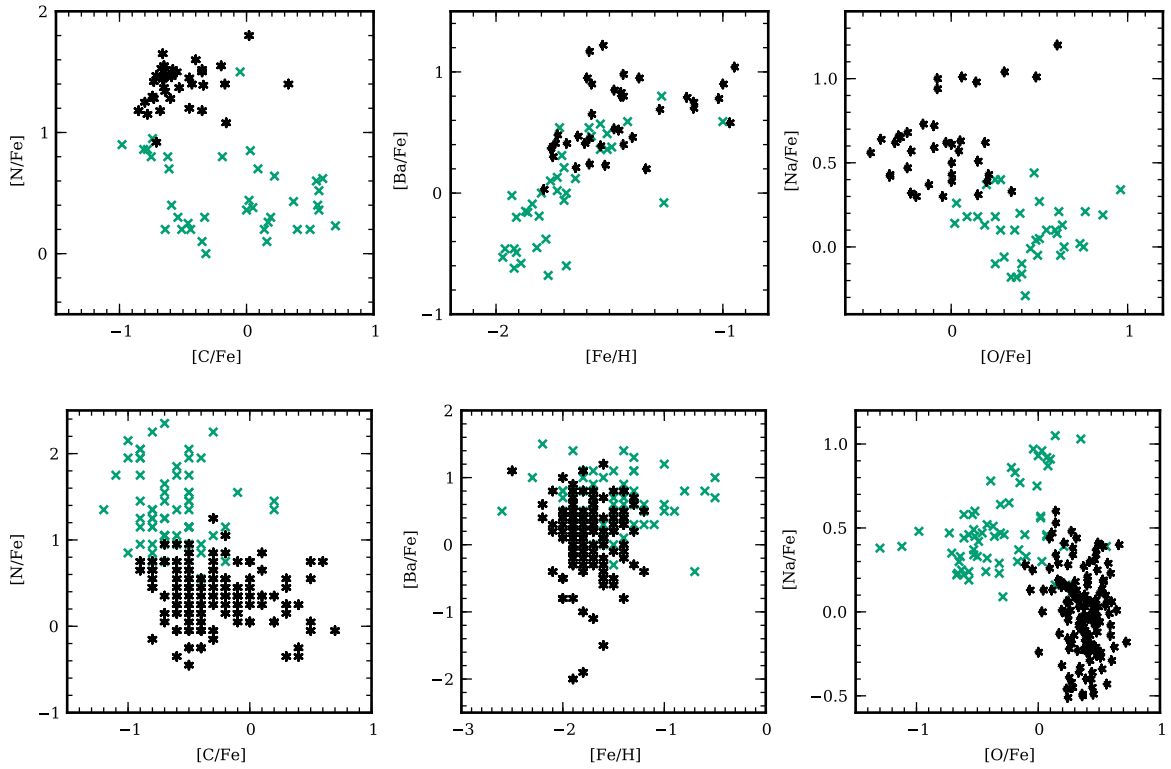

Figure 4.9 — The result of using two groups with k-means clustering on the (top row) Marino et al. (2012) dataset, and (bottom row) 221 star set. One group has been marked with $*$ and the other with $\times$.

Determining the optimal numbers of groups involved trying different number of groups to understand the groupings that were produced. The obvious starting place was two groups (Fig. 4.9). For the 221 stars, this created one group containing all the O-rich stars ([O/Fe] $\lesssim 0.17$) which are also N-poor (split at [N/Fe] ~ 1) and generally low in barium. The main driver of the separation is the nitrogen abundance, with a clear division between the two groups. This result was found for both the Marino et al. (2012) dataset and the 221 star set, though for Marino et al. (2012) the stars were more split in sodium than in oxygen.

For three groups (Fig. 4.10), it was not possible to have a unique solution, with the algorithm returning different results depending on its random starting seed. With the Marino et al. (2012) data there were two possibilities. One had all the N-poor stars ([N/Fe] $\lesssim 0.8$) as a group, and the N-rich stars being separated primarily due to their [Ba/Fe]. The other solution revealed that the O-rich stars consist of two distinct groups in terms of the [Fe/H], [Ba/Fe], [C/Fe] and [N/Fe]. This is the reason k-means clustering was used, as it can reveal details that could possibly not be obvious when using simple straight line cuts in two-dimensional parameters spaces.

As alluded to above, extreme outliers can drive the groupings in undesirable ways. This can be seen in the top row of Fig. 4.11, where the very N-poor stars create a separate group. To avoid this, these stars were removed from the dataset. It is known that their [N/Fe] was not precise as the pipeline was not sensitive to low nitrogen. Unlike the Marino et al. (2012) data, there was only one stable solution for three groups for the 221-star dataset (bottom row of Fig. 4.11). As with the second solution for the Marino et al. (2012) stars, this split the O-rich stars into two groups: C-poor/N-poor stars, C-rich/N-poor stars; and C-poor/N-rich stars. It was known that the very N-rich stars were also Fe-rich, so four groups were investigated to see if this extracted these stars as a separate grouping.

There were two possible groupings of four groups for Marino et al. (2012) (Fig. 4.12), with the primary difference between them being that the Na-rich stars. In one version, the very N-rich stars are a large separate group, while in the other version, it is the Fe-rich stars which form a large separate group. With more groups, the less precise 221-star subset created more possible solutions, with some being just subtly different from each other. One extreme

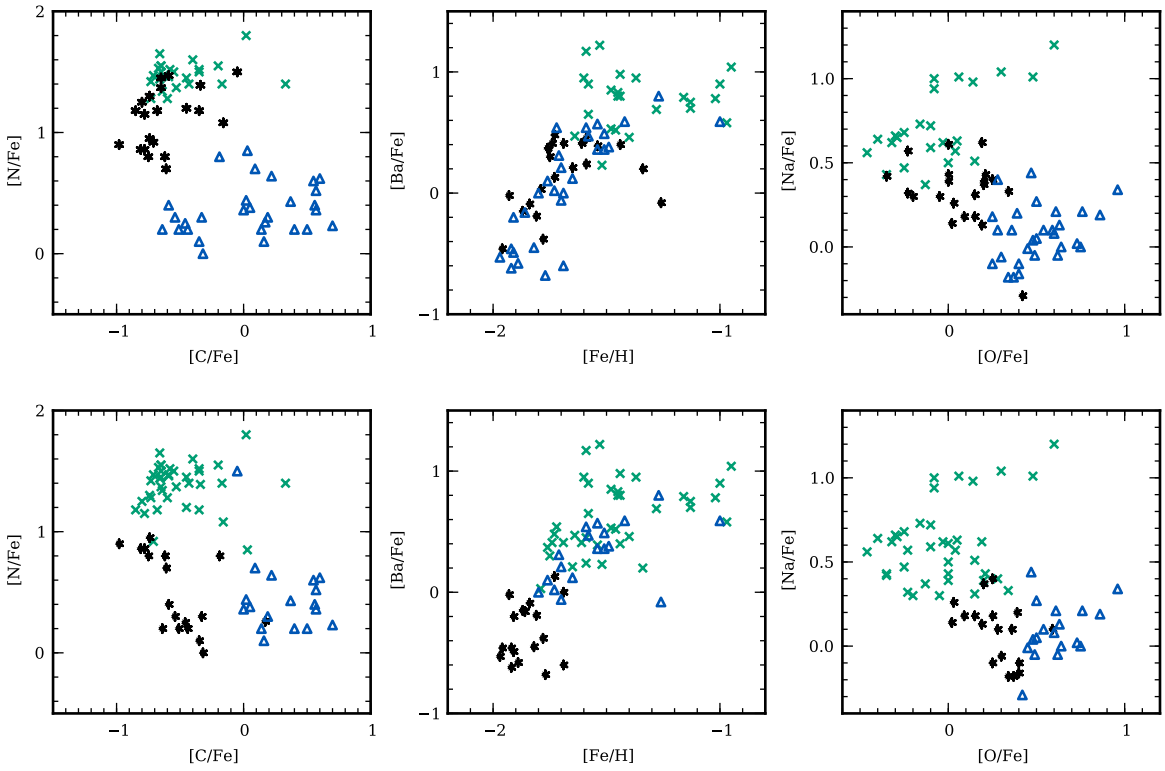

Figure 4.10 — Two possible results of using three groups with k-means clustering on Marino et al. (2012) dataset. Unlike with two groups (Fig. 4.9), there were two potential groupings found by the algorithm. The three groups are symbolized with $*$, $\times$ and $\triangle$.

version has all the O-rich stars as three groups and the Na-rich stars as one large group. The version that is used for subsequent discussion in this Chapter (bottom row of Fig. 4.13) has the very Na-rich stars forming one group, while the O-rich stars form two groups. The remaining Na-rich, O-poor stars form a fourth group. The selection of this grouping was driven by its replication of the grouping found for the Marino et al. (2012) stars (bottom row of Fig. 4.12).

It was decided to identify five groups in the Marino et al. (2012) dataset. Four groups did not isolate the stars with the extreme sodium abundances, with these stars being found in a group that consisted of a large range of metallicities and oxygen abundances, but the same barium abundances. Although five groups were used, two of the groups (#3a & #3b) were very similar in their properties so are sometimes discussed as one group.

Although we were able to define five groups from the Marino et al. (2011a, 2012) data, only four groups were attempted with 221 star set. This was because one of those groups (group #3b) found in Marino et al. (2011a, 2012) was primarily the result of it having higher barium abundance for its metallicity. This level of precision was not available in our data. As such, the same four overall groups were found, with group #3 having no subset that was s-process enhanced. Although Gratton et al. (2011) determined seven groups from the Johnson & Pilachowski (2010) dataset, we did not think that our sample with lower precision abundances would allow us to define that many groups. Any further division would have created signal out of noise.

The cluster centres of each group are given in Tables 4.5 and 4.6. In the context of this thesis, group #1 will be referred to as metal-poor, groups #2 & #3 as intermediate metallicity and #4 as metal-rich. This is similar to the labels given in Table 1.2 of the main population (MP), intermediate metallicity group (MInt), and RGB-a. By way of comparison, our group #1 is the equivalent of groups 4 & 6 in Gratton et al. (2011), our group #2 is their 1 & 5, our group #3 is their 2a & 3, and our group #4 is their 2b.

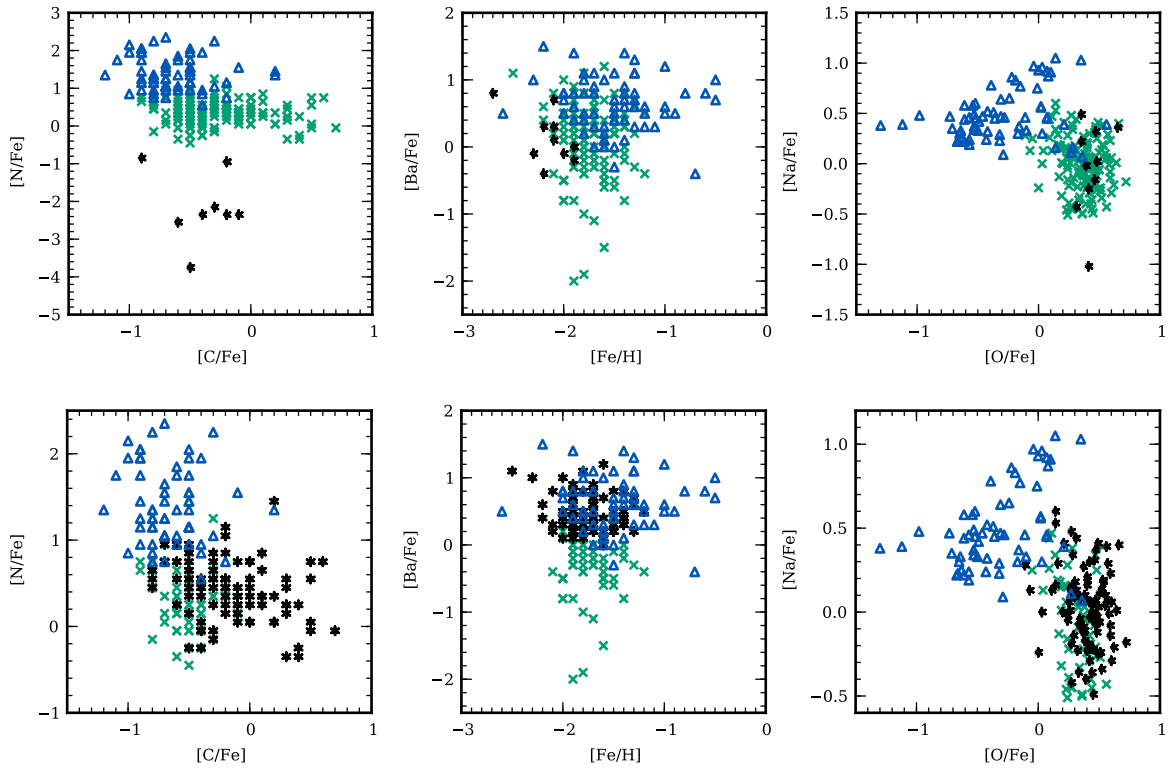

Figure 4.11 — The result of using three groups with k-means clustering on the 221-star dataset. The top row of plots illustrates one solution and how extreme outliers can drive the groupings, with the very N-poor stars found by the spectral matching pipeline creating a group of their own. The bottom row shows the single solution found for three for the 221 stars (minus the extreme-N outliers). The three groups are symbolized with $*$, $\times$ and $\triangle$.

4.4 Groupings in the Context of Abundances and the CMD

4.4.1 Groupings On The colour-magnitude diagram (CMD)

The stars of Marino et al. (2011a, 2012) were combined with Bellini et al. (2009a) and its high precision photometry and Figs. 4.14a, 4.14c and 4.15a show various CMDs with the groups found in the previous Section. Doing so gives a convincing demonstration that the k-means clustering does select physically different subsets of stars, lying on the identifiable RGB loci. The metal-poor group is clearly on the hot edge of the GB with little colour spread. As the metallicity increases, the stars are found at cooler positions. There are four stars in group #4 which are likely members of the RGB-a, the most metal-rich sequence in the cluster. These stars are found to be the most enriched in all the elements measured, except sodium where all of group #4 are equally enhanced (discussed in the next Sections).

As would be expected from their metallicity ranges, groups #2 and #3 have very similar magnitude and colour ranges, while group #3b is slightly cooler with a tight locus like group #1. As discussed in Section 6.3, group #3b could be an evolutionary extreme of group #3 or the end point of the sodium-oxygen anticorrelation trend before the stars begin to be sodium-oxygen correlated.

The correlation between metallicity and colour is expected from stellar evolutionary models. The small spread in [Fe/H] in group #1 correlates with a small spread on the CMD. Conversely, the larger spreads in iron for the intermediate metallicity groups are visible on the CMD. On the $T_{\rm eff}$-log g plane, a straight line was fitted through the group #1 stars, which could be used to produce a vertical plot of temperature deviation from the expected temperature for that gravity. The standard deviation of the temperatures in group #1 using this technique was 30 K. Group #2 were 100 ± 75 K cooler, #3 were 40 ± 90 K, #3b were 80 ± 30 K and #4 were 300 ± 60 K.

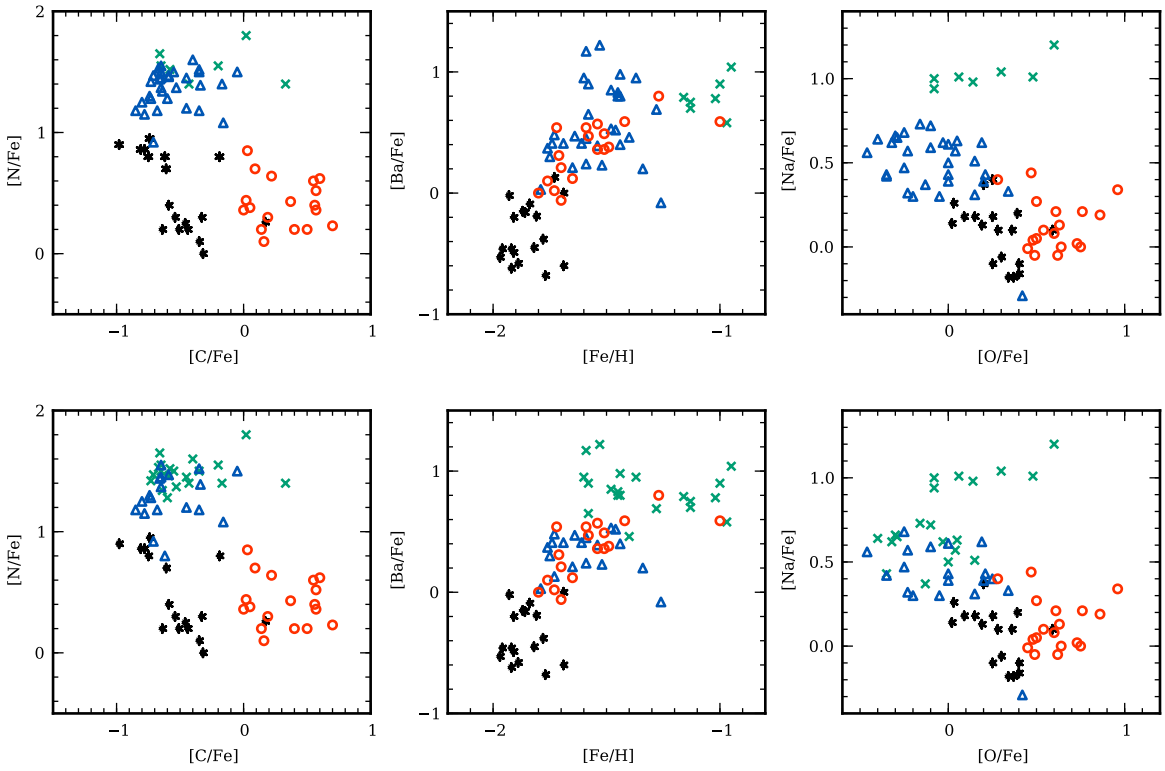

Figure 4.12 — Two possible solutions (top row & bottom row) resulting from using four groups with k-means clustering on Marino et al. (2012) set. Each group has a different symbol.

It is possible that star ID 215367 (Marino et al. 2011a numbering as this star is not in the van Loon et al. 2007 library) is an AGB star (circled in Figs. 4.14a, 4.14c and 4.15a), as it sits slightly to the left of the main locus of group #1 stars. This is most obvious in a U-$(U-V)$ CMD (Fig. 4.14c), as this region of the GB is at an almost constant U magnitude. Here, this star is at a much brighter U magnitude than would be expected for its $U-V$ colour. This star is found to have the lowest [C/Fe] (and [C/H]) of all the stars measured by Marino et al. (2012) (discussed in Section 4.4 and shown in Fig. 4.16). It is the most barium-rich of all the group #1 stars (Section 4.4).

Plotting the CMDs (Figs. 4.14b, 4.14d and 4.15b) for the 221 stars has the same conclusions as for Marino et al. (2011a, 2012) dataset. Compared to Figs. 4.14a, 4.14c and 4.15a there is more blending of the groups, which is a manifestation of the larger ranges of the metallicities of the groups than for Marino et al. (2011a, 2012). However at the bright end of the GB, there is still a tight locus of the most metal-poor stars. The metal-rich stars are also the coolest, as would be expected, and the two intermediate metallicity groups are inseparable.

Our larger sample size had nine stars that are on the well-defined AGB sequence (rectangle around region in Figs. 4.14b, 4.14d and 4.15b). These stars come from the metal-poor and intermediate metallicity groups and are all found in the carbon- and nitrogen-poor quadrant of the CN diagram. These, and other AGB stars, will discussed in Section 6.4, in the context of the potential absence of CN-strong stars on the AGB. The Johnson & Pilachowski (2010) dataset did not extend to magnitudes fainter than V = 13.5, which means there are only two members of the metal-rich RGB-a.

4.4.2 Sodium-Oxygen Anticorrelation

The k-means clustering of Marino et al. (2011a, 2012) dataset split the Na-O anticorrelation at about [Na/Fe] = 0.3, with groups #1 & #2 being oxygen-rich & sodium-poor, and groups #3 & #4 having the opposite properties (Fig. 4.17). The results confirm the results found by Johnson & Pilachowski (2010) and Marino et al. (2011a). They both found

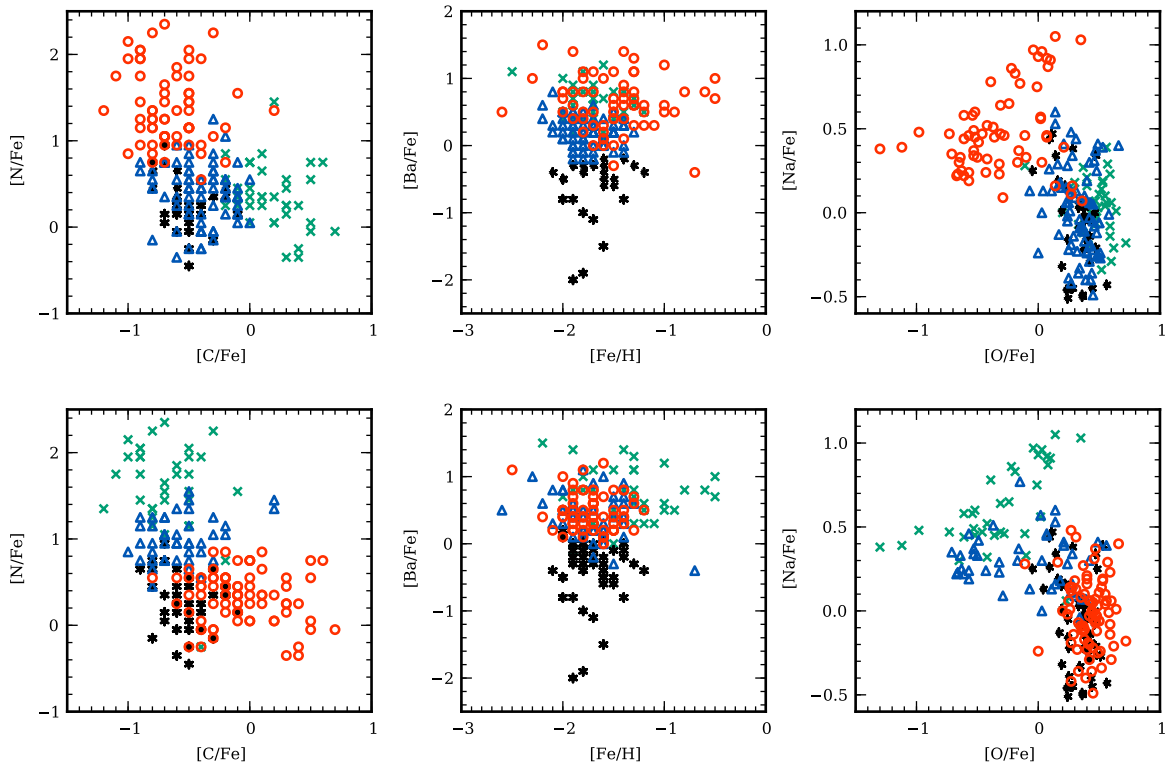

Figure 4.13 — Two possible solutions (top row and bottom row) resulting from using four groups with k-means clustering for the 221-star dataset. Each group has a different symbol.

that the intermediate metallicity stars displayed the well-known anticorrelation of monometallic clusters, while the metal-poor and metal-rich groups do not share this bimodal behaviour. The same result is observed for the clustering analysis of our data.

Plotting the abundances with respect to hydrogen instead of iron (Fig. 4.17c), the group #1 stars have the same [O/H] as group #3, with [Na/H] different by ~ 1 dex. Group #2 stars are about 0.5 dex enhanced in [O/H] compared to group #1 stars, and potentially slightly enhanced in sodium. If group #2 formed from the pollution of group #1 stars, this gas and dust would be enhanced in overall metallicity, oxygen and sodium. However if group #3 were formed after group #1, this would require an increase in metallicity and sodium, and a depletion in oxygen.

D'Antona et al. (2011) would have groups #3 and #3b at opposite ends of the evolutionary sequence that forms the sodium-oxygen anticorrelation. They theorized that the first stars of the second generation were sodium-rich, oxygen-poor and formed from pure AGB ejecta. As this ejected material was diluted by mixing the cluster's intra-cluster medium (ICM) with the surrounding interstellar medium (ISM), progressively oxygen-richer and sodium-poorer stars would form. This would continue until the AGB ejecta from these stars became the majority contributor to the gas of the cluster and produced sodium-rich stars. In this way, #3b could represent an extreme limit to sodium enhancement. The extension of group #2 into extremely high oxygen values is seen in the Marino et al. (2011a) dataset, but is not evident to the same extent in the larger Johnson & Pilachowski (2010) dataset.

Both Marino et al. (2011a, 2012) and our study show the **correlation** of sodium and oxygen in the most sodium-rich stars. This feature is not seen in monometallic clusters. The metal-rich stars of group #4 form this sequence, which would imply that they are the youngest stars of this sample, forming from the ejecta of the last supernovæ (SNe) in the cluster (though as discussed in Section 6.3, some propose it was not the last population to form in the cluster). Gratton et al. (2011) found this group to be the most enhanced in α-elements as well. The correlation between sodium and oxygen is most dramatically seen in Fig. 4.17a which used the Johnson & Pilachowski (2010) abundances. Here the correlation extends from [O/Fe] = −0.6 to 0.6.

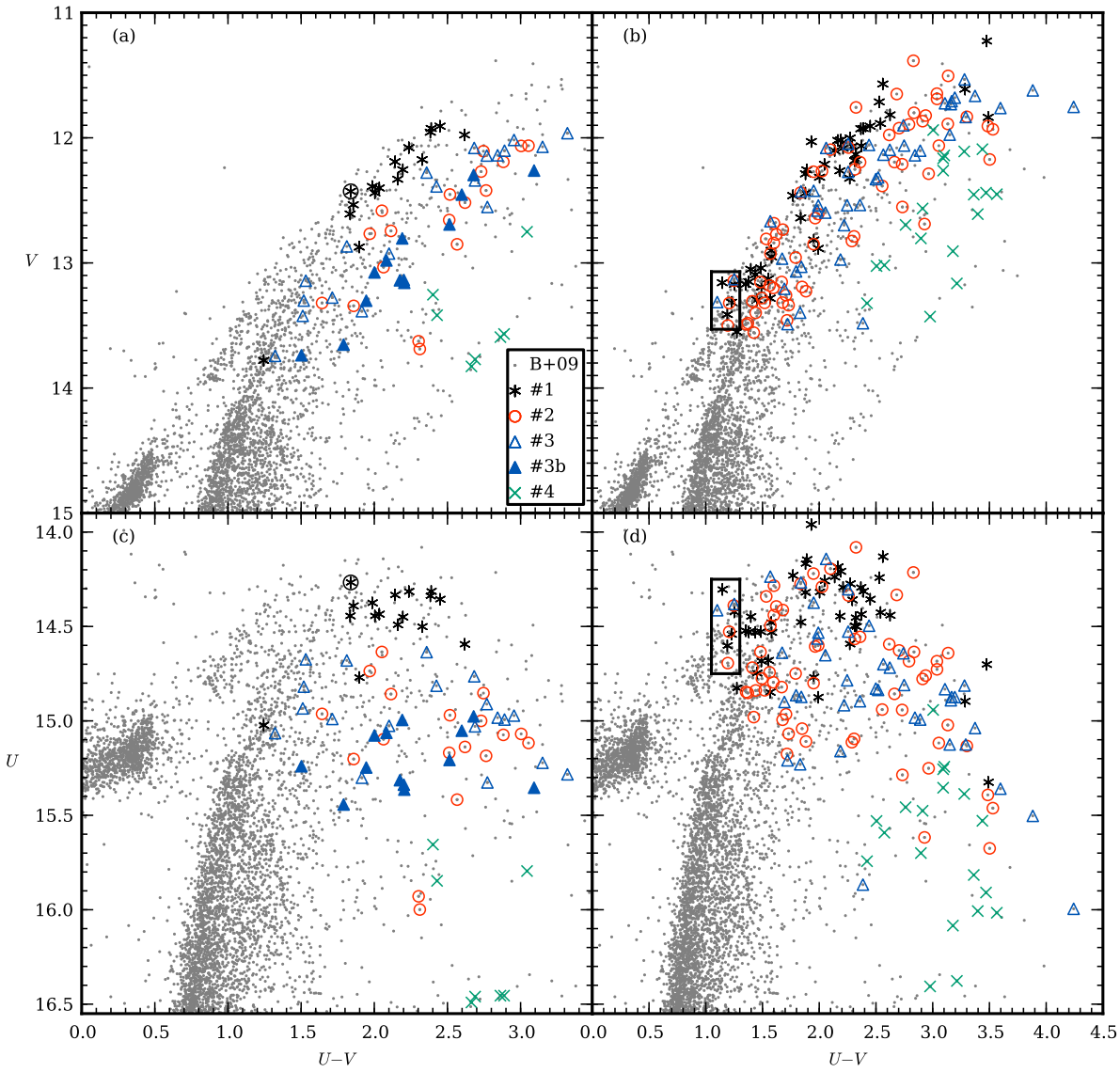

Figure 4.14 — (a) V-$(U-V)$, (c) U-$(U-V)$ CMD of the Marino et al. (2012) stars, with different symbols for the different groups as described in Table 4.6. (b) & (d) are the same for the 221 star set of this chapter. The small dots are the whole Bellini et al. (2009a) dataset. (a) & (c) The AGB star described in Section 4.4 is circled. (b) & (d) The nine stars surrounded by a rectangle that are between $13.0 > V > 13.5$ and $(U-V) < 1.4$ are highly likely to be AGB stars .

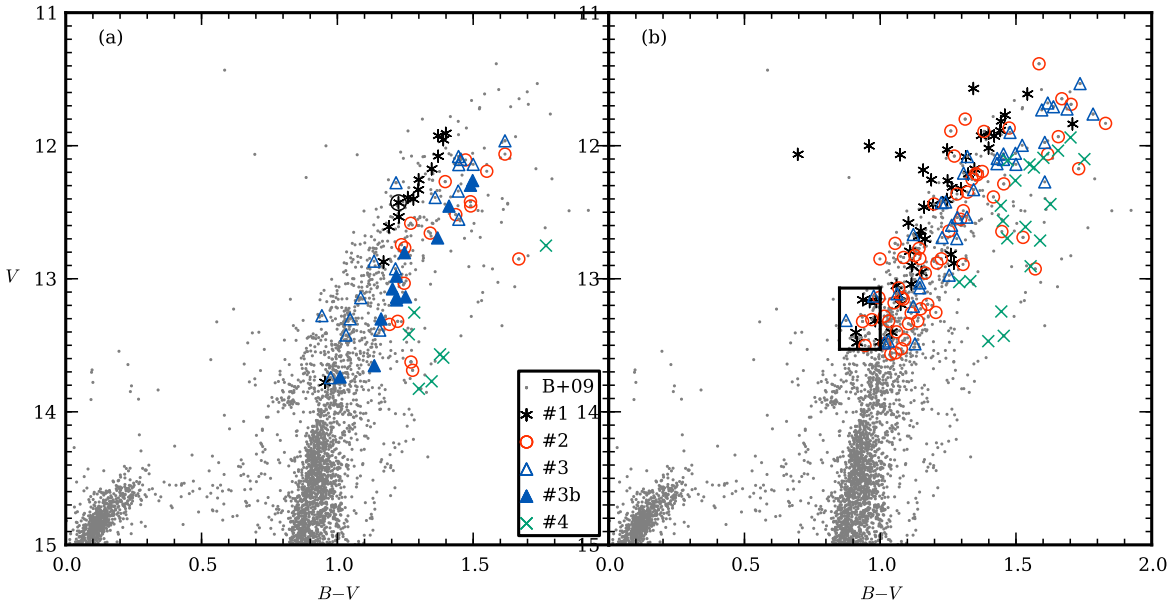

Figure 4.15 — (a) V-$(B-V)$ CMD of the Marino et al. (2012) stars, with different symbols for the different groups as described in Table 4.6. (b) The same for the 221-star set of this Chapter.

4.4.3 Carbon And Nitrogen

As with sodium-oxygen, there are roughly three regions of chemical abundances for carbon and nitrogen (Fig. 4.16): group #1 are C- and N-weak; group #2 are C-strong, N-weak; and groups #3 and #4 are C-weak, N-strong. There is a range of abundances in each grouping with #1 showing a range of 1 dex in [N/Fe] and about 0.6 dex in [C/Fe]. The intermediate metallicity groups have a range of 0.6 dex in [N/Fe] and [C/Fe]. Group #4, which has very few stars, ranges from [C/Fe] = −0.65 to 0.30.

Groups #3 and #3b of Marino et al. (2012) have similar ranges of [C/Fe] (Fig. 4.16b) but the #3b group form an upper limit for nitrogen for the intermediate metallicity groups. This is reinforced when the stars are plotted with [C/H] versus [N/H] (Fig. 4.16c). The group #3b stars have an average [N/H] = 0.01 ± 0.06, suggesting a maximum possible pollution for stars of this generation. Group #4 stars are found to have even higher nitrogen abundances with the four RGB-a stars having [N/H] > 0.45 ([N/Fe] > 1.4).

In monometallic clusters, the total C+N+O has been found to be constant (e.g., Carretta et al. 2005). In the case of ω Cen there is a large spread (Fig. 4.18). It was found that groups #1 and #2 have a straight-line relationship between [O/Fe] and [(C+N+O)/Fe] but with the other two groups having no correlation. Between [N/Fe] and [(C+N+O)/Fe], it is instead groups #3 and #4 that have the positive correlation. This illustrates that in the first two groups, it is nitrogen which is the dominant CNO species, while in the other two groups, it is oxygen. This is what would be expected based upon their relative abundances of nitrogen and oxygen.

In Marino et al. (2011a, 2012) (see our Table 4.6) there are 39 (53 %) stars in the N-rich groups and 35 (48 %) in the N-poor group, while in our work (see our Table 4.5) there are 148 (67 %) N-rich stars (groups #3 & #4) and 73 (33 %) N-poor stars (groups #1 & #2). We attribute this to a selection effect. The split in nitrogen groupings maps to the split in oxygen. In the Gratton et al. (2011) analysis, they had 574 (72 %) stars in O-poor groups (N-rich) and 223 (28 %) stars in O-rich groups (N-poor). So our groupings follow that of Gratton et al. (2011) in terms of the split of N-rich and N-poor stars. Our selection of stars was effectively based upon the selection of Johnson & Pilachowski (2010) through the use of their [Ca/Fe] and [O/Fe] abundances.

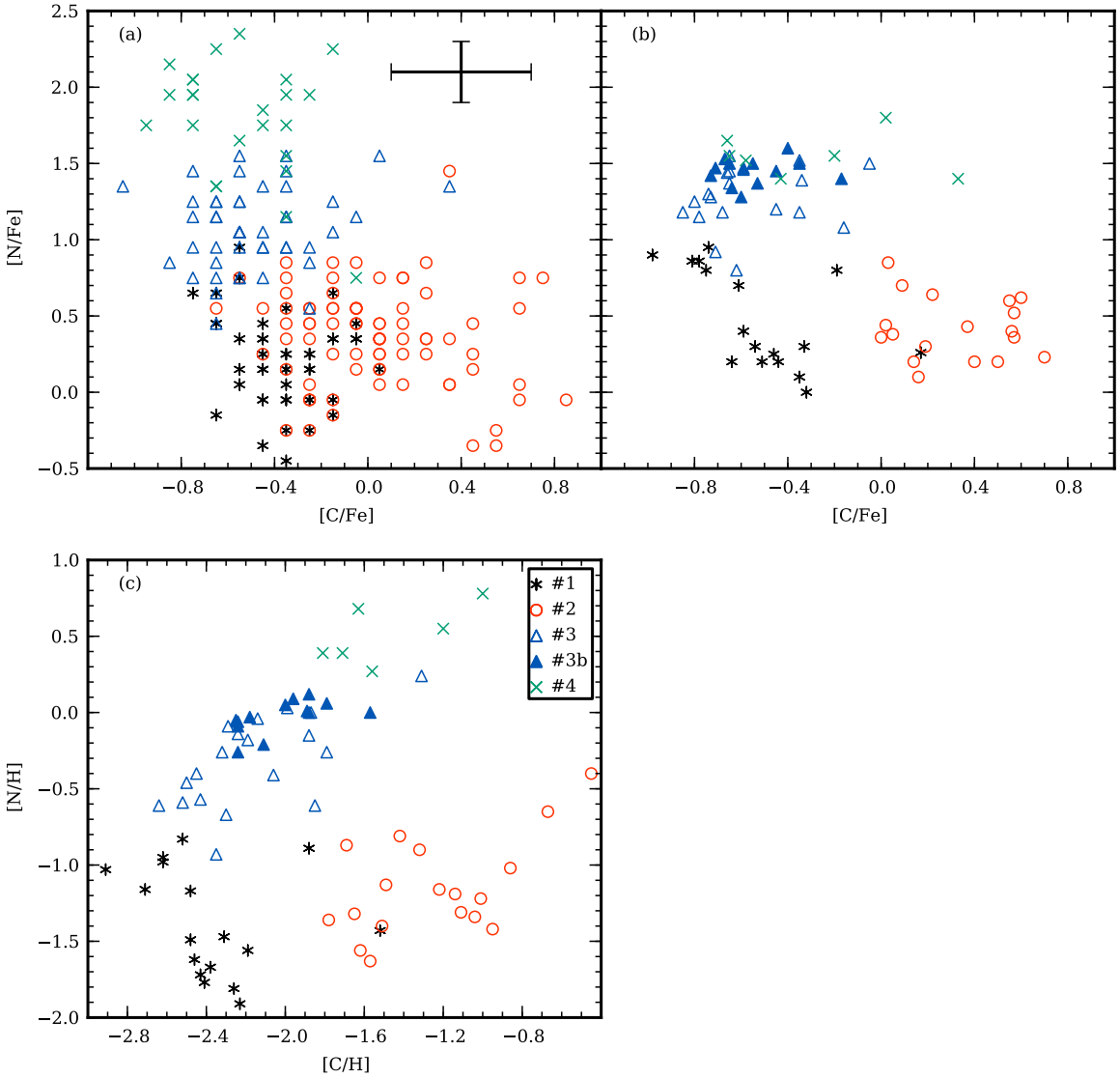

Figure 4.16 — Nitrogen against carbon for (a) this work and (b) & (c) Marino et al. (2011a, 2012). Uncertainties are shown in the bottom-left of each diagram. The C-N plane looks broadly similar to the Na-O plane. The metal-poor group (#1) is found to be deficient in both carbon and nitrogen, while the intermediate metallicity groups are bimodal. Group #3b shows an extreme enhancement of nitrogen. When considered with respect to iron (a) & (b), group #4 stars are very similar to those of group #3 in terms of their carbon abundance. However when they are considered with respect to hydrogen (c), their high metallicities result in a separate sequence, with some up to 0.8 dex higher than the solar value in nitrogen. The potential AGB star (Section 4.4) is the most carbon-deficient star in the Marino et al. (2011a, 2012) sample in (b) & (c).

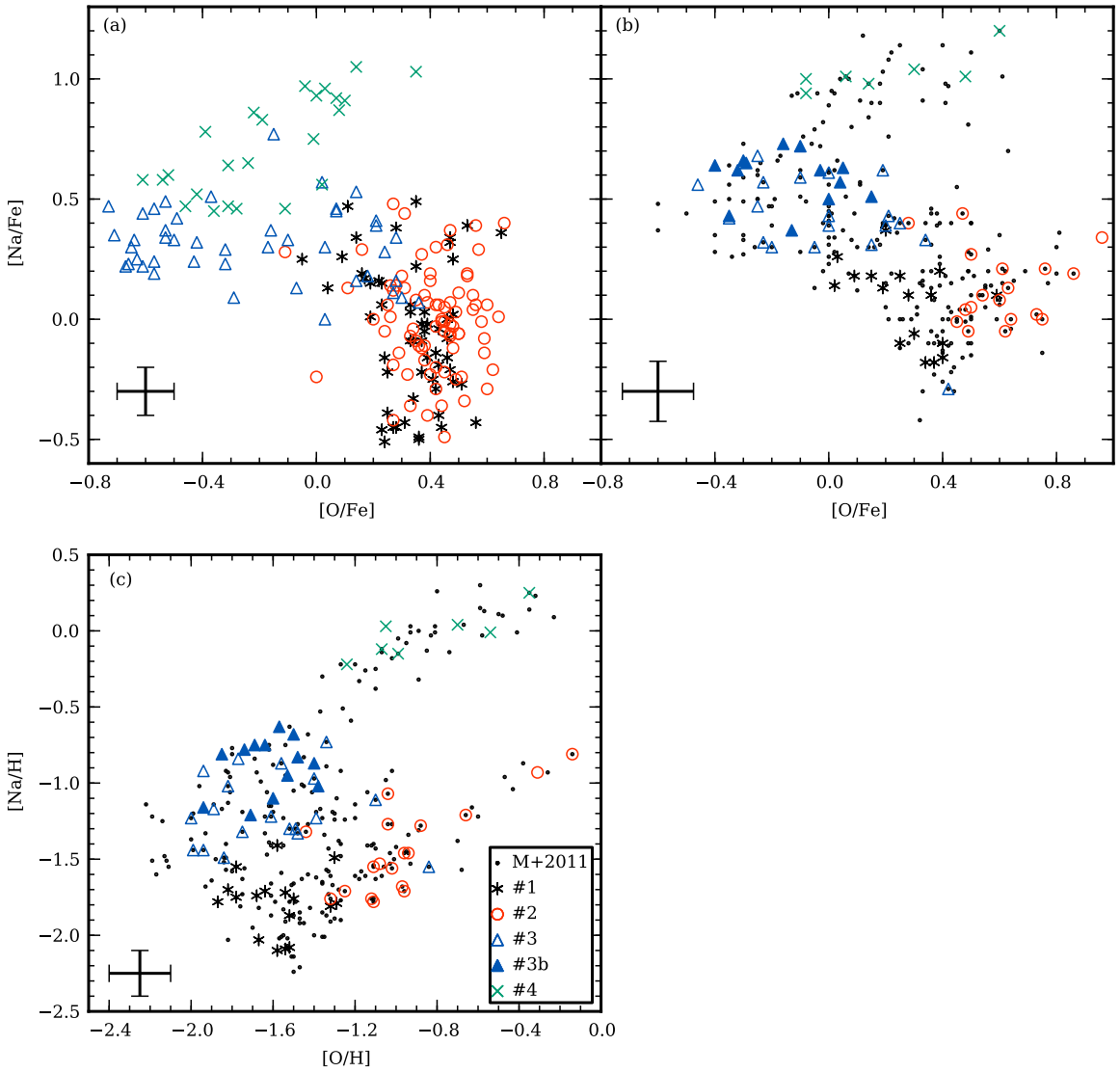

Figure 4.17 — The sodium-oxygen (anti)correlation for ω Cen of (a) this work and (b) & (c) Marino et al. (2011a, 2012). Symbols are as described in Tables 4.5 and 4.6 and uncertainties are shown in the bottom-left of each diagram. The small dots in (b) & (c) are the fuller Marino et al. (2011a) dataset. They illustrate that features observed (for instance the correlations within group #2 and #4) are not due to small numbers of stars. The sodium-oxygen anticorrelation is clearly present between groups #2 and #3. There is little separation between the two subgroups of #3, though potentially #3b is slightly more sodium-rich than #3. Group #1 is found to be the most sodium-poor on average but with an intermediate oxygen, both with respect to iron and hydrogen.

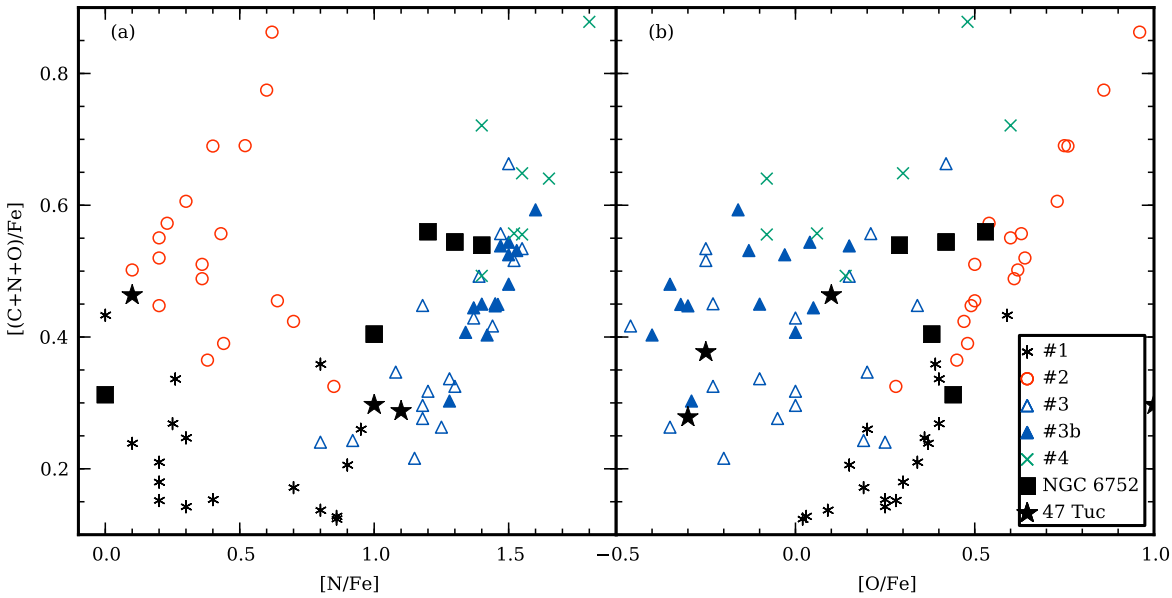

Figure 4.18 — The total C+N+O with respect to iron for the Marino et al. (2011a, 2012) dataset (using solar abundances from Anders & Grevesse 1989). Symbols as described in Table 4.6. Uncertainties are shown in the bottom-right of each diagram. Also included as sub-giant stars from 47 Tuc and NGC 6752 for comparison (Carretta et al. 2005). (a) the oxygen-rich groups (#1 & #2) have oxygen as their dominant CNO species, (b) while in the nitrogen-rich groups (#3 & #4) it is nitrogen. Unlike monometallic clusters, the total C+N+O is not constant.

4.4.4 s-process

A large range of s-process abundances is not typically observed in monometallic clusters. However, ω Cen does exhibit a very large range of abundances in elements such as barium. With a correlation between [Fe/H] and [Ba/Fe] (Fig. 4.19), the groupings were as would be expected from previous work (e.g., Johnson & Pilachowski 2010; Marino et al. 2011a). The metal-poor stars all had sub-solar abundances of barium with respect to iron, but with a very large range. Some stars had [Ba/Fe] = −0.8 while others had greater than the solar abundance in [Ba/H].

Unlike the other element combinations investigated in this study (C-N & Na-O), barium does not exhibit any differentiation between the intermediate metallicity groups of #2 and #3. This could require that any enhancements in metallicity and s-process happened before the anticorrelations.

The separation of group #3 from #3b is most evident (Fig. 4.19b). The two groups had about the same metallicity range, but a difference of about 0.5 dex in [Ba/Fe]. A caveat to this is that in Marino et al. (2011a) there were few stars at this metallicity/s-process abundance combination. They comment that at high barium abundances, the lines get too strong for accurate measurement. However we have kept them as a separate grouping due to their subtle separation in the other abundance planes that we investigated.

Neither Marino et al. (2011a, 2012) nor this work determined any r-process abundances. Johnson & Pilachowski (2010) did determine [Eu/Fe]. As noted by Gratton et al. (2011) there is no trend of [Eu/Fe] with [La/Fe], indicating that the contribution of the r-process to neutron-capture elemental abundances in the cluster are negligible. There is a potential increase in [Eu/H] at high [La/H], and the [La/Eu] abundance is dominated by changes in La. There is a larger scatter in [La/Fe] in the the metal-intermediate and metal-rich groups (almost 1 dex) but overall, in these groups, this ratio is constant.

4.5 Summary

This chapter presented the results of analyzing a 221-star subset of the van Loon et al. (2007) spectral library. These stars were selected as they had [O/Fe] abundances from Johnson & Pilachowski (2010), which allowed an analysis

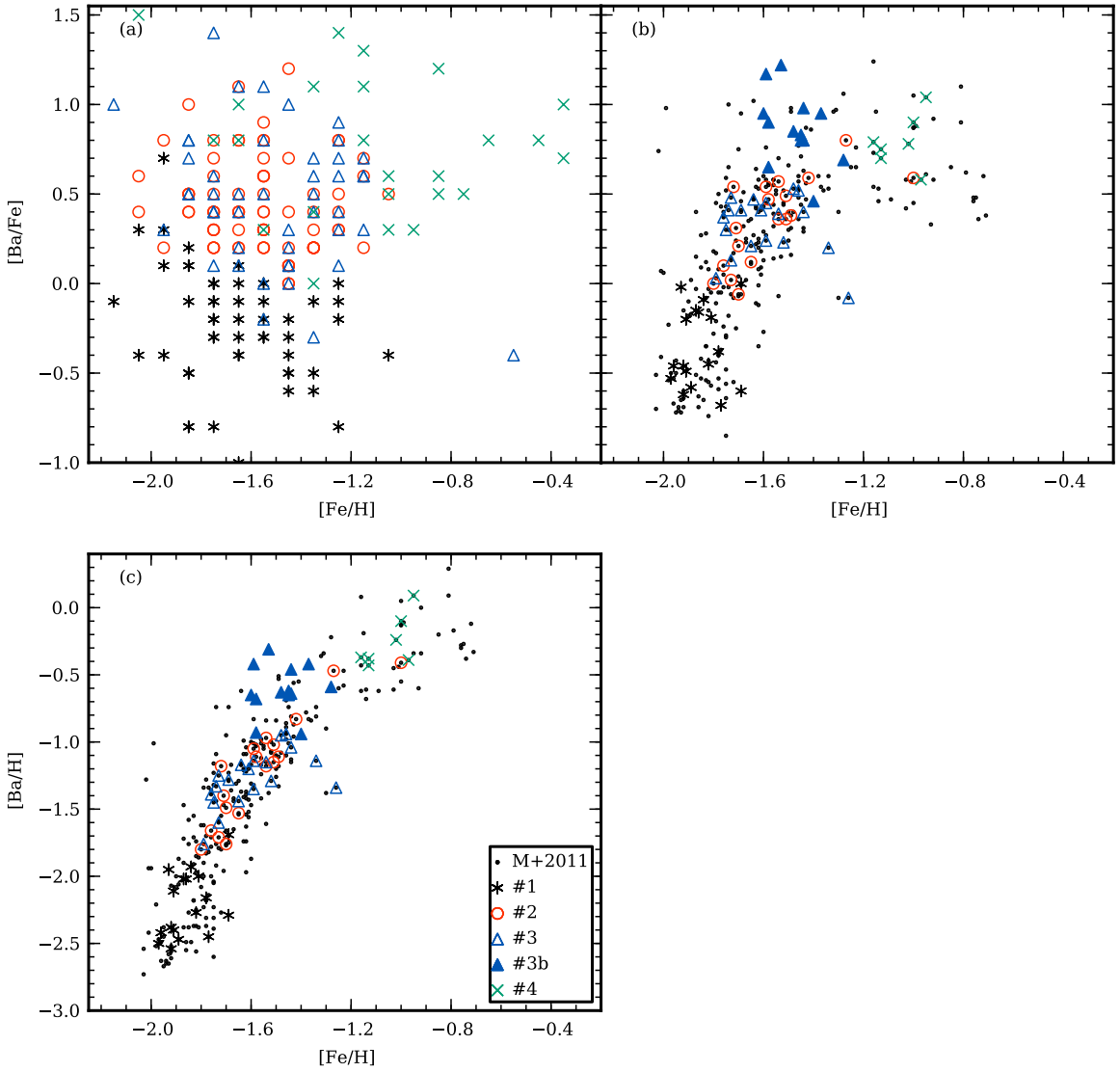

Figure 4.19 — The correlation between the metallicity of the stars and their s-process abundance for (a) this work and (b) & (c) Marino et al. (2011a, 2012). Uncertainties are shown in the bottom-right of each diagram. Only group #4 does not form part of the correlation, with the s-process abundance constant with respect to iron. One of the causes of the separation of group #3b from group #3 during the k-means clustering analysis is the roughly 0.5 dex difference in their [Ba/Fe].

that did not also rely on an estimate of the oxygen abundance. It was shown that the analysis returned results consistent with previous abundance analysis of ω Cen for carbon, nitrogen and barium. The stars were then grouped in chemically similar groups.

Using the Johnson & Pilachowski (2010) abundances as the basis does limit the analysis. They had a magnitude limit of $V < 13.5$, which meant it only just reached the magnitude level where it is possible to separate the AGB from the RGB. In the next chapter, the full van Loon et al. (2007) spectral library was analyzed using knowledge gained from this Chapter. Spectral indices were used to estimate [O/Fe]. It also used the same groupings found in this Chapter, developing criteria to apply them to independent datasets. The abundance results, and their implications of this Chapter, and the following, will be discussed in Chapter 6.

Chapter 5

ω Centauri: 848 Stars with Estimated [O/Fe]

The previous chapter investigated the abundances of 221 stars of ω Cen using known [O/Fe] from Johnson & Pilachowski (2010). This chapter discusses the creation of a 848 set of stars extracted from the van Loon et al. (2007) spectral library. As discussed previously, knowing [O/Fe] is vital for determining carbon and nitrogen from CH and CN molecular bands, due to the molecular equilibria that exists between CO, CH, CN (and other molecules) in the stellar atmosphere. In order to estimate oxygen abundances for these stars, spectral indices of CN and CH from van Loon et al. (2007) were used, taking advantage of the correlation between nitrogen and sodium, and the anticorrelation between sodium and oxygen. This allowed for a star to be classified as either oxygen rich or oxygen poor, and an appropriate [O/Fe] abundance used.

Section 5.1 describes how the [O/Fe] was estimated. Section 5.2 shows how the photometry was corrected for a difference between van Leeuwen et al. (2000) and Bellini et al. (2009a). Section 5.3 discusses the multiple analyses of each star that occurred for this Chapter. Section 5.4 describes the results and compares them to previous results from us and other researchers. Section 5.5 shows how the stars were placed into evolutionary groups. Section 5.6 discusses the abundances in terms of these groups.

This chapter is based primarily on Simpson & Cottrell (2013, accepted subject to revisions at submission of this thesis).

5.1 [O/Fe] Estimation from CN and CH Indices

In Chapter 4, the stars were selected from van Loon et al. (2007) to have abundances of [O/Fe] and [Ca/Fe] from Johnson & Pilachowski (2010). However for this analysis of the complete van Loon et al. (2007) library, these abundances are not known for all the stars. In the case of [Ca/Fe], a simple average value can be used. From Johnson & Pilachowski (2010) it was found that there was an overall mean [Ca/Fe] of 0.3 ± 0.1, with a very small positive correlation with metallicity. For stars with [Fe/H] < −1.8, ⟨[Ca/Fe]⟩ = 0.29; −1.8 > [Fe/H] > −1.6, ⟨[Ca/Fe]⟩ = 0.25; −1.6 > [Fe/H] > −1.4, ⟨[Ca/Fe]⟩ = 0.33; −1.4 > [Fe/H] > −1.2, ⟨[Ca/Fe]⟩ = 0.36; [Fe/H] > −1.2, ⟨[Ca/Fe]⟩ = 0.31. For all the stars analyzed in this Chapter, [Ca/Fe] = 0.3 was used.

The [O/Fe] abundance required a more nuanced approach. In Fig. 5.1 are the 291 stars that are in common between van Loon et al. (2007) and Johnson & Pilachowski (2010). There is a 1.5 dex range of [O/Fe], and as found in Chapter 4, there is a relationship between metallicity and oxygen abundance of these stars. At a particular metallicity, there could be the maximum range of [O/Fe], with the intermediate metallicity stars being both the most oxygen-rich and the most oxygen-poor stars in the cluster. Along with this range of metallicity, oxygen is involved in molecular equilibria with the two elements of interest: carbon and nitrogen.

For all the stars in the van Loon et al. (2007) library, there was a measurement of the S(3839) and CH(4300) indices[1] (Fig. 5.2). The first measured the CN band heads that extend blueward from 3883 Å and the second CH band at 4300 Å (the G band) (aee Harbeck et al. 2003 for the definitions used by van Loon et al. 2007).

There exists a correlation between these two indices and [O/Fe]. As shown in Fig. 5.3a, the oxygen-rich stars from Fig. 5.1 ([O/Fe] > 0.17), are found at lower S(3839) values than the oxygen-poor stars. This comes about

[1] It should be noted that these values used van Loon et al. (2007) normalized spectra.

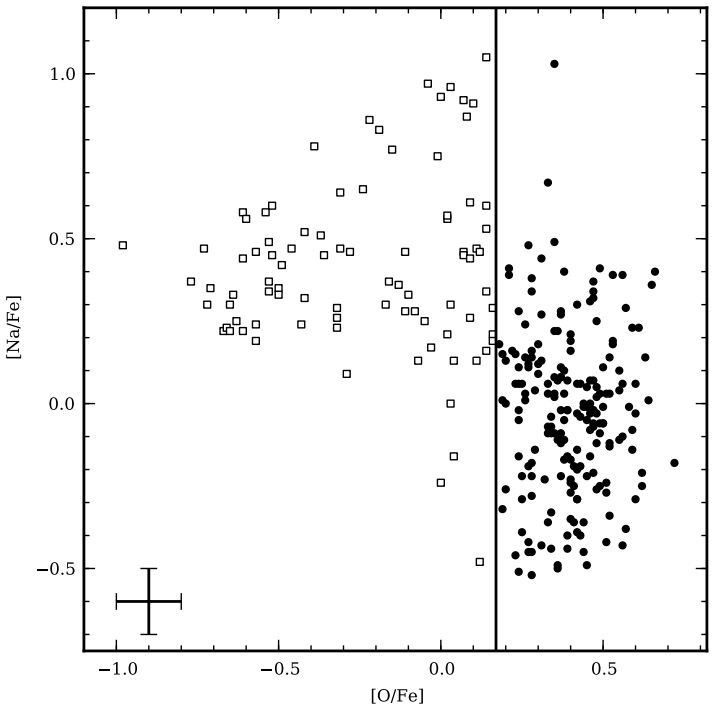

Figure 5.1 — [O/Fe] and [Na/Fe] determined by Johnson & Pilachowski (2010) for the 291 stars in common between it and van Loon et al. (2007). The vertical line is at [O/Fe] = 0.17, which was used as the divider between oxygen-poor (□) and oxygen-rich (•) stars as shown in Fig. 5.3. This definition of O-rich and O-poor stars is carried through to Fig. 5.3.

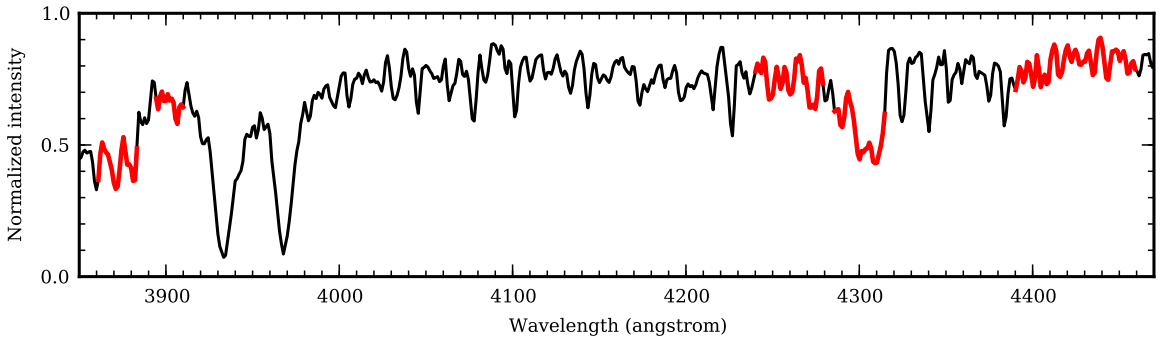

Figure 5.2 — Regions of the spectrum used for the spectral indices used by van Loon et al. (2007). The thick red lines on the left edge of the spectrum are for S(3839), and the lines on the right were used for CH(4300).

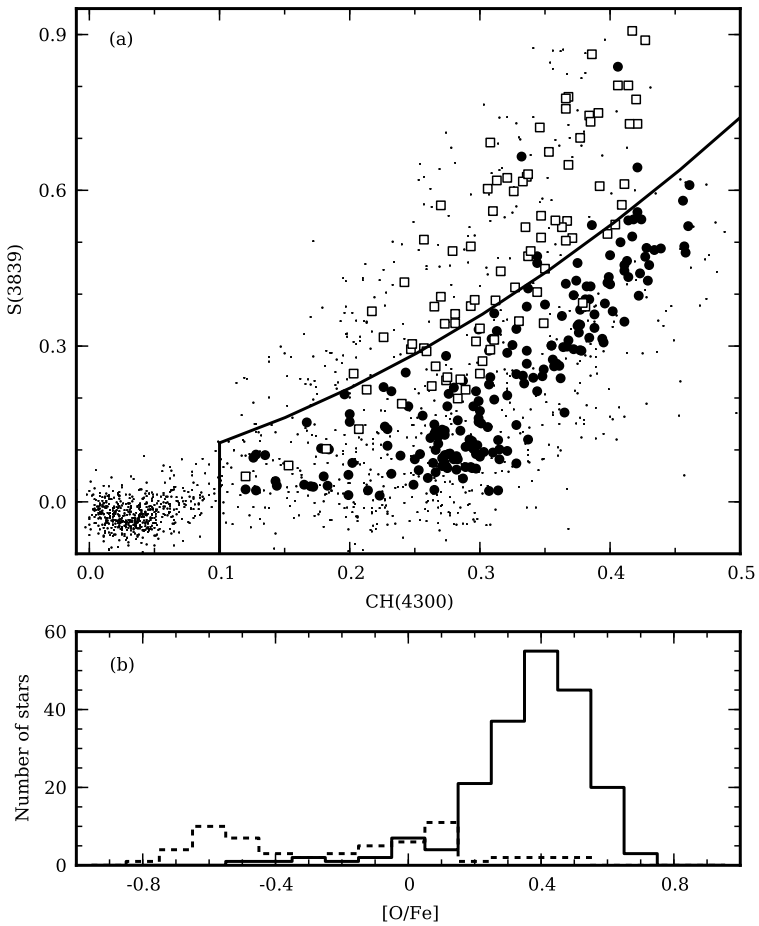

Figure 5.3 — (a) Positions of stars with [O/Fe] > 0.17 (•) and [O/Fe] < 0.17 (□) on the plane of CH and CN indices as found by van Loon et al. (2007). The line is a parabola that was selected to have as many of the O-rich stars below the line as possible. The small dots are the full van Loon et al. (2007) library. The concentration of stars with low values of both indices are the HB stars. (b) Histogram of the [O/Fe] abundance of stars above (solid line) and below (dashed) the line of (a). Note this subfigure excludes the HB stars.

because, the oxygen-rich stars are Na-poor and sodium is correlated with nitrogen. A line separating the two regions was created (in this case a parabola) that could be used to define oxygen-rich stars. It was decided to make sure that all the oxygen-rich stars were identified, at the loss of identifying some oxygen-poor stars as oxygen-rich (Fig. 5.3b). There were 27 stars (of 99 in total: 27 %) which were O poor ([O/Fe] < 0.17) which were below the parabola of Fig. 5.3a. They had a median [O/Fe] of −0.03. There were six O-rich stars (of 222 in total: 3 %) that were above the parabola, with a median [O/Fe] of +0.37. From now on in this Chapter, O-rich/O-poor refers to the stars below and above the parabola in Fig. 5.3a.

For O-rich stars, [O/Fe] = +0.4 was used as the input oxygen abundance for the spectral matching analysis. For the oxygen-poor stars, two values were investigated: [O/Fe] = −0.1 and −0.5, due to the range of possible [O/Fe] abundances for these O-poor stars. This means that the O-poor stars were analyzed twice.

5.2 Correcting for Systematic Differences in Photometry

For visible light, there were two sources of photometry for ω Cen used in this thesis: van Leeuwen et al. (2000) and Bellini et al. (2009a). The former was a proper motion study that used photographic plates observed in the

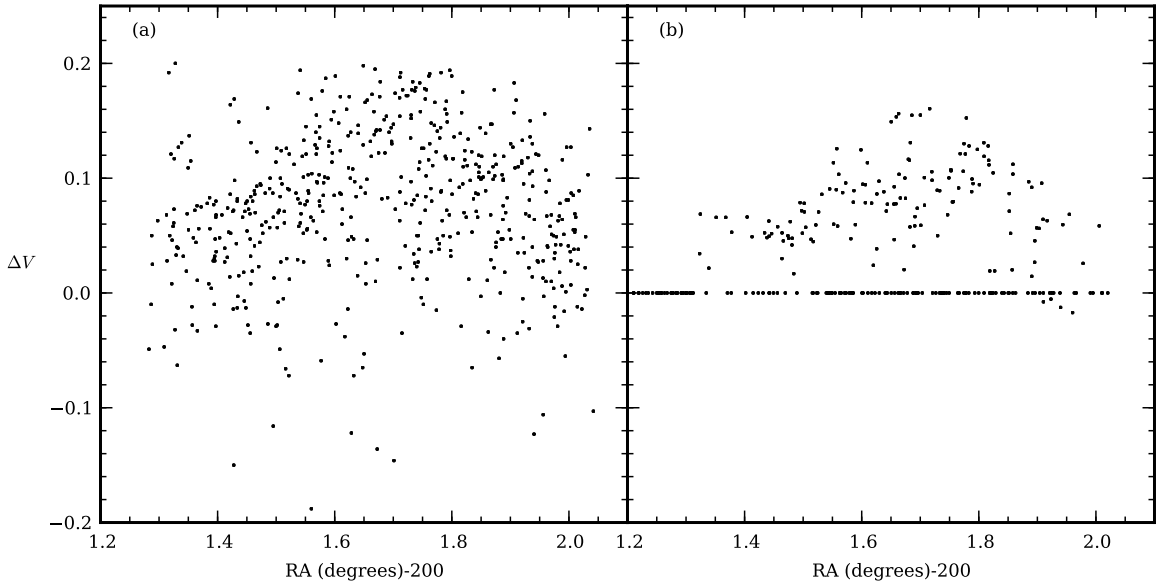

Figure 5.4 — (a) difference in the photometry between van Leeuwen et al. (2000) and Bellini et al. (2009a) ($\Delta V = V_{\mathrm{B+09}} - V_{\mathrm{vL+00}}$) as a function of the right ascension of the star. (b) the difference between the van Loon et al. (2007) photometry ($\Delta V = V_{\mathrm{corrected}} - V_{\mathrm{vL+00}}$) and that the corrected V magnitude for those stars that did not have Bellini et al. (2009a) photometry. The line of stars at $\Delta V = 0$ are those stars which were outside the observed region of Bellini et al. (2009a) and therefore had no correction applied to their photometry.

1930s and 1970s to identify cluster members, and to produce a photometric catalogue of the cluster. The latter was a CCD-based proper motion catalogue, described in Section 4.1.2. Using positional matching, there were 8322 matches between the two catalogues. These could be used to check for any systematic differences between the two catalogues, which would affect the T_{eff} and $\log g$ determination if the star did not not have Bellini et al. (2009a) photometry and only had van Leeuwen et al. (2000). It was found that ΔV between the two catalogues was not zero, nor constant with right ascension (Fig. 5.4). Instead stars close to the observed centre of the cluster had larger ΔV that those stars at the edges, with the Bellini et al. (2009a) photometry about 0.15 magnitudes fainter than the van Loon et al. (2007) photometry. The van Leeuwen et al. (2000) photometric reduction was not as robust in the very crowded core of the cluster. This change in V would translate to a change in the determined T_{eff} of the stars by 50–300 K across the $V-K$ range of the cluster.

The aim of this chapter was to analyze as many stars as possible and not be limited by the Bellini et al. (2009a) photometry, as had been the case in Chapter 4. Therefore a correction to the van Leeuwen et al. (2000) photometry was required so it was on the same abundance scale as Bellini et al. (2009a). The correction scheme was as follows: for stars in the observed region of Bellini et al. (2009a), but without Bellini et al. (2009a) photometry, the ten spatially closest stars which did have Bellini et al. (2009a) photometry were found. The average difference between van Leeuwen et al. (2000) and Bellini et al. (2009a) was found for these ten stars and that correction was applied to the unknown star's van Leeuwen et al. (2000) photometry. If the star was outside the observed region of Bellini et al. (2009a) then no correction was applied. Figure 5.4b shows the correction that was applied to these stars.

5.3 Spectral Matching Method

There were 1043 stars in common between the Two Micron All Sky Survey (2MASS) and van Loon et al. (2007) that also met the colour constraints of Alonso et al. (1999), in order to use the temperature-colour relationships described in Section 2.1. These stars could therefore have T_{eff}, $\log g$, [Fe/H], [C/Fe], [N/Fe], [Ba/Fe] determined

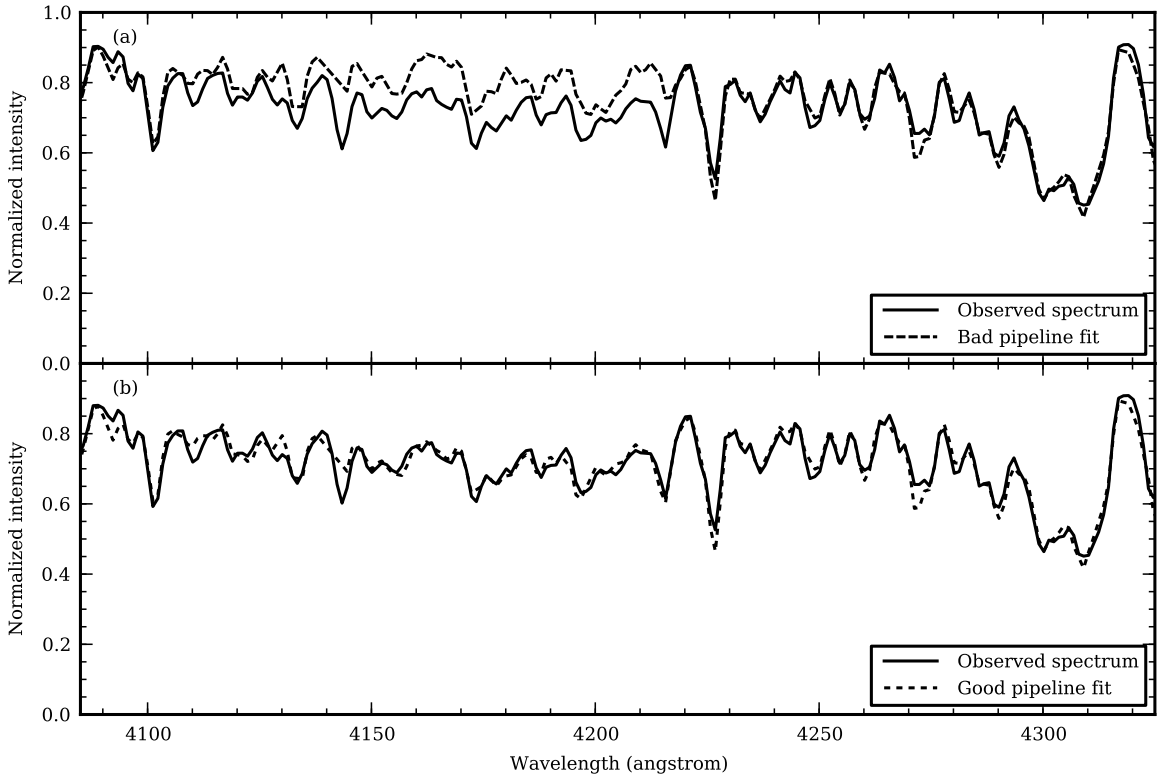

Figure 5.5 — Example of a star showing a bad fit due to search start position. (a) the spectral matching fit that resulted from a [N/Fe] initial abundance that was lower than the actual value ([N/Fe] = −0.5 instead of 0.0). Due to noise in the observed spectrum, the pipeline reached a local minimum and did not proceed to a better-fitting, nitrogen-richer abundance (b).

using the spectral matching pipeline described in Chapter 2, with a slight modification. For each star, three runs with three random starting positions were undertaken at the star's [O/Fe] abundances. This gave three values for [Fe/H], [C/Fe] and [N/Fe] for each [O/Fe] abundance for each star. A star had its abundance accepted if at least two of these runs resulted in the same value for all three elements (Fe, C, N). This allowed for stars where one starting position would not return a reasonable fit due to the parameter space search being trapped in a local minima (e.g., Fig. 5.5). The values reported in Tables 5.1 and 5.2 are the mode of value returned from the three runs. Of the 1043 stars, 912 (87 %) stars were accepted by these criteria. About 90 % of these 912 stars returned the same abundances on all three runs.

Breaking this down into O-rich and O-poor stars, there were 925 O-rich stars and 271 O-poor stars in the full set of 1043 stars. Of these, 678 of 925 (73 %) O-rich stars were kept and 234 of 271 (86 %) O-poor stars were kept. This result was expected as the O-rich stars include both N-poor stars and hotter stars. Both these groups are less likely to have 2 of the 3 runs converge. The spectral matching pipeline had a limit to how small the change in the strength of the spectral features could be before it stopped the search in that particular parameter. For instance, it would not continue to change the abundance of nitrogen in the model if the χ^2 changes by less than 0.00001.

To recap, the 1518 stars of the full van Loon et al. (2007) spectral library were reduced to 1043 stars through the constraints of Alonso et al. (1999), which were further reduced to 912 stars by the requirement for the spectral matching pipeline to return the same abundances from at least two of three random starting positions in its search.

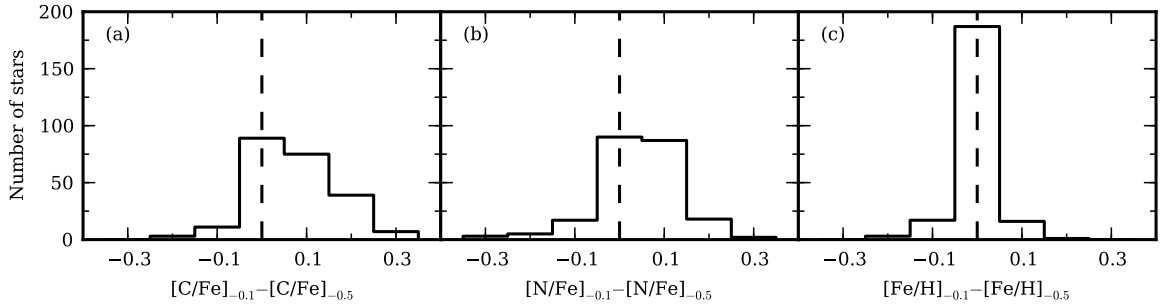

Figure 5.6 — Difference in (a) [C/Fe], (b) [N/Fe] and (c) [Fe/H] found using [O/Fe] = −0.1 and −0.5. These show that the different [O/Fe] input abundances do not significantly affect the output values of [C/Fe], [N/Fe] and [Fe/H]: 78 %, 87 % and 98 %, respectively, are within 0.1 dex. This justifies the adoption of a single oxygen abundance of [O/Fe] = −0.5 in the rest of this chapter for the O-poor stars.

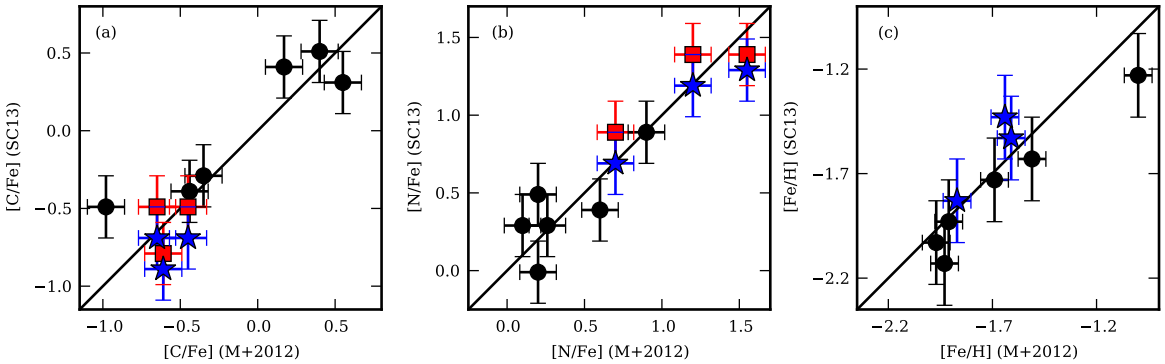

Figure 5.7 — The nine stars in common between this work and Marino et al. (2012) were used to determine systematic offsets. (a) [C/Fe] values were adjusted by 0.41 dex, (b) [N/Fe] by −0.51 and (c) [Fe/H] by +0.09. In (a) & (b), the abundances found using [O/Fe] = −0.1 (red circles) and −0.5 (blue stars) are shown. Those at the same [X/Fe] from Marino et al. (2012) are the same star. For [Fe/H], both oxygen-poor abundances returned the same [Fe/H].

Table 5.1 — Stellar parameters determined for the nine stars in common between Marino et al. (2012) and this work (≡ SC13). The LEID is the star label given by van Loon et al. (2007) and the ID is the numbering scheme from Marino et al. (2012). The [Fe/H], [C/Fe] and [N/Fe] are from Marino et al. (2012) and are shown for comparison.

LEID	ID	[Fe/H]		[C/Fe]		[N/Fe]		[O/Fe]	
vL+07	M+12	M+12	S13	M+12	S13	M+12	S13	M+12	S13
33139	250606	−1.00	−1.3	0.55	−0.1	0.60	0.9	0.86	+0.4
35090	246585	−1.64	−1.5	−0.65	−1.1	1.55	1.8	−0.25	−0.5
36156	245724	−1.97	−2.1	−0.44	−0.8	0.20	0.5	0.30	+0.4
37253	242745	−1.91	−2.0	−0.35	−0.7	0.10	0.8	0.37	+0.4
38115	241359	−1.69	−1.8	0.17	0.0	0.26	0.8	0.40	+0.4
46150	224500	−1.51	−1.7	0.40	0.1	0.20	1.0	0.49	+0.4
46194	225246	−1.87	−1.9	−0.61	−1.3	0.70	1.2	0.19	−0.5
48235	220325	−1.61	−1.6	−0.45	−1.1	1.20	1.7	0.00	−0.5
51091	215367	−1.93	−2.2	−0.98	−0.9	0.90	1.4	0.15	+0.4

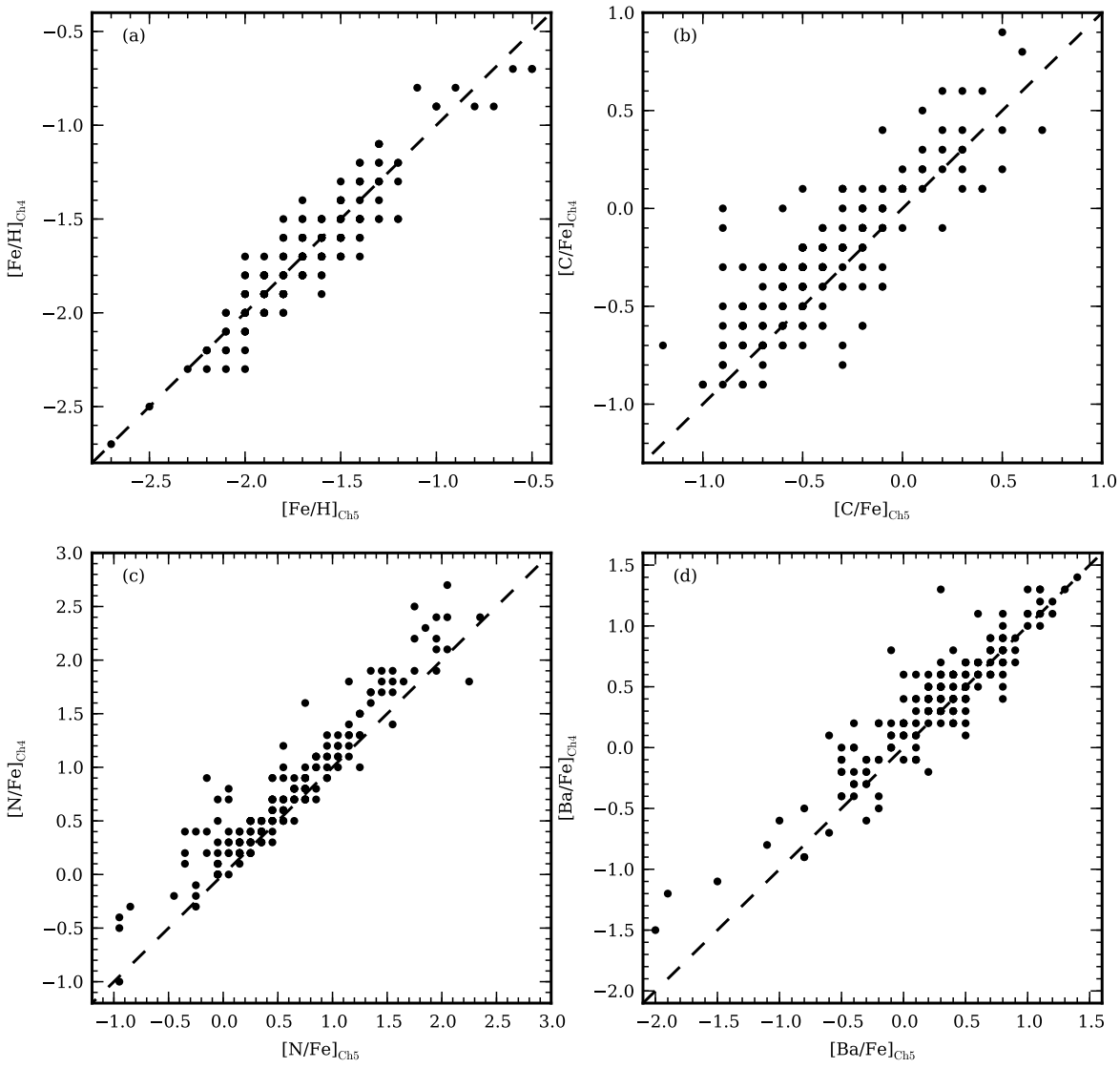

Figure 5.8 — Comparison of abundances found in Chapters 4 and 5 for (a) [Fe/H]; (b) [C/Fe]; (c) [N/Fe]; (d) [Ba/Fe]. In all cases the dashed line is the one-to-one line for comparison.

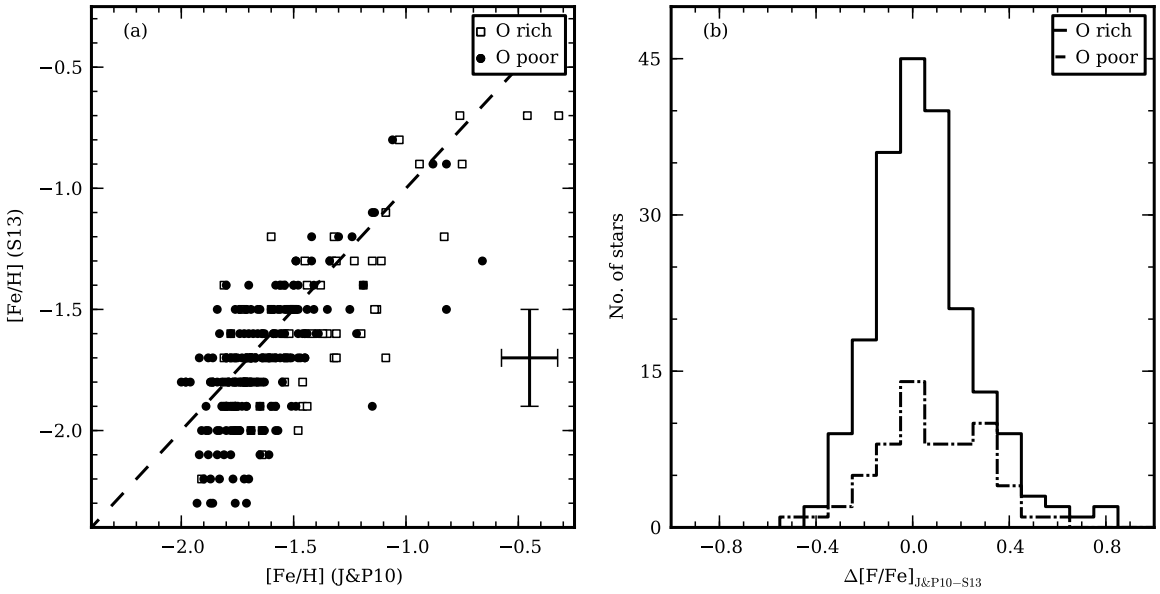

Figure 5.9 — Comparison of the [Fe/H] values found for the same stars in this work and those of Johnson & Pilachowski (2010). The straight line (a) is the one-to-one line for comparison.

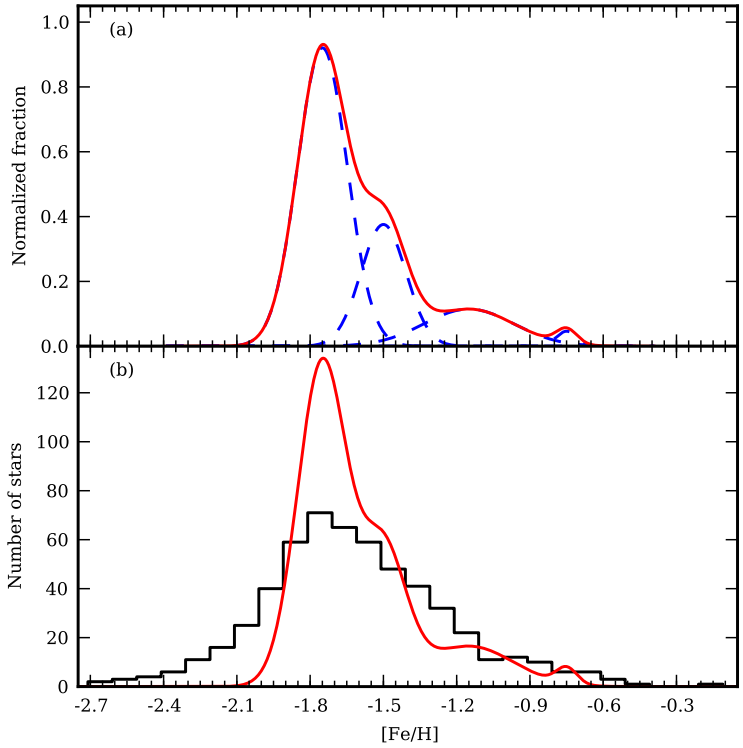

Figure 5.10 — (a) Metallicity histogram from Johnson & Pilachowski (2010), with a solid red line showing the best fitting result of adding together four Gaussians with $\mu_{[Fe/H]}$ of −1.75, −1.50, −1.15 and −0.75 (dashed blue curves). (b) [Fe/H] histogram of this study with the solid line from the top panel for guidance.

5.4 Cluster Membership & Quality Assurance

Cluster membership was determined using the radial velocity from van Loon et al. (2007) and membership probability from Bellini et al. (2009a). A star was classified as a cluster member if its radial velocity was 185 km s^{-1} < $v_{\rm rad}$ < 275 km s^{-1}; this excluded twelve stars of the 912. The membership probability of Bellini et al. (2009a) was only available for those stars that had positional matches to their photometric library. A cut off of 90 % was selected based up Figure 12 of Bellini et al. (2009a), which showed that the bulk of stars in the magnitude range of the van Loon et al. (2007) spectral library had membership probabilities above 90 %. These two criteria cut that number of stars to 848.

For the oxygen-poor stars, there were two values of [Fe/H], [C/Fe] and [N/Fe] due to the use of two [O/Fe] abundances (−0.1, −0.5). It did not make sense to simply take the average. The reason for using two values was that it was unknown how oxygen poor the star was simply from its CH(4300) and S(3839) indices. Taking the average of the [Fe/H], [C/Fe] and [N/Fe] abundances would not return the correct value for those stars that were at the extremes of the oxygen abundance. Inspection of the histograms in Fig. 5.6 showed that there was not a large difference between the [C/Fe], [N/Fe], [Fe/H] determined with [O/Fe] = −0.1 or −0.5. For [Fe/H], 83 % of the stars returned the same metallicity value and 98 % were within ±0.1 dex. For [C/Fe], 78 % were within ±0.1 dex, and for [N/Fe] it was 87 %. For this reason it was decided to use only one oxygen abundance for the oxygen-poor stars in the sample. As such subsequently all results in this Chapter have [O/Fe] = +0.4 for the O-rich stars, and [O/Fe] = −0.5 for the O-poor stars.

Of the 77 stars in Marino et al. (2012), nine[2] were is common with the 848 stars presented in this research (Fig. 5.7 and Table 5.1). These are the same stars as in Section 4.2. These nine stars provided a direct comparison for Fe, C and N, with the caveat that the abundances were determined with different [O/Fe] in Marino et al. (2012) to this Chapter. Assuming a straight line with a gradient of unity, the best fitting intercept for [Fe/H] was +0.09, [C/Fe] was +0.47 and [N/Fe] was −0.51. All subsequent values of [Fe/H], [C/Fe] and [N/Fe] have had these offsets applied (with the values rounded to one decimal place).

There were 197 stars in common between Chapter 4 and this Chapter. The missing stars were the result of them, either not meeting the new convergence criteria of Section 5.3, or that they only spectra that was in a low signal-to-noise observing run of van Loon et al. (2007) that were excluded from the analysis of this Chapter. There was some scatter between the results found (Fig. 5.8) but this was expected due to the changing value of [O/Fe]. Like in Figs. 3.16 and 3.17, there was a systematic offset in [N/Fe] for the different [O/Fe] inputs. As in Section 3.1.2, the cause of this was unknown but was only of the order of 0.1 dex so it did not of concern to the results of this Chapter and this thesis.

In Figs. 5.9 and 5.10, the [Fe/H] of this work and Johnson & Pilachowski (2010) are shown. There was some degeneracy in our values, but this is expected due to the lower resolution used here compared to in Johnson & Pilachowski (2010). We also found that the metallicity distribution was broadly similar with a long tail towards metal-rich abundances. The strength of the peak at [Fe/H] = −1.75 was not as great in our data, with a fraction of stars found at very low metallicities, which were found to have higher metallicities by Johnson & Pilachowski (2010).

Inspection of the full set of spectral fits showed that there was a temperature limit, above which there was little sensitivity to changes in the iron, carbon and nitrogen abundances in the model atmosphere. A value of $T_{\rm eff} \leq$ 4900 K was selected as the temperature limit (Fig. 5.11). A further limit was imposed that CH(4300)> 0.1 to exclude any HB stars (see Fig. 5.3a). This created a subset of 557 stars of the 848 cluster members, which had abundances determined from the input catalogue of 1015 stars with photometry and within the colour range of Alonso et al. (1999). Table 5.2 presents the abundance results for the 848 stars. On all subsequent figures, it is only the 557 star set that is plotted.

5.5 Clustering Analysis

From Chapter 4 it was known that there were at least four distinct groups of stars based upon their abundances. Each group had distinguishing abundance characteristics, which in this Chapter are used to place the stars into

[2] LEID36179 (ID 244812, Marino et al. 2011a) also matched but was excluded due to the extreme mismatch in its [N/Fe], as also found in Section 4.2.

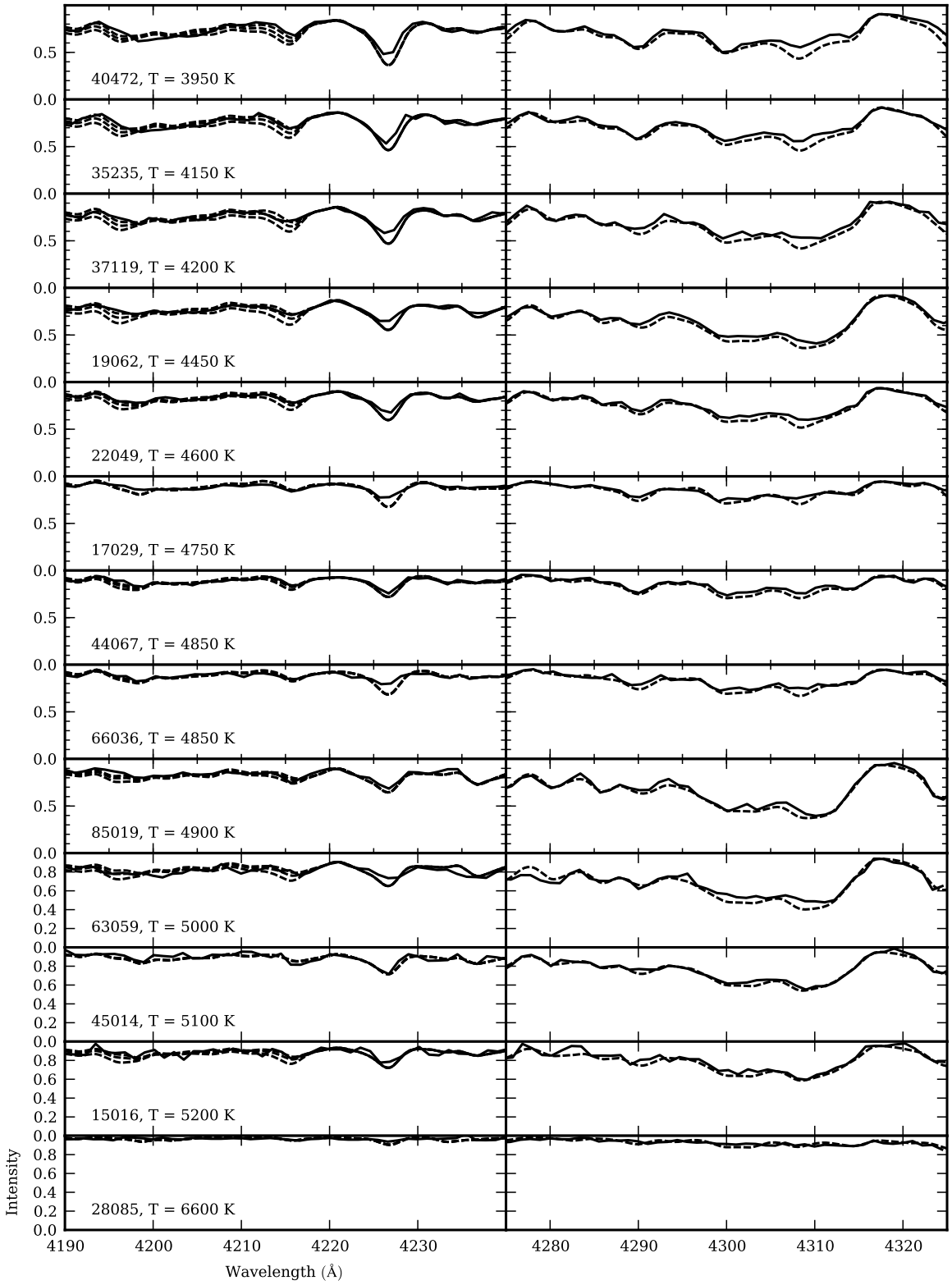

Figure 5.11 — Examples of the spectra across the temperature range in ω Cen. The solid line is the observed spectrum. The three dashed lines show the best fitting synthetic spectra with [N/Fe] ± 0.3.

Table 5.2 — Stellar parameters determined for the 912 stars. For each star an identifier from van Loon et al. (2007) (LEID) and 2MASS is given. For stars that also matched to Bellini et al. (2009a, B+09), their identifier is provided. In the full version of the table, the non-cluster members described in Section 5.5 are appended.

LEID	2MASS	B+09	$T_{\rm eff}$(K)	[Fe/H]	[C/Fe]	[N/Fe]	[Ba/Fe]	[O/Fe]	Group
42044	13260536-4728206	200024	3650	−1.5	0.2	2.5	0.7	0.4	4
35094	13262881-4725235	259071	3700	−1.2	−0.4	2.6	1.3	0.4	4
48150	13263981-4731069		3750	−1.9	0.9	1.2	1.5	0.4	2
25065	13270118-4720409		3850	−1.3	−0.9	2.4	0.3	−0.5	4
48120	13263304-4731003		3850	−1.7	0.4	1.2	0.2	0.4	2
47399	13271864-4730509	149466	3900	−1.6	0.1	0.8	0.1	0.4	2

(This table is available in its entirety in a machine-readable. A portion is shown here for guidance regarding its form and content.)

Table 5.3 — The cluster centres found using the grouping criteria described in Section 5.5 for the 557 stars. For each parameter, the average and standard deviation are given, along with the number of stars in each group. The symbol is the identifier used for that group in the figures.

#	Symbol	No.	[Fe/H]	[C/Fe]	[N/Fe]	[Ba/Fe]
1	∗	79	−1.7 ± 0.3	−0.2 ± 0.2	0.1 ± 0.5	−0.4 ± 0.4
2	○	254	−1.7 ± 0.4	0.1 ± 0.4	0.3 ± 0.5	0.7 ± 0.4
3	△	165	−1.7 ± 0.3	−0.5 ± 0.2	1.1 ± 0.3	0.4 ± 0.6
4	×	59	−1.1 ± 0.4	−0.5 ± 0.4	1.8 ± 0.5	0.7 ± 0.6

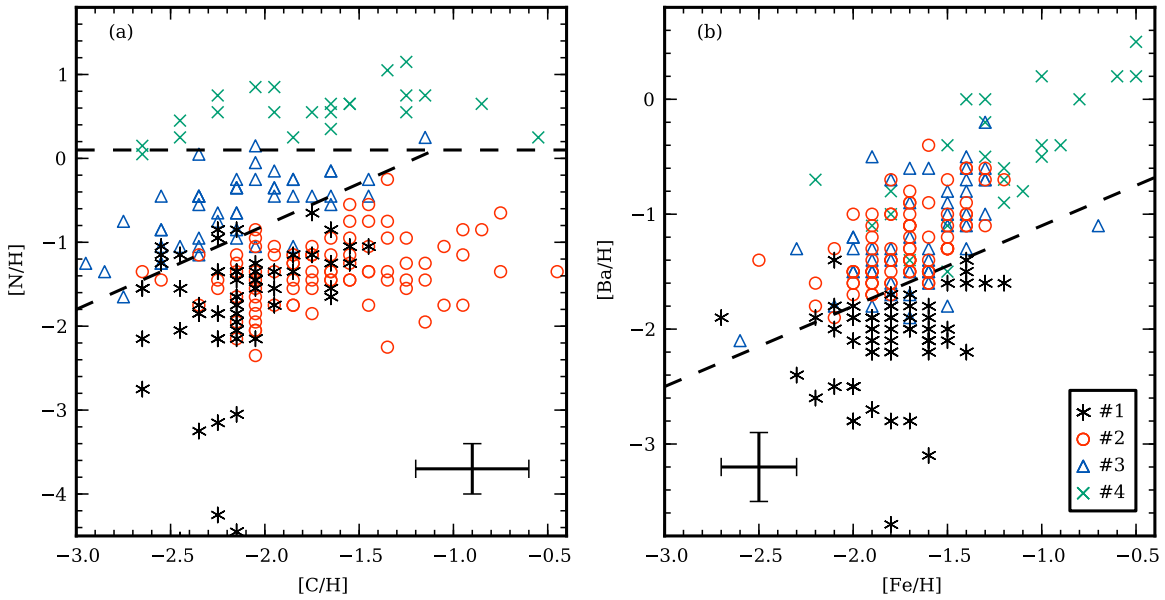

Figure 5.12 — (a) [N/H] versus [C/H], and (b) [Fe/H] versus [Ba/H] from Chapter 4, with the groupings as found in that paper using *k*-means clustering analysis. These planes were used to define the groups in this Chapter, with the dashed lines showing the divisions between each group. In (a), above the horizontal line is defined as group #4 for this Chapter, between that line and above the diagonal line is defined as group #3. All the stars below the diagonal line are defined as groups #1 and #2, and these groups are divided in (b) by the diagonal line: above, and not in the other groups, is group #2 and below is group #1.

groups without rerunning the k-means clustering analysis that was used in Chapter 4. For instance, the stars of group #4 were all much more nitrogen richer than any other group of stars of the cluster. Group #3 could be distinguished from groups #1 and #2 by its larger nitrogen abundance. In the carbon-nitrogen plane, groups #1 and #2 could not be distinguished easily but are separate in the [Ba/H]-[Fe/H] plane (Fig. 5.12).

A simple criteria was developed to place stars into groups. This had the advantage of using abundances that would be well-defined for some stars, but not well-defined for others. For example, the low-N stars, for which [N/Fe] was not very precise, were separated using barium abundances. These definitions could then also be easily applied to other abundance results. Group #4 stars were those for which [N/H] > 0.1, group #3 stars were those remaining stars where [N/H] > [C/H] + 1.2, group #2 were those remaining stars where [Ba/H] > 0.7 × [Fe/H] − 0.4, and group #1 were the rest of the stars. These divisions can be seen in Fig. 5.12, showing how well the Section 4.3 results fitted into the new criteria.

Using these criteria on the 221 stars from Chapter 4 resulted in essentially the same group classifications. Of the new group #1 stars, four had been in the group #2 of Chapter 4 and the rest had been group #1. In the new group #2, all but five were originally group #2 and these five were group #1. The new group #3 had two group #4 stars, ten group #1 and six group #2. This meant that 87 % of stars of the new group #3 were group #3 in Chapter 4. In the new group #4, two were old group #3 stars.

The mean abundances and standard deviations of the grouping of the 557 stars is given in Table 5.3, along with the symbols and colours used for these groups on subsequent figures (the same as used in Chapter 4).

5.6 Discussion

In this thesis an extensive set of atmospheres, parameters and abundances for 848 giant branch (GB) stars in ω Cen was compiled. We discuss these in the context of the methods used and in Chapter 6 they are discussed in the context of cluster evolutionary models.

The spectral resolution required the abundances inferred to be limited to 0.1 dex step sizes. This means that there are datum points that actually have several stars at the same value. For example, at [C/Fe] = 0.0, [N/Fe] = 0.4, there are 10 stars. In order to illustrate the density of stars at a given value, we show histograms in Fig. 5.13. In the case of [Fe/H] (Fig. 5.13a), they show that group #4 is definitely metal richer than the other groups, with hints that #1 is slightly metal poorer than the other two groups. Conversely Fig. 5.13d shows that group #1 is barium poorer than the other three groups. The histograms of carbon and nitrogen (Figs. 5.13b and 5.13c) show the bimodal nature of these elements.

The key driver behind this research was the determination of carbon and nitrogen abundances for stars in the globular cluster (GC) ω Cen (Fig. 5.14). In Chapter 4 it was shown that using carbon and nitrogen, groupings that were not previously seen can be discovered. There are four broad groupings of stars: two low-carbon groups, one with higher nitrogen than the other; and two carbon-deficient but nitrogen-rich groups. It was not possible to split that data of Johnson & Pilachowski (2010) into groups such as ours as there was no other abundance plane that correlates with the groupings that were found in carbon and nitrogen for the carbon-deficient groups (#1 and #2). They were the same in their oxygen and sodium abundance ranges. Compared to Chapter 4, it was found that group #3 extends to much carbon-poorer abundances, hinting at processing of carbon in group #1 or #2 (depending on the evolutionary model adopted) into nitrogen or sodium. By definition, group #4 was nitrogen rich, with a large range of carbon abundances. But this simple definition by its [N/H] abundance, also selected the metal- and sodium-rich stars, which form a separate GB on the colour-magnitude diagram (CMD) (Fig. 5.15).

The [Ba/Fe] results (Fig. 5.16) are consistent with previous results: the s-process abundance of stars rises rapidly at low metallicities and then flattens out at higher metallicities to a constant value. The same features have been observed by Johnson & Pilachowski (2010) and Marino et al. (2011a) (also shown in Figs. 1.3 and 4.19). Stanford et al. (2010) found the correlation with metallicity but their most metal-rich stars have intermediate barium abundances.

The lack of [O/Fe] was the driver behind the use of the CH(4300) and S(3839) indices as the estimator of oxygen abundance of the stars. We still do have [O/Fe] for 261 of these stars[3]. The resulting groupings in the Na-O plane (Fig. 5.17) mimic those found in Section 4.4.2 and Fig. 4.17 with the oxygen-rich stars consisting of two well-mixed groups in terms of their [O/Fe] and [Na/Fe], remembering that the groupings in Chapter 4 used sodium and

[3] This is more than the 221 stars reported in Chapter 4 because in that Chapter only those stars that also had photometry of Bellini et al. (2009a) were used.

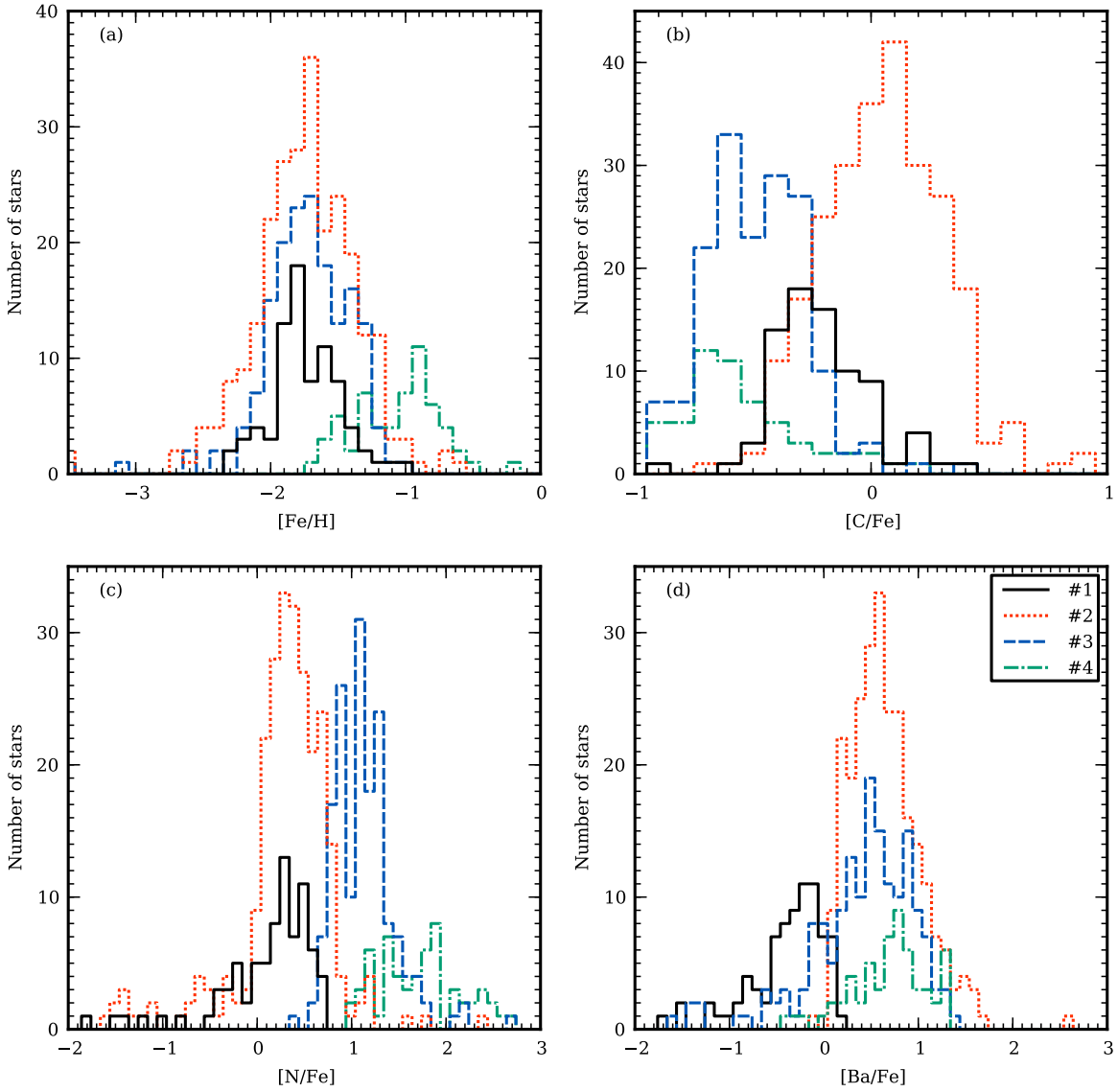

Figure 5.13 — For each of the inferred abundances, (a) [Fe/H], (b) [C/Fe], (c) [N/Fe] and (d) [Ba/Fe], histograms illustrate the concentration of stars at particular abundances. The different groups are indicated with different coloured and dashed lines.

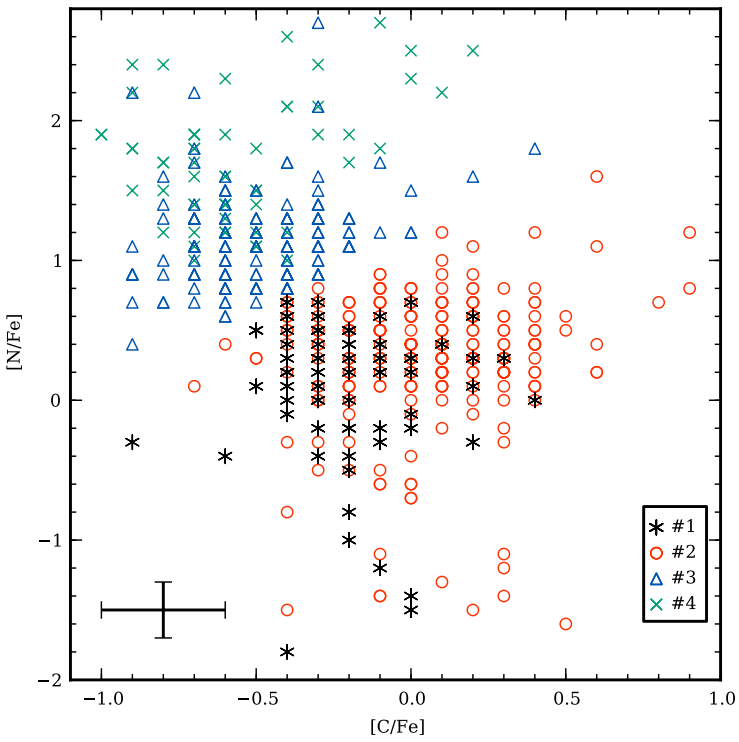

Figure 5.14 — [C/Fe] and [N/Fe] abundances for the four groups described in Section 5.5 and Table 5.3. The accompanying histograms are found on Fig. 5.13b ([C/Fe]) and Fig. 5.13c ([N/Fe]). It shows that there are four distinct regions when investigating carbon and nitrogen: a carbon-poor and nitrogen-poor group (#1) which is also iron-poor; a carbon-rich but nitrogen-poor group (#2); a carbon-poor but nitrogen-rich group (#3); and a very nitrogen-rich group (#4).

oxygen as part of their construction, whereas here they used only carbon, nitrogen, barium and iron. The Na-rich stars of group #4 form a sodium-oxygen distribution that is not observed in other clusters. The sodium-oxygen anticorrelation could be seen as the defining feature of a GC, but the metallicity distribution of ω Cen seems to require a modified version of this formation process due to the different yields that come from asymptotic giant branch (AGB) stars of different metallicities. How the helium affects these yields also needs to be understood. These are discussed in Chapter 6.

The CMD (Fig. 5.15) confirms that the nitrogen-rich group #4 is the metal-rich red giant branch (RGB)-a. The three other groups are mixed on the GB. The relative positions of the groups on the CMD suggest that group #1 was slightly bluer than the other groups. In order to investigate this further, a four degree polynomial was fitted along the edge of the GB. For each star, the normal distance from this line was found and this is plotted in the Fig. 5.18a. This normal distance was used instead of the $B-V$ difference as it did not exaggerate the effects at the bright end of the GB where it flattens out to a roughly constant V. In Fig. 5.18b, a histogram of this distance from the blue edge of the GB. It shows that group #4 stars are definitely found at larger, positive distances than the other groups. Group #1 has an average distance of 0.00 ± 0.06 magnitudes, group #2 is 0.06 ± 0.09, group #3 is 0.00 ± 0.17, and group #4 is 0.25 ± 0.15. So there is a suggestion that group #1 is bluer than the other groups but they are still within the uncertainty range of each other. This is consistent with group #1 being metal-poorer than the other groups, as metal-poorer stars are hotter (all else being equal).

5.7 Summary

In this Chapter and the previous Chapter, the $T_{\rm eff}$, $\log g$, [Fe/H], [C/Fe], [N/Fe], [Ba/Fe] were determined over 500 evolved stars of the GC ω Cen. This is the largest dataset for these elements in ω Cen. Using these abundances,

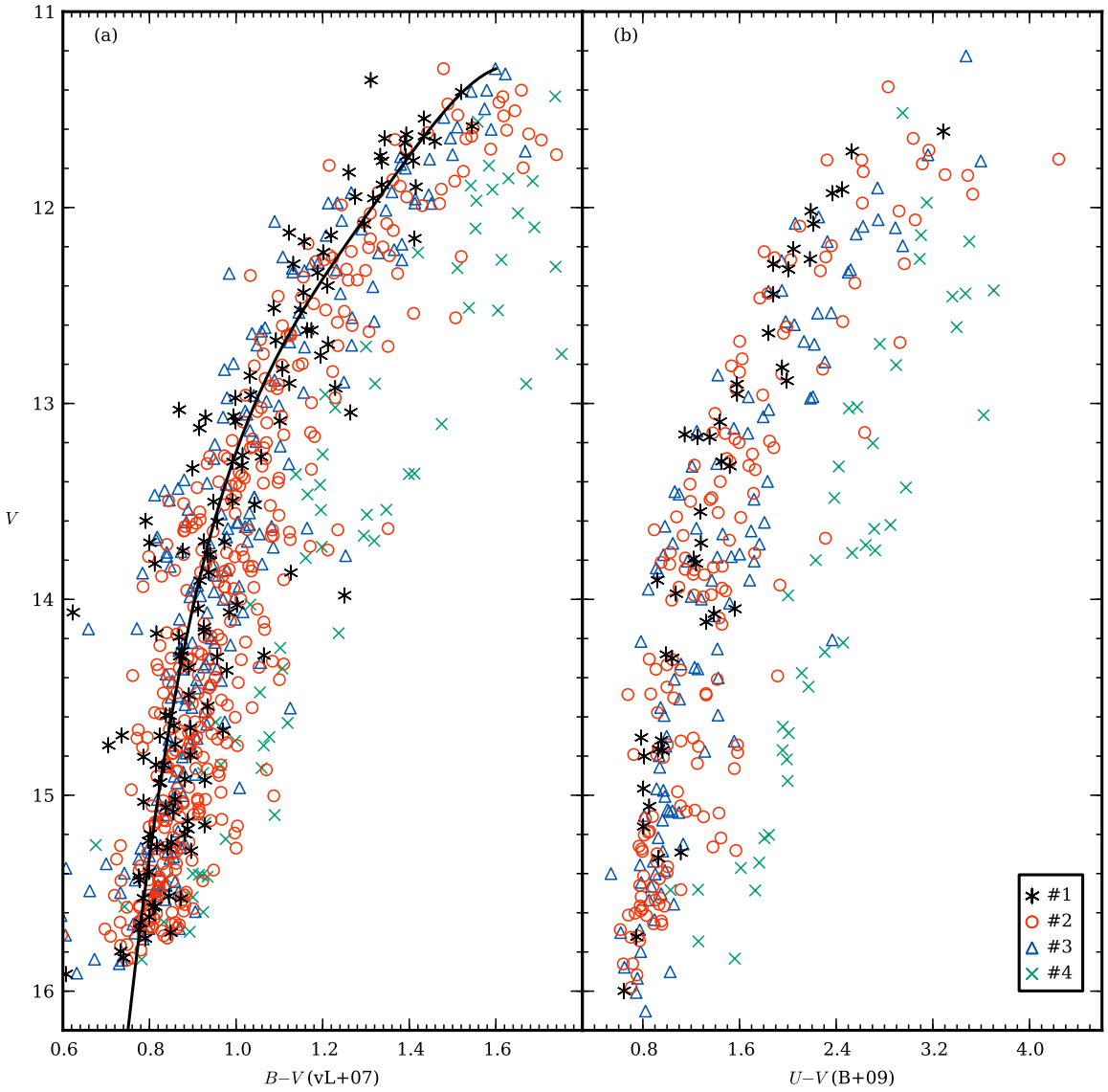

Figure 5.15 — (a) The four groups shown on a CMD using the photometry of van Loon et al. (2007, vL+07). The solid line is a four-degree polynomial that is used to define a locus of the GB. (b) The four groups shown on a CMD using the photometry of Bellini et al. (2009a, B+09). There are fewer stars than in (a) because not all of the stars in van Loon et al. (2007) were positionally matched to Bellini et al. (2009a).

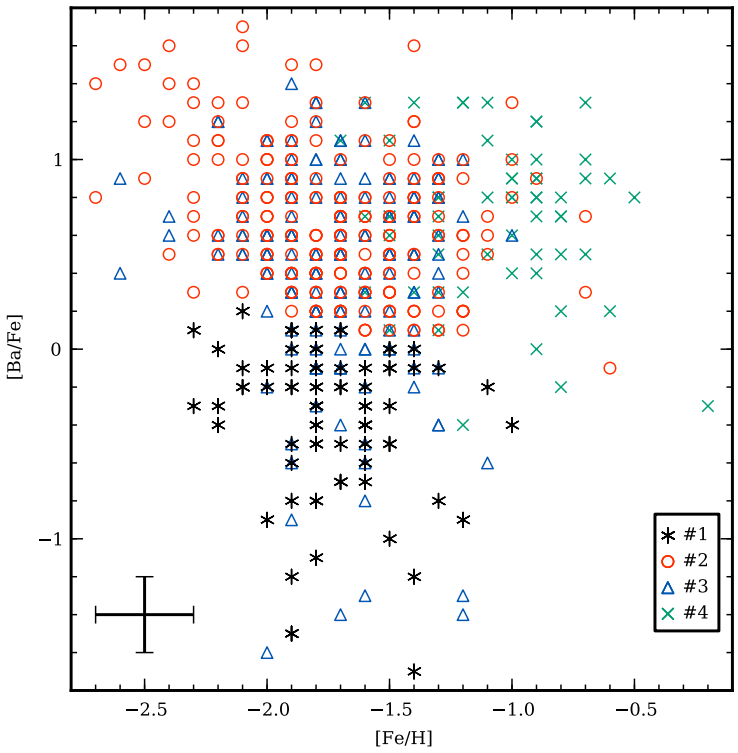

Figure 5.16 — [Ba/Fe] and [Fe/H] for the four groups described in Section 5.5 and Table 5.3. The accompanying histograms are found on Fig. 5.13a ([Fe/H]) and Fig. 5.13d ([Ba/Fe]). There are three regions in this abundance plane: a Fe-poor and Ba-poor region (group #1); a Fe-poor to Fe-intermediate and Ba-rich region (groups #2 and #3); and a Fe-rich and Ba-rich region (group #4).

homogeneous groups have been identified that need to be discussed in the context of evolutionary theories of ω Cen and other unusual GCs. The aim of determining these abundances is to consider them in the context of evolutionary models, and understand how they are consistent and inconsistent with these models.

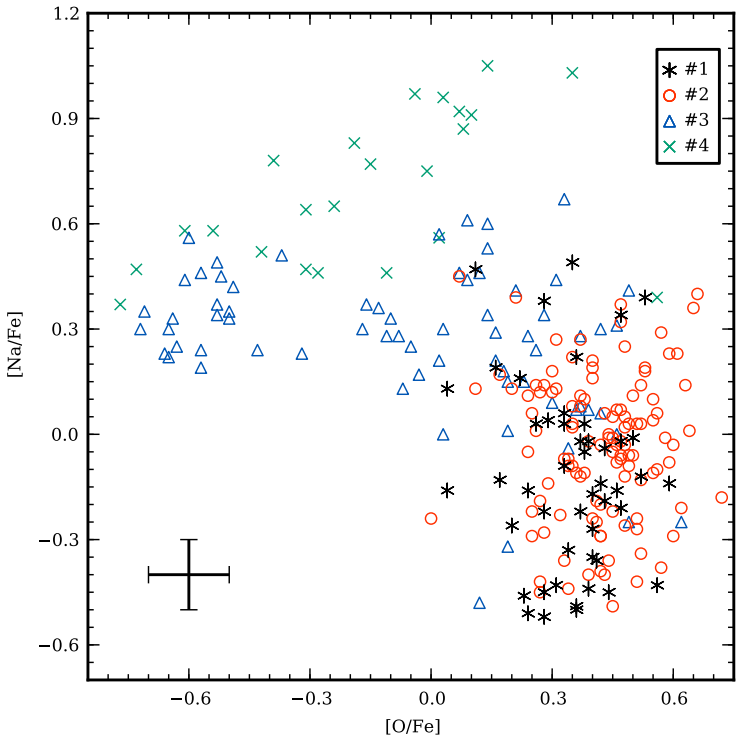

Figure 5.17 — There were 260 stars in common between this work and Johnson & Pilachowski (2010) and these stars are shown with their [O/Fe] and [Na/Fe] abundances from that work.

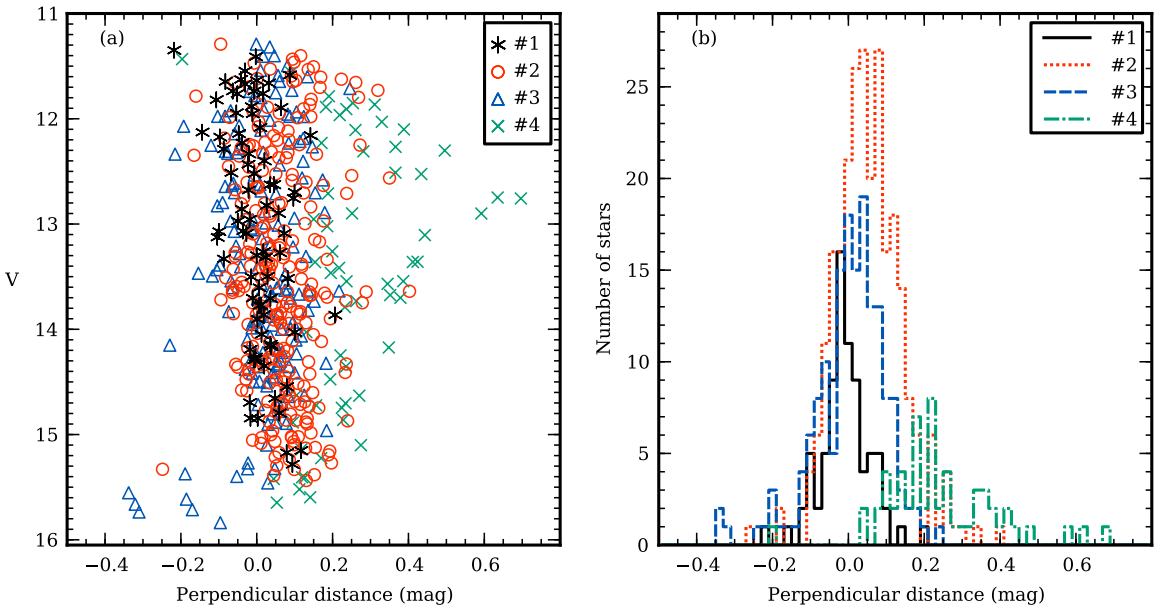

Figure 5.18 — (a) The GB locus of Fig. 5.15a was used to find the perpendicular distance of each star and then a "straightened CMD" was produced. (b) Histogram of the distances of stars from the GB locus. Group #4 is found to be redder than the other groups, while group #1 is on average slightly bluer than the other groups.

Chapter 6

Observational Evidence and Evolutionary Consequences

This thesis has been an exploration of using lower resolution spectra of giant branch (GB) and horizontal branch (HB) stars of globular clusters (GCs) to determine elemental abundances. Two monometallic clusters (47 Tuc and NGC 6752) and a multimetallic cluster (ω Cen) were investigated. Their observational results now need to be understood in the context of the formation theories of these GCs. First, we provide a summary of the key observational differences and similarities between these two types of GC.

As their descriptions would imply, the most obvious difference is that all of the stars of monometallic clusters have a single [Fe/H], while ω Cen is an (extreme) example of a multimetallic cluster which shows a range of metallicities in their stars. Of the about 160 known GCs of the Milky Way, there are five clusters which show a range of their [Fe/H]: ω Cen (Δ[Fe/H] ~ 1.5), M22 (Δ[Fe/H] ~ 0.14; Marino et al. 2009), M54 (Δ[Fe/H] ~ 0.19; Carretta et al. 2010a), NGC 3201 (Δ[Fe/H] < 0.4; Simmerer et al. 2013), and Terzan 5 (Δ[Fe/H] ~ 0.5; Ferraro et al. 2009)[1]. This implies that the formation processes of these multimetallic clusters is different to the bulk of GCs, and that even if ω Cen did form in the same way as these other multimetallic clusters, then it must have been an extremely unusual formation process.

It should be emphasized that ω Cen appears to straddle the line between a GC and a dwarf galaxy. With a mass of ~ 2.5×10^6 $M_\odot$ (van de Ven et al. 2006), it is smaller than the average dwarf galaxy, with small dwarf galaxies having masses of ~ 20×10^6 $M_\odot$ (Mateo 1998). But it has a larger mass than the typical simple stellar population GCs, whose average mass is ~ 1.9×10^5 $M_\odot$ (Mandushev et al. 1991). Its luminosity also sets it apart from other GCs, whose phyiscal extent are anticorrelated with luminosity: small clusters are the most luminous intrinsically. It may have a quite different history from other GCs of the Milky Way, with possibility it is the remnant core of a stripped dwarf galaxy (Freeman 1993; Bekki & Freeman 2003; Meza et al. 2005; Noyola et al. 2008).

In terms of the major chemical similarities, all well-studied Galactic GCs have anticorrelations between their light element abundances: in particular, sodium-oxygen and carbon-nitrogen (e.g., for ω Cen, see Figs. 1.2, 3.10, 3.28 and 5.14). In the case of ω Cen, the sodium-oxygen anticorrelation is more complicated with a group of stars which are **correlated** in their sodium and oxygen (Fig. 5.1). As shown in Chapters 4 and 5, these Na-O correlated stars are also metal-rich (Tables 4.5, 4.6 and 5.3).

A striking difference between the monometallic clusters and ω Cen is the huge range of s-process elemental abundances in the latter, while the former (mostly) show no range (Table 6.1). There are some monometallic clusters that show a range of neutron-capture elemental abundances. In M15 there is a range of Δ[Ba/Fe] ~ 0.15 (Sobeck et al. 2011). This cluster also has a 0.1 dex difference in [Fe/H] between the red HB and the red giant branch (RGB) stars. Along with its metallicity range, M22 has a correlated range of s-process elements, with [Ba/Fe] changing by 0.6 dex over a 0.2 dex range in [Fe/H] (Marino et al. 2011b). This gradient is about the same as that observed in ω Cen ([Ba/Fe] $\propto$ 3[Fe/H]). Another cluster with a similar range of s-process is NGC 1851 (Δ[Ba/Fe] ~ 0.6; Yong & Grundahl 2008), but this cluster does not have a metallicity range. A counterexample is NGC 3201 which, although having a metallicity range, does not have any range of its s-process abundances (Simmerer et al. 2012). So like ω Cen, a few clusters exhibit ranges in [Fe/H] and s-process element abundances, but usually to a lower level

[1] Both NGC 3201 and Terzan 5 have properties that would suggest that they are not "true" GCs (see Chapter 1).

Table 6.1 — Overview of the abundance results for the three clusters investigated in this thesis. The results are from this thesis unless otherwise indicated.

Cluster	[Fe/H]	[C/Fe]	[N/Fe]	[O/Fe]	[Na/Fe]	[Ba/Fe]
ω Cen	−2.0 to −0.5	−1.0 to +0.8	−0.5 to +2.5	−0.5 to +1.2[a]	−1.0 to +0.8[a]	−1.0 to +1.4
47 Tuc	−0.7[b]	−1.2 to −0.4	+0.3 to +2.1	−0.2 to +0.4[c]	+0.1 to +0.7[c]	+0.3[d]
NGC 6752	−1.5[b]	−1.0 to −0.5	+0.5 to +1.3	−0.2 to +0.7[e]	−0.2 to +0.9[e]	+0.05[f]

[a]Johnson & Pilachowski (2010); [b]Harris (1996); [c]Carretta et al. (2009); [d]Worley & Cottrell (2012); [e]Carretta et al. (2007); [f]Dobrovolskas et al. (2012)

Table 6.2 — Qualitative description and quantitative values of the four groups of ω Cen stars.

Group	[Fe/H]	[C/Fe]	[N/Fe]	[Ba/Fe]
#1	Low	Low	Low	Low
	−1.8	−0.4	0.3	−0.4
#2	Intermediate	High	Low	Intermediate
	−1.7	0.0	0.4	0.4
#3	Intermediate	Low	High	Intermediate
	−1.7	−0.5	1.0	0.5
#4	High	Low	High	High
	−1.3	−0.6	1.8	0.8

to that of ω Cen: i.e., Δ[Fe/H] = 2 dex compared to 0.2 dex, Δ[Ba/Fe] = > 1 dex compared to 0.6 dex. This again implies that there was a unique, or at least unusual, formation process for ω Cen. This Chapter in part looks at a variety of formation theories for ω Cen to understand how they can achieve the groupings that have been found in this thesis. It seeks to show which features are consistent and which features are not explained.

As discussed in various parts of this thesis, both helium and oxygen are of crucial importance to GC studies. However they are both technically difficult to make quantitative abundance determinations for. In the case of helium, its visible light spectral lines are no longer visible for stars cooler than A0 (Gray 2005) and in the hot HB stars, where the line could be present, diffusion and preferential settling of elements cause ambiguities in the abundances. Dupree et al. (1992) showed that the HeI infrared absorption line at 10,830 Å can be used in metal-poor RGB stars in the field and this was applied to ω Cen by Dupree et al. (2011). However there is still a limitation that the stars need to be hotter than 4500 K, such that the chromosphere reaches the necessary ~ 10,000 K for the transition to take place. Additionally, the observations of Dupree et al. (2011) required 2 h of exposures on each of their 12 stars with the Gemini South, an 8.2 m telescope.

Determinations of oxygen abundances suffer from similar problems (Meléndez et al. 2006). There is a neutral oxygen triplet at 0.77 μm but this can only be observed in FG dwarfs and subgiants. There are forbidden [OI] lines at 6300.311 Å which can be observed in GB stars. The lines usuable in GB stars require high S/N and high spectral resolution.

Section 6.1 discusses the radial distance and radial velocity distributions of the different groups. Section 6.2 looks at the different ages ranges in the cluster that have been proposed in the literature. Section 6.3 discusses the various evolutionary models for the cluster in the context of the abundance results found in this thesis. Section 6.4 investigates the abundances of asymptotic giant branch (AGB) stars in the cluster and compares this result to monometallic clusters.

6.1 Radial Distance and Radial Velocity Distribution of stars in ω Cen

ω Cen is one of the most flattened GCs (e.g., Geyer et al. 1983), indicating that it is rapidly rotating. It could be possible that mergers took place in the cluster's past that would leave a signature on the rotation of the different

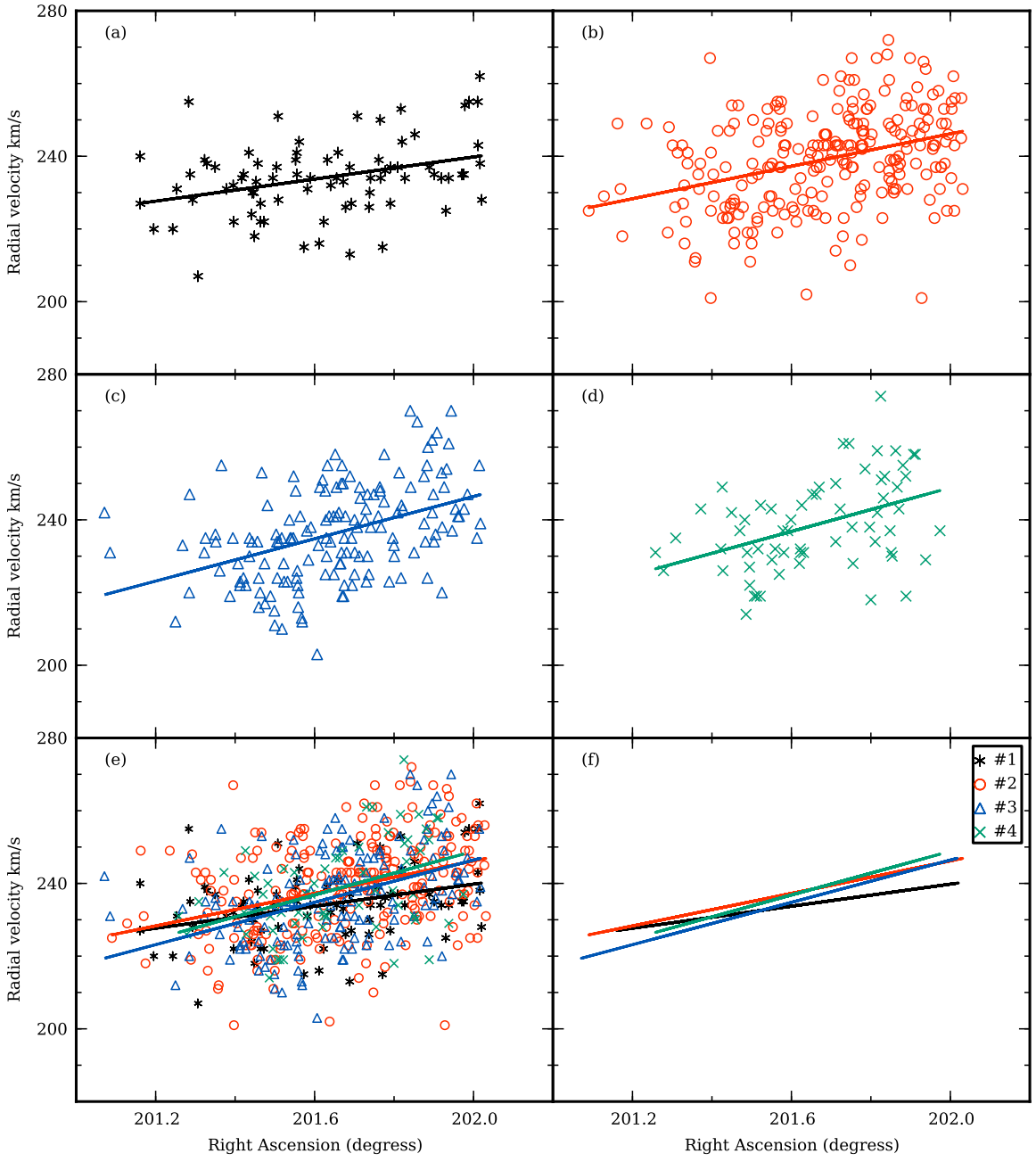

Figure 6.1 — The radial velocity distribution of ω Cen showing its rotation as its rotation axis is aligned with the north-south axis of the sky. (a), (b), (c) and (d) show the distribution for groups #1, #2, #3 and #4 respectively (Table 6.2) with a line of best fit through the data. (e) shows the combined result and (f) shows just the lines of best fit.

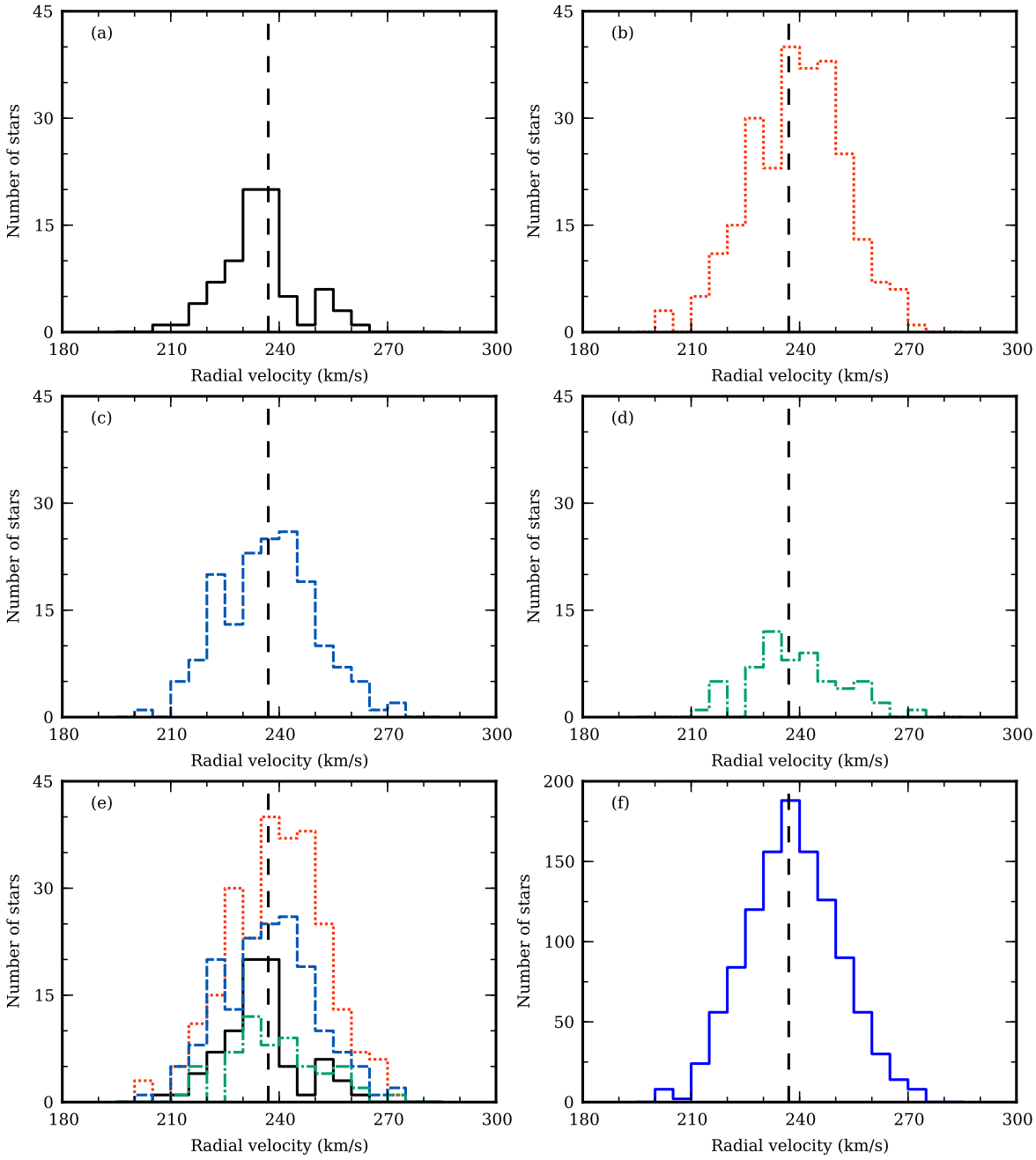

Figure 6.2 — The radial velocity distribution of ω Cen for the four groups (Table 6.2). The vertical dashed line in all the subfigures indicates the mean for the entire sample of stars (237 ± 13 km s^{-1}), (a), (b), (c) and (d) show the distribution for groups #1, #2, #3 and #4 respectively; (e) shows all four histograms from the previous subfigures; and (f) shows the combination of all four groups.

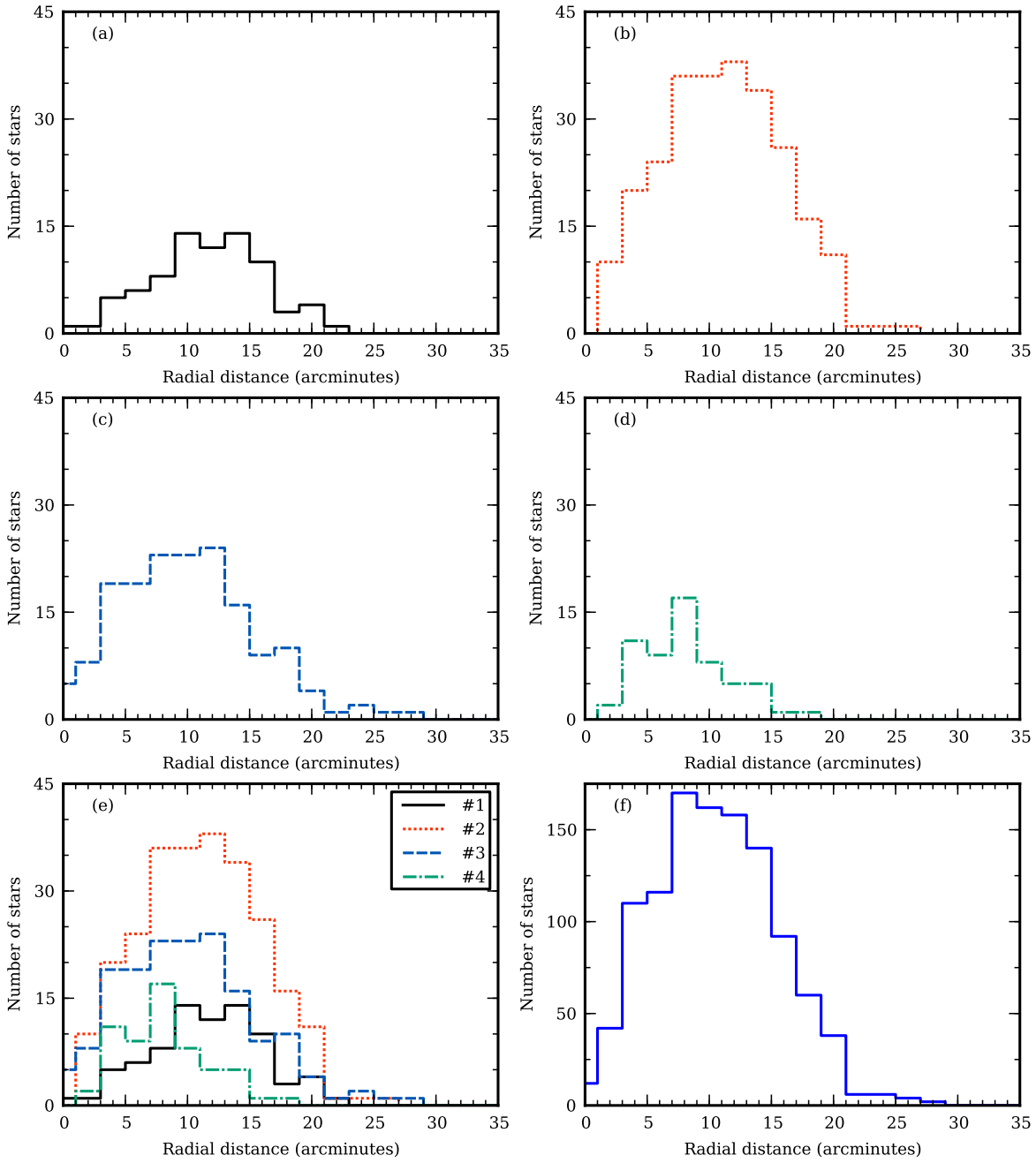

Figure 6.3 — The radial distance distribution of ω Cen for the four groups (Table 6.2). (a), (b), (c) and (d) show the distribution for groups #1, #2, #3 and #4 respectively. (e) shows all four histograms from the previous subfigures and (f) shows the combination of all four groups.

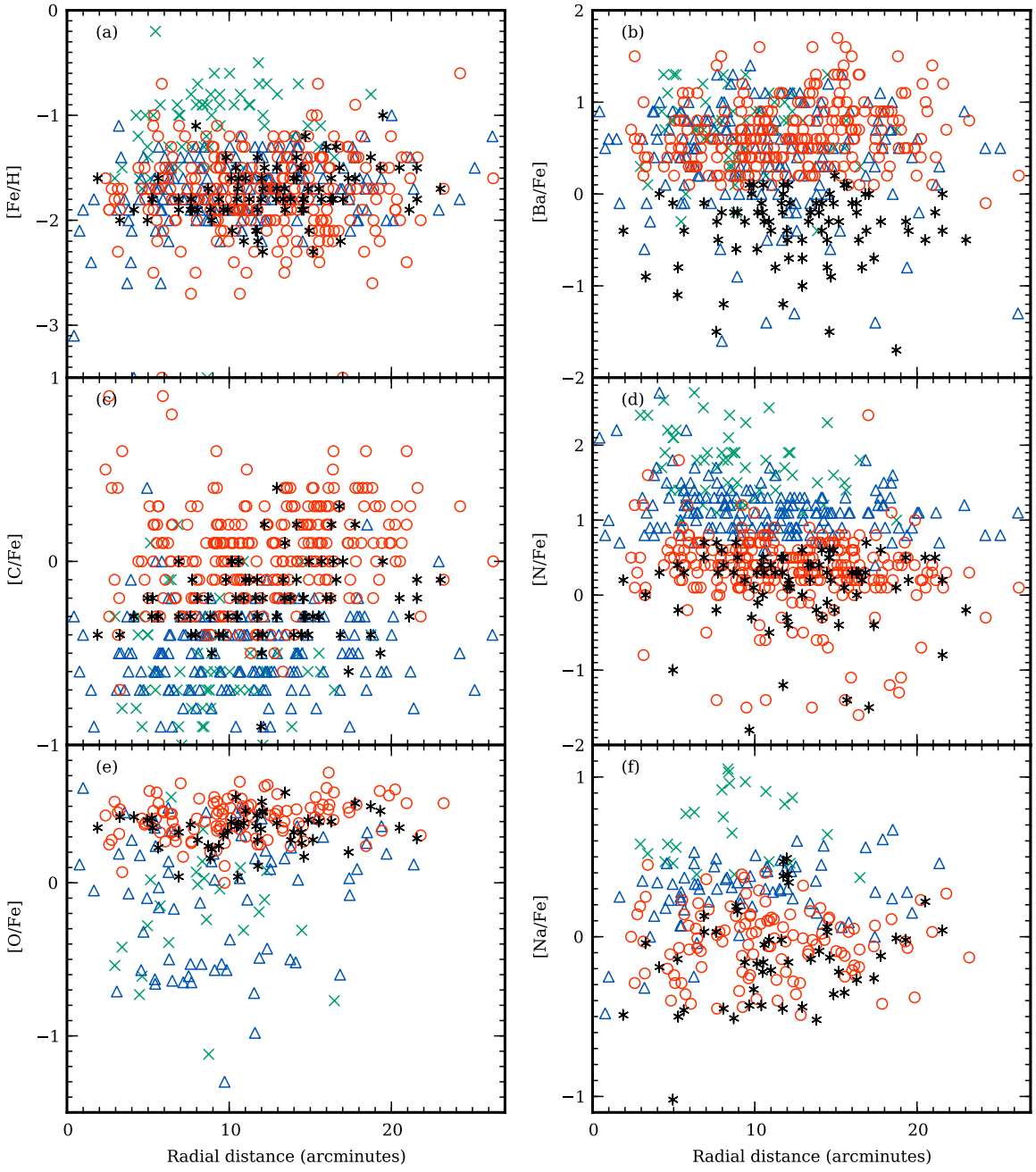

Figure 6.4 — The radial distance distribution of the different abundances of ω Cen stars. (a), (b), (c), (d), (e) and (f) show the distribution for groups [Fe/H], [Ba/Fe], [C/Fe], [N/Fe], [O/Fe], and [Na/Fe] respectively (the last two abundances are from Johnson & Pilachowski (2010)).

groups of stars identified in this thesis. At the core, the stars are orbiting at about 17 km s^{-1}, reducing to a constant 6 km s^{-1} at about 22′ from the centre (Scarpa & Falomo 2010).

A simple graphical test was performed (Fig. 6.1). The rotation axis of ω Cen is aligned with the north-south line on the plane of the sky, meaning that plotting radial velocity against right ascension shows the rotation of the cluster, with one side moving away from us slower than the other side. The radial velocity measurements of van Loon et al. (2007) were used, which had a mean of $\langle v_{\rm rad} \rangle = 237 \pm 13$ km s^{-1}, which is consistent with the canonical value of $\langle v_{\rm rad} \rangle = 233.2 \pm 0.4$ km s^{-1} (Meylan et al. 1995). Ultimately it is not possible to make any definitive conclusions from these distributions as there is little difference between the different groups. Looking at the spread of $v_{\rm rad}$, it does appear that group #1 (see Table 6.2 for a description of the groups) has a flatter distribution than the other groups (Fig. 6.2). Group #1 has the standard deviation of $\sigma_v = 10.5$ km s^{-1}, compared to the other groups with dispersions of 13.4 km s^{-1}, 13.1 km s^{-1} and 12.5 km s^{-1} respectively. The distributions of the stars in group #1 are skewed towards lower radial velocities while, group #2 are skewed towards higher radial velocities. However these effects are weak and suffer from small number statistics as there are few stars in any radial velocity bin. A more detailed analysis would be required to remove all the residuals and determine each stars rotational velocity around the core of the cluster, but this was not believed to be useful given the initial graphical tests.

Showing more obvious results are the radial distributions of the different groups (Fig. 6.3). Overall, the vast majority of stars have radial distances greater than 2′, with most stars > 5′. This means it is not possible to comment about the core region of the cluster. Overall, groups #1 and #2 track the distributions of all the stars (noting that they make up 28 % and 46 % of the stars respectively). Group #3 seems more centrally located, while the plurality of the group #4 stars are closer than 10′ to the core, compared to the other groups which are found at larger radial distances. This is consistent with the findings of Johnson & Pilachowski (2010) where the O-rich stars (groups #1 & #2) are found at all radial distances from the core, while the O-poor stars (groups #3 & #4) are only found closer to the core (Fig. 6.4e). These results are consistent with Norris et al. (1997), Hilker & Richtler (2000), Pancino et al. (2000), Bellini et al. (2009b), and Johnson et al. (2009), who all found that the metal-poor main population (MP) are less centrally concentrated than the metal-richer intermediate metallicity group (MInt). However these results are not consistent with Bellini et al. (2009b) with regards to the RGB-a (our group #4). Whereas they found it had the same radial distribution as MInt population (Table 1.2), which would be our groups #2 and #3, here we find that the groups #2 and #3 exist at larger radial distances than group #4. Looking at just the abundances of the stars (Fig. 6.4), apart from the aforementioned distribution of [O/Fe], only the very metal-rich and nitrogen-rich stars stand out as having different radial distribution in the cluster. This matches the experience in Fig. 6.3, where the group #4 stars were only found close to the core.

With the bias of this sample of stars against the core of the cluster, it was not possible to be conclusive about the radial distribution of the different groups. It was also necessary to take into account the fact the van Loon et al. (2007) spectral library was not perfectly centred on the cluster, meaning that it did not have consistent radial coverage of the cluster. With this in mind, it was beyond the scope of this thesis to be conclusive about any results regarding the radial distribution of stars in ω Cen. However for future work the location of the different groups is extremely useful to any formation theory that requires certain populations of stars to have formed more centrally due to core settling of gas.

6.2 How Long Did Star Formation Take?

One of the key questions regarding the formation and evolution of ω Cen is how long did it take for all the stars to form? In the literature, the time scale between the formation of the first population and the final population (which is not always the metal-richest population) ranges from < 1 Gyr (Herwig et al. 2012) up to 8 Gyr (Hilker & Richtler 2000). Recent results are given in Table 6.3. The age ranges between 2–4 Gyr are most commonly given, usually from isochrone fitting to the colour-magnitude diagram (CMD).

The reason that age estimates are so crucial to any evolutionary model is that it drives the selection of the types of stars that could have polluted the intra-cluster medium (ICM), which provided the gas from which the subsequent generations of stars formed. Any age range must be consistent with the ages of the normally invoked polluters of the ICM: AGB stars, fast rotating massive stars (FRMS) and/or supernovæ (SNe). In ω Cen, there is currently a contradiction between the stars that are invoked to produce the enhancements and depletions in light elements, and those that would have done the same for the s-process elements.

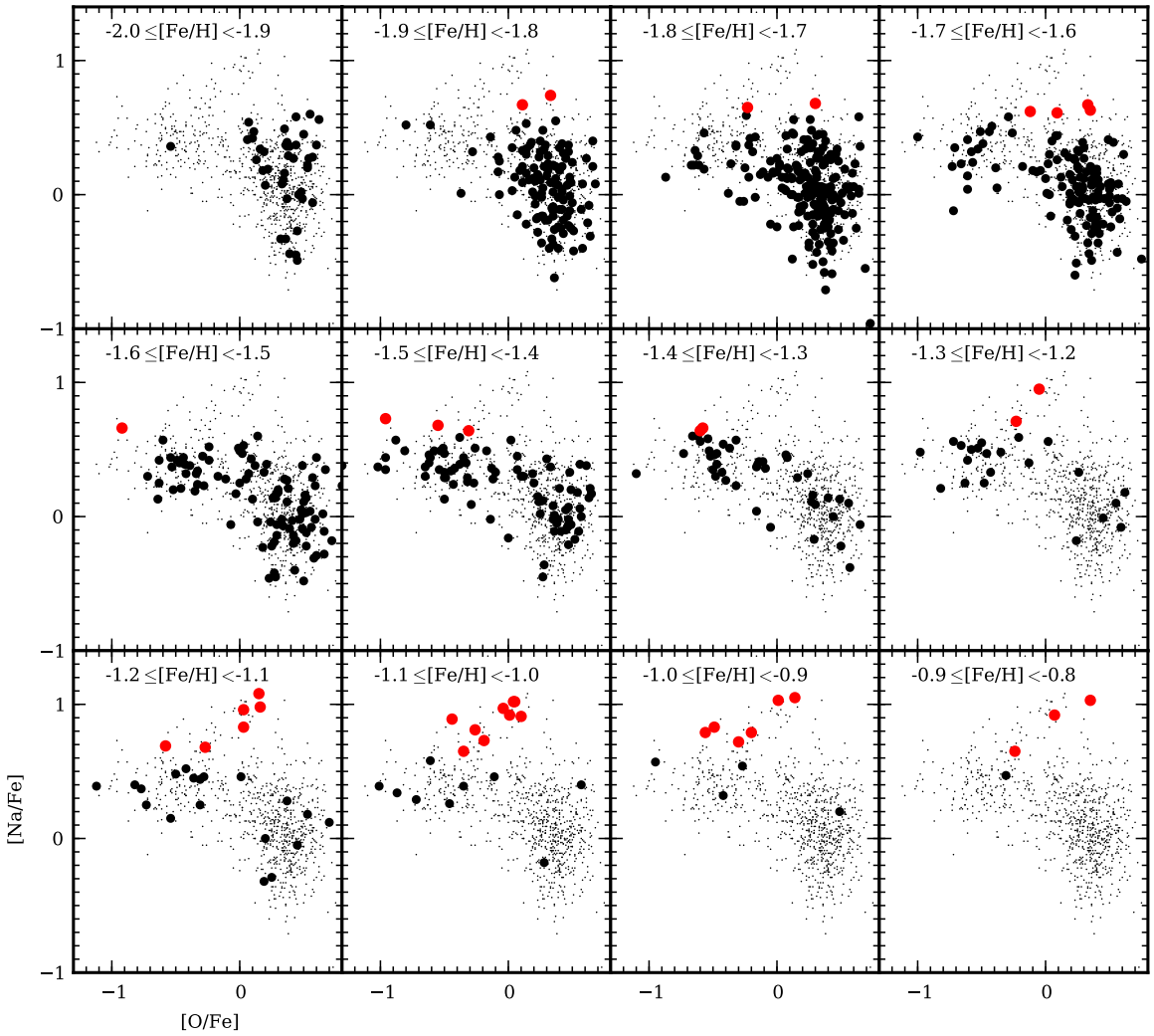

Figure 6.5 — The sodium-oxygen (anti)correlation for stars in ω Cen in metallicity bins of 0.1 dex using the Johnson & Pilachowski (2010) abundances. The red dots are those stars that belong to the sodium-oxygen **correlation** based upon their sodium abundances ([Na/Fe] > 0.6).

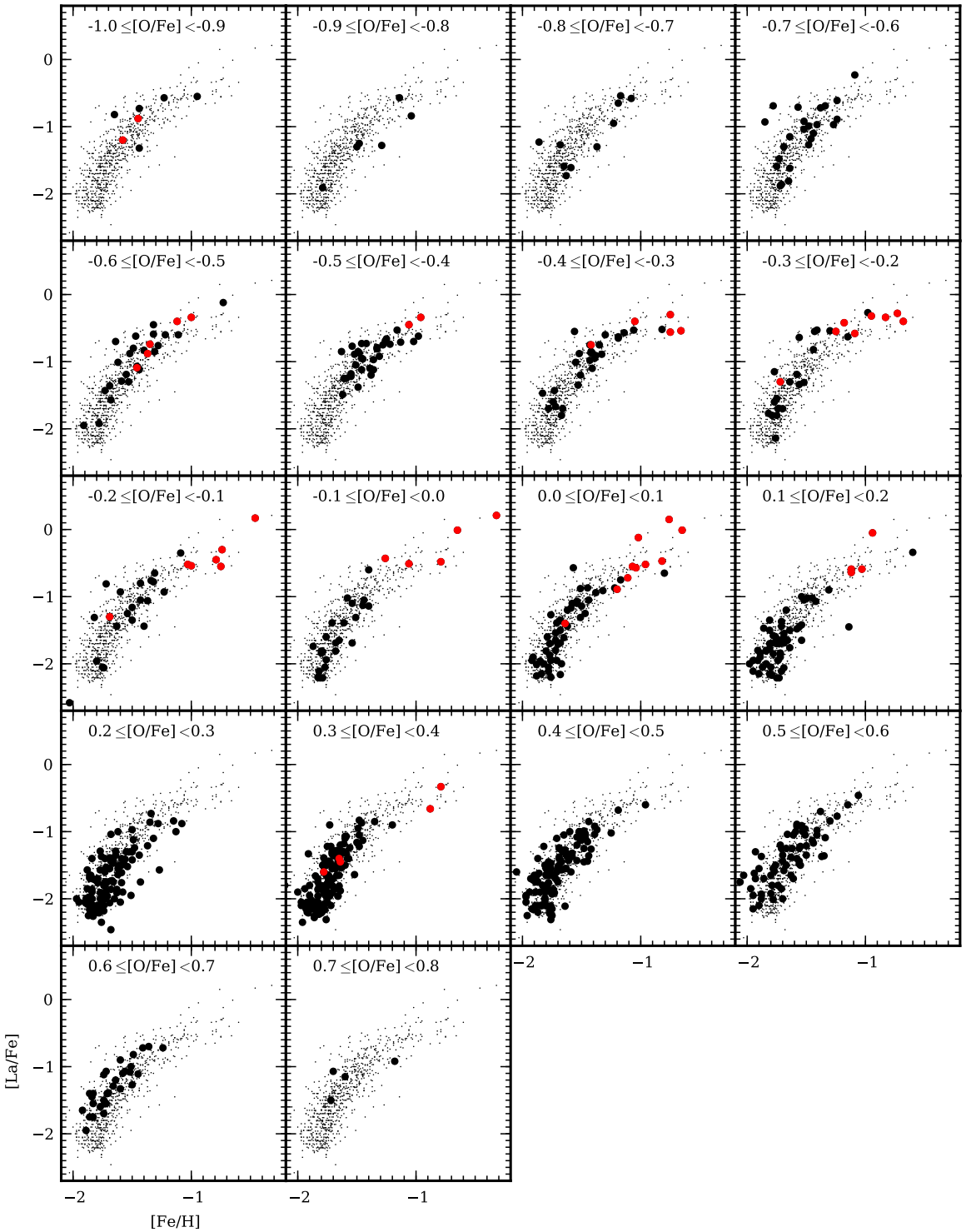

Figure 6.6 — The iron-lanthanum correlation for stars in ω Cen in [O/Fe] bins of 0.1 dex using the Johnson & Pilachowski (2010) abundances. The red dots are those stars that belong to the sodium-oxygen **correlation** based upon their sodium abundances ([Na/Fe] > 0.6).

Table 6.3 — Age ranges in the literature for ω Cen. The evolutionary stage is given for research that concentrated on one type of star.

Paper	Age range	Evolutionary stage
Norris & Da Costa (1995)	> 1 Gyr	RGB
Y.-W. Lee et al. (1999)	2 Gyr	main sequence (MS)
Hilker & Richtler (2000)	MInt 2–5 Gyr, RGB-a 5–8 Gyr	RGB
Hughes & Wallerstein (2000)	> 3 Gyr	main sequence turn-off (MSTO)
V. Smith et al. (2000)	2–3 Gyr	MSTO
Hilker et al. (2004)	3 Gyr	MSTO & sub-giant branch (SGB)
Hughes et al. (2004)	3–5 Gyr	MSTO
Rey et al. (2004)	4 Gyr	RGB
Sollima et al. (2005)	MInt < 2 Gyr after MP	RGB
Stanford et al. (2006)	2–4 Gyr	MSTO
Villanova et al. (2007)	6–7 Gyr	SGB
Johnson et al. (2009)	1–2 Gyr	RGB
D'Antona et al. (2011)	~ 250 Myr	
Herwig et al. (2012)	< 1 Gyr	

Table 6.4 — The models used by Sbordone et al. (2011) for interpreting sequences in ω Cen.

Model	ΔCNO	He (Y)
Reference	0.0	0.246
CNONa1	Δ[C/Fe] = −0.6, Δ[N/Fe] = +1.8, Δ[O/Fe] = −0.8, Δ[Na/Fe] = +0.8	0.246
CNONa2	Δ[C/Fe] = −0.6, Δ[N/Fe] = +1.4, Δ[O/Fe] = −0.8, Δ[Na/Fe] = +0.8	0.246
CNONa1+He	Δ[C/Fe] = −0.6, Δ[N/Fe] = +1.8, Δ[O/Fe] = −0.8, Δ[Na/Fe] = +0.8	0.4

One such contradiction involves AGB stars. The generally accepted location for the production of the main component of the s-process is low mass ($M < 3\,M_\odot$) AGB stars. These stars will take at least 1 Gyr to reach the stage of their life where they can pollute the ICM with s-process rich material. However, even the most massive of these low-mass stars will not have evolved before $M > 5\,M_\odot$ AGB stars begin polluting. It is these stars that are invoked as a possible source of material which creates the sodium-oxygen (anti)correlations in GCs. As shown in Figs. 6.5 and 6.6, the correlation of the iron and barium is independent of the sodium and oxygen abundances for the intermediate metallicity stars. This would mean that the barium polluting events must have occurred before the enhancements and depletions of sodium and oxygen. So age measurements of the different populations are important for their ability to constrain the different models.

Two aspects that have been missing from age estimations in the literature were helium and C+N+O enhancements. The blue main sequence (bMS) stars are proposed to be enhanced in helium relative to the red main sequence (rMS) stars (Norris 2004; King et al. 2012). Increasing the helium abundance of stars will increase their core temperature and decreases their opacity, making them hotter and brighter (all else remaining the same). They also evolve faster than the helium-poor stars, meaning they have a lower mass at a given age, allowing the bMS to be bluer and fainter than the rMS. This affects their positions on the CMD at later stages of their evolution. In addition, difference in C+N+O have usually not been considered. Marino et al. (2012) estimate that changing the C+N+O abundance by 1 dex could change an age estimation by over 3 Gyr.

Sbordone et al. (2011) calculated synthetic spectra based upon typical GC abundances (some of their isochrones are shown and described in Fig. 6.7 and Table 6.4). These spectra were then used to create synthetic CMD for a variety of band passes, one of which was the U and V used in this thesis. They noted that CNO variations will cause the greatest variation in the U and B bands due to the molecular lines in these regions of the spectrum. Their base isochrone had a metallicity of –1.62 ($Z = 0.001$, $Y = 0.246$) with an age of 12 Gyr. Three other abundance combinations were investigated: one enhanced in nitrogen and sodium by 1.8 dex and 0.8 dex respectively and

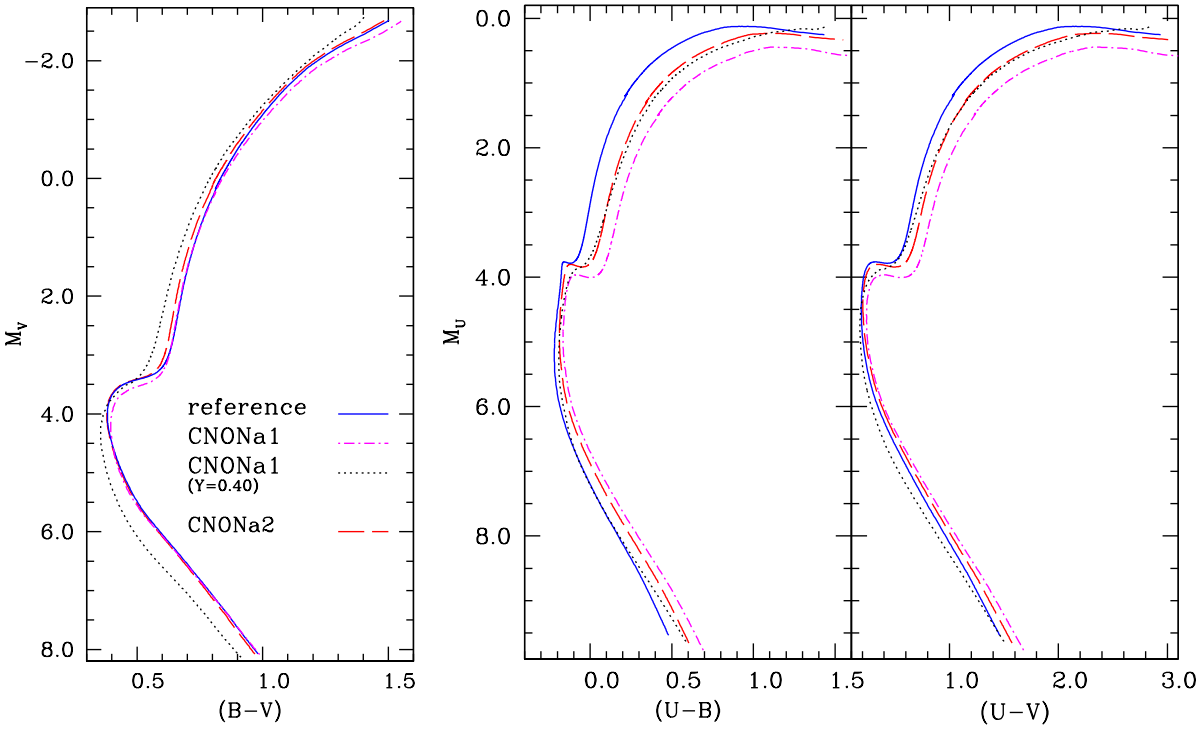

Figure 6.7 — Combination of Figures 10 and 11 from Sbordone et al. (2011) showing the possible degeneracy between isochrones with differing C+N+O and helium abundances for understanding the sequences in ω Cen. The different isochrones are explained in the text and in Table 6.4.

depleted in carbon and oxygen by 0.6 dex and 0.8 dex (CNONa1); one with the same enhancement in C, Na and O but only enhanced by 1.4 dex in nitrogen (CNONa2); and the same as the first but with $Y = +0.4$ (CNONa1+He). The C+N+O mass fraction was twice the reference value in CNONa1, while CNONa2 had the same value as the reference. This is similar to a hypothesized situation in ω Cen: group #3 has a larger C+N+O total than group #2 stars (Fig. 4.18), and from D'Ercole et al. (2008, 2010) where the equivalent of group #3 would be enhanced in helium. They found that for the visible light broad band pass filter, the CNONa1+He and CNONa2 were indistinguishable for much of the RGB on the CMD (Fig. 6.7). This would concur with what was found in this thesis: that groups #2 and #3 are blended on the CMD. But of course, their work used a monometallic isochrone and could not be directly applied to the GB of ω Cen. Sbordone et al. (2011) supplies a useful caveat to any age estimations: there is some degeneracy between the possible isochrones that could be present on the CMD of a cluster like ω Cen.

One controversial age estimation is Villanova et al. (2007), who were the first to identify that there were at least four distinct SGBs in the cluster. Using isochrones, they determined that one of the oldest populations of stars had a metallicity of [Fe/H] = −1.7. This is accepted as part of any self-enrichment model, as it is not possible to radically remove metals from the cluster. That is what would be required to have the first generation metal-richer than a subsequent population, excluding an influx of very metal-poor gas, which seems very unlikely as it would require a radical change of the interstellar medium (ISM) surrounding the cluster. However, they also gave a coeval population with [Fe/H] = −1.1, which could be the result of a collision of two gas clouds of different compositions. The second star forming event would have been 4–6 Gyr later and the final population formed 1–2 Gyr after this. This age and ordering has been disputed. In Marino et al. (2012), they argue that Villanova et al. (2007) did not take into account the C+N+O variations between the various subpopulations. So instead of the metal-poor and metal-rich groups being coeval, the metal-rich group is ~ 2 Gyr younger. Marino et al. (2012) suggest that similar corrections need to be applied to previous age estimates in the literature, with their estimate of a 1 dex change in C+N+O being the equivalent of 3 Gyr age differences in the isochrones.

The most recent age determination using isochrones was by Joo & Y.-W. Lee (2013), who used updated versions of the Yonsei-Yale isochrones that allow for enhancements of the He and C+N+O. Their results are given in

Table 6.5. They assumed the five subpopulations of Johnson & Pilachowski (2010), adopting that paper's [Fe/H] peaks, and used the [(C + N + O)/Fe] of the different populations from Marino et al. (2012). The free parameters in Joo & Y.-W. Lee (2013) were the age of the isochrone and its helium content. They determined the primordial population (labelled "G1") that was almost coeval with a metal-richer population (G2) with [Fe/H] = −1.81 and −1.51 respectively. They found that both of these populations would have primordial helium content (Y = 0.23). Their next forming population (G3), with a metallicity of [Fe/H] = −1.31, had the highest He content ($Y = 0.41 \pm 0.02$), forming about 1 Gyr after G1 and G2. This is the population that makes up the bMS and the extreme blue horizontal branch stars. This is the first group with a (small amount of) CNO enhancement (Δ[CNO/Fe] = 0.14). The last two populations (G4 & G5) were coeval within uncertainties, forming 0.6 ± 0.6 Gyr after G3. These two populations were also found to be enhanced by a similar amount of He as G3. They would also have the highest [CNO/Fe], 0.47 dex greater than G1 and G2. Based upon the [Fe/H] and their positions in the CMD, their G1 is the equivalent of our #1, G2 and G3 are the equivalent of #2 and #3; and G4 and G5 are #4. A topic that returns continuously in this sort of discussion is the barium content of these populations. If G1 and G2 are coeval, there must have been some internal inhomogeneity in the star forming cloud to explain the large difference (up to 1 dex) between the s-process content of these two populations.

One of the most extreme age estimates comes from Li et al. (2012). They used an EA-type eclipsing binary consisting of two early-type MS stars, and estimated that one member had an age of 16 Gyr and while the other was only 1.19 Gyr old! No such extreme age range has appeared anywhere else in the literature. They only had a light curve for the binary, so its abundance is not known. Based upon the binary's photometry, it would be located in the blue straggler region of the CMD ($B-V \sim 0.2$, $V \sim 17$). It was identified by Bellini et al. (2009a) as being a member of the cluster with a membership probability of over 90 %. So it cannot be explained away as a field star that by chance is in the same direction as ω Cen in the sky. Whether their age estimate is correct is beyond the scope of this thesis, but clearly this star warrants further observations to understand if it really has a 1 Gyr old member.

It is clear that there must have been some period of extended star formation in ω Cen's past in order to explain all the different abundances present in the cluster. Throughout this time of star formation, self-enrichment was taking place to alter the composition of the ICM. This enrichment seems likely to have occurred in conjunction with dilution from the ISM. Models incorporating these aspects are discussed in the next Section.

6.3 Evolutionary Models

From the work presented in this thesis there are several abundance features that need to be explained by any evolutionary model of ω Cen: the overall metallicity distribution of the stars; the Na-O abundance (anti)correlations; the rapid increase of s-process element abundance with Fe, which flattens at high metallicity; and the C-N abundance distribution. Any model of the evolution of ω Cen must start with a primordial population (group #1) with the lowest metallicity observed in the cluster, and which will also have high oxygen, low carbon, intermediate-to-low nitrogen, and low barium. It is the intermediate metallicity stars (groups #2 & #3) that exhibit the N-C and Na-O anticorrelations, but have indistinguishable distributions of [Ba/Fe] with [Fe/H]. Finally, we have the anomalous RGB-a stars, with their high metallicity, high nitrogen, Na-O **correlation**, but no further enhancement of barium over their metal-poorer cousins. Also requiring explanation are the constant r-process abundances, and the very slowly increasing α-element abundance with [Fe/H].

With regards to the metallicity of the primordial population, in Section 1.2.2 and Fig. 1.3 are results from Pancino et al. (2011b) who found three very metal-poor (VMP) SGB stars in ω Cen, with [Fe/H] ≈ −2.0. This is lower than the [Fe/H] = −1.7 peak in the metallicity distribution (Fig. 1.6) found by other researchers. There are two possibilities for their origin: (1) they are amongst the oldest stars in the cluster, or (2) they are remnants of another cluster that merged with ω Cen. They do have low [Ba/Fe], which would be consistent with an in situ formation hypothesis, since the other low-Fe stars in the cluster also have low [Ba/Fe]. However disk, halo and bulge stars also have −0.5 < [Ba/Fe] < 0.0 for [Fe/H] − 2.0 (Koch et al. 2008; Ishigaki et al. 2010). So their barium abundance does not provide evidence for their origin. However their [C/Fe] and [N/Fe] abundances do seem to be inconsistent with the rest of the cluster (Fig. 1.4). The low-metallicity stars in the cluster were found to have low carbon and low nitrogen (with the caveat of comparing evolved and unevolved stars). This result has been found both in this thesis (Section 4.4.3 and Figs. 4.16 and 5.14) and in the literature (see Figure 2 of Marino et al. 2012). At this stage, these stars are unusual and more of them need to be discovered and analyzed in order to understand their origin and abundance properties.

Table 6.5 — Four different evolutionary sequences for ω Cen. Joo & Y.-W. Lee (2013) is based upon isochrones, D'Antona et al. (2011) is designed to explain the Na-O anticorrelation, Herwig et al. (2012) has a model using Galactic plane passages, and Valcarce & Catelan (2011) is a generic model based upon the mass of the progenitor structure. The details for Herwig et al. (2012) are copied from their table 5. In each case the population that each ascribes to the bMS is highlighted.

Generation	Joo & Y.-W. Lee (2013)	D'Antona et al. (2011)	Herwig et al. (2012)	Valcarce & Catelan (2011)
1	[Fe/H] = −1.81, Y = 0.2	metal-poor	Low Fe; normal He, La; high α, high (from r-process) Eu	[Fe/H] ∼ −1.7 O-richest, Na-poorest
2	[Fe/H] = −1.51, Y = 0.2, 0.1 ± 0.4 Gyr	O-poor, He-rich, (**bMS**), 80 Myr	Low O, intermediate Fe; high He (**bMS**), N, Na, n-capture	[Fe/H] ∼ −1.5, He- and Na-rich, O-poor (**bMS**)
3	[Fe/H] = −1.31, Y = 0.4, 1.1 ± 0.4 Gyr (**bMS**) some CNO enhancement	O-int, He-int	High Fe, C+N+O; higher N, He, n-capture	[Fe/H] ∼ −0.75, He- and Na-rich, O-poor
4	[Fe/H] = −1.01, Y = 0.38, 1.7 ± 0.4 Gyr, max. CNO enhancement	O-rich, 90 Myr	Low (medium) Fe; normal He, medium O, Na, high C, n-capture	[Fe/H] ∼ −1.5 to −1.2, probably O- and Na-int
5	[Fe/H] = −0.62, Y = 0.39, 1.7 ± 0.4 Gyr, max. CNO enhancement	Na-O correlated pop., 150 Myr		

Self-enrichment is a method for creating the sodium-oxygen anticorrelations in GCs. This uses a combination of AGB star winds and SNe to pollute the ICM and also to expel extra gas. An alternate model proposes the merger of gas clouds with different compositions (e.g. Icke & Alcaíno 1988). The merger of gas clouds has the problem that it would require a contrived explanation of the α-element similarities and the light element differences in GC stars.

In D'Antona et al. (2011) they discuss the models of D'Ercole et al. (2008, 2010), which modelled the monometallic cluster NGC 2808, in the context of ω Cen. They used super-AGB star yields to show a qualitative match to the Na-O anticorrelation and correlation in ω Cen. In their model, the first stars of the second generation were the most oxygen poor (our group #3), forming from pure AGB ejecta from the first generation of stars, which had accumulated at the centre of the cluster. These stars were very helium-rich (corresponding to the bMS). This pure ejecta material was then diluted by "pristine" gas from the surrounding ISM, which reduced its sodium abundance and increased its oxygen abundance. Type 1A SNe caused the remaining gas to be expelled, stopping more star formation. This occurred when the [O/Fe] and [Na/Fe] had returned to the values that were present during the primordial generation (our group #2). A final star formation period took place that used the pure ejecta of the first second-generation stars, with these ejecta having a correlated abundance of sodium and oxygen. This formed the group #4 stars of this thesis. Since any dilution by the ISM would result in an anticorrelation, this model requires that the surrounding region of the galaxy be cleared of residual gas, so that the ICM be pure AGB ejecta. They also note that this requires there to be a delay, in order for the AGB stars to be great enough in quantity to have produced enough gas. This whole process "must not exceed a few 10^8 years".

In Herwig et al. (2012), they identified Galactic plane passages as a potential mechanism for stripping the cluster of gas, and stimulating star formation events, as opposed to SNe. Their evolutionary sequence would have our group #1 as the primordial population, followed by group #3 forming and then group #4. The last population formed would be group #2 from the gas of the group #1 stars, and after all residual gas had been stripped by a Galactic plane passage. This theory would require all GCs to be undergoing Galactic plane passages in order to account for the sodium-oxygen anticorrelations, and would not explain the Fe-Ba correlation, as the last generation of stars would form from gas that had been expelled from lower-mass AGB, which are rich in s-process elements.

The same order of groups would result from the formation model of Valcarce & Catelan (2011). Group #1 would form and pollute the environment with sodium-rich, oxygen-poor material from the winds of massive stars. The core-collapse SNe of group #1 would compress this gas, starting the formation of the second generation, composed of our group #3 stars. Gas would once again accumulate at the cluster core from the ejecta of SNe of group #1, and winds of lower-mass group #1 stars and massive group #3 stars. A third period of star formation would take place to create the Fe-rich, Na-O correlated, group #4 stars. Finally more gas would accumulate from the winds of all generations of stars and form the oxygen-rich, sodium-poor group #2. Again an aspect they do not take into account is how the neutron-capture element profile are enhanced. Why would the final generation of stars, formed from the winds of all the previous generation of stars, have the same s-process element range as the second generation of stars, which formed from only the first generation ejecta? It would also require the processing of nitrogen to carbon, since the group #2 stars are much more carbon rich than any of the other groups and also at the same carbon abundance as the group #1 stars, which form the first generation.

Carretta et al. (2010b) investigated the abundance distribution of M54 and the Sagittarius dwarf spheroidal (Sgr dSph) galaxy to see if it could be seen as a precursor to an ω Cen-like object. One focus was on how the equivalent of our group #4 (metal-rich, nitrogen-rich) population of stars could be formed in a GC environment. They found that the stars that make up the Sgr dSph consist of stars that are metal-rich, so they suggested a model in which the Fe-rich stars were accreted by ω Cen from its parent galaxy and did not form in the cluster itself. They propose an inhomogeneous formation process in the cluster itself, where the metal-intermediate groups would form 10–30 Myr after the metal-poor groups in an unmixed region of the cluster. In the metal-poor region, 6–8 $M_\odot$ AGB stars would form as the core collapse SNe are occurring in the metal-intermediate region. Somehow the gas does not accumulate and instead the next star formation process occurs simultaneously in the two regions: the metal-poor region from the winds of 5–6 $M_\odot$ stars and from 6–8 $M_\odot$ AGB stars in the metal-intermediate region. In this way, the metal-poor region is forming the very O-poor extension of the Na-O anticorrelation. Again this does not appear to explain the barium abundances, as the second generation of the metal-rich region would have formed from the well-mixed gas that formed its first generation. Why would iron and barium be correlated?

Monometallic cluster models invoke SNe as a source of energy that can be injected into the system which can remove gas that needs to be ejected from the cluster before further generations can form (i.e., iron-rich material from SNe). Gas also needs to be ejected in order to stop star formation. Dopita & G. Smith (1986) and Krause et al. (2012) argued that for clusters more massive than $\sim 10^7$ $M_\odot$, the gravitational potential would have been too large for SNe to remove gas. This is about the mass of the present day ω Cen but it is thought that the GCs were much larger in their youth. Leigh et al. (2013) investigated using black holes as a possible method to remove gas from GCs during the star formation era. They found that a black hole would accrete a significant mass fraction of the cluster (50–80 %) in 10–100 Myr. Another possible aspect of black holes would have the ability to change the first generation's initial mass function while the first generation is still forming. The most massive stars could have evolved and formed black holes before the first generation had actually finished its star formation, and these black holes could have removed gas from the ICM. Of course in order for the second generation to form, the black holes must be removed from the cluster, lest they remove all the gas before the second generation can form. Leigh et al. (2013) do suggest it would be possible to remove them from the cluster through gravitational interactions. It does seem likely that there would have been some black holes in ω Cen due to core collapse SN that would have occurred in its youth. Although there has been no direct evidence for black holes existing in the cluster today, there is some circumstantial evidence for the existence in the core (Lu & Kong 2011; Jalali et al. 2012 but see also Anderson & van der Marel 2010). How the black holes would affect the abundance pattern of the cluster needs to be understood.

This section has outlined a variety of formation models for ω Cen and aspects of those models. Each seeks to explain some of the observed features of the cluster. It would seem that the s-process abundance spread is the major unexplained feature of any of these models. Perhaps as suggested by D'Antona et al. (2011), the s-process is a "red herring" and requires a new theory of s-process enrichment. As they state, the sodium-oxygen anticorrelation only occurs in GCs and not in field stars. This is because of the compact nature of GCs and the effect this has on the stellar winds. In the same vein, perhaps the s-process enhancement of ω Cen is the result of something unique to its environment, and other multimetallic clusters? But of course although these multimetallic clusters all have s-process abundance ranges, we have the counterexample of NGC 3201, which has a metallicity spread but no s-process spread.

The unique nature of ω Cen suggests that it underwent a formation process that is unique amongst Galactic GCs. It is highly likely that ω Cen formed from a gas cloud that was much more massive that the present mass of

the cluster. However mass alone cannot be the sole cause of its anomalous abundance compared to other clusters. Although in science, contrived and fine-tuned models are to be avoided, in this case we may be looking at a very unique set of circumstances that formed this unusual cluster.

6.4 Asymptotic Giant Branch Stars

In Section 3.3 it was found that there was **not** a lack of CN-strong stars on the AGB of 47 Tuc. This was in contrast to previous work with NGC 6752, which had found there were no CN-strong stars on the AGB of that cluster (Norris et al. 1981; Campbell et al. 2010). Conversely, NGC 1851, mentioned before as having an s-process abundance range, has a quadrimodal distribution of CN band strengths in its RGB and AGB populations (Campbell et al. 2012).

This lack of CN-strong stars on the AGB of NGC 6752 is in contrast to the RGB where the stars are equally CN-weak and CN-strong. As shown in Fig. 1.2, NGC 6752 has an extended HB, similar in morphology to that of ω Cen. However the situation with the HB of ω Cen is more complicated due to its multiple populations.

Due to the range of ages, metallicities and helium content of ω Cen, there will potentially be as many distinct AGBs as there are distinct RGBs. This means that it is almost certain that some of the stars that are being referred to in this thesis, and in other works, as RGB stars, will in fact be AGB stars. In the context of the Large Magellanic Cloud there was an estimate that the "number of early-AGB stars lying hidden in the broad RGB may be as high as 30 % of the total number of RGB+AGB stars" (Cole et al. 2000). This level of contamination will also be affected by how many of these stars actually ascend the AGB. D'Cruz et al. (2000) estimated that as many as 30 % of the HB stars are extreme in their colour, which could mean that they evolve directly to white dwarfs, never passing up the AGB. As such it is not possible to identify all of the AGB stars of the cluster. In addition there will be an overlapping of isochrones of different iron, age, CNO, and helium on the AGB and RGB (see Fig. 6.7). This will affect the metal-poor RGBs more than the metal-rich ones, since it will be the metal-rich AGB stars that will be contaminating the metal-poor RGBs.

However, at least in the ω Cen sample investigated by Marino et al. (2012), there does not appear to be a lot of contamination, with the metal-richer groups (our groups #2 & #3) not overlapping the most metal-poor group (our group #1) (see Figs. 4.14a, 4.14c and 4.15a). In the case of Marino et al. (2012) there is only one potential AGB star (Section 4.4.1). This star has a low [N/Fe] and [C/Fe], which would fit with the findings of Campbell et al. (2010).

There were two spectral indices measured by van Loon et al. (2007) in their spectral library of ω Cen that are of interest to this thesis: the S(3839) and CH(4300) indices[2]. The first measured the CN band around 3839 Å and the second CH band at 4300 Å (the G band). They used the definition of Harbeck et al. (2003), where $F_{\lambda 1-\lambda 2}$ is the average flux level between the two wavelengths in angstroms:

$$\mathrm{S}(3839) = -2.5 \log \left(\frac{F_{3861-3884}}{F_{3894-3910}} \right), \tag{6.1}$$

$$\mathrm{CH}(4300) = -2.5 \log \left(\frac{2F_{4285-4315}}{F_{4240-4280} + F_{4390-4460}} \right). \tag{6.2}$$

Fig. 6.8a shows the S(3839) and CH(4300) indices for all the stars determined in Chapter 4, with a curved line dividing the O-rich stars (Section 5.1) from the O-poor stars. The clump of stars in the lower-left quadrant of both subfigures of Fig. 6.8 with CH(4300)< 0.9 are HB stars. This has been separated from the GB by a vertical line. The groups of stars which were deficient in nitrogen (see Figs. 4.16 and 5.14) are almost all below the dividing line, while group #3 (C-weak, N-strong) stars are placed above the line. The (metal-rich) group #4 are found to be on both sides of the line. For this group there is a much larger variation in S(3839) than in CH(4300), which would correspond to their larger range of [N/Fe] than [C/Fe]. From Section 4.4, there are nine potential AGB stars in the 221-star subset of van Loon et al. (2007) for which [C/Fe] and [N/Fe] were determined. These nine AGB stars have small to medium strength CN and CH bands based upon their S(3839) and CH(4300) indices.

All this gives good evidence that the S(3839) and CH(4300) indices of van Loon et al. (2007) can be used to define the CN strength of the stars. This would be expected as S(3839) is designed to measure the strength of a CN spectral feature. To extend the sample of AGB stars from just those for which a [C/Fe] and [N/Fe] was determined in Chapter 4, the photometry of Bellini et al. (2009a) was used to separate the AGB from the RGB

[2] It should be noted that these values used van Loon et al. (2007) normalized spectra.

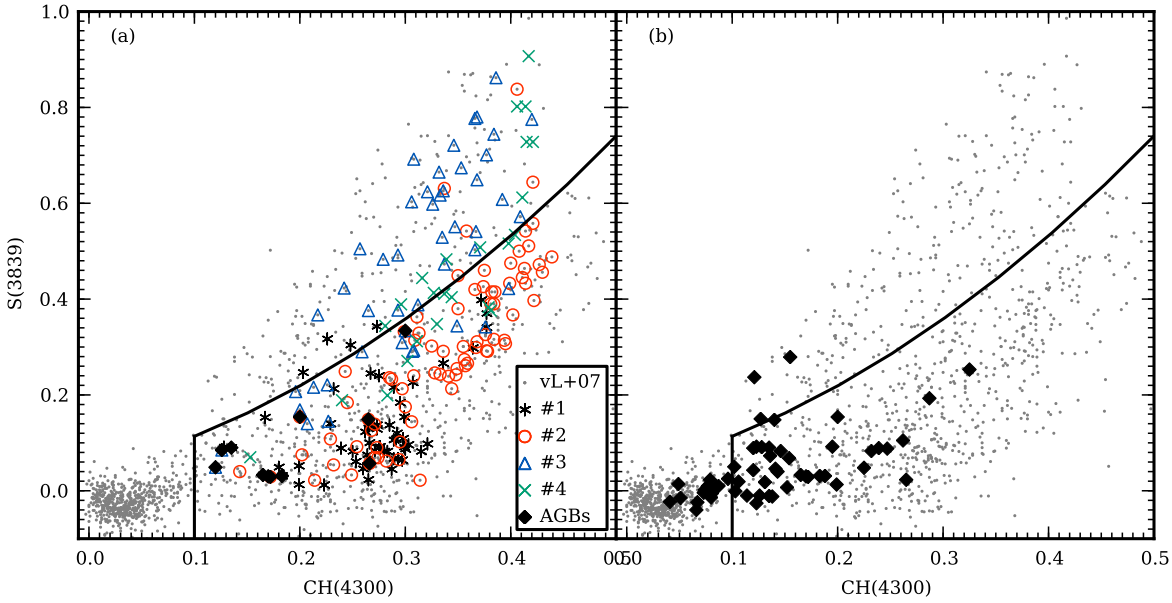

Figure 6.8 — (a) The four groups of stars in ω Cen with their CN [S(3839)] and CH [CH(4300)] indices as found by van Loon et al. (2007). The diamonds are the AGB stars identified in Section 4.4. The curved line separates the oxygen-rich stars (below the line) from the oxygen-rich stars. This serves as a divider between CN-weak and CN-strong stars. The vertical line divides the HB from the GB in these diagrams. The small dots in all subplots show all the stars in the van Loon et al. (2007) dataset. (b) Highlighting all the 55 AGB stars identified in the entire van Loon et al. (2007) library based upon their position in the CMD of Bellini et al. (2009a).

from $12.6 < V < 14.2$. By eye, over 200 AGB stars were defined from the Bellini et al. (2009a) sample (out of over 60,000 probable cluster members). These stars then gave 55 AGB stars in the overall van Loon et al. (2007) sample for which there was also Bellini et al. (2009a) photometry.

All the van Loon et al. (2007) stars identified as AGB stars have low S(3839) and CH(4300) indices (see Fig. 6.8b). In the case of the CN index, they are all less than 30 % of the maximum value measured for any star by van Loon et al. (2007). The vertical line places 18 of the 55 stars (33 %) in the HB part of the diagram. Some of these stars may not be HB stars but are too hot to easily determine their CN strength from these indices. Of the remaining 37, only two of these AGB stars (5 %) are significantly above the line. From this we would infer that more than 90 % of this AGB are CN-weak.

Instead of using the S(3839) and CH(4300) indices, the results of Chapter 5 can be used instead, with their determinations of [C/Fe] and [N/Fe]. Of the 55 AGB stars identified in the van Loon et al. (2007) spectral library, 42 were analyzed in Chapter 5, with 22 of the 42 being cool enough ($T_{\rm eff} \leq 4900$ K; Section 5.4) for reliable carbon and nitrogen abundances. These stars had an average metallicity of $\langle$[Fe/H]$\rangle = -2.0 \pm 0.3$, so these stars represent a metal-poor subset of the cluster. This would be expected based upon the assumption that these stars are members of the metal-poor population. However, their [N/Fe] were distributed evenly from −0.5 to 1.4 dex (Fig. 6.9). Their groupings determined in Chapter 5 were such that there were 4 stars were in group #1 (18 %), 8 in #2 (36 %), 10 in #3 (45 %), and none in #4.

The reason for this discrepancy between the stars S(3839) index and its [N/Fe] abundance becomes clear when the two values are plotted against each other (Fig. 6.10). It is found that although there is a correlation between these two, there is a degeneracy of [N/Fe] for the low values of S(3839). As such it is not possible to use the S(3839) index alone to determine the CN strength for such a wide range of temperatures as is present in this analysis. As the temperature is increased the strength of the CN strength will decrease (for all else remaining the same).

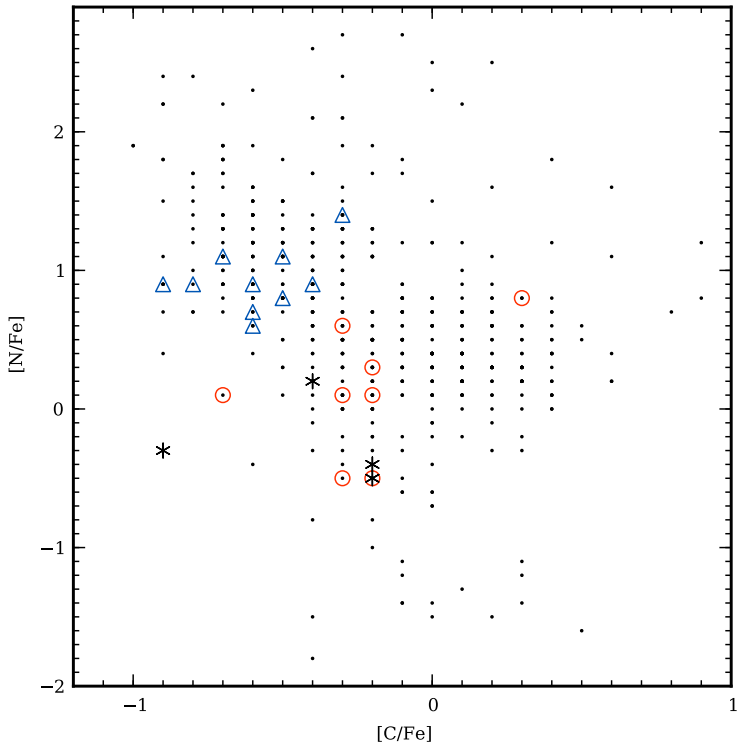

Figure 6.9 — [C/Fe] and [N/Fe] abundances of the AGB stars in ω Cen in the 557 star sample of Chapter 5.

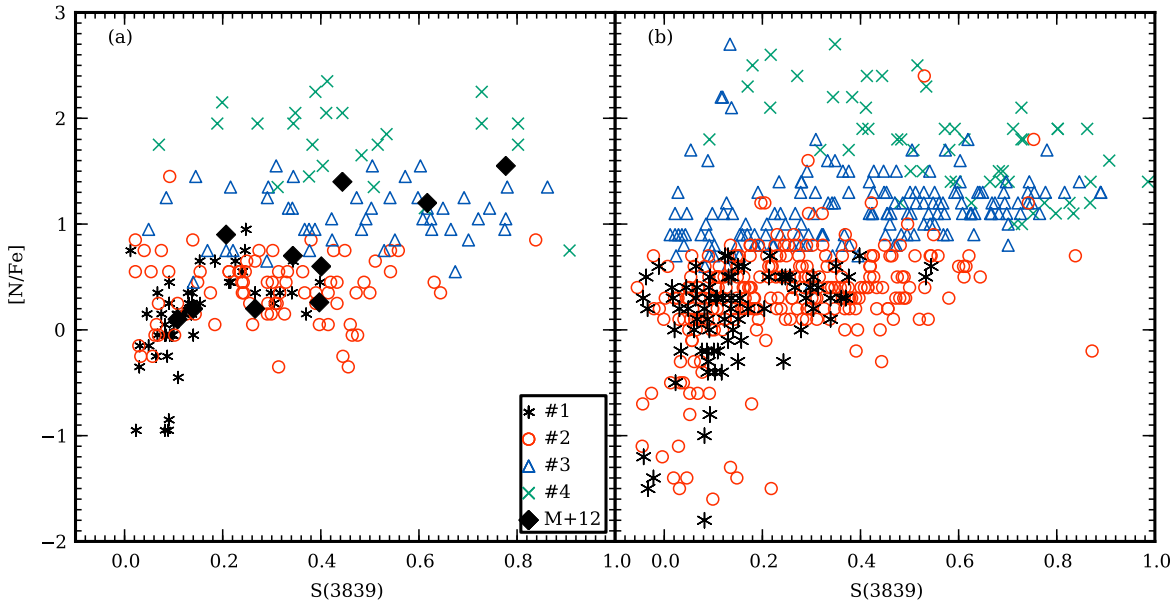

Figure 6.10 — The [N/Fe] abundance against the S(3839) spectral index determined for ω Cen stars by van Loon et al. (2007). (a) Shows the results from the 221 star sample of Chapter 4 as well as the results from the nine stars in common with Marino et al. (2012) using their [N/Fe]. (b) Shows the results from 557 star sample of Chapter 5.

What is found is that identifiable AGB stars of ω Cen have a large range of [N/Fe] but only a small range of [C/Fe] compared to the rest of the cluster. Only one of these stars was found to have a supersolar abundance of carbon, with the rest having an average of $\langle[C/Fe]\rangle = -0.5$. Based upon Fig. 5.13b, this would place them mostly in the realm of groups #1 and #3. It should be remembered that AGB stars have undergone further mixing processes to those stars on the RGB, which could affect their surface abundance of carbon and nitrogen. All of these AGB stars that were in common with Johnson & Pilachowski (2010) were found to be oxygen rich, which is consistent with their location on Figs. 5.3a and 6.8a. Their combination of low carbon and high oxygen means that they have a much lower [C/O] ratio than most of the stars in the cluster, with a mean of -0.90 ± 0.21 dex compared to -0.26 ± 0.43 dex for the entire cluster. One possibility is that the carbon-rich AGB stars do not return to this region of the AGB, hence the lack of them in this sample. This could be the result of them being the helium-rich population in the cluster. This would be inconsistent with the model of D'Antona et al. (2011), where it is the oxygen-poor group of stars that are enhanced in helium.

Chapter 7

Conclusions

Globular clusters (GCs) have long been a testing ground for models of stellar evolution, as they provide a group of stars that are all at the same distance from the observer. With their large numbers of stars, the clusters are intrinsically bright, and therefore can be observed at large distances. However, their evolution is more complicated than previously assumed. Even though most are monometallic, they show correlations and anticorrelations between their light elements. This is interpreted to be the result of a primordial population of stars, which polluted the intra-cluster medium (ICM), and from which younger generations of stars formed. Along with being monometallic, most of these clusters do not show any range of abundances of their neutron-capture elements.

However, the massive GC, ω Cen, has been found to be different (but also similar) to these other clusters. It is not monometallic at all, having a range of at least 1.5 dex in the metallicity of its stars. Correlated with this iron abundance is the abundance of its s-process elements. Over about a change in [Fe/H] of 0.4 dex, the [Ba/Fe] increases by about 1.5 dex. Like the monometallic clusters, there is an anticorrelation of sodium and oxygen, but there is a complication: there is a group of stars that are **correlated** in their sodium and oxygen abundances. This group is also the most metal-rich group in the cluster.

In order to explore the abundances of ω Cen using low resolution spectra, an automated spectral matching pipeline was created. This pipeline used a combination of photometry and spectroscopy to determine basic stellar parameters and elemental abundances for each star. The $V-K$ colour of the star was used to determine the star's $T_{\rm eff}$ and $\log g$ using the empirical temperature-colour relationships of Alonso et al. (1999, 2001). For the clusters investigated in this thesis, matching of synthetic spectra to the observed spectrum was used to find the elemental abundances. This spectral matching pipeline took into account molecular equilibria that exist between CO, CH, and CN. These equilibria mean that any abundance determination of [C/Fe] and [N/Fe] using the molecular lines of CH and CN must have a good understanding of the [O/Fe] abundance of the stars in question. The spectra were automatically normalized by mapping the observed spectrum onto the synthetic spectrum. The abundance was then determined by iteratively refining the abundance from an initial estimation until the best fitting synthetic spectrum was found.

In order to assure the quality of the abundances determined by the spectral matching pipeline for ω Cen, two monometallic clusters were used as test-cases: 47 Tuc and NGC 6752. These clusters were selected as they were of similar metallicities to, respectively, the metal-rich and metal-poor stars of ω Cen. They were also used to understand how different methods of determining [O/Fe] would affect the carbon and nitrogen abundances that were found for the stars. In the case of 47 Tuc, there were two sources of spectroscopy. The first was a large sample of 94 stars from AAOmega on Anglo-Australian Telescope (AAT), which covered the red giant branch (RGB), horizontal branch (HB), and asymptotic giant branch (AGB). The second was a smaller sample of 13 stars from the Southern African Large Telescope (SALT). For NGC 6752, 11 RGB stars were analyzed from spectra acquired with AAOmega. In the case of both clusters, the expected anticorrelation between nitrogen and carbon was found, consistent with results found from other researchers for (unevolved) stars in each cluster.

The van Loon et al. (2007) spectral library provides a large sample of spectra of giant branch and horizontal branch stars of ω Cen. Combining this spectral data with high precision photometric data and previously determined [O/Fe] and [Ca/Fe] abundances of these stars, [C/Fe] and [N/Fe] were determined for over 200 new stars in the cluster (Chapter 4). These results confirmed the results of Marino et al. (2012): that the low metallicity stars have both low carbon and nitrogen, while the intermediate groups show an anticorrelation of carbon and nitrogen.

Combining these carbon and nitrogen data with sodium, oxygen and barium abundances, and using k-means clustering, four groupings of stars were found:

- A low-metallicity group #1 ($\langle$[Fe/H]$\rangle$ = −1.9) which is deficient in carbon and nitrogen relative to iron, but not oxygen.
- Two intermediate metallicity groups ($\langle$[Fe/H]$\rangle$ = −1.6) which are anti-correlated in Na-O and C-N. Group #2 are high in C and O, while group #3 are high in Na and N. Both these groups have the same metallicity and barium range. There is a potential subgroup of group #3, which was labelled #3b which has a higher barium than the rest of the group and higher Na and N without any differences in its O and C.
- A metal-rich group #4 ($\langle$[Fe/H]$\rangle$ = −1.1) which is enhanced in Na, N, and showing a correlation of Na with O. This group has the highest average barium of all the groups.

In Chapter 5, the van Loon et al. (2007) spectral library was again used, with stellar parameters and elemental abundances ([Fe/H], [O/Fe], [C/Fe], [N/Fe] and [Ba/Fe]) determined for 848 members of the GC ω Cen. In addition over 100 non-cluster members were also analyzed. This is one of the largest abundance analysis of this GC in the literature, complementing the work of Johnson & Pilachowski (2010). With limits imposed due to the spectral resolution of the spectra, we are confident of the nitrogen abundances for 557 stars with $T_{\rm eff} \leq 4900$ K.

This work confirmed what was found in Chapter 4 regarding the relative abundances of four different groups of stars. We identified a metal-poor group of stars (our group #1) that is oxygen rich, while poor in sodium, nitrogen and carbon. This group exists on the bluest edge of the giant branch of the colour-magnitude diagram, which matches to its metallicity (metal-poorer stars are hotter). We believe this to be the oldest extant population in the cluster.

Groups #2 and #3 form the bulk of the stars in our sample, and probably the cluster. In Chapter 4, we showed that these stars have similar ranges of barium and iron, potentially making them coeval, or one forming from the ejecta of the other group. This requires processes that change the abundance of oxygen, sodium, carbon and nitrogen, while not affecting the metallicity or s-process abundance of the stars. These two groups form the extended Na-O anticorrelation that is typical of a GC. Of course, these groups show a metallicity range that is not present in a simple-stellar population GC.

Group #4 are the extreme stars of our sample. They have the highest Fe, N, Na, Ba of all the stars. They are potentially the last population of stars to form in the cluster, due to their high iron content. Even if not the last population of stars to form, they are certainly one of the later groups. Their Na-O correlation is not observed in other GCs. This could require the mass of ω Cen to retain the gas that would normally be lost in other clusters but here was kept and formed this generation of stars.

Due to the biased nature of our sample of stars, we have avoided drawing conclusions about the radial aspects of these groups. We find evidence that the nitrogen-rich stars are not found at large radial distances in the cluster, being more centrally concentrated. This matches to the work of Johnson & Pilachowski (2010) who found that O-poor stars are similarly centrally concentrated. This would make them our groups #3 and #4 stars, which have both low oxygen and high nitrogen. Which is the driver here? Are they nitrogen rich because they are oxygen poor, or vice versa?

High precision photometry was used to define 39 AGB stars in the van Loon et al. (2007) sample. Their S(3839) and CH(4300) indices provided a good measure of the CN strength of the star. The majority of AGB stars were found to be CN-weak. The hypothesis that differing helium abundances could cause such an effect in mono-metallic clusters does not fit this result, as this AGB is associated with the most metal-poor stars in the cluster and therefore will not have any helium enhancement.

7.1 Future Work

The Johnson & Pilachowski (2010) abundance analysis is a fantastic resource, with 20 different chemical elements determined for over 850 giant branch (GB) stars in ω Cen. It was however magnitude limited to $V < 13.5$. This did not allow for it to reach stars on the AGB, nor include many stars that belong to the metal-rich RGB-a. It would be desirable to observe stars further down the GB at high resolution. Currently, there is not a large catalogue of abundances for the sub-giant branch (SGB) and main sequence (MS) at higher spectral resolutions. This would

extend the work of Stanford et al. (2007) and Pancino et al. (2011b), where the surface composition will show the composition of the gas from which these stars formed.

To extend the results of this thesis, helium abundances in MS and GB stars in ω Cen (and other clusters) are crucial. These are a key aspect to fully understanding its chemical evolution. Currently it is speculated that one or more of the intermediate metallicity populations are helium enhanced, but it is crucial to understand which ones as this drives the choice of polluters and the order in which the different populations formed. This work would link back to the CN-weak/CN-strong research interest, where one of the hypotheses is that a high helium abundance causes horizontal branch stars to evolve directly to the white dwarf phase.

As discussed in Chapter 6, the carbon and nitrogen abundances of AGB stars needs further investigation. Since the RGBs of clusters do have CN-strong and CN-weak stars in approximately equal proportion, this would suggest that something is happening to the CN-strong stars of NGC 6752. One possibility is that the CN-strong stars are undergoing some mixing process that depletes their surface CN composition. Another is that the CN-strong stars are evolving directly from horizontal branch stars to white dwarfs. As part of this thesis work and in Simpson et al. (2012), it was found that the observable AGB stars of ω Cen are all CN-weak as given by their CN-index, but not according to their [N/Fe]. In this case, it could be that the AGB that we are observing are the more evolved stars of the metal-poor population of the cluster, which is CN-weak already. Investigation of this would be useful and to see if further AGBs can be identified in the cluster's colour-magnitude diagram (CMD). Of particular interest would be the AGB associated with the metal-rich RGB of the cluster. This has the potential for identifying stars that belong to its AGB due to its largest separation from the main bulk of the RGB on the CMD.

One cluster not studied in this thesis was NGC 2419. With the anomalous luminosity for its size, NGC 2419 warrants further observations. Currently there are few analyses of its stars and they are contradictory as to whether it has a spread of its iron abundance (Sandquist & Hess 2008; Cohen et al. 2010; Cohen & Kirby 2012; Mucciarelli et al. 2012). With the high precision, long exposures available with the Hubble Space Telescope (HST), investigating the main sequence photometrically for multiple populations could help to determine the extent of the anomalous behaviour of this cluster. Its luminosity suggests something strange happened in its formation. It can either be thought of as too physically large for its luminosity or too luminous for its physically extent. Understanding anomalous clusters like it and ω Cen provides a test for formation theories of "ordinary" globular clusters like 47 Tuc. It is also one of the most distant clusters, so observations of it will be difficult.

From SALT, we have three sets of spectra of 47 Tuc, NGC 362, and NGC 6752 that require analyses. In this thesis only the spectra from 47 Tuc was analyzed and only then in a preliminary sense, without the proper [O/Fe] for the stars. There have been few large analyses of [C/Fe] and [N/Fe] for evolved stars in these clusters so these datasets will greatly extend our knowledge of the abundances of these clusters. In addition, in the observing queue is a multi-object spectroscopy (MOS) observation of about 20 stars of ω Cen with the aim of increasing the number of for AGB stars in our sample.

With regards to SALT and its reference stars, which are used for aligning the instrument, could also be useful for abundances. These stars are selected by the observer when setting up the proposal and are usually around $V \sim 15$. This is about the magnitude of the blue straggler stars and the extreme horizontal branch stars in clusters with apparent brightnesses like ω Cen. Both of these types stars are not well-studied and could provide interesting results. One issue with using these reference stars is that the slits used by the instrument are wide ($5''$) which means that the spectra acquired will have a very low spectral resolution ($R \sim 1000$). However, they will have a large signal and will come at no extra cost to the observer when planning an observation. The analysis of the reference star spectra already acquired from 47 Tuc, NGC 362, and NGC 6752 is another area to investigate.

Appendix A

Data Tables

A.1 47 Tuc Results

Results for 47 Tuc stars from the AAOmega spectra with [O/Fe] derived from δC (Section 3.1).
Results for 47 Tuc stars from the AAOmega spectra with [O/Fe] derived from [Na/Fe] (Section 3.1.2).
Results for 47 Tuc stars from SALT MOS spectra (Section 3.2)

Bibliography

Albrow, M. D., Gilliland, R. L., Brown, T. M., Edmonds, P. D., Guhathakurta, P., & Sarajedini, A. (2001). "The Frequency of Binary Stars in the Core of 47 Tucanae". In: ApJ 559, pp. 1060–1081 (cit. on p. 11).

Allen, C. W. & Cox, Arthur N. (2000). *Allen's Astrophysical Quantities*. 4th. New York: Springer (cit. on p. 20).

Alonso, A., Arribas, S., & Martínez-Roger, C. (1999). "The effective temperature scale of giant stars (F0-K5). II. Empirical calibration of $T_{\rm eff}$ versus colours and [Fe/H]". In: A&AS 140, pp. 261–277 (cit. on pp. 19–21, 64, 88, 89, 93, 121).

— (2001). "Erratum: The effective temperature scale of giant stars (F0-K5). II. Empirical calibration of $T_{\rm eff}$ versus colours and [Fe/H]". In: A&A 376, p. 1039 (cit. on pp. 19, 20, 121).

Anders, E. & Grevesse, N. (1989). "Abundances of the elements - Meteoritic and solar". In: Geochim. Cosmochim. Acta 53, pp. 197–214 (cit. on pp. 23, 29, 82).

Anderson, J. (1997). "Mass Segregation in Globular Clusters M92, 47 Tucanae, and Omega Centauri". PhD thesis. University of California, Berkeley (cit. on p. 5).

— (2002). "Main-Sequence Observations with HST". In: *Omega Centauri, A Unique Window into Astrophysics*. Ed. by F. van Leeuwen, J. D. Hughes, & G. Piotto. Vol. 265. Astronomical Society of the Pacific Conference Series, p. 87 (cit. on p. 5).

— (2003). "Astrometry with HST: the Promise and the Perils". In: *New Horizons in Globular Cluster Astronomy*. Ed. by G. Piotto, G. Meylan, S. G. Djorgovski, & M. Riello. Vol. 296. Astronomical Society of the Pacific Conference Series, p. 125 (cit. on p. 5).

Anderson, J., Piotto, G., King, I. R., Bedin, L. R., & Guhathakurta, P. (2009). "Mixed Populations in Globular Clusters: Et Tu, 47 Tuc?" In: ApJ 697, pp. L58–L62 (cit. on p. 4).

Anderson, J. & van der Marel, R. P. (2010). "New Limits on an Intermediate-Mass Black Hole in Omega Centauri. I. Hubble Space Telescope Photometry and Proper Motions". In: ApJ 710, pp. 1032–1062 (cit. on p. 116).

Asplund, M., Grevesse, N., Sauval, A. J., & Scott, Pat (2009). "The Chemical Composition of the Sun". In: ARA&A 47.1, pp. 481–522 (cit. on p. 16).

Audi, G., Wapstra, A. H., & Thibault, C. (2003). "The Ame2003 atomic mass evaluation: (II). Tables, graphs and references". In: *Nuclear Physics A* 729.1. The 2003 NUBASE and Atomic Mass Evaluations, pp. 337–676. ISSN: 0375-9474 (cit. on p. 15).

Bedin, L. R., Piotto, G., Anderson, J., Cassisi, S., King, I. R., Momany, Y., & Carraro, G. (2004). "ω Centauri: The Population Puzzle Goes Deeper". In: ApJ 605, pp. L125–L128 (cit. on p. 5).

Bekki, K. & Freeman, K. C. (2003). "Formation of ω Centauri from an ancient nucleated dwarf galaxy in the young Galactic disc". In: MNRAS 346, pp. L11–L15 (cit. on p. 103).

Bellini, A., Piotto, G., Bedin, L. R., Anderson, J., Platais, I., Momany, Y., Moretti, A., Milone, A. P., & Ortolani, S. (2009a). "Ground-based CCD astrometry with wide field imagers. III. WFI@2.2m proper-motion catalog of the globular cluster ω Centauri". In: A&A 493, pp. 959–978 (cit. on pp. 8, 21, 23, 63–67, 75, 78, 85, 87, 88, 93, 95, 96, 99, 114, 117, 118).

Bellini, A., Piotto, G., Bedin, L. R., King, I. R., Anderson, J., Milone, A. P., & Momany, Y. (2009b). "Radial distribution of the multiple stellar populations in ω Centauri". In: A&A 507, pp. 1393–1408 (cit. on p. 109).

Belserene, E. P. (1959). "Magnitudes and colors in omega Centauri." In: AJ 64, pp. 58–64 (cit. on p. 2).

Bergbusch, P. A. & Stetson, P. B. (2009). "A New Color-Magnitude Diagram for 47 Tucanae: A Statistical Analysis". In: AJ 138, pp. 1455–1464 (cit. on p. 37).
Briley, M. M., Harbeck, D., Smith, G. H., & Grebel, E. K. (2004). "On the Carbon and Nitrogen Abundances of 47 Tucanae's Main-Sequence Stars". In: AJ 127, pp. 1588–1593 (cit. on pp. 4, 54, 55).
Briley, M. M., Smith, V. V., Suntzeff, N. B., Lambert, D. L., Bell, R. A., & Hesser, J. E. (1996). "Sodium abundance variations in main-sequence stars of the globular cluster 47 Tucanae". In: Nature 383, pp. 604–606 (cit. on p. 4).
Brown, J. A. & Wallerstein, G. (1992). "High-resolution CCD spectra of stars in globular clusters. VII - Abundances of 16 elements in 47 Tuc, M4, and M22". In: AJ 104, pp. 1818–1830 (cit. on p. 34).
— (1993). "High resolution CCD spectra of stars in globular clusters. VIII - The self-enrichment history of Omega Centauri". In: AJ 106, pp. 133–141 (cit. on p. 10).
Brown, J. A., Wallerstein, G., & Oke, J. B. (1990). "High-resolution CCD spectra of stars in globular clusters. V - Carbon, nitrogen, and oxygen abundances in stars in 47 Tuc, M4, and M22". In: AJ 100, pp. 1561–1574 (cit. on pp. 34, 55).
Burbidge, E. M., Burbidge, G. R., Fowler, W. A., & Hoyle, F. (1957). "Synthesis of the Elements in Stars". In: RMP 29, pp. 547–650 (cit. on pp. 12, 14, 15).
Campbell, S. W., Yong, D., Wylie-de Boer, E. C., Stancliffe, R. J., Lattanzio, J. C., Angelou, G. C., D'Orazi, V., Martell, S. L., Grundahl, F., & Sneden, C. A. (2012). "Cyanogen in NGC 1851 Red Giant Branch and Asymptotic Giant Branch Stars: Quadrimodal Distributions". In: ApJ 761, p. L2 (cit. on p. 117).
Campbell, S. W., Yong, D., Wylie-de Boer, E. C., Stancliffe, R. J., Lattanzio, J. C., Angelou, G. C., Grundahl, F., & Sneden, C. A. (2010). "The case of the disappearing CN-strong AGB stars in Galactic Globular Clusters - preliminary results". In: Mem. Soc. Astron. Italiana 81, p. 1004 (cit. on pp. 4, 55, 117).
Cannon, R. D., Croke, B. F. W., Bell, R. A., Hesser, J. E., & Stathakis, R. A. (1998). "Carbon and nitrogen abundance variations on the main sequence of 47 Tucanae". In: MNRAS 298, pp. 601–624 (cit. on p. 4).
Cannon, R. D. & Stobie, R. S. (1973). "Photometry of southern globular clusters I. Bright stars in omega Centauri". In: MNRAS 162, p. 207 (cit. on p. 2).
Carretta, E., Bragaglia, A., Gratton, R. G., Lucatello, S., Bellazzini, M., Catanzaro, G., Leone, F., Momany, Y., Piotto, G., & D'Orazi, V. (2010a). "Detailed abundances of a large sample of giant stars in M 54 and in the Sagittarius nucleus". In: A&A 520, A95 (cit. on pp. 2, 4, 103).
— (2010b). "M54 + Sagittarius = ω Centauri". In: ApJ 714, pp. L7–L11 (cit. on p. 116).
Carretta, E., Bragaglia, A., Gratton, R. G., Lucatello, S., Catanzaro, G., Leone, F., Bellazzini, M., Claudi, R., D'Orazi, V., Momany, Y., Ortolani, S., Pancino, E., Piotto, G., Recio-Blanco, A., & Sabbi, E. (2009). "Na-O anticorrelation and HB. VII. The chemical composition of first and second-generation stars in 15 globular clusters from GIRAFFE spectra". In: A&A 505, pp. 117–138 (cit. on pp. 1, 3, 4, 34, 36, 37, 40, 50, 51, 55, 104).
Carretta, E., Bragaglia, A., Gratton, R. G., Lucatello, S., & Momany, Y. (2007). "Na-O anticorrelation and horizontal branches. II. The Na-O anticorrelation in the globular cluster NGC 6752". In: A&A 464, pp. 927–937 (cit. on pp. 3, 56, 57, 59–61, 104).
Carretta, E., Gratton, R. G., Lucatello, S., Bragaglia, A., & Bonifacio, P. (2005). "Abundances of C, N, O in slightly evolved stars in the globular clusters NGC 6397, NGC 6752 and 47 Tuc". In: A&A 433, pp. 597–611 (cit. on pp. 4, 55, 57, 59, 61, 62, 79, 82).
Castelli, F. & Kurucz, R. L. (2003). "New Grids of ATLAS9 Model Atmospheres". In: *Modelling of Stellar Atmospheres*. Ed. by N. Piskunov, W. W. Weiss, & D. F. Gray. Vol. 210. IAU Symposium, 20P (cit. on p. 29).
Cayrel de Strobel, G., Soubiran, C., Friel, E. D., Ralite, N., & François, P. (1997). "A catalogue of [Fe/H] determinations: 1996 edition". In: A&AS 124, pp. 299–305 (cit. on p. 34).
Cohen, J. G. & Kirby, E. N. (2012). "The Bizarre Chemical Inventory of NGC 2419, An Extreme Outer Halo Globular Cluster". In: ApJ 760, p. 86 (cit. on pp. 1, 123).
Cohen, J. G., Kirby, E. N., Simon, J. D., & Geha, M. (2010). "NGC 2419-Another Remnant of Accretion by the Milky Way". In: ApJ 725, pp. 288–295 (cit. on pp. 1, 123).
Cole, A. A., Smecker-Hane, T. A., & Gallagher III, J. S. (2000). "The Metallicity Distribution Function of Red Giants in the Large Magellanic Cloud". In: AJ 120, pp. 1808–1829 (cit. on p. 117).
Cole, A. A., Smecker-Hane, T. A., Tolstoy, E., Bosler, T. L., & Gallagher, J. S. (2004). "The effects of age on red giant metallicities derived from the near-infrared CaII triplet". In: MNRAS 347, pp. 367–379 (cit. on p. 12).
Cool, A. M., Haggard, D., Arias, T., Brochmann, M., Dorfman, J., Gafford, A., White, V., & Anderson, J. (2013). "HST/ACS Imaging of Omega Centauri: Optical Counterparts of Chandra X-Ray Sources". In: ApJ 763, p. 126 (cit. on p. 11).

Cottrell, P. L. (2013). "47 Tucanæ reduced spectra". private communication (cit. on p. 50).
Cottrell, P. L. & Da Costa, G. S. (1981). "Correlated cyanogen and sodium anomalies in the globular clusters 47 TUC and NGC 6752". In: ApJ 245, pp. L79–L82 (cit. on p. 1).
Crawford, S. M., Still, M., Schellart, P., Balona, L., Buckley, D. A. H., Dugmore, G., Gulbis, A. A. S., Kniazev, A., Kotze, M., Loaring, N., Nordsieck, K. H., Pickering, T. E., Potter, S., Romero Colmenero, E., Vaisanen, P., Williams, T. B., & Zietsman, E. (2010). "PySALT: the SALT science pipeline". In: *Society of Photo-Optical Instrumentation Engineers (SPIE) Conference Series*. Vol. 7737. Society of Photo-Optical Instrumentation Engineers (SPIE) Conference Series (cit. on pp. xii, 50).
D'Antona, F., D'Ercole, A., Marino, A. F., Milone, A. P., Ventura, P., & Vesperini, E. (2011). "The Oxygen versus Sodium (Anti)Correlation(s) in ω Cen". In: ApJ 736, p. 5 (cit. on pp. 77, 112, 115, 116, 120).
D'Antona, F., Gratton, R. G., & Chieffi, A. (1983). "CNO self-pollution in globular clusters - A model and its possible observational tests". In: Mem. Soc. Astron. Italiana 54, pp. 173–198 (cit. on p. 4).
D'Antona, F. & Ventura, P. (2007). "A model for globular cluster extreme anomalies". In: MNRAS 379, pp. 1431–1441 (cit. on p. 1).
Darwent, B. B. (1970). *Bond dissociation energies in simple molecules*. NSRDS-NBS. U.S. National Bureau of Standards; for sale by the Supt. of Docs., U.S. Govt. Print. Off., p. 52 (cit. on p. 23).
Davies, M. B. (1997). "Cataclysmic variable production in globular clusters". In: MNRAS 288, pp. 117–128 (cit. on p. 11).
D'Cruz, N. L., O'Connell, R. W., Rood, R. T., Whitney, J. H., Dorman, B., Landsman, W. B., Hill, R. S., Stecher, T. P., & Bohlin, R. C. (2000). "Hubble Space Telescope Observations of New Horizontal-Branch Structures in the Globular Cluster ω Centauri". In: ApJ 530, pp. 352–356 (cit. on p. 117).
de Marcillac, P., Coron, N., Dambier, G., Leblanc, J., & Moalic, J.-P. (2003). "Experimental detection of α-particles from the radioactive decay of natural bismuth". In: Nature 422, pp. 876–878 (cit. on p. 15).
Decin, L., Shkedy, Z., Molenberghs, G., Aerts, M., & Aerts, C. (2004). "Estimating stellar parameters from spectra. I. Goodness-of-fit parameters and lack-of-fit test". In: A&A 421, pp. 281–294 (cit. on p. 29).
Decressin, T., Meynet, G., Charbonnel, C., Prantzos, N., & Ekström, S. (2007). "Fast rotating massive stars and the origin of the abundance patterns in galactic globular clusters". In: A&A 464, pp. 1029–1044 (cit. on p. 1).
D'Ercole, A., D'Antona, F., Ventura, P., Vesperini, E., & McMillan, S. L. W. (2010). "Abundance patterns of multiple populations in globular clusters: a chemical evolution model based on yields from AGB ejecta". In: MNRAS 407, pp. 854–869 (cit. on pp. 113, 115).
D'Ercole, A., Vesperini, E., D'Antona, F., McMillan, S. L. W., & Recchi, S. (2008). "Formation and dynamical evolution of multiple stellar generations in globular clusters". In: MNRAS 391, pp. 825–843 (cit. on pp. 113, 115).
Di Criscienzo, M., D'Antona, F., Milone, A. P., Ventura, P., Caloi, V., Carini, R., D'Ercole, A., Vesperini, E., & Piotto, G. (2011). "NGC 2419: a large and extreme second generation in a currently undisturbed cluster". In: MNRAS 414, pp. 3381–3393 (cit. on p. 11).
Di Criscienzo, M., Ventura, P., D'Antona, F., Milone, A., & Piotto, G. (2010). "The helium spread in the globular cluster 47 Tuc". In: MNRAS 408, pp. 999–1005 (cit. on p. 4).
Dobrovolskas, V., Kučinskas, A., Andrievsky, S. M., Korotin, S. A., Mishenina, T. V., Bonifacio, P., Ludwig, H.-G., & Caffau, E. (2012). "Barium abundance in red giants of NGC 6752. Non-local thermodynamic equilibrium and three-dimensional effects". In: A&A 540, A128 (cit. on p. 104).
Dopita, M. A. & Smith, G. H. (1986). "The potential for supernova-induced chemical enrichment of protoglobular cluster clouds". In: ApJ 304, pp. 283–294 (cit. on p. 116).
D'Orazi, V., Gratton, R. G., Pancino, E., Bragaglia, A., Carretta, E., Lucatello, S., & Sneden, C. A. (2011). "Chemical enrichment mechanisms in ω Centauri: clues from neutron-capture elements". In: A&A 534, A29 (cit. on pp. 9, 10).
Dupree, A. K., Sasselov, D. D., & Lester, J. B. (1992). "Discovery of a fast wind from a field population II giant star". In: ApJ 387, pp. L85–L88 (cit. on p. 104).
Dupree, A. K., Strader, J., & Smith, G. H. (2011). "Direct Evidence for an Enhancement of Helium in Giant Stars in Omega Centauri". In: ApJ 728, p. 155 (cit. on pp. 10, 11, 104).
Eggen, O. J. (1992). "Asymptotic giant branch stars near the sun". In: AJ 104, pp. 275–313 (cit. on p. 34).
— (1998). "Evolutionary Oddities in Old Disk Population Clusters". In: AJ 115, pp. 2435–2452 (cit. on p. 34).
Eggen, O. J. & Iben, Jr. I. (1991). "First giant branch and asymptotic giant branch stars in nearby aggregates". In: AJ 101, pp. 1377–1407 (cit. on p. 34).

Ferraro, F. R., Dalessandro, E., Mucciarelli, A., Beccari, G., Rich, R. M., Origlia, L., Lanzoni, B., Rood, R. T., Valenti, E., Bellazzini, M., Ransom, S. M., & Cocozza, G. (2009). "The cluster Terzan 5 as a remnant of a primordial building block of the Galactic bulge". In: Nature 462, pp. 483–486 (cit. on pp. 1, 2, 103).

Ferraro, F. R., Sollima, A., Pancino, E., Bellazzini, M., Straniero, O., Origlia, L., & Cool, A. M. (2004). "The Discovery of an Anomalous Subgiant Branch in the Color-Magnitude Diagram of ω Centauri". In: ApJ 603, pp. L81–L84 (cit. on p. 5).

Freeman, K. C. (1993). "Globular Clusters and Nucleated Dwarf Ellipticals". In: *The Globular Cluster-Galaxy Connection*. Ed. by G. H. Smith & J. P. Brodie. Vol. 48. Astronomical Society of the Pacific Conference Series, p. 608 (cit. on p. 103).

Freeman, K. C. & Rodgers, A. W. (1975). "The Chemical Inhomogeneity of Omega Centauri". In: ApJ 201, p. L71 (cit. on p. 2).

Frogel, J. A., Persson, S. E., & Cohen, J. G. (1981). "Infrared photometry of red giants in the globular cluster 47 Tucanae". In: ApJ 246, pp. 842–865 (cit. on p. 34).

Geyer, E. H. (1967). "Eine Dreifarbenphotometrie von Omega Centauri (NGC 5139)". In: ZAp 66, p. 16 (cit. on p. 2).

Geyer, E. H., Nelles, B., & Hopp, U. (1983). "Ellipticity variations within some globular clusters of the Galaxy and the Magellanic Clouds". In: A&A 125, pp. 359–367 (cit. on p. 104).

Gratton, R. G., Bonifacio, P., Bragaglia, A., Carretta, E., Castellani, V., Centurion, M., Chieffi, A., Claudi, R., Clementini, G., D'Antona, F., Desidera, S., François, P., Grundahl, F., Lucatello, S., Molaro, P., Pasquini, L., Sneden, C. A., Spite, F., & Straniero, O. (2001). "The O-Na and Mg-Al anticorrelations in turn-off and early subgiants in globular clusters". In: A&A 369, pp. 87–98 (cit. on p. 62).

Gratton, R. G., Carretta, E., & Bragaglia, A. (2012). "Multiple populations in globular clusters. Lessons learned from the Milky Way globular clusters". In: A&A Rev. 20, p. 50 (cit. on p. 1).

Gratton, R. G., Carretta, E., Bragaglia, A., Lucatello, S., & D'Orazi, V. (2010). "The second and third parameters of the horizontal branch in globular clusters". In: A&A 517, A81 (cit. on p. 11).

Gratton, R. G., Johnson, C. I., Lucatello, S., D'Orazi, V., & Pilachowski, C. A. (2011). "Multiple populations in ω Centauri: a cluster analysis of spectroscopic data". In: A&A 534, A72 (cit. on pp. 72, 74, 77, 79, 82).

Gratton, R. G., Sneden, C. A., & Carretta, E. (2004). "Abundance Variations Within Globular Clusters". In: ARA&A 42, pp. 385–440 (cit. on p. 1).

Gray, D. F. (2005). *The Observation and Analysis of Stellar Photospheres*. 3rd. Cambridge: Cambridge University Press. ISBN: 0521851866 (cit. on pp. 24, 104).

Grundahl, F., Briley, M. M., Nissen, P. E., & Feltzing, S. (2002). "Abundances of RGB stars in NGC 6752". In: A&A 385, pp. L14–L17 (cit. on p. 4).

Grundahl, F., VandenBerg, D. A., Stetson, P. B., Andersen, M. I., & Briley, M. M. (2000). "Exploring star clusters using Strömgren uvby photometry". In: *Liege International Astrophysical Colloquia*. Ed. by A. Noels, P. Magain, D. Caro, E. Jehin, G. Parmentier, & A. A. Thoul. Vol. 35. Liege International Astrophysical Colloquia, p. 503 (cit. on p. 62).

Halley, E (1714). "An Account of Several Nebulae or Lucid Spots Like Clouds, Lately Discovered among the Fixt Stars by Help of the Telescope". In: *Philosophical Transactions* 29.338-350, pp. 390–392 (cit. on p. 1).

Harbeck, D., Smith, G. H., & Grebel, E. K. (2003). "CN Abundance Variations on the Main Sequence of 47 Tucanae". In: AJ 125, pp. 197–207 (cit. on pp. 4, 85, 117).

Harris, W. E. (1996). "A Catalog of Parameters for Globular Clusters in the Milky Way". In: AJ 112, p. 1487 (cit. on pp. 1–4, 57, 104).

Hartigan, J. A. & Wong, M. A. (1979). "Algorithm AS 136: A K-Means Clustering Algorithm". In: J. R. Stat. Soc. 28.1, p. 100. ISSN: 00359254 (cit. on p. 69).

Herwig, F., VandenBerg, D. A., Navarro, J. F., Ferguson, J., & Paxton, B. (2012). "From the Color-Magnitude Diagram of ω Centauri and (Super-)asymptotic Giant Branch Stellar Models to a Galactic Plane Passage Gas Purging Chemical Evolution Scenario". In: ApJ 757, p. 132 (cit. on pp. 109, 112, 115).

Hilker, M., Kayser, A., Richtler, T., & Willemsen, P. G. (2004). "The extended star formation history of ω Centauri". In: A&A 422, pp. L9–L12 (cit. on p. 112).

Hilker, M. & Richtler, T. (2000). "ω Centauri - a former nucleus of a dissolved dwarf galaxy? New evidence from Strömgren photometry". In: A&A 362, pp. 895–909 (cit. on pp. 12, 109, 112).

Hinkle, K., Wallace, L., Valenti, J., & Harmer, D. (2000). *Visible and Near Infrared Atlas of the Arcturus Spectrum 3727-9300 A*. Astronomical Society of the Pacific (cit. on p. 29).

Hughes, J. & Wallerstein, G. (2000). "Age and Metallicity Effects in ω Centauri: Strömgren Photometry at the Main-Sequence Turnoff". In: AJ 119, pp. 1225–1238 (cit. on p. 112).
Hughes, J., Wallerstein, G., van Leeuwen, F., & Hilker, M. (2004). "The Giant Branches of ω Centauri: Multiwavelength Observations of Evolved Stars". In: AJ 127, pp. 980–990 (cit. on p. 112).
Iben Jr., I. (1964). "The Surface Ration of N^{14} to C^{12} during Helium Burning." In: ApJ 140, p. 1631 (cit. on p. 6).
Icke, V. & Alcaíno, G. (1988). "Is Omega Centauri a merger?" In: A&A 204, p. 115 (cit. on p. 115).
Iliadis, Christian (2007). *Nuclear Physics of Stars*. Physics Textbook. John Wiley & Sons. 680 pp. ISBN: 9783527406029 (cit. on p. 12).
Ishigaki, M., Chiba, M., & Aoki, W. (2010). "Chemical Abundances of Outer Halo Stars in the Milky Way". In: PASJ 62, pp. 143– (cit. on p. 114).
Ivanova, N., Heinke, C. O., Rasio, F. A., Taam, R. E., Belczynski, K., & Fregeau, J. (2006). "Formation and evolution of compact binaries in globular clusters - I. Binaries with white dwarfs". In: MNRAS 372, pp. 1043–1059 (cit. on p. 11).
Jalali, B., Baumgardt, H., Kissler-Patig, M., Gebhardt, K., Noyola, E., Lützgendorf, N., & de Zeeuw, P. T. (2012). "A Dynamical N-body model for the central region of ω Centauri". In: A&A 538, A19 (cit. on p. 116).
Johnson, C. I., Kraft, R. P., Pilachowski, C. A., Sneden, C. A., Ivans, I. I., & Benman, G. (2005). "A 235 Star Sample Sodium, Magnesium, and Aluminum Abundance Study in the Globular Clusters M3 (NGC 5272) and M13 (NGC 6205)". In: PASP 117, pp. 1308–1324 (cit. on pp. 20, 21).
Johnson, C. I. & Pilachowski, C. A. (2010). "Chemical Abundances for 855 Giants in the Globular Cluster Omega Centauri (NGC 5139)". In: ApJ 722, pp. 1373–1410 (cit. on pp. 6, 7, 9, 10, 17, 21, 23, 28, 63, 64, 66–69, 72, 74, 76, 77, 79, 82, 84–86, 92, 93, 96, 101, 104, 108–111, 114, 120, 122).
Johnson, C. I., Pilachowski, C. A., Michael Rich, R., & Fulbright, J. P. (2009). "A Large Sample Study of Red Giants in the Globular Cluster Omega Centauri (NGC 5139)". In: ApJ 698, pp. 2048–2065 (cit. on pp. 109, 112).
Joo, S.-J. & Lee, Y.-W. (2013). "Star Formation Histories of Globular Clusters with Multiple Populations. I. ω Cen, M22, and NGC 1851". In: ApJ 762, p. 36 (cit. on pp. 113–115).
Keller, L. D., Pilachowski, C. A., & Sneden, C. (2001). "$^{12}C/^{13}C$ in Metal-poor Field Halo Giants". In: AJ 122, pp. 2554–2560 (cit. on p. 23).
King, I. R., Bedin, L. R., Cassisi, S., Milone, A. P., Bellini, A., Piotto, G., Anderson, J., Pietrinferni, A., & Cordier, D. (2012). "Hubble Space Telescope Observations of an Outer Field in Omega Centauri: A Definitive Helium Abundance". In: AJ 144, p. 5 (cit. on pp. 5, 112).
Koch, A. & McWilliam, A. (2008a). "A New Abundance Scale for the Globular Cluster 47 Tuc". In: AJ 135, pp. 1551–1566 (cit. on p. 39).
— (2008b). "Erratum: ''a New Abundance Scale for the Globular Cluster 47 Tuc'' (2008, AJ, 135, 1551)". In: AJ 136, p. 518 (cit. on p. 39).
Koch, A., McWilliam, A., Grebel, E. K., Zucker, D. B., & Belokurov, V. (2008). "The Highly Unusual Chemical Composition of the Hercules Dwarf Spheroidal Galaxy". In: ApJ 688, pp. L13–L16 (cit. on p. 114).
Krause, M., Charbonnel, C., Decressin, T., Meynet, G., Prantzos, N., & Diehl, R. (2012). "Superbubble dynamics in globular cluster infancy. I. How do globular clusters first lose their cold gas?" In: A&A 546, p. L5 (cit. on p. 116).
Kravtsov, V., Alcaíno, G., Marconi, G., & Alvarado, F. (2010). "Evidence of the inhomogeneity of the stellar population in the differentially reddened globular cluster NGC 3201". In: A&A 512, p. L6 (cit. on p. 1).
Lee, J.-W., Kang, Y.-W., Lee, J., & Lee, Y.-W. (2009). "Enrichment by supernovae in globular clusters with multiple populations". In: Nature 462, pp. 480–482 (cit. on p. 1).
Lee, Y.-W., Joo, J.-M., Sohn, Y.-J., Rey, S.-C., Lee, H.-C., & Walker, A. R. (1999). "Multiple stellar populations in the globular cluster ω Centauri as tracers of a merger event". In: Nature 402, pp. 55–57 (cit. on pp. 6, 112).
Lee, Y.-W., Joo, S.-J., Han, S.-I., Chung, C., Ree, C. H., Sohn, Y.-J., Kim, Y.-C., Yoon, S.-J., Yi, S. K., & Demarque, P. (2005). "Super-Helium-rich Populations and the Origin of Extreme Horizontal-Branch Stars in Globular Clusters". In: ApJ 621, pp. L57–L60 (cit. on p. 11).
Leigh, N. W. C., Böker, T., Maccarone, T. J., & Perets, H. B. (2013). "Gas depletion in primordial globular clusters due to accretion on to stellar-mass black holes". In: MNRAS, p. 492 (cit. on p. 116).
Li, K., Qian, S.-B., & Leung, K.-C. (2012). "Detection of a Second-generation Binary in the Globular Cluster ω Centauri". In: ApJ 755, p. 83 (cit. on p. 114).
Lindegren, L. (2010). "Gaia: Astrometric performance and current status of the project". In: *IAU Symposium*. Ed. by S. A. Klioner, P. K. Seidelmann, & M. H. Soffel. Vol. 261. IAU Symposium, pp. 296–305 (cit. on p. 17).

Lu, T.-N. & Kong, A. K. H. (2011). "Radio Continuum Observations of 47 Tucanae and ω Centauri: Hints for Intermediate-mass Black Holes?" In: ApJ 729, p. L25 (cit. on p. 116).

MacQueen, J. (1967). "Some methods for classification and analysis of multivariate observations". In: *Proc. Fifth Berkeley Sympos. Math. Statist. and Probability (Berkeley, Calif., 1965/66)*. Berkeley, Calif.: Univ. California Press, Vol. I: Statistics, Vol. I: Statistics (cit. on p. 69).

Mandushev, G., Staneva, A., & Spasova, N. (1991). "Dynamical masses for Galactic globular clusters". In: A&A 252, pp. 94–99 (cit. on p. 103).

Marino, A. F., Milone, A. P., Piotto, G., Cassisi, S., D'Antona, F., Anderson, J., Aparicio, A., Bedin, L. R., Renzini, A., & Villanova, S. (2012). "The C+N+O Abundance of ω Centauri Giant Stars: Implications for the Chemical-enrichment Scenario and the Relative Ages of Different Stellar Populations". In: ApJ 746, p. 14 (cit. on pp. 5, 7, 10, 21, 63, 68–83, 90, 93, 112–114, 117, 119, 121).

Marino, A. F., Milone, A. P., Piotto, G., Villanova, S., Bedin, L. R., Bellini, A., & Renzini, A. (2009). "A double stellar generation in the globular cluster NGC 6656 (M 22). Two stellar groups with different iron and s-process element abundances". In: A&A 505, pp. 1099–1113 (cit. on pp. 2, 103).

Marino, A. F., Milone, A. P., Piotto, G., Villanova, S., Gratton, R. G., D'Antona, F., Anderson, J., Bedin, L. R., Bellini, A., Cassisi, S., Geisler, D., Renzini, A., & Zoccali, M. (2011a). "Sodium–Oxygen Anticorrelation and Neutron-capture Elements in Omega Centauri Stellar Populations". In: ApJ 731, p. 64 (cit. on pp. 5–7, 9, 10, 17, 21, 63, 72, 74–77, 79–83, 93, 96).

Marino, A. F., Sneden, C. A., Kraft, R. P., Wallerstein, G., Norris, J. E., Da Costa, G. S., Milone, A. P., Ivans, I. I., Gonzalez, G., Fulbright, J. P., Hilker, M., Piotto, G., Zoccali, M., & Stetson, P. B. (2011b). "The two metallicity groups of the globular cluster M 22: a chemical perspective". In: A&A 532, A8 (cit. on p. 103).

Massari, D., Ferraro, F. R., Dalessandro, E., Lanzoni, B., Mucciarelli, A., & Origlia, L. (2013). "Terzan 5: a Fossil Remnant of the Galactic Bulge". In: *ArXiv e-prints* (cit. on p. 2).

Mateo, M. L. (1998). "Dwarf Galaxies of the Local Group". In: ARA&A 36, pp. 435–506 (cit. on p. 103).

McWilliam, A. (1998). "Barium Abundances in Extremely Metal-poor Stars". In: AJ 115, pp. 1640–1647 (cit. on p. 16).

Meléndez, J., Shchukina, N. G., Vasiljeva, I. E., & Ramírez, I. (2006). "Permitted Oxygen Abundances and the Temperature Scale of Metal-poor Turnoff Stars". In: ApJ 642, pp. 1082–1097 (cit. on p. 104).

Merrill, P. W. (1952). "Spectroscopic Observations of Stars of Class". In: ApJ 116, p. 21 (cit. on p. 6).

Meshik, A. P., Hohenberg, C. M., Pravdivtseva, O. V., & Kapusta, Ya. S. (2001). "Weak decay of ^{130}Ba and ^{132}Ba: Geochemical measurements". In: Phys. Rev. C 64 (3), p. 035205 (cit. on p. 16).

Meylan, G., Mayor, M., Duquennoy, A., & Dubath, P. (1995). "Central velocity dispersion in the globular cluster ω Centauri." In: A&A 303, p. 761 (cit. on p. 109).

Meza, A., Navarro, J. F., Abadi, M. G., & Steinmetz, M. (2005). "Accretion relics in the solar neighbourhood: debris from ωCen's parent galaxy". In: MNRAS 359, pp. 93–103 (cit. on p. 103).

Michaud, G., Richer, J., & Richard, O. (2008). "Abundance Anomalies in Horizontal Branch Stars and Atomic Diffusion". In: ApJ 675, pp. 1223–1232 (cit. on p. 11).

Michaud, G., Vauclair, G., & Vauclair, S. (1983). "Chemical separation in horizontal-branch stars". In: ApJ 267, pp. 256–270 (cit. on p. 11).

Milone, A. P., Piotto, G., Bedin, L. R., King, I. R., Anderson, J., Marino, A. F., Bellini, A., Gratton, R. G., Renzini, A., Stetson, P. B., Cassisi, S., Aparicio, A., Bragaglia, A., Carretta, E., D'Antona, F., Di Criscienzo, M., Lucatello, S., Monelli, M., & Pietrinferni, A. (2012). "Multiple Stellar Populations in 47 Tucanae". In: ApJ 744, p. 58 (cit. on p. 34).

Milone, A. P., Piotto, G., King, I. R., Bedin, L. R., Anderson, J., Marino, A. F., Momany, Y., Malavolta, L., & Villanova, S. (2010). "Multiple Stellar Populations in the Galactic Globular Cluster NGC 6752". In: ApJ 709, pp. 1183–1194 (cit. on p. 4).

Moni Bidin, C., Villanova, S., Piotto, G., Moehler, S., Cassisi, S., & Momany, Y. (2012). "Spectroscopy of horizontal branch stars in ω Centauri". In: A&A 547, A109 (cit. on p. 11).

Moni Bidin, C., Villanova, S., Piotto, G., Moehler, S., & D'Antona, F. (2011). "The Peculiar Properties of Horizontal-branch Stars in ω Centauri". In: ApJ 738, p. L10 (cit. on p. 11).

Mucciarelli, A., Bellazzini, M., Ibata, R. A., Merle, T., Chapman, S. C., Dalessandro, E., & Sollima, A. (2012). "News from the Galactic suburbia: the chemical composition of the remote globular cluster NGC 2419". In: MNRAS 426, pp. 2889–2900 (cit. on pp. 1, 123).

Nataf, D. M., Gould, A., Pinsonneault, M. H., & Stetson, P. B. (2011). "The Gradients in the 47 Tuc Red Giant Branch Bump and Horizontal Branch are Consistent with a Centrally Concentrated, Helium-enriched Second Stellar Generation". In: ApJ 736, p. 94 (cit. on p. 4).
National Nuclear Data Center (2013). *NuDat 2 database*. URL: http://www.nndc.bnl.gov/nudat2/ (visited on 01/23/2013) (cit. on pp. 15, 16).
Norris, J. E. (2004). "The Helium Abundances of ω Centauri". In: ApJ 612, pp. L25–L28 (cit. on pp. 5, 10, 112).
— (2012). "CN, CH region line list". private communication (cit. on p. 29).
Norris, J. E., Cottrell, P. L., Freeman, K. C., & Da Costa, G. S. (1981). "The abundance spread in the giants of NGC 6752". In: ApJ 244, pp. 205–220 (cit. on pp. 4, 55, 117).
Norris, J. E. & Da Costa, G. S. (1995). "The Giant Branch of omega Centauri. IV. Abundance Patterns Based on Echelle Spectra of 40 Red Giants". In: ApJ 447, p. 680 (cit. on pp. 5–7, 10, 112).
Norris, J. E., Freeman, K. C., & Da Costa, G. S. (1984). "The anticorrelation of cyanogen and CH on the giant branch of 47 Tucanae". In: ApJ 277, pp. 615–622 (cit. on p. 34).
Norris, J. E., Freeman, K. C., Mayor, M., & Seitzer, P. (1997). "The Giant Branch of omega Centauri: The Dependence of Kinematics on Abundance". In: ApJ 487, p. L187 (cit. on pp. 6, 109).
Norris, J. E., Freeman, K. C., & Mighell, K. J. (1996). "The Giant Branch of omega Centauri. V. The Calcium Abundance Distribution". In: ApJ 462, p. 241 (cit. on p. 34).
Norris, J. E. & Pilachowski, C. A. (1985). "The sodium-nitrogen correlation within globular clusters". In: ApJ 299, pp. 295–302 (cit. on pp. 36, 59).
Noyola, E., Gebhardt, K., & Bergmann, M. (2008). "Gemini and Hubble Space Telescope Evidence for an Intermediate-Mass Black Hole in ω Centauri". In: ApJ 676, pp. 1008–1015 (cit. on p. 103).
Origlia, L., Ferraro, F. R., Bellazzini, M., & Pancino, E. (2003). "A Near-Infrared Spectroscopic Screening of the Red Giant Populations in ω Centauri". In: ApJ 591, pp. 916–924 (cit. on p. 6).
Origlia, L., Rich, R. M., Ferraro, F. R., Lanzoni, B., Bellazzini, M., Dalessandro, E., Mucciarelli, A., Valenti, E., & Beccari, G. (2011). "Spectroscopy Unveils the Complex Nature of Terzan 5". In: ApJ 726, p. L20 (cit. on p. 2).
Pancino, E., Ferraro, F. R., Bellazzini, M., Piotto, G., & Zoccali, M. (2000). "New Evidence for the Complex Structure of the Red Giant Branch in ω Centauri". In: ApJ 534, pp. L83–L87 (cit. on pp. 5, 6, 109).
Pancino, E., Mucciarelli, A., Bonifacio, P., Monaco, L., & Sbordone, L. (2011a). "The subgiant branch of ω Centauri seen through high-resolution spectroscopy. II. The most metal-rich population". In: A&A 534, A53 (cit. on p. 6).
Pancino, E., Mucciarelli, A., Sbordone, L., Bellazzini, M., Pasquini, L., Monaco, L., & Ferraro, F. R. (2011b). "The subgiant branch of ω Centauri seen through high-resolution spectroscopy. I. The first stellar generation in ω Cen?" In: A&A 527, A18 (cit. on pp. 5, 7, 114, 123).
Pancino, E., Pasquini, L., Hill, V., Ferraro, F. R., & Bellazzini, M. (2002). "High-Resolution Spectroscopy of Metal-rich Giants in ω Centauri: First Indication of Type Ia Supernova Enrichment". In: ApJ 568, pp. L101–L105 (cit. on p. 6).
Petrucci, Ralph H., Herring, F. Geoffrey, Madura, Jeffry D, & Bissonnette, Carey (2001). *General Chemistry: Principles and Modern Applications*. 10th. Pearson Canada. ISBN: 978-0-13-206452-1 (cit. on p. 22).
Pilachowski, C. A., Sneden, C., Kraft, R. P., & Langer, G. E. (1996). "Proton Capture Chains in Globular Cluster Stars. I. Evidence for Deep Mixing Based on Sodium and Magnesium Abundances in M13 Giants". In: AJ 112, p. 545 (cit. on p. 12).
Piotto, G., Bedin, L. R., Anderson, J., King, I. R., Cassisi, S., Milone, A. P., Villanova, S., Pietrinferni, A., & Renzini, A. (2007). "A Triple Main Sequence in the Globular Cluster NGC 2808". In: ApJ 661, pp. L53–L56 (cit. on pp. 4, 5).
Piotto, G., Milone, A. P., Anderson, J., Bedin, L. R., Bellini, A., Cassisi, S., Marino, A. F., Aparicio, A., & Nascimbeni, V. (2012). "Hubble Space Telescope Reveals Multiple Sub-giant Branch in Eight Globular Clusters". In: ApJ 760, p. 39 (cit. on p. 4).
Piotto, G., Villanova, S., Bedin, L. R., Gratton, R. G., Cassisi, S., Momany, Y., Recio-Blanco, A., Lucatello, S., Anderson, J., King, I. R., Pietrinferni, A., & Carraro, G. (2005). "Metallicities on the Double Main Sequence of ω Centauri Imply Large Helium Enhancement". In: ApJ 621, pp. 777–784 (cit. on p. 5).
Prochaska, J. X. & McWilliam, A. (2000). "On the Perils of Hyperfine Splitting: A Reanalysis of MN and SC Abundance Trends". In: ApJ 537, pp. L57–L60 (cit. on p. 24).
R Development Core Team (2011). *R: A Language and Environment for Statistical Computing*. ISBN 3-900051-07-0. R Foundation for Statistical Computing. Vienna, Austria (cit. on p. 69).

Ramdani, A. & Jorissen, A. (2001). "Evolution of the dust mass loss with luminosity along the giant branch of the globular cluster 47 Tucanae". In: A&A 372, pp. 85–94 (cit. on p. 34).
Ramírez, I., Meléndez, J., & Chanamé, J. (2012). "Oxygen Abundances in Low- and High-α Field Halo Stars and the Discovery of Two Field Stars Born in Globular Clusters". In: ApJ 757, p. 164 (cit. on p. 4).
Rey, S.-C., Lee, Y.-W., Ree, C. H., Joo, J.-M., Sohn, Y.-J., & Walker, A. R. (2004). "CCD Photometry of the Globular Cluster ω Centauri. II. Stellar Populations and Age-Metallicity Relation". In: AJ 127, pp. 958–979 (cit. on pp. 6, 112).
Sandquist, E. L. & Hess, J. M. (2008). "Evolved Stars in the Core of the Massive Globular Cluster NGC 2419". In: AJ 136, pp. 2259–2285 (cit. on p. 123).
Sarajedini, A., Bedin, L. R., Chaboyer, B., Dotter, A., Siegel, M., Anderson, J., Aparicio, A., King, I. R., Majewski, S., Marín-Franch, A., Piotto, G., Reid, I. N., & Rosenberg, A. (2007). "The ACS Survey of Galactic Globular Clusters. I. Overview and Clusters without Previous Hubble Space Telescope Photometry". In: AJ 133, pp. 1658–1672 (cit. on p. 3).
Sbordone, L., Salaris, M., Weiss, A., & Cassisi, S. (2011). "Photometric signatures of multiple stellar populations in Galactic globular clusters". In: A&A 534, A9 (cit. on pp. 112, 113).
Scarpa, R. & Falomo, R. (2010). "Testing Newtonian gravity in the low acceleration regime with globular clusters: the case of ω Centauri revisited". In: A&A 523, A43 (cit. on p. 109).
Schwarzschild, M. & Härm, R. (1967). "Hydrogen Mixing by Helium-Shell Flashes". In: ApJ 150, p. 961 (cit. on p. 17).
Shetrone, M. D. & Keane, M. J. (2000). "Spectral Comparison of Red Giants in the Second-Parameter Globular Cluster Pair NGC 288 and NGC 362". In: AJ 119, pp. 840–850 (cit. on pp. 11, 56).
Simmerer, J. A., Ivans, I. I., & Filler, D. (2012). "Chemical Compositions of Stars in the Globular Cluster NGC 3201: Tracers of Multi-Epoch Star Formation". In: *American Astronomical Society Meeting Abstracts 219*. Vol. 219. American Astronomical Society Meeting Abstracts, p. 152.07 (cit. on p. 103).
Simmerer, J. A., Ivans, I. I., Filler, D., François, P., Charbonnel, C., Monier, R., & James, G. (2013). "Star-to-star Iron Abundance Variations in Red Giant Branch Stars in the Galactic Globular Cluster NGC 3201". In: ApJ 764, p. L7 (cit. on pp. 1, 103).
Simpson, J. D. & Cottrell, P. L. (2013). "Spectral matching for abundances of 848 stars of the giant branches of the globular cluster ω Centauri". In: MNRAS 433, pp. 1892–1902 (cit. on pp. xii, 85).
Simpson, J. D., Cottrell, P. L., & Worley, C. C. (2012). "Spectral matching for abundances and clustering analysis of stars on the giant branches of ω Centauri". In: MNRAS 427, pp. 1153–1167 (cit. on pp. xii, 12, 63, 123).
Skrutskie, M. F. et al. (2006). "The Two Micron All Sky Survey (2MASS)". In: AJ 131, pp. 1163–1183 (cit. on p. 19).
Smith, V. V., Suntzeff, N. B., Cunha, K., Gallino, R., Busso, M., Lambert, D. L., & Straniero, O. (2000). "The Chemical Evolution of the Globular Cluster ω Centauri (NGC 5139)". In: AJ 119, pp. 1239–1258 (cit. on p. 112).
Smith, V. V., Terndrup, D. M., & Suntzeff, N. B. (2002). "Carbon Isotopic Abundances in the Red Giants of ω Centauri (NGC 5139)". In: ApJ 579, pp. 832–840 (cit. on p. 23).
Sneden, C. A. (1973). "Carbon and Nitrogen Abundances in Metal-Poor Stars." PhD thesis. The University of Texas at Austin (cit. on p. 27).
Sneden, C. A., Cowan, J. J., & Gallino, R. (2008). "Neutron-Capture Elements in the Early Galaxy". In: ARA&A 46, pp. 241–288 (cit. on pp. xii, 14).
Sobeck, J. S., Kraft, R. P., Sneden, C. A., Preston, G. W., Cowan, J. J., Smith, G. H., Thompson, I. B., Shectman, S. A., & Burley, G. S. (2011). "The Abundances of Neutron-capture Species in the Very Metal-poor Globular Cluster M15: A Uniform Analysis of Red Giant Branch and Red Horizontal Branch Stars". In: AJ 141, p. 175 (cit. on pp. 9, 103).
Sollima, A., Pancino, E., Ferraro, F. R., Bellazzini, M., Straniero, O., & Pasquini, L. (2005). "Metallicities, Relative Ages, and Kinematics of Stellar Populations in ω Centauri". In: ApJ 634, pp. 332–343 (cit. on pp. 6, 112).
Soubiran, C., Le Campion, J.-F., Cayrel de Strobel, G., & Caillo, A. (2010). "The PASTEL catalogue of stellar parameters". In: A&A 515, A111 (cit. on p. 34).
Stanford, L. M., Da Costa, G. S., & Norris, J. E. (2010). "Abundances of C, N, Sr, and Ba on the Red Giant Branch of ω Centauri". In: ApJ 714, pp. 1001–1014 (cit. on pp. 5, 7, 9, 24, 96).
Stanford, L. M., Da Costa, G. S., Norris, J. E., & Cannon, R. D. (2006). "The Age and Metallicity Relation of ω Centauri". In: ApJ 647, pp. 1075–1092 (cit. on pp. 6, 112).
— (2007). "Abundances on the Main Sequence of ω Centauri". In: ApJ 667, pp. 911–929 (cit. on p. 123).

Steinhaus, H. (1956). "Sur la division des corps matériels en parties". In: *Bull. Acad. Polon. Sci. Cl. III.* 4, 801–804 (1957) (cit. on p. 69).
Taylor, M. B. (2005). "TOPCAT & STIL: Starlink Table/VOTable Processing Software". In: *Astronomical Data Analysis Software and Systems XIV*. Ed. by P. Shopbell, M. Britton, & R. Ebert. Vol. 347. Astronomical Society of the Pacific Conference Series, p. 29 (cit. on p. 64).
Trimble, V. (1975). "The origin and abundances of the chemical elements". In: RMP 47, pp. 877–976 (cit. on p. 12).
Tucholke, H.-J. (1992). "Astrometry of globular clusters. I - Relative proper motions for stars in 47 Tuc. II - Relative proper motions and the space motion of NGC 362". In: A&AS 93, pp. 293–310 (cit. on p. 34).
Valcarce, A. A. R. & Catelan, M. (2011). "Formation of multiple populations in globular clusters: another possible scenario". In: A&A 533, A120 (cit. on pp. 115, 116).
van de Ven, G., van den Bosch, R. C. E., Verolme, E. K., & de Zeeuw, P. T. (2006). "The dynamical distance and intrinsic structure of the globular cluster ω Centauri". In: A&A 445, pp. 513–543 (cit. on p. 103).
van Leeuwen, F., Le Poole, R. S., Reijns, R. A., Freeman, K. C., & de Zeeuw, P. T. (2000). "A proper motion study of the globular cluster ω Centauri". In: A&A 360, pp. 472–498 (cit. on pp. 21, 23, 64, 67, 85, 87, 88).
van Loon, J. T., van Leeuwen, F., Smalley, B., Smith, A. W., Lyons, N. A., McDonald, I., & Boyer, M. L. (2007). "A spectral atlas of post-main-sequence stars in ω Centauri: kinematics, evolution, enrichment and interstellar medium". In: MNRAS 382, pp. 1353–1374 (cit. on pp. xii, 11, 12, 17, 19, 21, 22, 24, 27, 29, 33, 44, 50, 62–69, 71, 72, 76, 82, 84–90, 93, 95, 99, 109, 117–119, 121, 122).
Vesperini, E., McMillan, S. L. W., D'Antona, F., & D'Ercole, A. (2011). "Binary star disruption in globular clusters with multiple stellar populations". In: MNRAS 416, pp. 355–360 (cit. on p. 11).
Villanova, S., Carraro, G., Scarpa, R., & Marconi, G. (2010). "Abundance analysis of a sample of evolved stars in the outskirts of ω Centauri". In: New A 15, pp. 520–529 (cit. on pp. 5, 7, 9).
Villanova, S., Piotto, G., King, I. R., Anderson, J., Bedin, L. R., Gratton, R. G., Cassisi, S., Momany, Y., Bellini, A., Cool, A. M., Recio-Blanco, A., & Renzini, A. (2007). "The Multiplicity of the Subgiant Branch of ω Centauri: Evidence for Prolonged Star Formation". In: ApJ 663, pp. 296–314 (cit. on pp. 5, 112, 113).
Wallerstein, G., Iben Jr., I., Parker, P., Boesgaard, A. M., Hale, G. M., Champagne, A. E., Barnes, C. A., Käppeler, F., Smith, V. V., Hoffman, R. D., Timmes, F. X., Sneden, C. A., Boyd, R. N., Meyer, B. S., & Lambert, D. L. (1997). "Synthesis of the elements in stars: forty years of progress". In: RMP 69, pp. 995–1084 (cit. on pp. 12, 15).
Worley, C. C. (2009). "Exploration of s-process elemental abundances in globular cluster stars using medium- and high-resolution spectra." PhD thesis. University of Canterbury (cit. on pp. 34, 56).
— (2013). "Normalized spectra and [Na/Fe] abundances of 47 Tuc stars". private communication (cit. on pp. 4, 36, 38–40, 50, 51, 55, 57).
Worley, C. C. & Cottrell, P. L. (2012). "Medium-Resolution s-process Element Survey of 47 Tuc Giant Stars". In: PASA 29, pp. 29–41 (cit. on pp. 4, 9, 21, 34, 36–38, 51, 57, 104).
Worley, C. C., Cottrell, P. L., Freeman, K. C., & Wylie-de Boer, E. C. (2009). "Differential chemical abundance analysis of a 47 Tucanæ asymptotic giant branch star with respect to Arcturus". In: MNRAS 400, pp. 1039–1048 (cit. on p. 34).
Worley, C. C., Cottrell, P. L., McDonald, I., & van Loon, J. T. (2010). "Heavy-element abundances in low-gravity globular cluster stars: 47 Tuc*". In: MNRAS 402, pp. 2060–2074 (cit. on p. 34).
Wylie-de Boer, E. C. (2006). "Nucleosynthesis and S-process Element Formation in Giant Stars". PhD thesis. University of Canterbury (cit. on p. 34).
Yong, D. & Grundahl, F. (2008). "An Abundance Analysis of Bright Giants in the Globular Cluster NGC 1851". In: ApJ 672, pp. L29–L32 (cit. on p. 103).
Yong, D., Grundahl, F., Johnson, J. A., & Asplund, M. (2008). "Nitrogen Abundances in Giant Stars of the Globular Cluster NGC 6752". In: ApJ 684, pp. 1159–1169 (cit. on pp. 4, 57).
Zucker, D. B., de Silva, G., Freeman, K. C., Bland-Hawthorn, J., & Hermes Team (2012). "The Galactic Archaeology with HERMES Survey". In: *Galactic Archaeology: Near-Field Cosmology and the Formation of the Milky Way*. Ed. by W. Aoki, M. Ishigaki, T. Suda, T. Tsujimoto, & N. Arimoto. Vol. 458. Astronomical Society of the Pacific Conference Series, p. 421 (cit. on p. 17).